the Energy to Lead

gti

FINAL REPORT

GTI PROJECT NUMBER 21874

Characterization and Fitness for Service of Corroded Cast Iron Pipe

Contract Number: DTPH56-15-T-00006

Report Issued
February 15, 2018

Prepared For
U.S. Department of Transportation
Pipeline and Hazardous Materials Safety Administration
Office of Pipeline Safety
Chris McLaren
chris.mclaren@dot.gov

Technical Team
Daniel Ersoy
Oren Lever
Khalid Farrag
Brian Miller

Project Manager
Kristine Wiley
R&D Manager, GTI
kristine.wiley@gastechnology.org

Technical Contact
Daniel Ersoy
R&D Executive Director, GTI
daniel.ersoy@gastechnology.org

Gas Technology Institute
1700 S. Mount Prospect Rd.
Des Plaines, Illinois 60018

Signature Page

			Date
AUTHOR			
Daniel A. Ersoy	*Title:*	Daniel Ersoy//S// R&D Exec. Dir. and PI	02/15/2018
CO-AUTHOR			
Oren Lever	*Title:*	Oren Lever//S// Principal Engineer	02/15/2018
CO-AUTHOR			
Khalid Farrag	*Title:*	Khalid Farrag//S// Sr. Institute Engineer	02/15/2018
CO-AUTHOR			
Brian J. Miller	*Title:*	Brian J. Miller//S// Chief Technologist	02/15/2018
REVIEWED BY			
Kristine Wiley	*Title:*	Kristine Wiley//S// R&D Manager and PM	02/15/2018

Legal Notice

This information was prepared by Gas Technology Institute ("GTI") for U.S. DOT/PHMSA under agreement DTPH56-15-T-00006.

Neither GTI, the members of GTI, the Sponsor(s), nor any person acting on behalf of any of them:

Makes any warranty or representation, express or implied with respect to the accuracy, completeness, or usefulness of the information contained in this report, or that the use of any information, apparatus, method, or process disclosed in this report may not infringe privately-owned rights. Inasmuch as this project is experimental in nature, the technical information, results, or conclusions cannot be predicted. Conclusions and analysis of results by GTI represent GTI's opinion based on inferences from measurements and empirical relationships, which inferences and assumptions are not infallible, and with respect to which competent specialists may differ.

Assumes any liability with respect to the use of, or for any and all damages resulting from the use of, any information, apparatus, method, or process disclosed in this report; any other use of, or reliance on, this report by any third party is at the third party's sole risk.

The results within this report relate only to the items reviewed.

Table of Contents

Table of Figures

Page

List of Tables

Page

Executive Summary

This project final report provides a Cast Iron (CI) Fitness-For-Service (FFS) model, calculator, and method for operators to characterize and grade graphitic corrosion defects on cast iron natural gas pipe. This will help make monitoring, repair, and replacement decisions, as well as prioritize their replacement program decisions leading to improved safety and supply stability.

Cast iron piping was installed over a period spanning more than 100 years, leading to a great range of variability in the material. Different manufacturing processes, chemistries, and designs have led to a wide range of material characteristics and performance levels. Even when operators assess their cast iron piping systems and find corrosion, especially graphitic corrosion, they are left without sound engineering guidance if the corrosion and wall loss found are an integrity threat or allowable within the design and operational restrictions of the installation.

Accordingly, operators need FFS guidance for cast iron piping that can be consulted when graphitic corrosion defects and wall loss are identified in cast iron piping systems. Having FFS guidance in the form of a remaining factor of safety for cast iron assets will immediately provide a go/no-go decision for immediate threat defects, and will also provide validated engineering guidance to prioritize mains and service replacement programs. The highest risk piping can be identified and scheduled for prioritized replacement.

As part of this project a detailed literature search on cast iron materials was conducted. The report summarizes the history, use, composition, microstructure, mechanical properties, metallurgy, and corrosion characteristics of gray cast iron in general and cast iron used for natural gas distribution systems in specific. The review includes a detailed explanation of graphitic corrosion of gray cast irons and the effect of graphitic corrosion on residual pipe strength. A set of field testing and sampling considerations, including a table of standards and methods to obtain mechanical, physical, and chemical properties from in service pipelines was developed.

A summary was developed of cast iron failure incidents, as well as the associated loads and stresses on cast iron pipes due to external loads and environmental conditions. This included a review of the parameters affecting cast iron corrosion and an analysis of the loads and stresses which the cast iron pipes are subjected to in the field. Additionally, the review and summary of design codes for cast iron pipes was completed.

A method for measurement of graphitic corrosion in the field was developed with detailed guidance on measurement of corrosion defects to be used as part of the FFS model input. This included a general set of guidelines an operator will use to characterize the type and severity of graphitic corrosion on a cast iron pipeline in the field. This will allow the operator to consistently and reliably develop part of the input data needed to run the FFS cast iron model.

Using Finite Element Analysis, Design of Experiments, and Statistical Regression a CI FFS model for graphitic corrosion defects was developed. The model can be used to determine the critical defect size and characteristics that could lead to premature piping failure. The results of the model were incorporated into an Excel-based, end-user calculator. A user's/training manual was developed and a set of examples were created to facilitate implementation of the FFS model with the end user.

A first-pass validation of the FFS model was completed through the analysis of select cast iron field failures. The failure data was compared against the FFS model results applied to the same situations. An analysis was also conducted on the effect that uncertainty of input values would have on the model results. This was done through Monte Carlo simulations that allowed the inclusion of measurement uncertainty for input variables such as diameter, thickness, material strength, corrosion defect geometry, etc.

Finally, the report summarizes the basis and specific recommendations for a comprehensive, testing-based validation program for the developed FFS model. The program considers and lists the gray iron materials testing specifications, consensus standards for mechanical testing, currently available (new) gray cast iron materials, vintage piping samples to consider, and how many testing replicates are recommended for each material type.

GTI thanks the project sponsor, the Pipeline and Hazardous Materials and Safety Administration, for its financial and program support, as well as the industry members of the project Technical Advisory Panel for their technical guidance during this effort.

1. Introduction

Cast iron gas mains have been installed since the 1830's and they are still in service in many U.S. cities. About 32,400 miles of cast iron main is estimated to be in service in 2012, with about 50% of these pipes located within four states: New Jersey, New York, Massachusetts, and Pennsylvania. Consistent with the 49 CFR federal requirements, local distribution companies (LDC) have developed procedures for surveillance of their cast iron facilities to identify problems and take appropriate action concerning leak, breakage, and graphitization.

Recently, there have been two significant incidents in Philadelphia and Allentown, PA resulting from the failure of cast iron mains in the gas distribution system. Failures in these incidents were in 12-inch gas cast iron mains that were installed in 1942 and 1928; respectively.

These incidents prompted the state regulators in PA to evaluate and modify the utilities' procedures regarding the frequencies of the cast iron surveillance. Cast iron pipelines' vulnerability and their integrity are further highlighted in the PHMSA Safety Advisory Bulletin. This requires gas operators to implement a program, based on factors such as age, pipe diameter, operating pressure, soil corrosiveness, existing graphitic damage, leak history, and external loading, to identify and replace in a planned, timely manner cast iron piping systems.

This project provides a Fitness-For-Service (FFS) model, calculator, and method for operators to characterize and grade graphitic corrosion defects on cast iron natural gas pipe. This will help make monitoring, repair, and replacement decisions, as well as prioritize their replacement program decisions leading to improved safety and supply stability.

Background

Cast iron piping was installed over a period spanning more than 100 years, leading to a great range of variability in the material. Different manufacturing processes, chemistries, and designs have led to a wide range of material characteristics and performance levels. Even when operators assess their cast iron piping systems and find corrosion, especially graphitic corrosion (sometimes improperly termed graphitization), they are left without sound engineering guidance if the corrosion and wall loss found are an integrity threat or allowable within the design and operational restrictions of the installation. Accordingly, operators need FFS guidance for cast iron piping that can be consulted when graphitic corrosion defects and wall loss are identified in cast iron piping systems. Having FFS

guidance in the form of a remaining factor of safety (F.S.) for cast iron assets will immediately provide a go/no-go decision for immediate threat defects, and will also provide validated engineering guidance to prioritize mains and service replacement programs. The highest risk piping can be identified and scheduled for prioritized replacement.

Pipeline owners are increasingly required to find new methods for a proactive condition assessment of their assets and determining the FFS in support of prioritizing cast iron pipe replacement programs.

Replacement of the vintage cast iron pipes in urban areas can be technically difficult, extremely expensive, and can pose secondary risks. On the other hand, the failure of these vintage pipes in the urban environments has a higher potential risk of adverse consequences.

Even when it has been possible to measure defects on cast iron pipe walls, there is little to no guidance whether the pipes with the defects are still fit for service. Steel piping has an abundance of such guidance. For example, the API 5L steel pipe operators can rely on ASEM B31G - Manual for Determining the Remaining Strength of Corroded Pipelines, RSTRENG software for determining remaining strength of corroded pipe, and API 579-1 FFS guides to help make such monitoring, repair, and replacement decisions. Cast iron pipe and material is vastly different. It has extremely low ductility, a different and much more brittle failure mode, built-in stress risers in the form of flake graphite, different joining designs, and a much larger variability in its physical and mechanical properties.

There is a need for a guidance document on how to characterize the cast iron materials, properties, corrosion defects, and environmental, operational, and loading conditions. Then, this information with a validated FFS model can be used to determine the severity and risk of the corrosion damage to the cast iron pipe.

Project Objectives

- Provide a Fitness-For-Service (FFS) model and method for operators to characterize and grade graphitic corrosion defects on cast iron natural gas pipes. This will help operators make monitoring, repair, and replacement decisions, as well as prioritize accelerated replacement decisions related to cast iron mains and services.
- Summarize and categorize the required input parameters to the FFS model related to cast iron material, graphitic corrosion geometry and characteristics, and operational environment.

- Validate the FFS model by comparing its output to a statistically analyzed set of historical cast iron failure data.
- Provide the model in an easy to use, Excel-based calculator with an associated training manual and examples of the model use.
- Provide a physical testing program to fully validate the FFS model (a potential follow on effort).

Acknowledgements

GTI thanks the project sponsor, the Pipeline and Hazardous Materials and Safety Administration for its financial and program support and the industry members of the project Technical Advisory Panel for their technical support of this effort.

2. Cast Iron Materials Literature Search

This section of the report summarizes a literature search and review on cast iron materials and corrosion.

A brief background section discusses the history of cast iron, its use as a pipeline material, general composition, corrosion, and the categories/types.

After the background section is a detailed section on gray cast iron microstructure, composition, and mechanical properties. The typical properties of currently produced gray cast irons, as well as the defect-free and corroded properties of in-field, exhumed gray cast iron pipes are compared. Much of the research was performed on gray cast iron pipe used in the water industries. However, this work is highly relevant to the natural gas distribution piping systems, since the same pipe is used across both sectors.

This section also provides a detailed explanation of graphitic corrosion of gray cast irons along with short explanations of other corrosion mechanisms like pitting, stress corrosion cracking, corrosion in waters, etc. The effect of graphitic corrosion on residual pipe strength is then presented.

Appendix A provides a draft summary of field testing and sampling considerations, including a table of standards and methods to obtain mechanical, physical, and chemical properties from in service pipelines.

Select mechanical property information from this literature review was used as inputs to the finite element modeling and stress analysis tasks of this project. The corrosion information was incorporated into the project task on field corrosion characterization.

Finally, this review also demonstrated the great variability of gray cast iron pipe mechanical properties in the field, as well as corrosion morphology. This reinforces the need for systematic field sampling to properly bound a fitness-for-service analysis of specific pipeline systems.

Background

History

Ancient records indicate that the Chinese were making iron castings as early as the 6th century before Christ. Various Chinese temples with cast iron roofs a thousand years old appear to be in first class condition today. In the 12th century A.D., iron progress shifted to European countries, principally Germany, Belgium, France, Italy, and England.

By the 1700's European production included bells, cannon, gunshot, pipe, stoves, and cast iron cooking utensils. Figure 1 [1] shows a cast iron water pipe laid in 1644 to supply water to the Fountains of Versailles and is still in use over 300 years later.

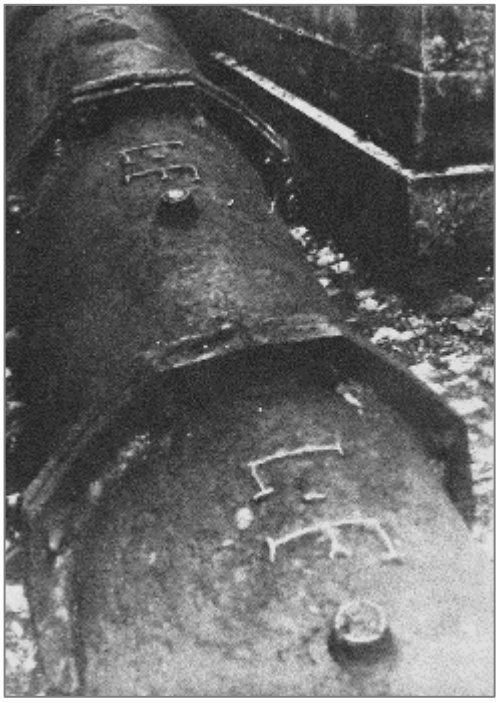

Figure 1. Cast iron water pipe laid in 1644 to supply the Fountains of Versailles, still in use after 300 years. The initials "L.F." are for Louis XIV of France.

The first casting made in America was produced at Saugus Iron Works near Lynn, Mass., shortly after its establishment in 1642. Soon after, foundries appeared in Connecticut, Rhode Island, New Jersey, Virginia, the Carolinas, Pennsylvania, and Maryland.

Natural Gas Industry Use

Significant gray cast iron was installed up through 1950-1960 as part of the U.S. natural gas and water infrastructure distribution systems. Examples of natural gas distribution piping installations are shown in Figure 2 to Figure 5.

Figure 2. Cast iron gas pipe installation showing bell and spigot joint.

Figure 3. Cast iron gas pipe installation showing flange and bolted connection.

Figure 4. Large diameter cast iron gas pipe about to undergo video inspection.

Figure 5. Cast iron cast iron gas pipe in a congested joint trench.

Graphitic Corrosion

Three examples of graphitic corrosion on natural gas cast iron pipe are shown in Figure 6 to Figure 8. Corrosion in general, and graphitic corrosion in particular, will be discussed in the paper under the corrosion section.

Figure 6. Cast iron gas pipe corrosion.

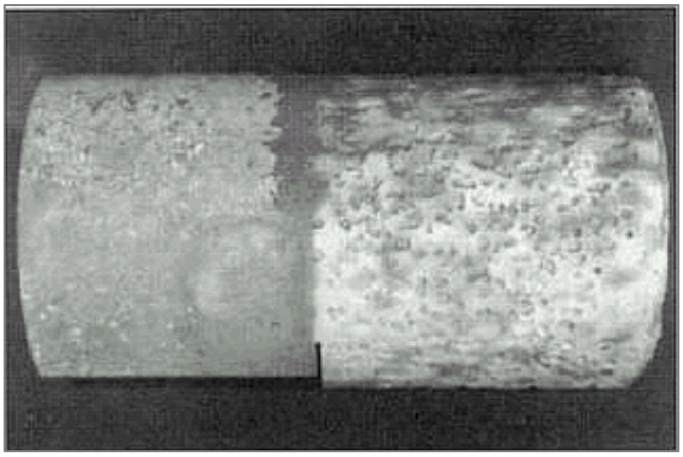

Figure 7. Cast iron gas pipe corrosion before and after grit blasting.

Figure 8. Cast iron gas pipe graphitic corrosion and pitting.

General Composition

Cast iron is mainly an alloy of carbon, silicon, and iron where there is more carbon present than can be retained in solid solution in austenite, a typically high temperature form of iron. Cast iron therefore contains decomposition products like free graphite or cementite (an iron carbide). The carbon content in cast irons is usually more than 1.7 weight percent and less than 4.5 weight percent. This high percentage of carbon makes the cast iron brittle and not workable, except by casting, hence its name - cast iron. The range of carbon and silicon for common cast irons as compared with steel is shown in Figure 9 [2].

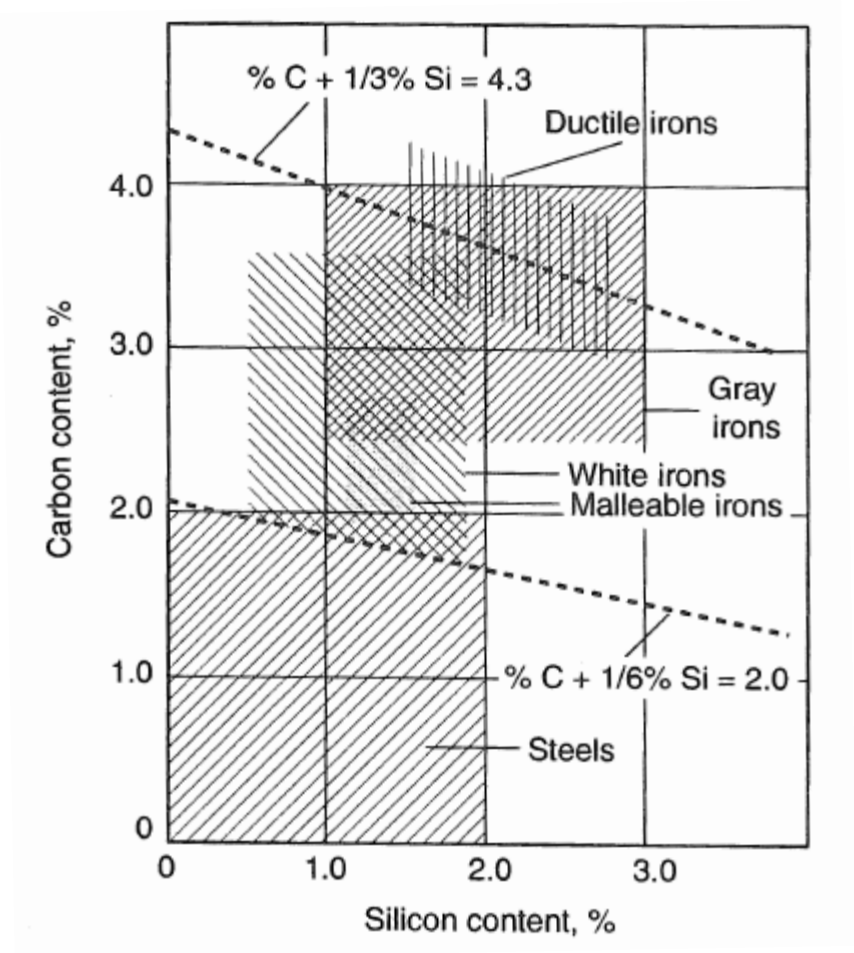

Figure 9. Approximate ranges of carbon and silicon for steel and various cast irons.

Cast iron can therefore solidify according to the thermodynamically metastable iron - iron carbide system, Fe-Fe(3)C, or the stable iron-graphite system. When the metastable path is followed, the rich carbon phase is iron carbide; when the stable solidification path is followed, the rich carbon phase is graphite.

Silicon is a graphitizing agent and is usually added in amounts around one half to two percent, but much higher in certain silicon irons. Cast iron also contains manganese, phosphorous, and sulfur; all as byproducts of the refining process.

Special alloying elements like copper, molybdenum, nickel, and chromium are added to change the chemical and mechanical properties. These will be discussed in a later section of this report.

Main Cast Iron Groupings

The main groups of cast irons are:
1. Gray cast iron
2. White cast iron
3. Malleable iron
4. Ductile (nodular) iron
5. Alloy cast iron

Gray vs. White

The term "gray" and "white" as applied to cast iron refer to the appearance of the fracture of the casting. The gray iron fractures with a dark, gray fracture, where the white cast iron shows a light gray or almost white fracture as shown in Figure 10 [3].

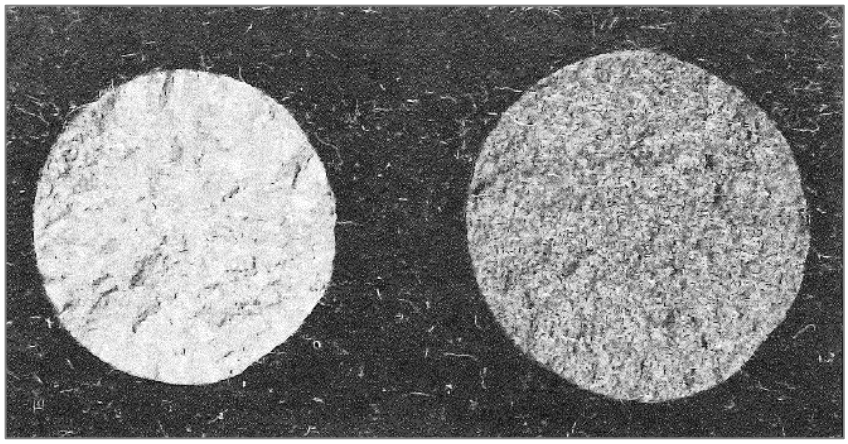

Figure 10. Fracture appearance of white cast iron, left; gray cast iron, right.

For the remainder of this report we will focus on unalloyed (i.e., base), gray cast iron since this the type of cast iron that natural gas distribution pipes and fittings have been made from.

Gray Cast Iron Microstructural, Chemical, and Mechanical Properties

Introduction

Gray cast iron, or gray iron, is the most widely used of all cast irons. It is manufactured more than the other four types combined.

In general, gray cast iron has good compressive strength, wear resistance, castability, low notch sensitivity, and high damping capacity. It is also has a good manufacturing economy, better castability than steel, and low shrinkage in the casting mold.

Gray iron must be selected in a way to satisfy three basic structural requirements:
1. The required graphite shape and distribution
2. The carbide-free (chill-free) structure
3. The required matrix.

Gray iron typically refers to a broad class of ferrous casting alloys normally characterized by a microstructure of flake graphite in a ferrous matrix. Gray irons are in essence iron-carbon-silicon alloys that usually contain 2.5% to 4% C, 1 to 3% Si, and additions of manganese, depending on the desired microstructure. Sulfur and phosphorous are also present in small amounts as residual impurities.

Classification of Gray Cast Iron

In general, gray cast irons are classified on the basis of tensile strength.

ASTM A48

A simple method to classify gray irons is found in *ASTM A48 - Standard Specification for Gray Iron Castings*. This specification classifies the various gray cast iron types in terms of tensile strength, expressed in ksi. So, a class 20 cast iron has a tensile strength of 20,000 psi (or 20 ksi), a class 30 is 30ksi, and so on. Chemical analysis alone is not sufficient to designate a cast iron because of the wide range of mechanical properties that can be obtained.

Generally, it can be assumed that the following properties of gray cast irons increase with increasing tensile strength from class 20 to class 60:
1. All strengths, including strength at elevated temperature
2. Ability to be machined to a fine finish
3. Modulus of elasticity
4. Wear resistance

Likewise, the following properties decrease with increasing tensile strength, so that low-strength irons often perform better than high-strength irons when these properties are important:

1. Machinability
2. Resistance to thermal shock
3. Damping capacity
4. Ability to be cast in thin sections

Microstructure of Gray Cast Iron

The microstructure is as important as the chemical analysis in determining the final properties of gray cast iron castings. The microstructure consists of two primary parts: the graphite flakes and the metal matrix surrounding the flakes. The matrix structure of gray cast iron can be changed somewhat easily by heat treatment once the casting is formed, but the graphite flakes are slightly influenced by heat treatment.

Steps for Examination

Examination of cast iron microstructure is done in two steps:

1. First a specimen is sanded and polished with progressively finer abrasives. Then it is viewed under the microscope at 25X and then 100X to establish the size and distribution of graphite that is present. This is done by comparing the microstructure with standard charts, see Figure 11 and Figure 12 [4]. An example of unetched graphite structure is shown in Figure 13.

These charts are made for comparison of unetched specimens at 100X magnification.

2. Second, the specimen is etched with the recommended reagent to make the matrix structure visible. The structure is viewed and recorded with microscopic examination.

Figure 14 is the etched microstructure of the same sample shown in Figure 13. The primary metal matrix phase is pearlite. Additional examples of typical matrix structures for gray iron are shown in Figure 15 [5].

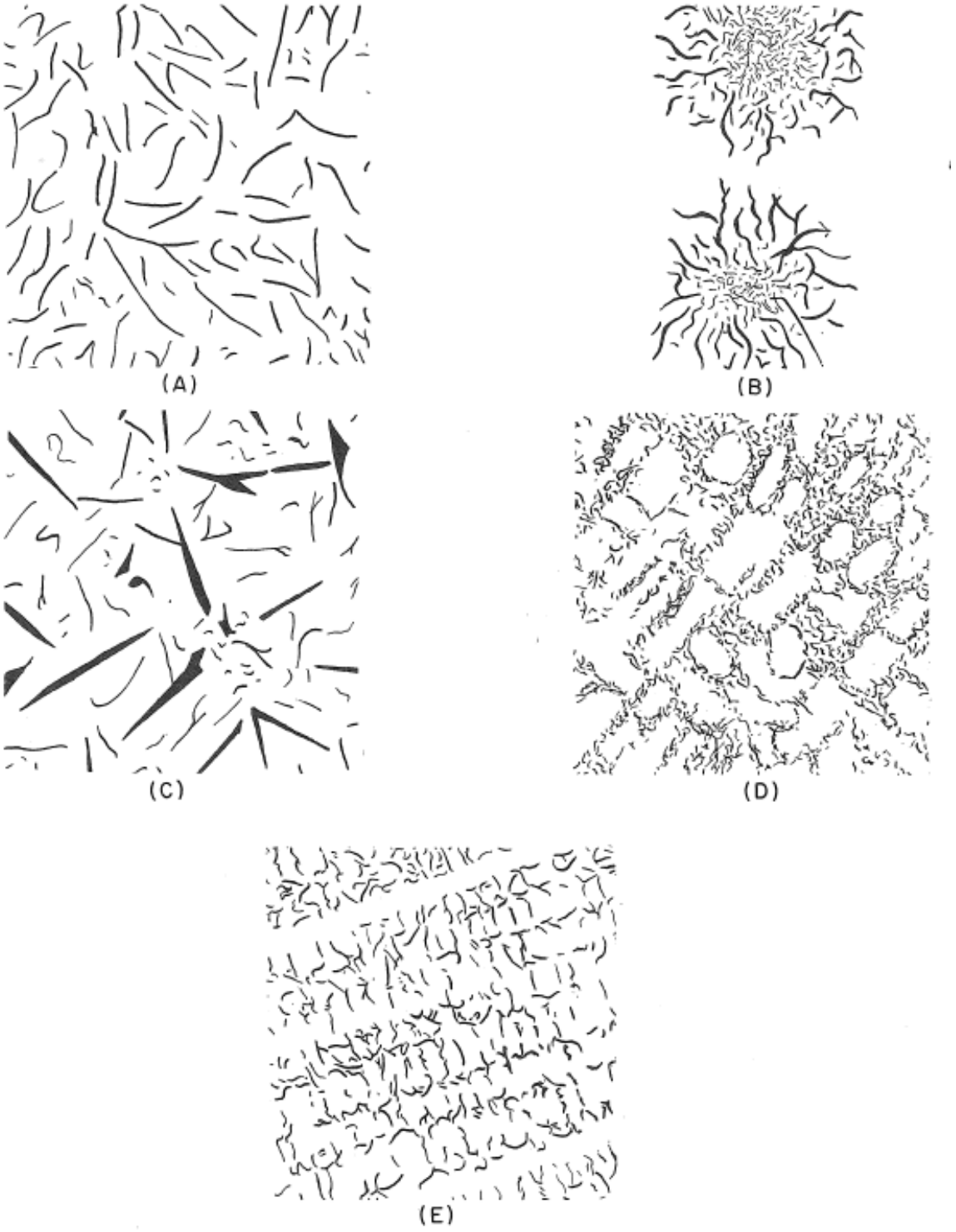

Figure 11. Graphite flake types in gray irons - ASTM and AFS standards, 100X.
Type A, uniform distribution, random orientation.
Type B, rosette groupings, random orientation.
Type C, superimposed flake sizes, random orientation.
Type D, inter-dendritic segregation, random orientation.
Type E, inter-dendritic segregation, preferred orientation.

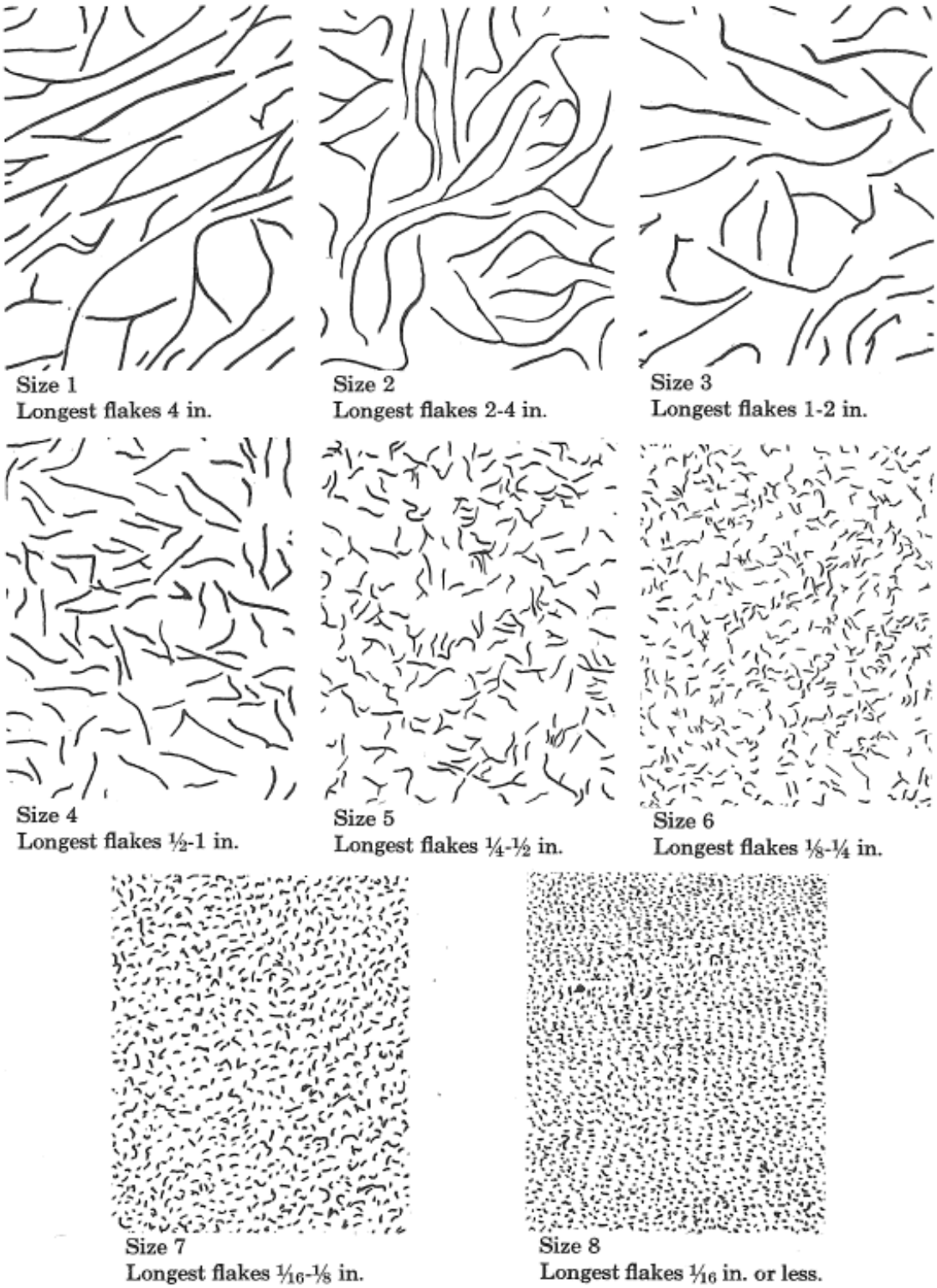

Figure 12. Gray flake size in gray irons, 100X.

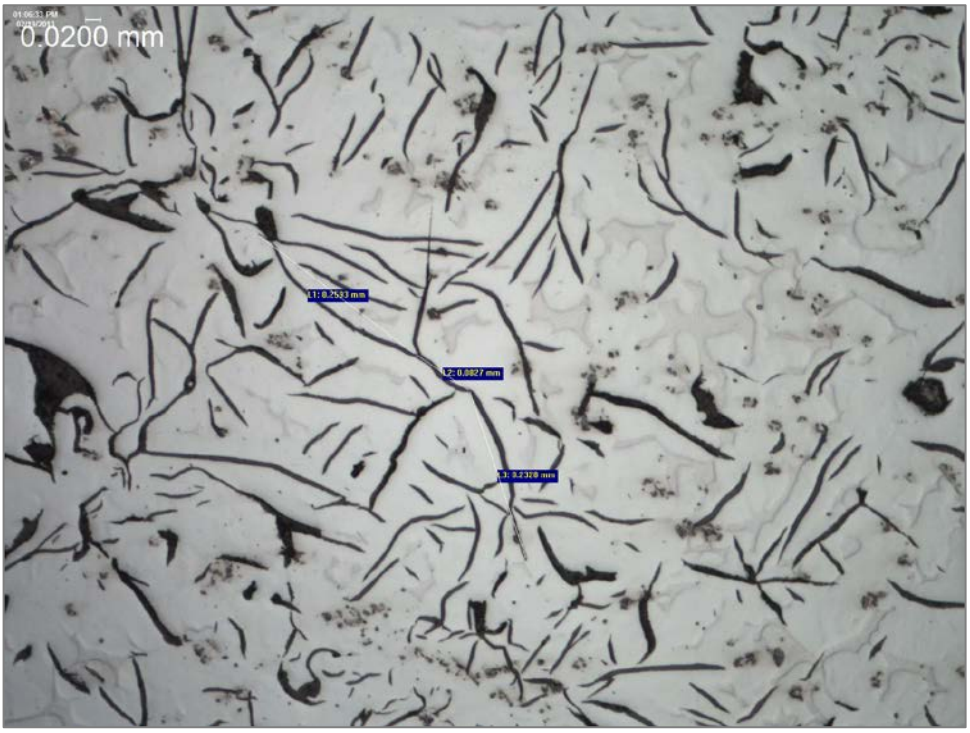

Figure 13. Unetched gray cast iron flake structure.

Figure 14. Etched gray cast iron microstructure, primarily pearlite.

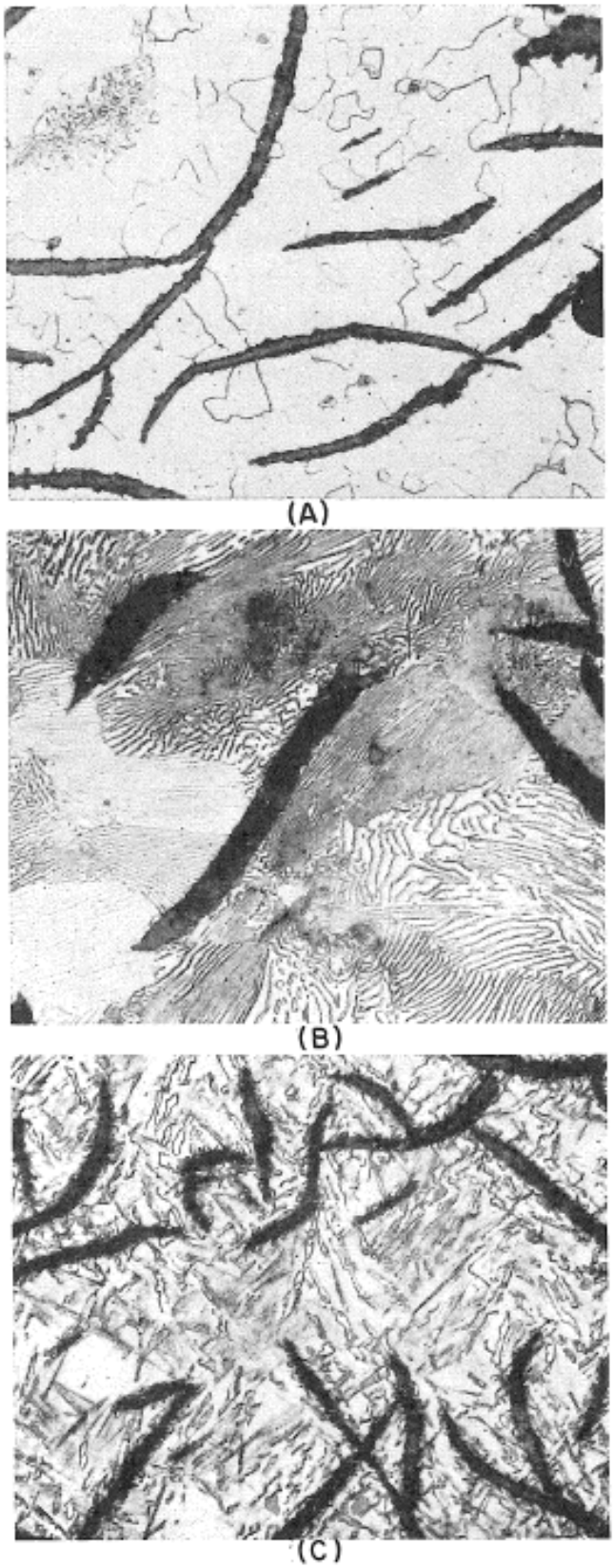

Figure 15. Microstructure of typical gray cast irons. A, with ferritic matrix, etched, 250X. B, matrix of pearlite, etched. 500X. C, acicular matrix, etched. 500X.

Metallurgy of Gray Iron

The metallurgy of cast irons is very complex and cannot be represented on the binary iron-carbon diagram used for steel metallurgy.

Carbon Equivalent

The basic composition of cast irons is often defined or described in terms of a carbon equivalent factor, C.E. This factor provides a relationship of the percent carbon and silicon in gray iron to its capacity to produce graphite. The relationship is shown in Equation 1 below:

$$C.E. = T.C. + 1/3\ (\%Si) \qquad \text{(Equation 1)}$$

T.C. = Total Carbon

Phosphorous can be included in the formula, but is omitted because of the low phosphorous content in domestic pig irons. For example, if an iron contains 3.4% C and 2.4% Si, the C.E. = 4.2%.

The carbon equivalent has metallurgical significance by influencing the mode of solidification of the iron, and therefore its basic microstructure. Irons with C.E. over 4.3% are called hypereutectic and those below 4.3% are called hypoeutectic cast irons.

The average effect of C.E. on tensile strength is shown in Figure 16 [5].

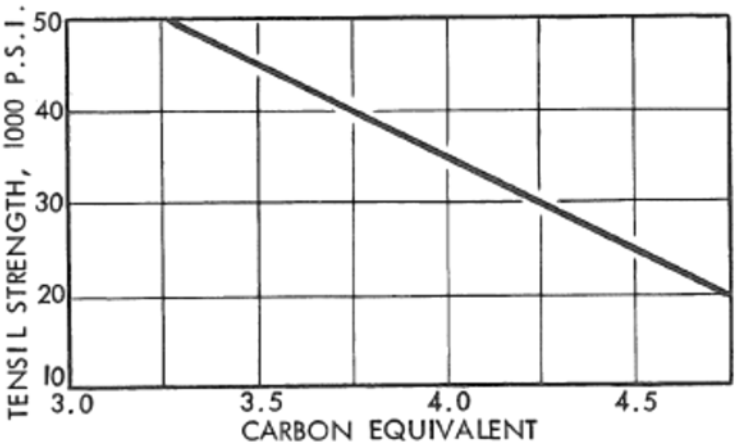

Figure 16. Relationship between carbon equivalent and tensile strength of gray iron test specimens.

Carbon-Silicon Categories and Combinations

Another method to represent or categorize the type of cast iron structure for various carbon-silicon combinations is shown in Figure 17 [3].

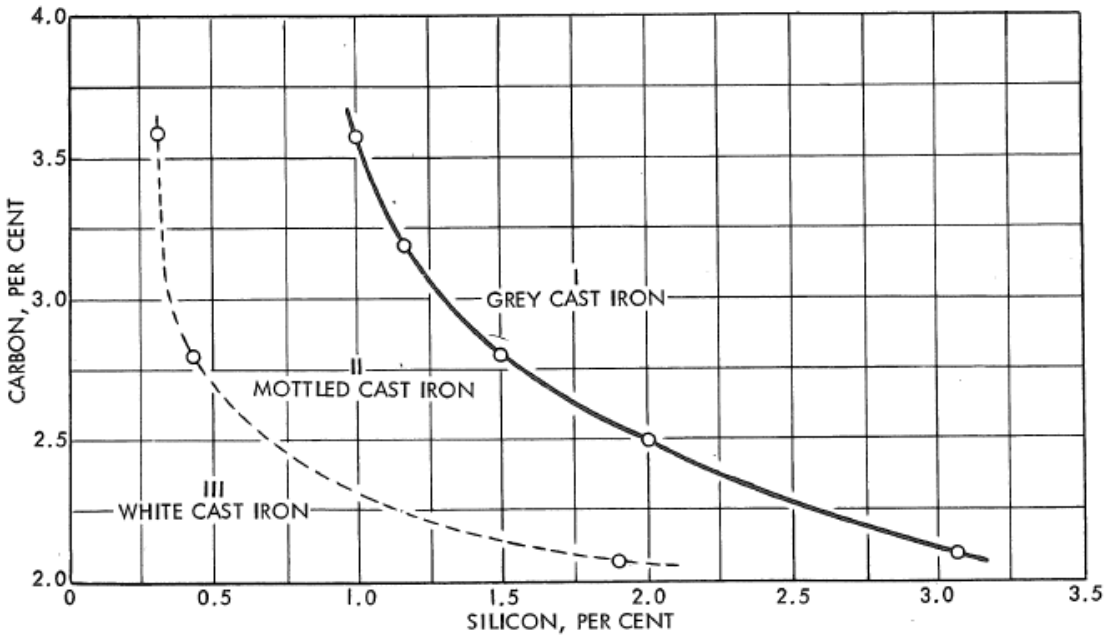

Figure 17. Composition limits for gray, mottled, and white cast irons.

Silicon is the strongest graphitizer of all the elements that are added to cast iron, therefore it is the main element that determines the relative properties of combined and graphitic carbon that will be present in the final casting. Therefore, the foundry metallurgist can control the properties of the cast iron by adjusting the silicon content relative to the amount of carbon and thickness of the casting.

In commercial castings, the gray iron typically solidifies under non-equilibrium conditions. The cooling rate (a function of section thickness) and chemical composition determine the microstructure of the gray iron and therefore its properties.

Cooling Rate vs. Microstructural Properties

The properties of hypoeutectic gray cast iron cooled at different rates is shown in Table 1 [3].

Table 1. Effect of cooling rate on microstructure and properties of gray cast iron

COOLING RATE	MICROSTRUCTURE *	REMARKS	BHN
FAST	P + C (WHITE IRON)	EXTREMELY HARD AND BRITTLE	325–500
MODERATELY FAST	P + C + G (MOTTLED IRON)	GREATEST STRENGTH, HARD TO MACHINE	250
MODERATE	P + G	BEST HIGH TEST IRONS; CLOSE GRAINED	200
MODERATELY SLOW	P + G + F	FAIR STRENGTH, EASY MACHINING, FAIR FINISH	150
SLOW	F + G	LOW STRENGTH, OPEN GRAINED MACHINES SOFT	100

* P =PEARLITE C =CEMENITE G =GRAPHITE F =FERRITE

Very rapid cooling (also low silicon and low carbon contents) results in the retention of the metastable structure of free carbide and pearlite. Martensite or even some retained austenite may also be present. Very slow cooling promotes the stable system, which consists of ferrite and graphite.

An example of mixed microstructure for gray cast iron is shown in Figure 18. This cast iron contains ferrite, pearlite, graphite, and steadite. Explanations and additional examples of cast iron microstructures are presented in a later section of this report.

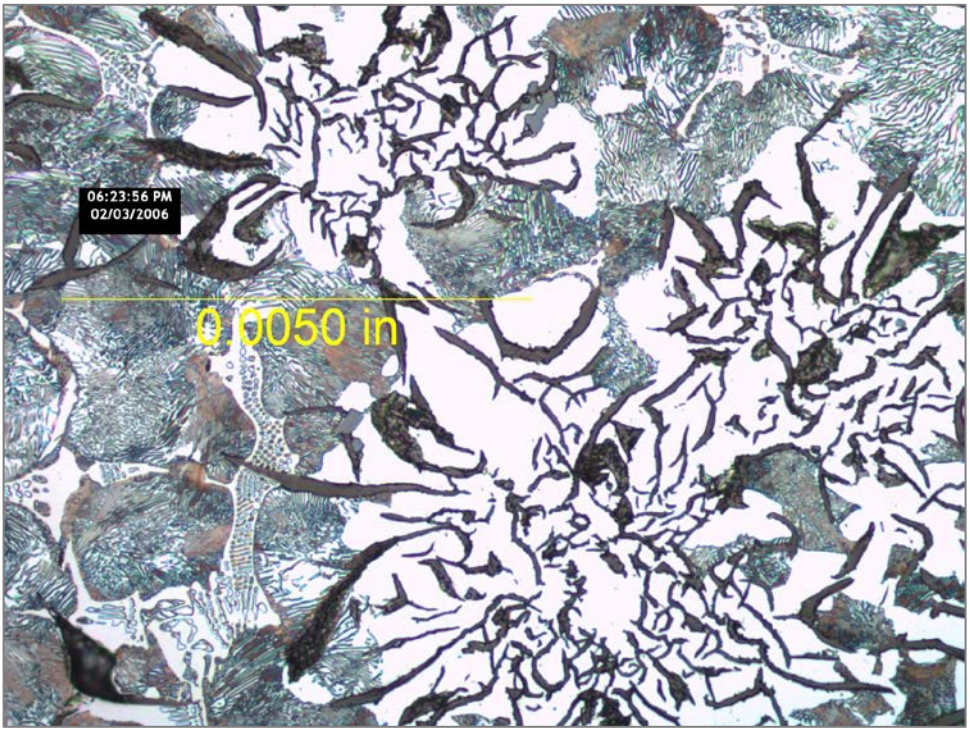

Figure 18. Example of gray cast iron microstructure showing ferrite (white), pearlite (gray lamellar), graphite (black flakes), and steadite (intergranular white with circular pattern).

The rate of cooling also influences the grain size and the size of the graphite flakes. Slow cooling promotes soft coarse structures, and rapid cooling, fine grained, hard structures. The effect of wall thickness on tensile strength and hardness of typical gray irons is shown in Figure 19 [5].

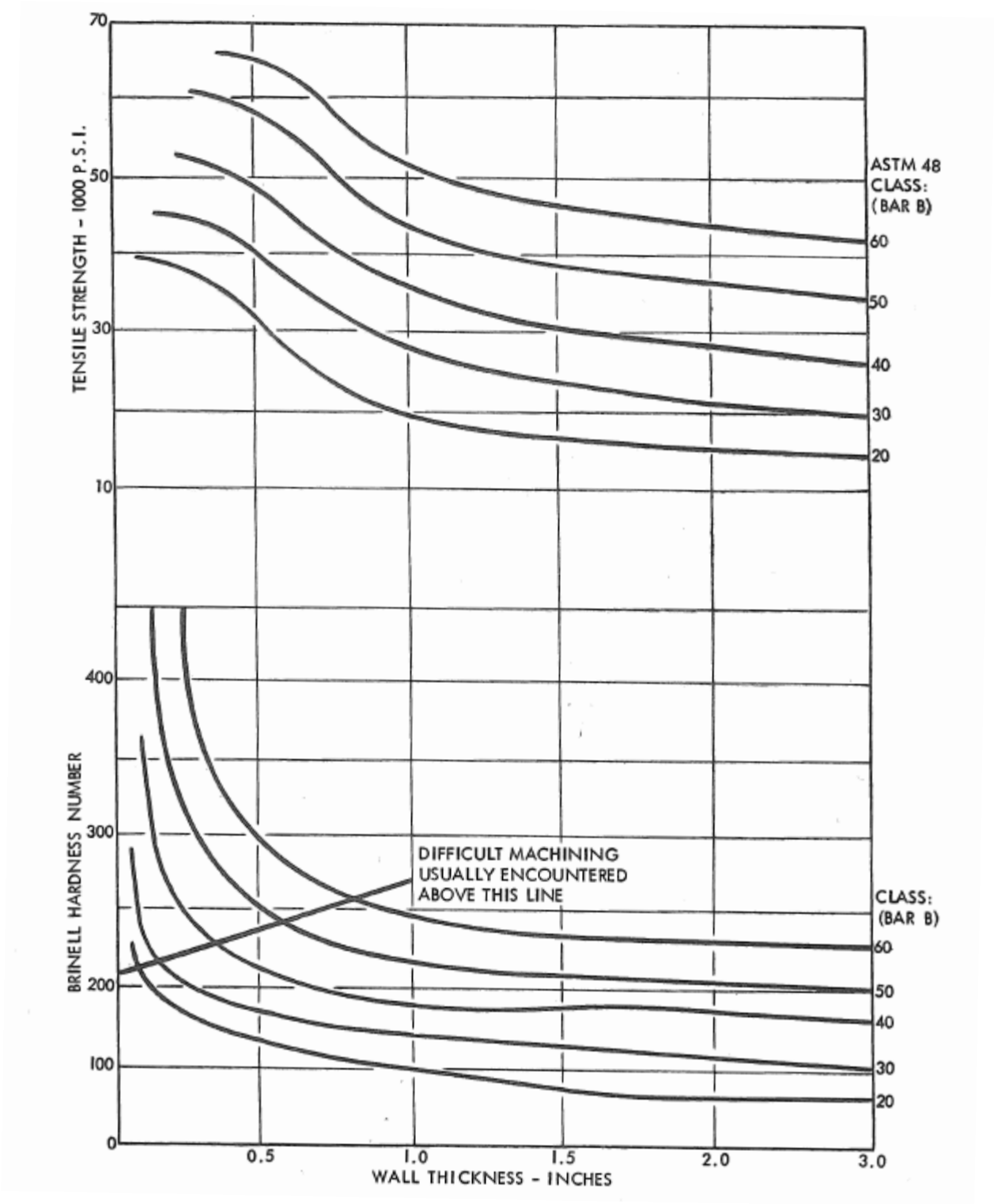

Figure 19. Effect of wall thickness on tensile strength and hardness of typical gray irons.

Section Thickness Types

Gray cast irons may also be grouped or categorized into four types according to the dominant section thickness. These four groups are shown in Table 2 [3]. The types are: S, A, P, and H.

Table 2. Basic gray cast irons grouped according to dominant section thickness

DOMINANT SECTION THICKNESS INCHES	TYPE	CLASS	TENSILE STRENGTH	TYPICAL COMPOSITION PERCENTAGE					APPLICATION
				T.C.	Si	Ni	Mo	Cr	
LESS THAN 0.5 IN.	S	BASE: IRON	25,000	3.5	2.5	---	---	---	LIGHT CASTING OF ABOUT 3/8 IN. MAXIMUM THICKNESS. TOTAL CARBON RANGE FROM 3.4 TO 3.8% AND SILICON FROM 2.4 TO 2.8%
		NCI-35-S	35,000	3.5	2.5	0.75	1.50	---	
		NCI-40-S	40,000	3.5	2.5	0.30	0.60	---	
0.15 TO 1.00	A	BASE IRON	30,000	3.3	2.3	---	---	---	AUTOMOTIVE CASTINGS, ENGINE HEADS, COMPRESSOR BLOCKS, TOTAL CARBON RANGES FROM 3.25 TO 3.40% AND SILICON FROM 2.2 TO 2.4%
		NCI-35-A	35,000	3.3	2.3	0.75	0.30	---	
		NCI-40-A	40,000	3.3	2.3	1.25	0.25	0.35	
		NCI-45-A	45,000	3.3	2.3	1.50	0.30	0.40	
		NCI-50-A	50,000	3.3	2.3	2.00	0.35	0.60	
0.5 TO 2.5	P	BASE IRON	35,000	3.1	2.0	---	---	---	PRESSURE CASTINGS FOR MEDIUM SIZE VALVE AND PUMPS (3" to 12") AND FOR ENGINE AND COMPRESSOR CASTINGS. TOTAL CARBON RANGES FROM 3.0 TO 3.25% AND SILICON FROM 1.5 TO 2.2%
		NCI-40-P	40,000	3.1	2.0	0.75	0.30	---	
		NCI-45-P	45,000	3.1	2.1	1.00	---	0.35	
		NCI-50-P	50,000	3.1	2.1	1.25	0.30	0.40	
		NCI-55-P	55,000	3.1	2.1	1.50	0.30	0.60	
1.5 MINIMUM	H	BASE IRON	35,000	3.0	1.5	---	---	---	FOR HEAVY SECTIONS HAVING THICKNESSES OF FROM 1/2 INCHES THICK AND UP. TOTAL CARBON RANGES FROM 2.8 TO 3.1% AND SILICON FROM 1.0 TO 1.8%.
		NCI-40-H	40,000	3.0	1.5	1.00	---	---	
		NCI-45-H	45,000	3.0	1.5	1.25	0.50	---	
		NCI-50-H	50,000	3.0	1.5	2.00	0.35	0.50	
		NCI-55-H	55,000	3.0	1.5	2.5	---	1.00	

Castings with the thinnest sections require the highest percentages of carbon and silicon.

Alloy Classifications

Gray cast irons may also be grouped or categorized into five broad alloy classifications, including:

Unalloyed, base iron

Ni Alloy

Ni-Cr Alloy

Ni-Mo Alloy
Ni-Cr-Mo Alloy

These types (S, A, P, and H) and the alloy combinations give greater flexibility in achieving the required tensile strength for a given section thickness.

A similar plot is shown below in Figure 20 [6]. This shows the influence of section thickness on the tensile strength and hardness for an ASTM A48 series of gray irons as cast in 1.2 inch diameter bars.

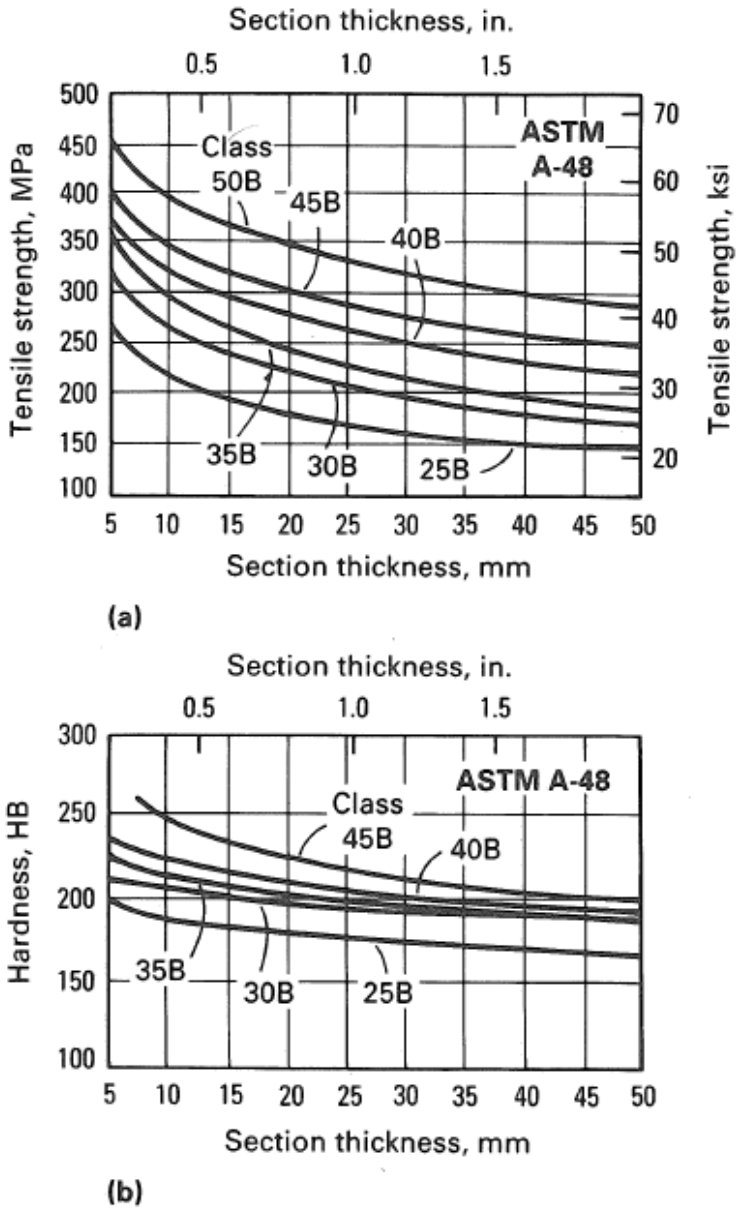

Figure 20. (a) Tensile strength and (b) Hardness vs. section thickness for a series of gray cast irons (per ASTM A48).

Effects of Major Alloying Elements in Gray Cast Irons

The elements present and/or added into gray cast iron are commonly divided into two groups: Graphitizers and Carbide Stabilizers.

Graphitizers promote graphite formation and include: silicon, aluminum, titanium, nickel, and copper.

Carbide stabilizers tend to retain the carbon in the form of iron carbides and include: manganese, molybdenum, chromium, and vanadium.

The effects of the alloying elements in gray cast iron are:

Carbon

A high carbon content increases the amount of graphite or Fe(3)C. High carbon and silicon contents increase the graphitization potential of the iron as well as its castability. However, they both decrease the chilling tendency, so the strength is adversely affected as shown in an earlier figure; this is due to ferrite promotion and the coarsening of pearlite.

Silicon

Silicon is the strongest graphitizer of all the alloying elements. Silicon forms Fe(3)Si leaving the carbon to form free graphite. The upper limit of effectiveness for silicon alloy additions is about 3.0% Si.

Manganese

Manganese content varies as a function of what the desired matrix is. Typically, it can be as low as 0.1% for ferritic irons and as high as 1.2% for pearlitic irons, because manganese is a strong pearlite promoter. The effect of sulfur must be balanced by the effect of manganese. Without manganese in the iron, undesired iron sulfide (FeS) will form at grain boundaries, resulting severely reduced mechanical properties. If the sulfur content is balanced by manganese, then manganese sulfide (MnS) will form, but it will be distributed within the grains, making it nearly harmless.

Nickel

Nickel assists with graphitization, but is only about half as effective as silicon. Nickel promotes casting density and freedom from casting porosity, by allowing lower silicon content. Nickel uniformly hardens and strengthens the casting matrix by changing the structure from coarse to fine pearlite, and even progressively to the harder and stronger

martensite phase. Nickel also refines the grains to smaller sizes and finely disperses the graphite, both having the effect of increasing strength and toughness.

Chromium

Chromium forms stable carbides and promotes formation of finely laminated and harder pearlite. These effects result in increasing strength and hardness of the cast product.

Molybdenum

Promotes finer pearlite, increasing strength and hardness of the matrix and casting.

Copper

Copper is a graphitizer, but only about one fifth as effective as silicon.

Vanadium

Vanadium is a powerful grain refiner, resulting in finer grain sizes which provide significant increases in hardness. Vanadium also acts as a carbide former, resulting further strength enhancement.

Phosphorous and Sulfur

These two elements are the most common, minor elements and are always present in the composition as a byproduct of the pig iron production. They can be as high as 0.15% for low-quality iron and are considerably less for high-quality iron. Vintage cast irons (e.g., pre-WWII) tend to have higher phosphorus and sulfur levels than contemporary gray and/or ductile cast irons. Higher levels of phosphorous and sulfur result in reductions of strength and toughness and increase in sulfides and phosphides in the final casting.

Typical Unalloyed Composition Ranges

The range of compositions for typical, unalloyed common cast irons is presented in Table 3 [6].

Table 3. Range of compositions for typical unalloyed common cast irons

	Composition, %				
Type of iron	C	Si	Mn	P	S
Gray	2.5-4.0	1.0-3.0	0.2-1.0	0.002-1.0	0.02-0.25
Compacted graphite	2.5-4.0	1.0-3.0	0.2-1.0	0.01-0.1	0.01-0.03
Ductile	3.0-4.0	1.8-2.8	0.1-1.0	0.01-0.1	0.01-0.03
White	1.8-3.6	0.5-1.9	0.25-0.8	0.06-0.2	0.06-0.2
Malleable	2.2-2.9	0.9-1.9	0.15-1.2	0.02-0.2	0.02-0.2

The typical composition range for low- (20B) and high-grade (55B) unalloyed gray iron (flake graphite iron) cast in sand molds is given in Figure 11 [7].

Table 4. Composition of unalloyed gray irons

ASTM A 48 class	Carbon equivalent	Composition, %				
		C	Si	Mn	P	S
20B	4.5	3.1-3.4	2.5-2.8	0.5-0.7	0.9	0.15
55B	3.6	≤3.1	1.4-1.6	0.6-0.75	0.1	0.12

The carbon and silicon levels found in the commercial gray irons vary widely, as shown in the figure below Table 5 [7].

Table 5. Carbon and silicon levels for commercial gray iron

Type of iron	Total carbon, %	Silicon, %
Class 20	3.40-3.60	2.30-2.50
Class 30	3.10-3.30	2.10-2.30
Class 40	2.95-3.15	1.70-2.00
Class 50	2.70-3.00	1.70-2.00
Class 60	2.50-2.85	1.90-2.10

Graphite Morphology

The mechanical and physical properties of gray iron are governed in part by the shape, size, amount, and distribution of the graphite flakes.

In tension, gray cast iron is more brittle than most metals due to the distribution of graphite flakes in an iron matrix. The graphite flakes have virtually no strength in tension, they also act as stress concentrators and crack initiators under such loading, leading to an overall decrease in mechanical properties. In compression, on the other hand, the graphite flakes serve to transmit stresses and the overall response is governed by the response of the graphite-iron system. For example, tensile strength for ASTM A48 class 20, Table 9 shows that the compressive strength is 83 ksi while the tensile strength is only 22 ksi.

A method for evaluating graphite flake distribution and size is given in *ASTM A247 - Standard Test Method for Evaluating the Microstructure of Graphite in Iron Castings*.

Graphite Flake Distributions

There are five graphite flake distributions: A to E.

Type A

The graphite flakes are randomly distributed and oriented throughout the iron matrix. This type if found in irons that solidify with a minimum amount of undercooling. Type A is desired to optimize mechanical properties.

Type B

The graphite rosettes are formed in irons near the eutectic composition and solidify with more undercooling than Type A graphite. This type is commonly used in thin sections (e.g., 3/8 inch thick) and along the surfaces of thicker sections.

Type C

The graphite occurs in hypereutectic irons, particularly those with high carbon content. This type precipitates during primary freezing of the iron (Kish graphite) and is often straight, coarse plates; this greatly reduces the mechanical properties of the iron and provides a rough surface when machined.

Type D

The graphite forms when there is a large amount of undercooling, but not enough to cause carbide formation. This type is in the interdendritic regions. Type D is randomly distributed, Titanium and aluminum promote undercooled graphite structures. The iron matrix is usually ferrite which is weaker than pearlite, so the underlying strength of the matrix is lower.

Type E

The same as Type D, but a preferred orientation vs. random distribution.

Graphite Flake Sizes

There are eight graphite flake sizes.

Graphite flake sizes are also categorized in ASTM A247. Large flakes are associated with irons that have high C.E. values and slow cooling rates. Strongly hypoeutectic irons and those with rapid solidification generally have small, short flakes. Small flakes maximize tensile properties.

Graphite Flake Length Effect on Strength

A plot showing the effect of graphite flake length on tensile strength for gray cast irons is shown in Figure 21 [8].

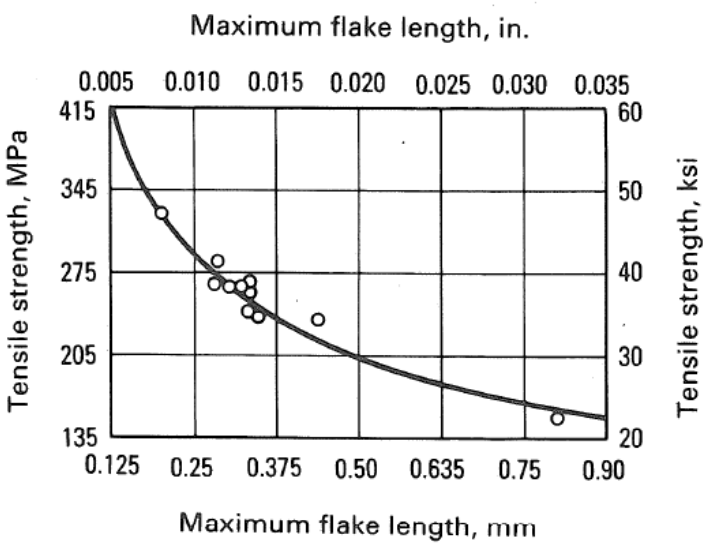

Figure 21. Effect of maximum graphite flake length on the tensile strength of gray iron.

The larger/longer flakes result in a significant decrease in the tensile strength. As noted earlier in this report, these flakes act as stress concentrators, "built into" the cast iron structure.

Gray Iron Matrix Structure

Common Phases in Gray Iron

The three most common phases in gray irons are ferrite, cementite, and pearlite. An etchant like 2% nital is typically used to reveal the microstructural phases.

Ferrite

Ferrite is a soft, low-carbon, alpha-iron phase with low tensile strength, but high ductility. Ferrite is promoted by graphitizers such as silicon and slow cooling rates. An example of ferrite is shown in Figure 22.

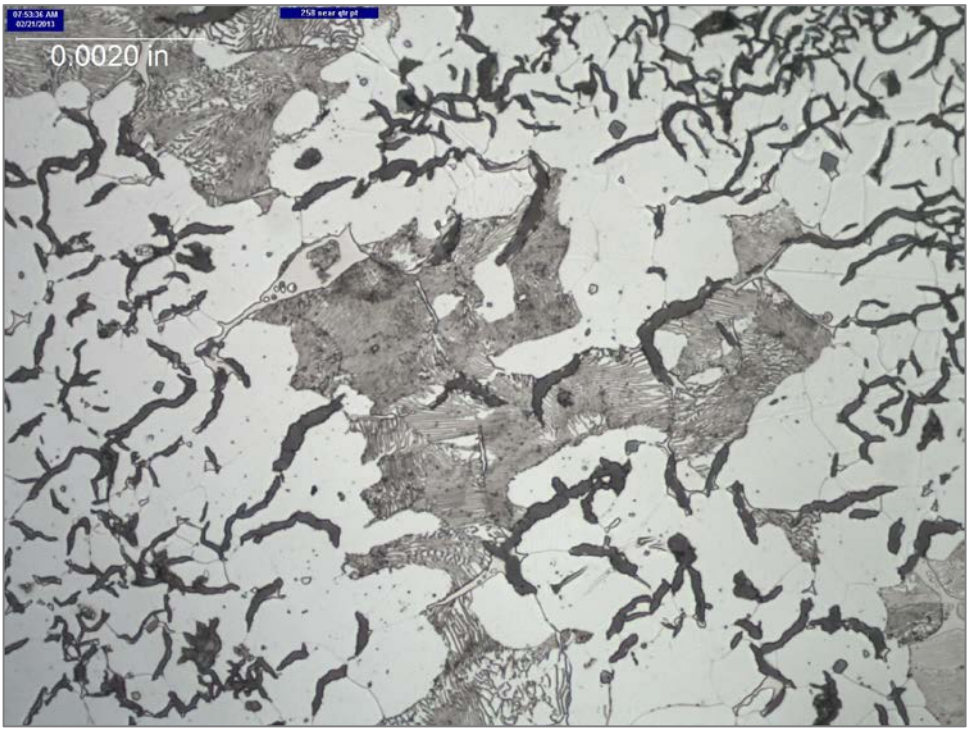

Figure 22. Etched gray cast iron microstructure. The white areas are ferrite.

Cementite

Also known as eutectic carbide, is a hard, brittle intermetallic compound of iron and carbon. It forms in areas where there is rapid cooling rates such as thin sections, corners, and the surface of the castings. Irons with low C.E. values and low silicon levels are likely to contain cementite. An example of cementite is shown in Figure 23.

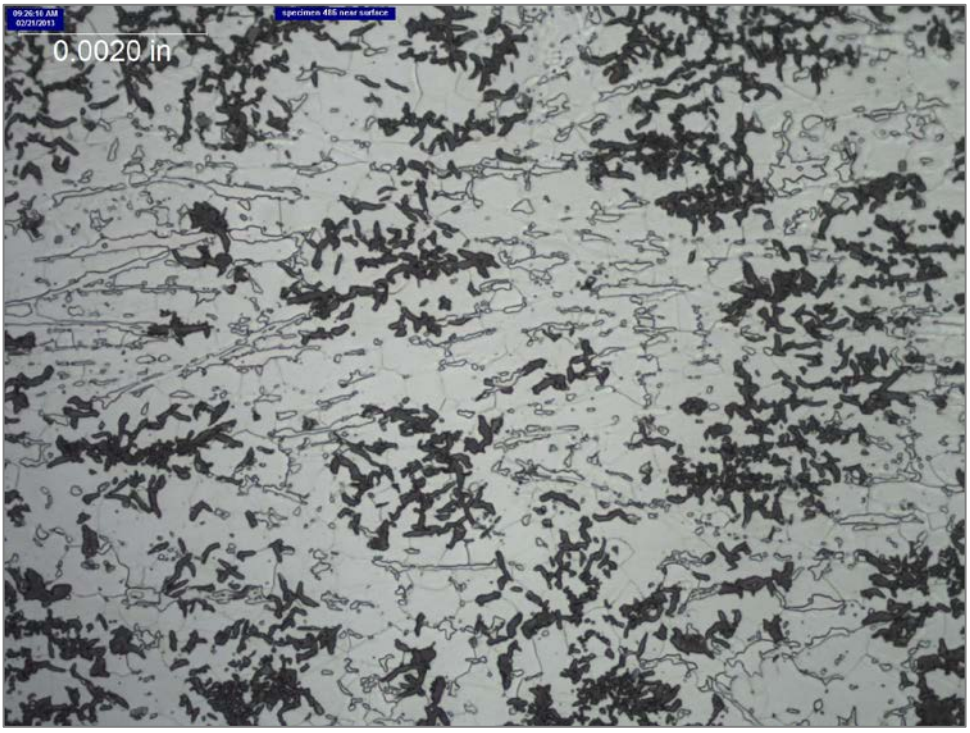

Figure 23. Etched gray cast iron microstructure. The white, horizontal banded structure is cementite and dispersed primarily at the ferrite boundaries.

Pearlite

This is the eutectoid transformation product and consists of lamellar plates of ferrite and cementite. It is harder and stronger than ferrite, but has lower ductility. The hardness and tensile strength of pearlite depend primarily on the spacing of the plates. Higher values of both are found in pearlite with finer spacing of the plates, which is associated with more rapid cooling rates and alloying.

Tensile Strength and Hardness of Individual Phases

The tensile strength, ductility, and hardness ranges for these major/common phases is shown in Table 6 [7].

Table 6. Common gray iron phase mechanical property ranges

Phase	Tensile strength, MPa (ksi)	Elongation, %	Hardness, HB
Ferrite	272-290 (39.5-42)	61	75
Pearlite	862 (125)	10	200
Cementite	…	…	550

Steadite

An iron-phosphide eutectic, is commonly found at grain boundaries in gray irons with phosphorus contents greater than 0.02%. Steadite, like iron carbides, can decrease the mechanical properties of the iron. Steadite is common in vintage gray cast irons (e.g., pre-WWII) due to their higher phosphorous content. An example of steadite is shown in Figure 24.

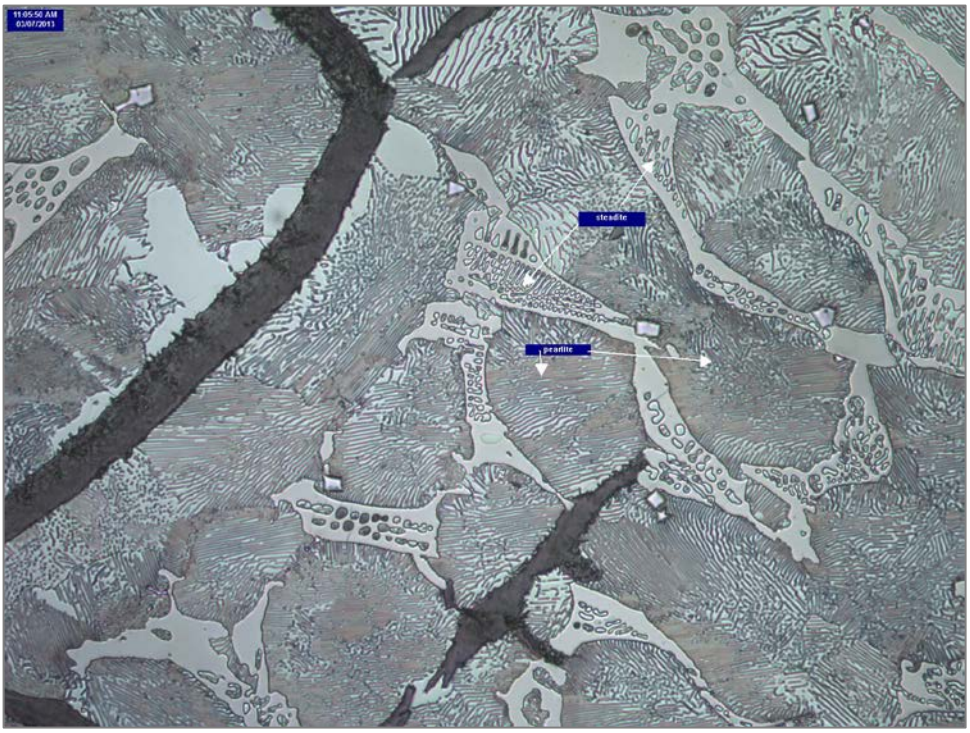

Figure 24. Etched gray cast iron microstructure. The light gray phase with rows of holes is steadite. The steadite is located on the ferrite/pearlite boundaries.

Manganese sulfides

Are commonly found and evenly distributed in the matrix of gray irons.

Titanium carbides or carbonitrides

Are often in gray iron, especially when titanium is deliberately added to prevent the formation of nitrogen fissure defects.

Other (less common) Phases in Gray Iron

Bainite, Martensite, and Austenite can be produced through different heat treatments and alloy additions. They are not typical in the base gray cast irons and will not be discussed further in the paper.

Composite Microstructure Matrix Hardness

Hardness values for combinations of graphite and other matrix phases are shown in Table 7 [7].

Table 7. Hardness ranges for various combinations of gray iron microstructures

Microstructure	Hardness, HB
Ferrite + graphite	110-140
Pearlite + graphite	200-260
Pearlite + graphite + massive carbides	300-450
Bainite + graphite	260-350
Tempered martensite + graphite	350-550
Austenite + graphite	140-160

Section Sensitivity

The solidification of gray iron castings is controlled by the chemical composition and the cooling rate of the iron in the casting. Composition generally remains constant once the melt is poured into the mold, with little segregation. Therefore, the cooling rate is the controlling variable that influences the final microstructure.

The cooling rate can vary within the mold and is itself a function of many variables such as: pouring temperature, pouring rate, volume of iron to be cooled, surface area of the iron, thermal conductivity of the mold, number of castings in a mold, locations of cores, gates, and riser, etc. Therefore, the microstructure can have variation across the mold and also through the wall section at one location depending on these variables coupled with the chemical composition.

To illustrate this, one can see in Figure 25 [9] that the hardness and microstructural phase changes in a wedge specimen across its thickness. The structure changes from: white iron, to mottled iron, to ferritic iron, to mixed ferritic and pearlitic iron, to pearlitic gray iron as one goes from a thin to a thick section.

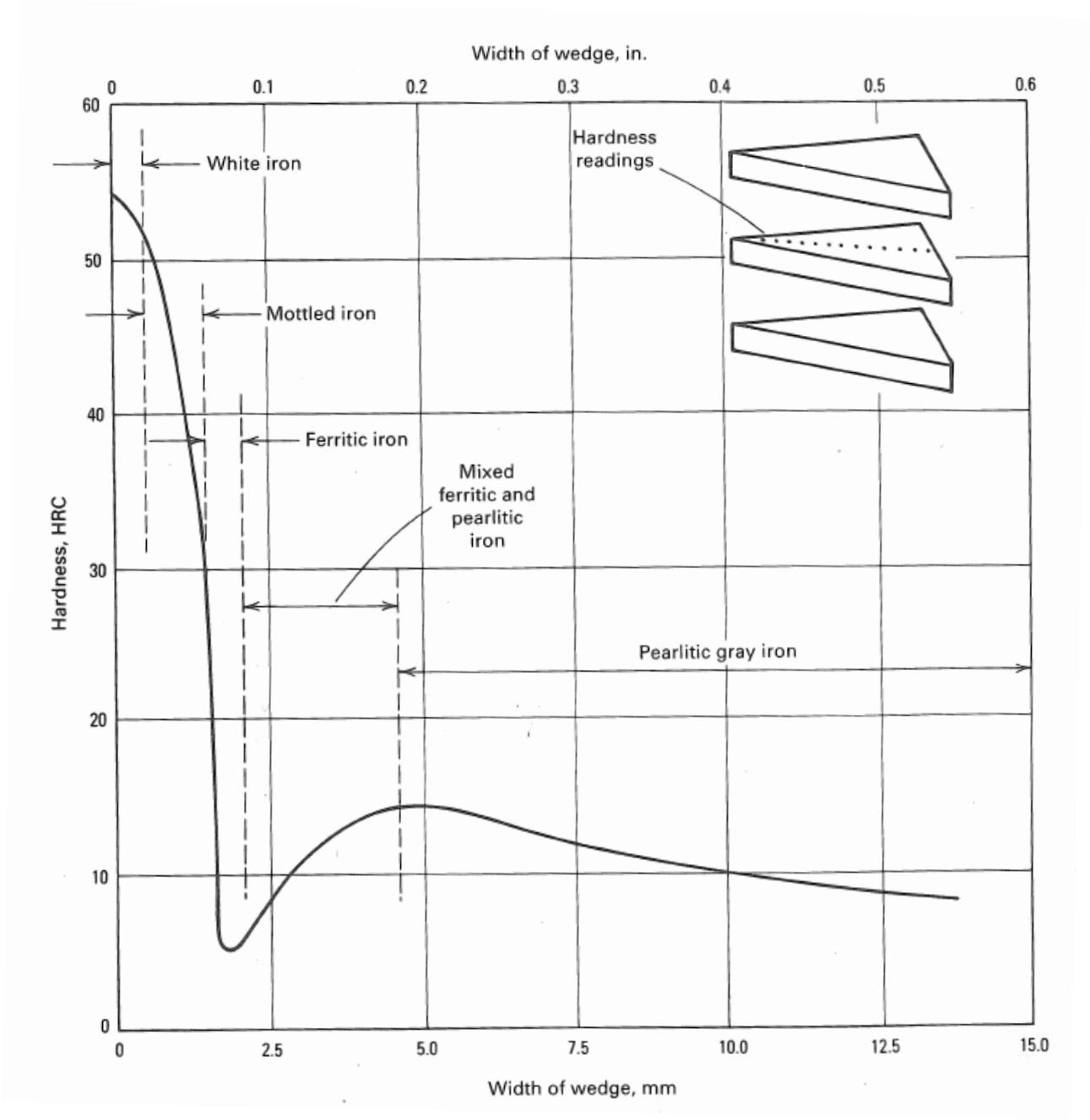

Figure 25. Effect of section thickness on hardness and structure. Hardness readings were taken at increasing distance from the tip of a cast wedge section.

Tensile strength decreases with increasing section size for all classes of gray iron. For example, an ASTM A48 grade gray iron of class 45 in a 1 inch section will develop only 30 ksi of strength in a 3 inch section due to larger graphite flakes and reduction in combined carbon leading to more ferrite and less pearlite in the matrix (along with coarser pearlite).

Room Temperature Mechanical/Tensile Properties

Graphite morphology and matrix characteristics affect the mechanical properties of gray iron.

Higher tensile strength and modulus of elasticity are obtained with irons containing small flakes, which is promoted by low C.E. values and faster cooling rates. Pearlite refinement and stabilization of acicular structures provide increased hardness, tensile strength, and wear resistance.

Tension (tensile bar) and transverse (beam loading) tests on bars are the most common methods for evaluating the strength of gray iron. The transverse test measures the strength in bending and also gives a maximum deflection value. By its nature, gray iron behaves as a brittle material in tension, with no measurable elongation after fracture. Yield strength, elongation, and reduction of area are seldom determined for gray iron in standard tension testing.

For ASTM A48 classes, the minimum *specification* values are shown in Table 8 [7]. These bars were tested per ASTM A438 - Standard Test Method for Transverse Testing of Gray Cast Iron.

Table 8. Approximate tensile strength and transverse breaking loads of gray irons

ASTM class(a)	Approximate tensile strength		Corrected transverse breaking load(a)					
			A bar(b)		B bar(c)		C bar(d)	
	MPa	ksi	kN	lb	kN	lb	kN	lb
20	138	20	4.00	900	8.01	1800	26.69	6 000
25	172	25	4.56	1025	8.90	2000	30.25	6 800
30	207	30	5.12	1150	9.79	2200	33.81	7 600
35	241	35	5.67	1275	10.68	2400	36.92	8 300
40	276	40	6.23	1400	11.57	2600	40.48	9 100
45	310	45	6.85	1540	12.46	2800	43.15	9 700
50	345	50	7.45	1675	13.34	3000	48.04	10 300
60	414	60	8.56	1925	15.12	3400	55.60	12 500

(a) For separately cast test specimens produced in accordance with ASTM A 48, ASTM A 278, ASME SA278, FED QQ-1-652, or any other specification that designates ASTM A 438 as the test method. Included in specifications only by agreement between producer and purchaser. (b) 22.4 mm (0.88 in.) diam; 305 mm (12 in.) between supports. (c) 30.5 mm (1.20 in.) diam; 457 mm (18 in.) between supports. (d) 50.8 mm (2.00 in.) diam; 610 mm (24 in.) between supports

Tensile and Compressive Strength

Tensile strength is considered in selecting gray iron for items intended for static loads in direct tension or bending. Depending on the uncertainty of loading, a factor of safety of 2 to 12 have been used in figuring allowable design stresses. *Typical* strength values (tensile, torsional, compressive, bending fatigue, traverse load, and hardness) are presented in Table 9 [7].

Table 9. Typical mechanical properties of as-cast standard gray iron test bars

ASTM A48 class	Tensile strength		Torsional shear strength		Compressive strength		Reversed bending fatigue limit		Transverse load on test bar B		Hardness, HB
	MPa	ksi	MPa	ksi	MPa	ksi	MPa	ksi	kN	lbf	
20	152	22	179	26	572	83	69	10	8.23	1850	156
25	179	26	220	32	669	97	79	11.5	9.67	2175	174
30	214	31	276	40	752	109	97	14	11.23	2525	210
35	252	36.5	334	48.5	855	124	110	16	12.68	2850	212
40	293	42.5	393	57	965	140	128	18.5	14.12	3175	235
50	362	52.5	503	73	1130	164	148	21.5	16.01	3600	262
60	431	62.5	610	88.5	1293	187.5	169	24.5	16.46	3700	302

The compressive strength of gray iron is typically three to four times that of the tensile strength. A comparison of compressive versus tension stress strain curves for two classes of gray iron is shown in Figure 26 [10].

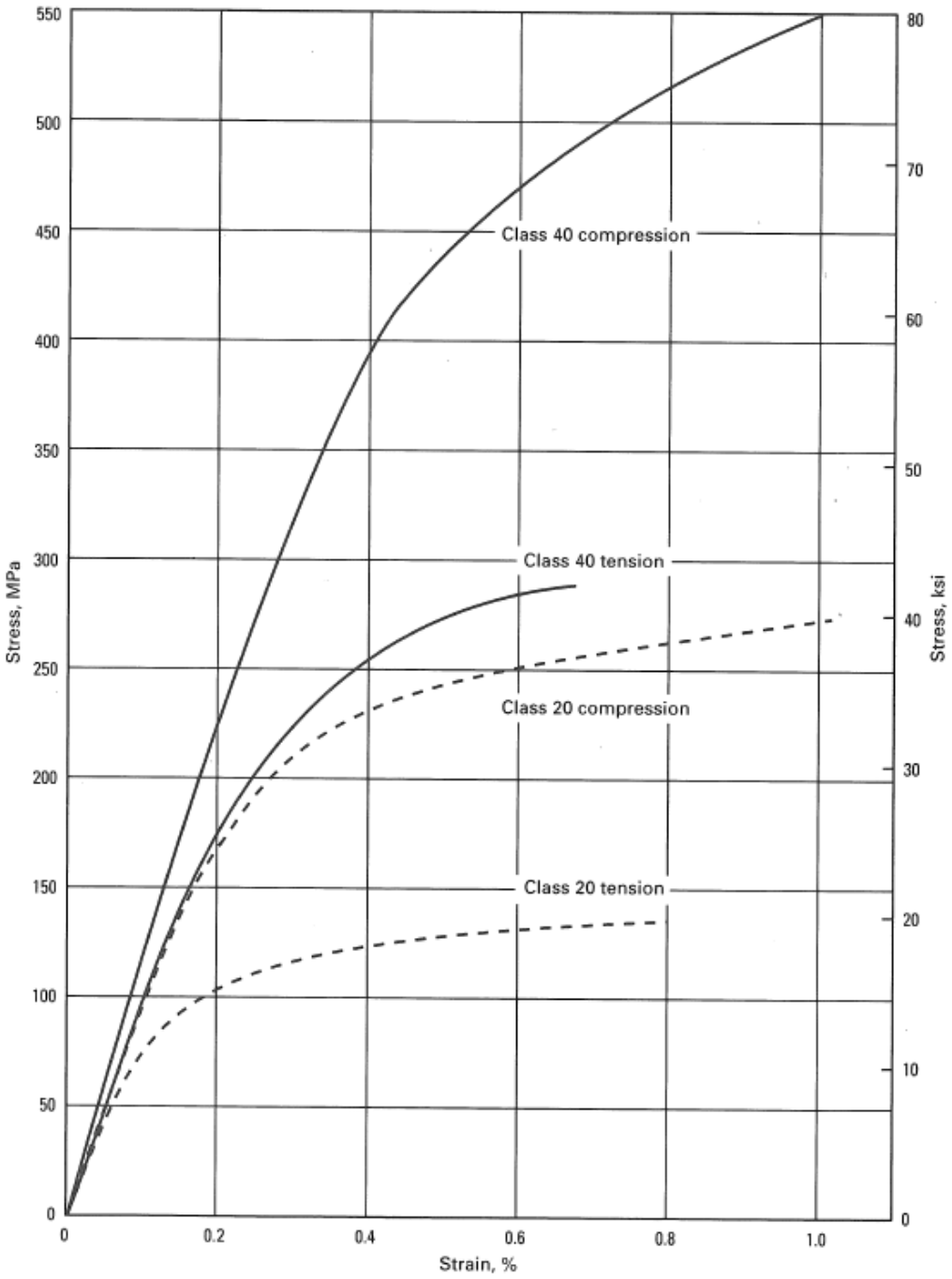

Figure 26. Comparison of stress-strain curves in tension and compression for a class 20 and class 40 gray cast iron.

Elongation

Gray cast iron's elongation at fracture is very low, typically around 0.6% and is therefore seldom reported. This mechanical measure is of little use to the designer.

Modulus of Elasticity

Typical stress-strain curves for three classes of gray irons are shown in Figure 27. Gray iron force/stress-strain behavior in tension is characterized by a quasilinear relationship, with a fairly linear segment corresponding to low values of applied stress, which afterward begins to curve showing a certain mild excursion into the inelastic domain. Gray iron therefore does not purely obey the linear Hooke's law (the initial tangent modulus).

A convenient method to characterize this semi-linear response is to use the secant modulus. The secant modulus is obtained from the slope of the line connecting the origin of the stress-strain curve with the point corresponding to one-fourth the tensile strength. Secant modulus is also sometimes reported using the point corresponding to failure or tensile strength.

The one quarter modulus is considered a conservative value for most engineering work, since design loads are seldom as high as one-fourth the tensile strength and the deviation of the stress-strain curve from linearity is usually less than 0.01% at these loads. The ratio between the two moduli of elasticity (Young's/secant) is an indication of the deviation from the linear-elastic behavior of the material.

A typical force/stress-strain plot for a gray cast iron specimen in tension is shown in Figure 27 [11].

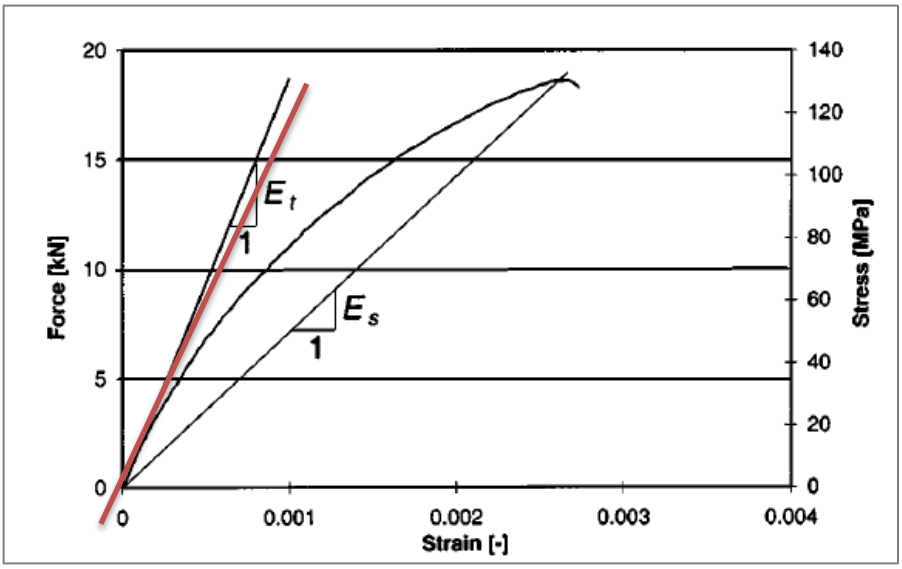

Figure 27. Definition of the initial tangent (Young's) modulus, Ei, and the secant modulus of elasticity at failure, Es, on a typical tension force/stress-strain curve. An approximate ¼ secant modulus line is added in red.

The modulus of elasticity of as-cast gray iron classes is shown in Table 10 [7].

Table 10. Typical moduli of elasticity of as-cast standard gray iron test bars

ASTM A 48 class	Tensile modulus		Torsional modulus	
	GPa	10^6 psi	GPa	10^6 psi
20	66-97	9.6-14.0	27-39	3.9-5.6
25	79-102	11.5-14.8	32-41	4.6-6.0
30	90-113	13.0-16.4	36-45	5.2-6.6
35	100-119	14.5-17.2	40-48	5.8-6.9
40	110-138	16.0-20.0	44-54	6.4-7.8
50	130-157	18.8-22.8	50-55	7.2-8.0
60	141-162	20.4-23.5	54-59	7.8-8.5

The modulus of gray iron varies considerably more than the moduli for most other metals. Therefore, if using the observed strain to calculate stress, it is important to measure the modulus of the particular gray iron specimen being considered.

A significant range of modulus values exist due to section size and chemical analysis variation, see Figure 28 [7].

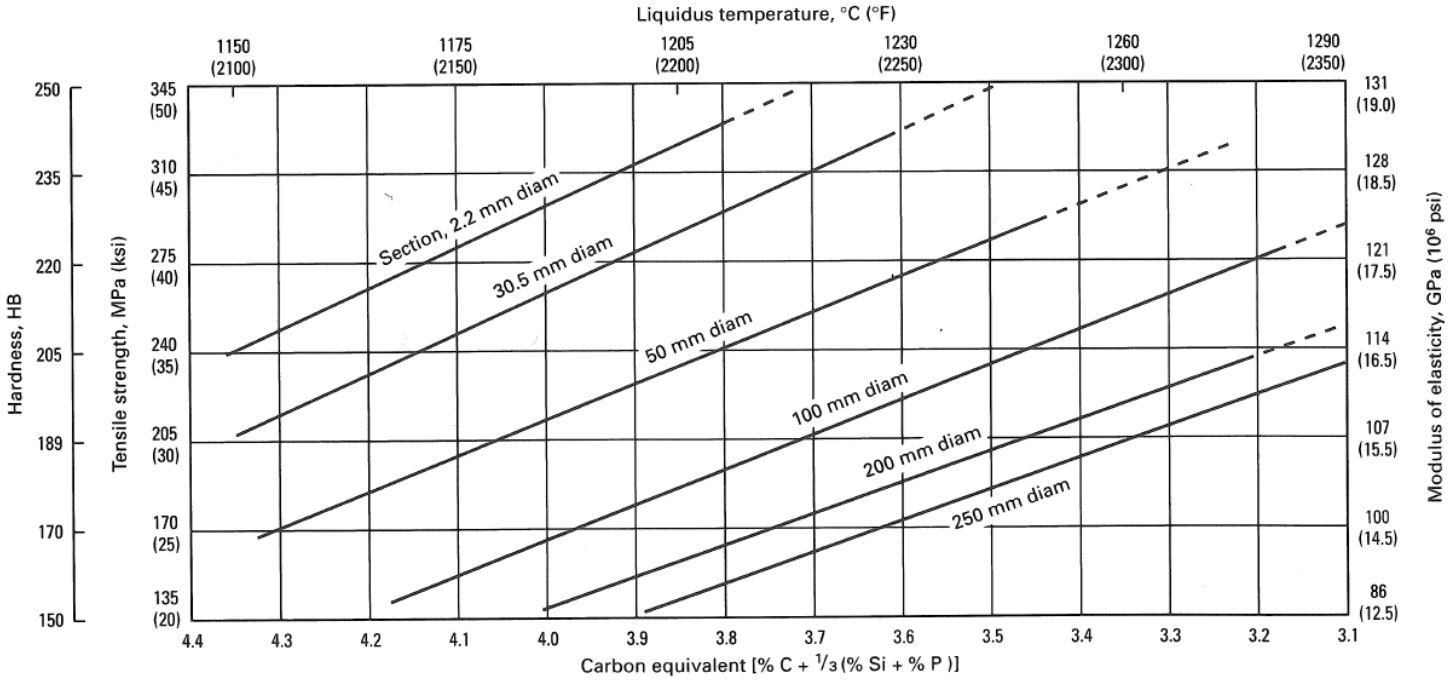

Figure 28. Interrelationship of mechanical properties, section diameter, and carbon equivalent of gray iron.

Hardness and Hardness-to-Tensile Relationship

Hardness tests, on either test bars or castings, are used as an approximate measure of tensile strength. Relationships between Brinell hardness and tensile strength generally follow the pattern shown in Figure 29 [12].

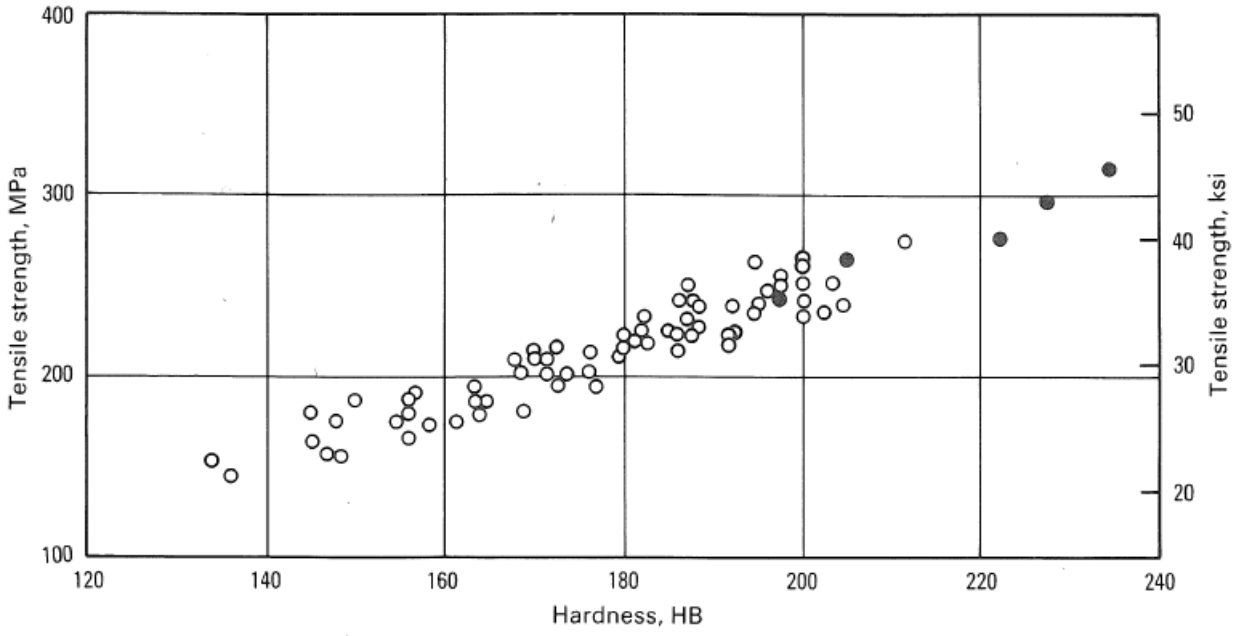

Figure 29. Relationship between tensile strength and Brinell hardness for a series of inoculated gray irons from a single foundry. Open circles are unalloyed gray iron; close circles are alloy gray iron.

Historical Casting Methods for Gray Iron Pipe

Gray cast iron is a legacy material for the water and natural gas industry, throughout the world.

Two primary types of casting methods, pit and spin casting, were used to produce gray cast iron pipes [13]. Pit casting involved the use of upright sand molds assembled in pits. Spin casting used horizontal, spinning molds made of sand or metal. The metal molds were water cooled.

Initially, the first cast iron pipes used were manufactured using pit casting method, then in the 1920's this process was replaced by the centrifugal (spin) casting technology. At present, all new pipes (for the water industry) are made of ductile iron using similar centrifugal casting technology.

These different casting methods produced profound differences in the metallurgy of the pipe materials [14]. Pit cast iron typically has large ASTM Type C flakes, where spun cast typically have much finer ASTM Type D flakes throughout the bulk of the pipe wall, with a small amount of Type C or Type A flakes on the inside surface of the pipe. In the work by Makar and McDonald (2007) they present ASTM standard flake types and sizes for a group of pit and spun cast gray iron pipes, see Table 11 [15].

Table 11. ASTM standard flake types and sizes from field exhumed pit and spun cast gray iron pipes

	ASTM flake type[a]			ASTM flake size[b]		
Sample	Inner surface	Center	Outer surface	Inner surface	Center	Outer surface
Pit cast	C	C	C	4	4	4
Spun Cast 1	A	D	D	6	8	7
Spun Cast 2	C	D	D	5	7	8
Spun Cast 3	C	D	D	5	8	8
Spun Cast 4	C	C–D	D	4	5–8	8
Spun Cast 5	C	C–D	D	4	5–8	8

[a]In ASTM A 247 the flake type indicates how the graphite flakes are distributed in the metal matrix. Type A indicates uniformly distributed, apparently randomly oriented flakes; Type C indicates randomly oriented flakes of widely varying sizes and Type D a very fine pattern of flakes surrounding areas without graphite.

[b]In ASTM A 247 the sizes refer to a range of values as measured at 100× magnification that vary geometrically from 1 to 128 mm. Size 3 corresponds to approximately 16–32 mm at this magnification, Size 4 to 8–16 mm, Size 5 to 4–8 mm, Size 6 to 2–4 mm, Size 7 to 1–2 mm, and Size 8 to 0–1 mm.

The same body of research reported the tensile stress-strain curves for the same pit and spun cast gray iron pipes, see Figure 30 [15].

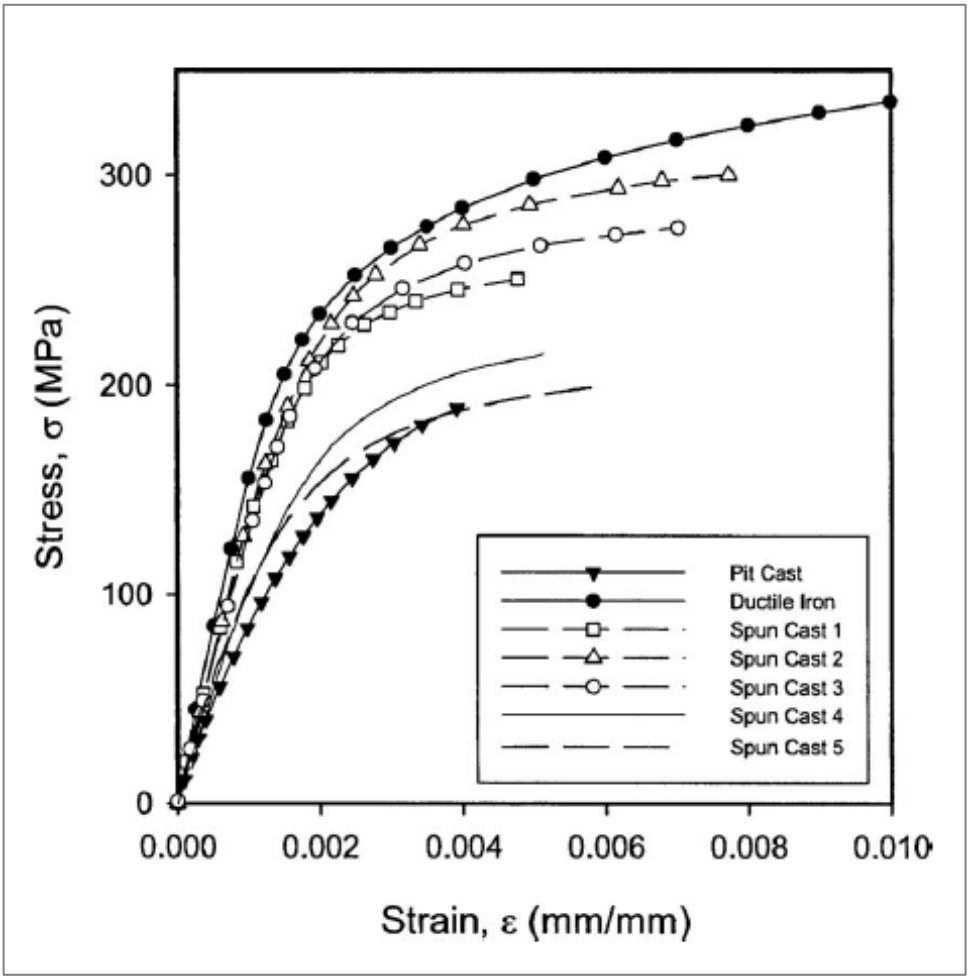

Figure 30. Typical tensile stress-strain curves for pit cast pipe, spun cast samples, and ductile iron.

The pit cast pipe from the study is typical of those expected for gray iron with the same flake type and size. However, the spun cast gray iron exhibited more of a "knee" on its stress-strain curves, similar to ductile iron which is plotted as well.

The ductility measurements for pit cast gray iron was 0.4% or less and for the spun cast it was not much higher at 0.9% maximum. Ductile iron exhibited ductility on the range of 1.5% to 4%.

Exhumed Gray Cast Iron Pipe Properties

There are several potential factors that contribute, directly or indirectly, to in service pipe failures, the primary being a combination of corrosion and mechanical action. Such factors lead to failures by cracking, circumferentially or longitudinally, as shown in Figure 31 [11].

Figure 31. Longitudinally cracked (84), circumferentially cracked (72), and temporarily repaired, clamped (71) pipes.

Many of the gray cast iron pipes in US cities are old and, as such, are expected to exhibit a wide range of mechanical properties. Even though those old pipes having a lower-than-anticipated strength may have performed well over the years, owing to a healthy factor of safety used in design, their aging, and hence overall loss of strength, may have reduced their factors of safety to potential hazardous levels, and such pipes need to be identified. Certain pipes may be subjected to higher-than anticipated loads in selected locations and therefore fail, despite having an adequate strength.

Therefore, a good understanding of the mechanical properties of cast iron pipes in a particular distribution system is very important. It can lead to a realistic evaluation of the strength of pipes in the system, and hence of their current factor of safety, or fitness for service.

There is only a small set of researchers that have done tests on cast iron pipes; and these being mostly water vs. natural gas carrying pipes. As noted earlier in this report, the water pipe data is directly applicable to natural gas distribution pipe performance. Seica and Packer compiled this research in their 2002 study and the summary table of mechanical properties is shown in Table 12 [11].

Table 12. Comparison of mechanical properties of gray cast iron pipes [16,17,18,19,20]

Type of cast iron	Reference	Age of pipes	Tensile strength (MPa)	Compressive strength[c] (MPa)	Modulus of rupture (MPa)	Secant elastic modulus (MPa)	Fracture toughness (MPa$\sqrt{m}$)
Pit	Rajani et al. (2000)	64–115 years	33–267	n/a	132–378	38,000–168,000	5.7–13.7
Pit & spun	Conlin and Baker (1991)	Out of service pipes	137–212	n/a	n/a	n/a	10.5–15.6
Pit & spun	**This study (2002)[a]**	**50–124 years[b]**	**47–297**	**519–1,047**	**164–349**	**23,000–150,000**	n/a
Spun	Yamamoto et al. (1983)	22–79 years	100–150	n/a	20–250	n/a	n/a
Spun	Caproco Corrosion (1985)	22–28 years	70–217	n/a	n/a	n/a	n/a
Spun	Ma and Yamada (1994)	21–32 years	40–320	n/a	120–320	n/a	n/a
Spun	Rajani et al. (2000)	22–61 years	135–305	n/a	194–445	43,000–159,000	10.3–15.4

[a]Please refer to the "Test Results" section.

[b]Where data were available.

[c]Ultimate strength (as opposed to yield strength). (1 m = 3.281 ft, 1 MPa = 0.145 ksi.)

These test data reveal that there are notable differences between the mechanical properties of pit and spun cast iron pipes and, within each type of material, there is notable scatter. This suggests that different manufacturing technologies employed at different times had a clear impact on the mechanical properties of cast iron.

Spin casting resulted in improved tensile strength over the pit casting process primarily due to an improved graphite structure and reduction in the incidence of casting voids.

Exhumed Pipe Strengths (with corrosion and/or defects present)

Seica and Packer conducted mechanical testing on fifty "as is" condition cutouts from various cast iron pipes. These samples included any corrosion or other defects. A summary of the distribution of tensile strengths is shown in Figure 32 [11]. The tests revealed that the strengths ranged from 8.6 ksi (59 MPa) to 35.4 ksi (244 MPa). The specifications for the pipes indicated 11, 18, and 21 ksi (75, 125, and 145 MPa) per the three specifications for these pipe grades.

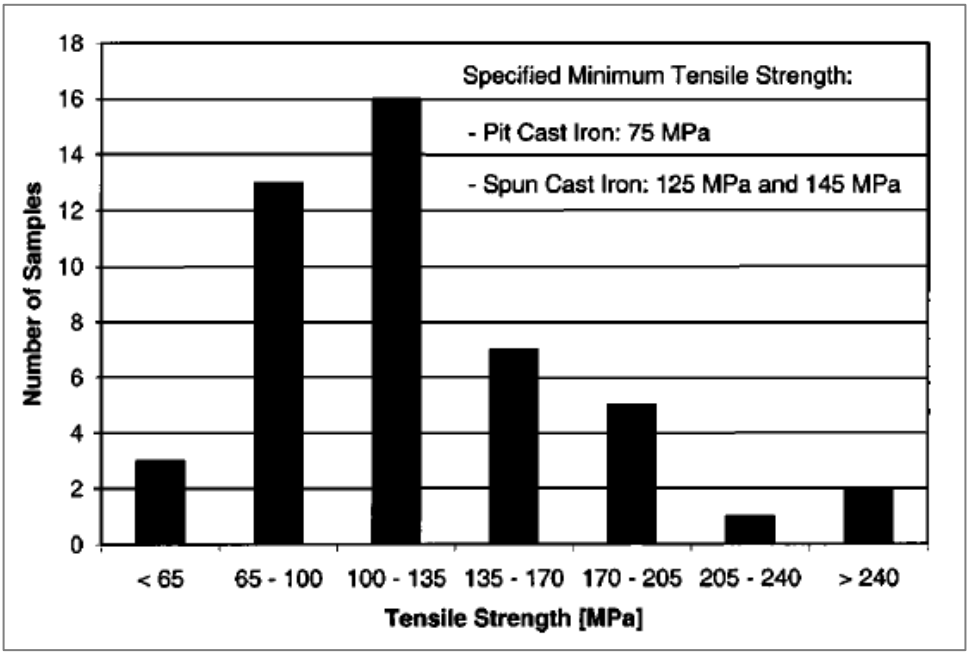

Figure 32. Distribution of the tensile strength for tested cast iron round specimens (total of 50 pipe cutouts for tensile testing).

A comparison between the material tensile strength and the age of the pipe is shown in Figure 33 [11]. Most the pipes were older than 76 years when they were exhumed, it is assumed that these were manufactured by pit casting methods. The pipes younger than this were assumed to be spun cast.

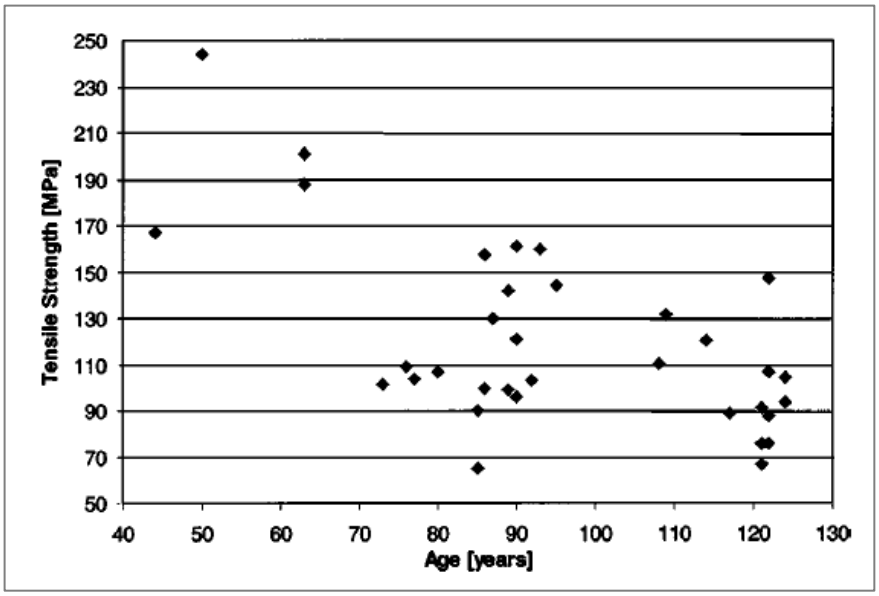

Figure 33. Comparison of the material tensile strength versus the age of the pipe when exhumed.

Exhumed Pipe Strengths (with no corrosion or defects present)

This same body of work also tested "metal only" cutouts, where there were no corrosion spots or manufacturing defects as determined by radiography inspection, i.e., they used corrosion- and defect-free areas of the pipe for tensile testing. Six pipes were tested and the results are presented in Figure 34 [11]. The tensile strengths ranged from 19 to 43 ksi (131 to 297 MPa).

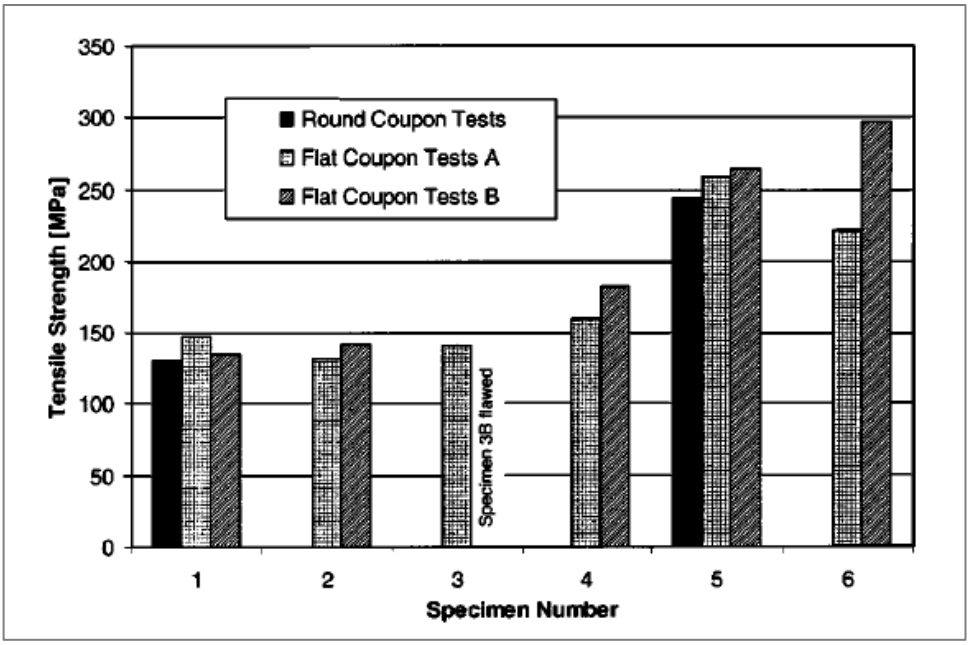

Figure 34. Comparison of the tensile strength for specimens obtained from similar pipes. Round coupons were the as is samples; Flat coupons are the defect free samples.

Gray Cast Iron Corrosion

In this section we will review the forms of corrosion applicable to gray cast iron. We will focus especially on graphitic corrosion, which is the most important form of corrosion for buried, gray cast iron pipe systems.

Forms of Corrosion that are a Concern for Cast Iron Pipe

Cast iron exhibits the same general forms of corrosion as other metals and is especially similar to steels. The most common corrosion forms are listed below.

- Selective leaching (graphitic corrosion in gray irons)
- Pitting/Alkali attack
- Stress corrosion
- Uniform or general attack
- Erosion-corrosion
- Galvanic or two-metal corrosion
- Crevice corrosion
- Intergranular corrosion
- Corrosion fatigue
- Fretting corrosion

Graphitic corrosion (sometimes called graphitization) and pitting are the most serious threats. Stress corrosion is less likely but if the conditions are right it is a possibility. With the thick-walled cast iron pipes and potential for alkali passivation, uniform/general corrosion is of lesser concern relative to the others.

Graphitic Corrosion a Form of Dealloying

High Profile Graphitic Corrosion Pipe Failures

Graphitic corrosion of gray cast iron has reached the public eye because of failures of underground pipelines, particularly those handling hazardous materials, like natural gas. Graphitically corroded pipe has cracked because of soil settlement or impact by excavating or earth-moving equipment. In cases explosions, fires, and fatalities have occurred [21].

Process of Graphitic Corrosion

Dealloying is a corrosion process where one constituent of an alloy is removed, leaving an altered residual structure. It was first reported in 1886 on copper-zinc alloys (brasses) and has since been reported on virtually all copper alloys as well as on cast

irons and other alloy systems [22]. Other terms for dealloying include parting, selective leaching, selective attack, and specifically for cast irons, graphitic corrosion (sometimes erroneously called graphitization which is a high temperature, heat treatment term).

Environments Conducive to Graphitic Corrosion

Graphitic corrosion is unique to cast irons and is a form of selective leaching attack. It is observed in gray cast irons in relatively mild environments in which selective leaching of iron leaves behind a graphite network (soft, porous black residue on the surface) that progressively grows into the bulk of the iron section. The selective leaching of the iron takes place because the graphite is cathodic to the iron and the gray iron structure establishes an excellent galvanic cell due to the interlocking graphite flake network. This form of corrosion generally occurs when corrosion rates are low. If the metal corrodes more rapidly, the entire surface (including the graphite) is removed and uniform or general attack occurs.

Graphitic corrosion produces a weakened spot on the pipe that may not be able to withstand the internal pressure and the superimposed external loading, especially bending, from heavy earth loads and/or a washout under the joint. The corroded area can be picked away with a screwdriver or pocket knife, see Figure 35 [23].

Figure 35. Graphitic corrosion of cast iron elbow.

Graphitically corroded gray cast iron still has some strength. In well-packed soil, it can withstand internal pressures of up to about 500 psi. However, frost heave or any other bending stress from earth loads, washout, or impact on the pipe will also tend to break it [24].

Cast iron is prone to graphitic corrosion in soft water, acidic water, brackish water, and water containing low levels of hydrogen sulfide. Soils lead to this same type of attack [25]. Graphitic corrosion of gray cast iron pipe by anaerobic bacteria is common [24].

Graphitic Corrosion Attributes

Graphitic corrosion usually occurs in three ways [26]:

1. Sometimes just the surface of the pipe graphitizes/corrodes, forming a graphitic coating on the exterior of the pipe. Often this protects the pipe well, leading to a long service life.
2. Other times, a graphitically corroded plug forms in the pipe wall. This pipe may serve for years, but if a pressure surge or water hammer (in water pipe) occurs, the plug may blow out.
3. Finally, the whole wall may graphitize/corrode, and if the pipe is subjected to a heavy earth load, or perhaps a washout under a joint, a circumferential break occurs.

Examples of Graphitic Corrosion

Three examples of graphitic corrosion were shown earlier in this report, see Figure 6 to Figure 8. Additional examples of graphitic corrosion of cast iron pipes are shown in Figure 36 to Figure 38 below [27].

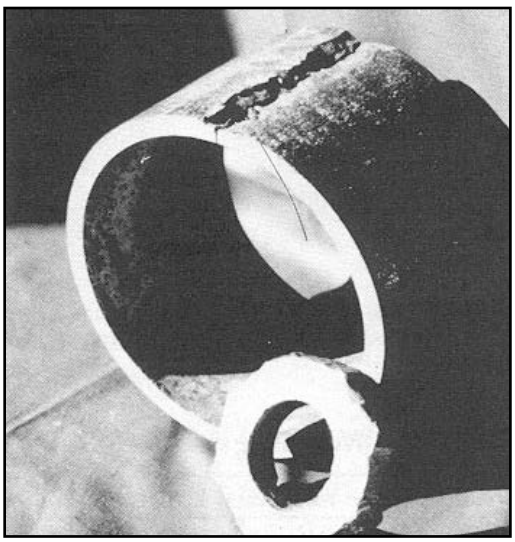

Figure 36. An 8 in. diameter gray iron pipe that failed due to graphitic corrosion. Severe graphitic corrosion occurred along the bottom external surface (rotated to the 12 O'clock position) where the pipe rested on wet soil.

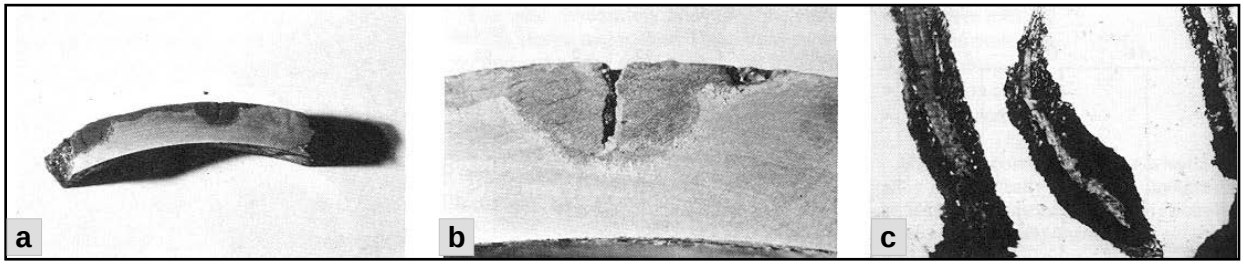

Figure 37. The pipe shown in Figure 36 above. (a) External surface exhibiting severe graphitic corrosion. (b) Close-up of the region shown in (a). (c) Micrograph of symmetrical envelopes of graphitically corroded cast iron surrounding flakes of graphite.

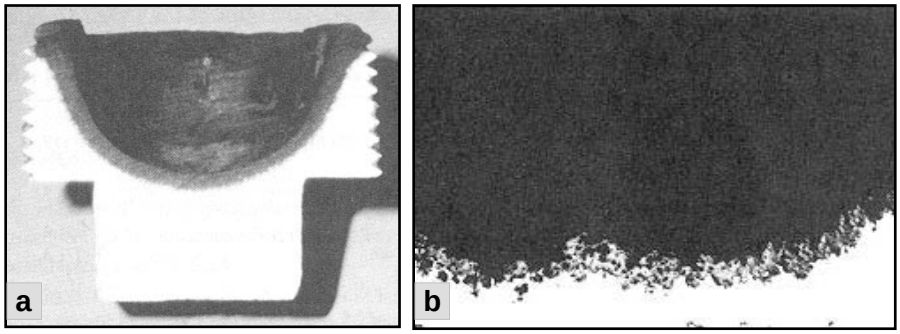

Figure 38. Example of graphitic corrosion of (a) pipe plug, (b) pump shell clearly showing the graphite residue left behind as the iron matrix dissolved.

Three more examples of a porous graphite corrosion on the outside of cast iron water pipe are shown in Figure 39 [22]; and in Figure 40 and Figure 41 on natural gas distribution cast iron pipes.

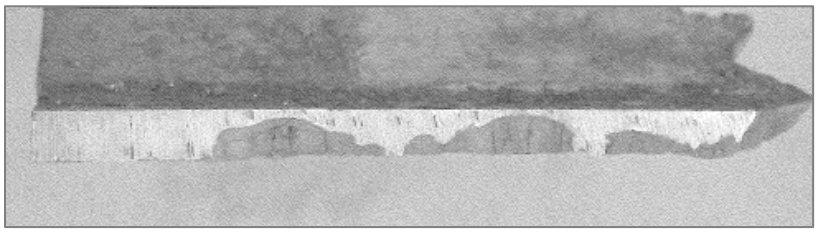

Figure 39. Dark, graphite corrosion on the exterior of a cast iron water main.

3

Figure 40. Dark, graphite corrosion on the exterior of a cast iron gas main.

Figure 41. Dark, graphite corrosion near the entrance to a joint on the exterior of a cast iron gas main.

Microstructure of Graphite Corrosion

The typical microstructure of a graphitically corroded surface is shown in Figure 42 and Figure 43 below [27,28], and Figure 44.

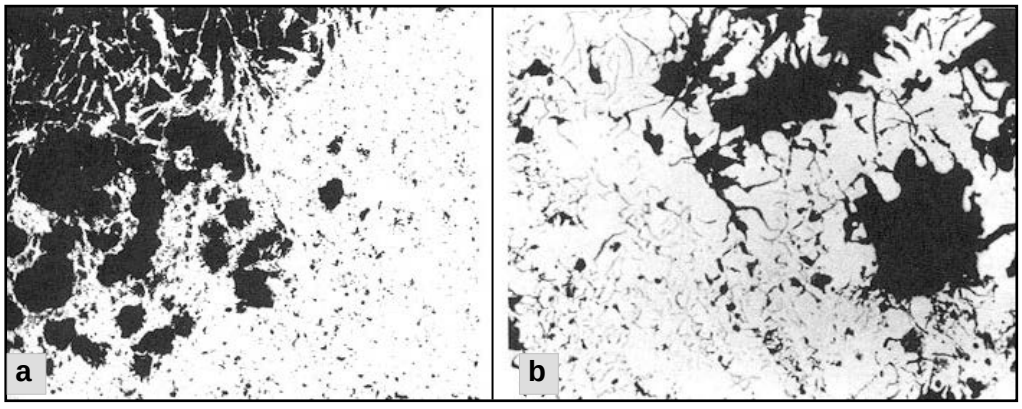

Figure 42. Microstructure of a failed water pipe. (a) A lacy network of porous residue, 27x. (b) Porosity associated with the graphitic structure, 135x.

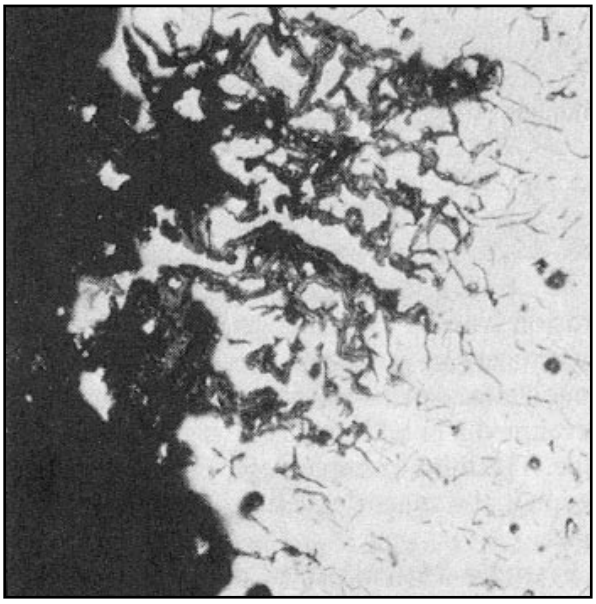

Figure 43. Example of microstructure of graphitic corrosion showing typical deterioration of exposed surface due to dissolution/leaching of metal matrix.

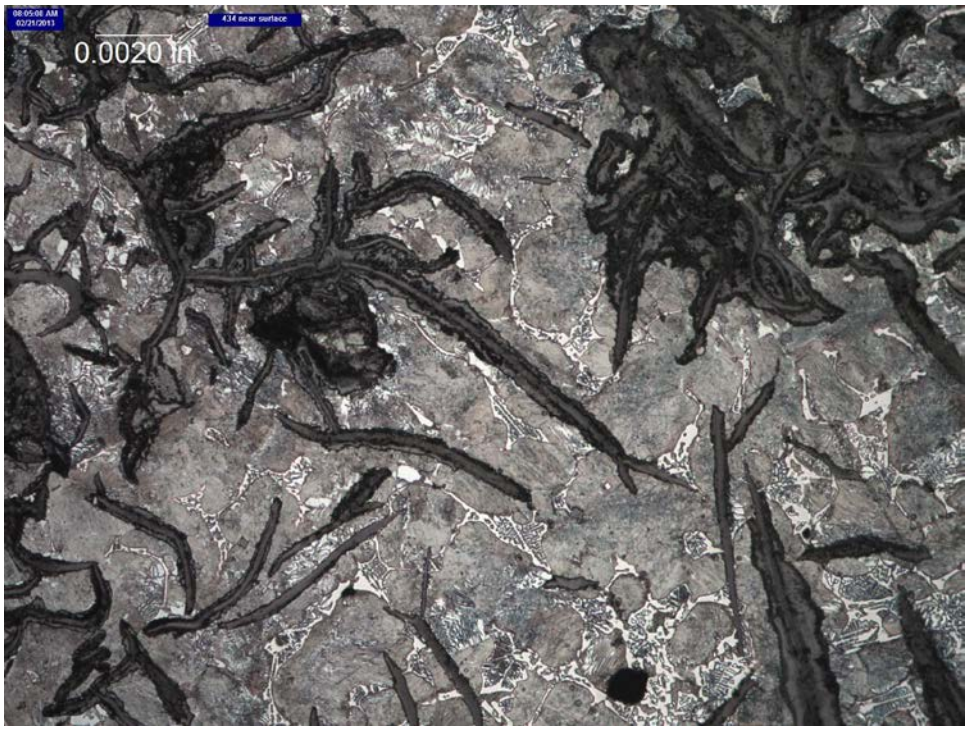

Figure 44. Example of microstructure of graphitic corrosion showing dealloyed regions around the large graphite flakes, i.e. expanded dark areas.

Graphitic corrosion can cause significant problems because there are no dimensional changes, but the cast iron loses its strength. This is dangerous for pressure-containing situations. The porosity can extend a considerable distance into the pipe wall from the surface. In tests of severely corroded cast iron pipe without a continuous path of porosity, the graphitic corrosion products *have* withstood pressures of several hundred pound per square inch. The danger is that the graphite layer can give way or break at any time due to shock or movement.

Chloride and sulfate contamination greatly increase the chance of graphitic corrosion.

Pitting and Crevice Corrosion

The presence of chlorides and/or crevices present conditions that are very favorable to pitting and/or crevice corrosion in cast irons.

Pitting of cast iron has been reported in calm seawater in addition to chloride solutions (since seawater contains a substantial amount of chloride ions). High additions of silicon, nickel, chromium and molybdenum aid in pitting resistance but need to be added in the levels discussed in the alloying section of this report to be effective.

Gray cast iron has a greater susceptibility to pitting than malleable cast iron. The pitting factor of cast iron is shown in Table 13 [29].

Table 13. Pitting factor of cast iron

Type	Corrosion rate (mm/year)	Pitting factor
Gray cast iron	0.02	10.9
Ferritic spheroidal gray cast iron	0.025	14.7
Malleable cast iron	0.045	4.9
Pearlitic gray cast iron	0.003	9.3
Spheroidal graphite Ni cast iron	0.07	6.7
White cast iron	0.045	10.00

Stress Corrosion Cracking (SCC) of Cast Irons

Stress corrosion cracking is observed in cast irons under certain combinations of environment and stress. Because stress is necessary to initiate SCC and because design factors often limit stresses in castings to low levels, SCC is not observed as often in cast irons as steels. However, under certain conditions SCC can be a serious problem. Environments that may cause SCC in unalloyed cast irons include sodium hydroxide and seawater when combined with a tensile stress and stress concentrations.

Gray iron can contain graphite in the form of interlocking flakes that produce a "notch effect", increasing the effect of applied tensile stresses.

Corrosion of Cast Iron in Alkali Solutions

Alkalies include sodium hydroxide (NaOH), potassium hydroxide (KOH), sodium silicate (Na_4O_4Si), and other materials that contain sodium, potassium, or lithium. Aqueous solutions of these salts carry sodium hydroxide. Unalloyed cast irons exhibit generally good resistance to alkalies, approximately equivalent to that of steel and are not substantially attacked by *dilute* alkalies at any temperature.

Gray irons have an approximate corrosion rate of 5 mpy when the concentration of NaOH is < 70% as shown in Figure 45 [30].

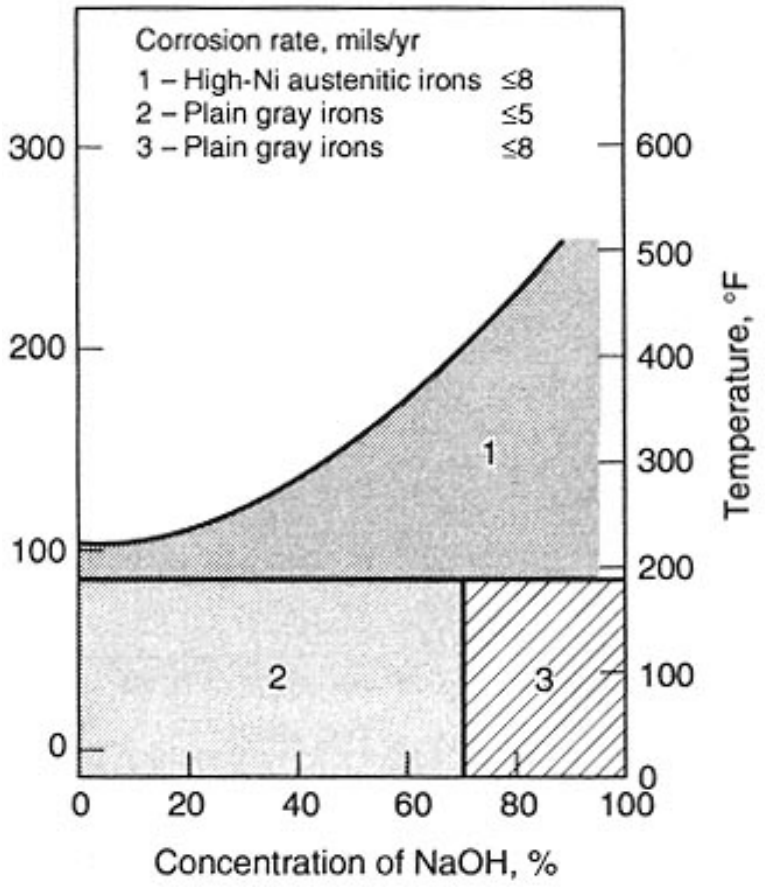

Figure 45. Corrosion of cast irons in NaOH as a function of alkali concentration and temperature.

The boundary between the alkaline and neutral zones marking the first appearance of greater corrosion resistance is at a pH of 9 to 10. A very low concentration only of the stronger alkalies, such as sodium hydroxide, tri-sodium phosphate, and sodium silicate, is required to throw the solution on the alkaline side of this boundary. A somewhat higher concentration of the weaker alkaline substances, as sodium carbonate and ammonia, is required, and the very weak alkalies like borax and di-sodium phosphate, even in substantial concentration, barely attain the alkaline zone.

Corrosion by alkalies *is* often characterized by pitting and localized attack. This would seem to be explained by the tendency of alkalies to produce cathodic films and therefore concentrate the attack on given areas. The size and shape of the pits will depend on the relative magnitude of the film-forming tendency and the rate of anodic reaction. A high

film-forming tendency will force the anodic corrosion into small areas, and pits will be small and deep and will penetrate relatively rapidly.

Another undesirable phenomenon often connected with alkali corrosion is embrittlement by hydrogen. Hydrogen produced in caustic solution in a nascent state, either by electric current or by corrosion, will penetrate the metal in a variety of ways and produce permanent embrittlement.

Corrosion in Water

Unalloyed and low-alloy cast irons are the primary cast irons used in water. The corrosion of unalloyed cast iron in water is determined by its ability to form protective scales. Calcium carbonate scales (formed in hard water) slow corrosion rates. Generally, corrosion rates in water will be a function of the contaminants present. Chlorides always increase the corrosion rates of unalloyed cast irons.

Aqueous (salt solution) cast iron corrosion studies were completed by Mehra and Soni [31] on 3.26% C, 2.25% Si gray iron; a summary of their results are listed below:

- It was found that KCl and NaCl were the major contributors (of the 12 major salts of concern) to accelerating corrosion of cast iron.
- The levels of NaCl and KCl used in the study were 600 ppm (part per million) each.
- The ion levels were Na^+ 236 ppm, K^+ 315 ppm, Cl^- 285-364 ppm.
- The two most significant anions were chlorides and sulfates.
- Corrosion rates for KCl and NaCl solutions were 6 mpy (mils per year) each. Together they would be about 12 mpy.
- The corrosion rate of a combined solution of 12 salts (≤ 600 ppm each) was 16-30 mpy.
- Halide ions contributed the most to corrosion, with sulfate and nitrate ions at an intermediate level, and carbonate and bicarbonate having minimal effect.

Independent data from Shell Development Company [32] on cast iron corrosion supports the Mehra and Soni results.

Seawater presents some special problems for cast irons. In general, iron objects will corrode 5 times faster in sea than in fresh water (for general corrosion). Seawater contains about 3.4% salt and is slightly alkaline (pH 8). The salt content will increase pitting and since it makes an excellent electrolyte, it greatly enhances galvanic corrosion

and therefore selective leaching. Gray iron may experience graphitic corrosion in calm seawater. Intermittent exposure to seawater is even worse.

The Handbook of Corrosion Data [33] lists the use of cast iron in salt water as: Not Recommended (from ambient to 100F) = Severe corrosion effect, unsatisfactory, not acceptable, do not use. The corrosion rate of gray cast iron in moderately flowing sea water can be between 20-60 mpy (temperature range of 50-86F), see Figure 46 [34].

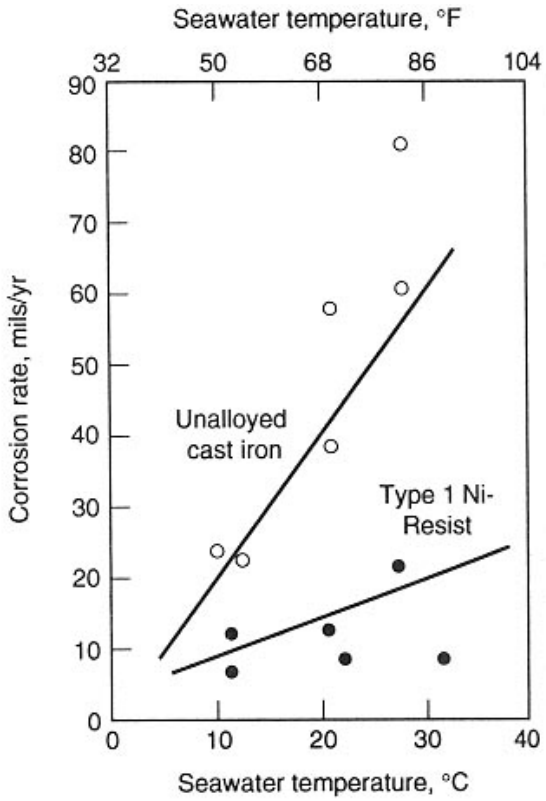

Figure 46. Corrosion of cast irons in flowing seawater.

In *quiet* (still) sea water the major concerns are graphitic and pitting corrosion, Figure 47 [35].

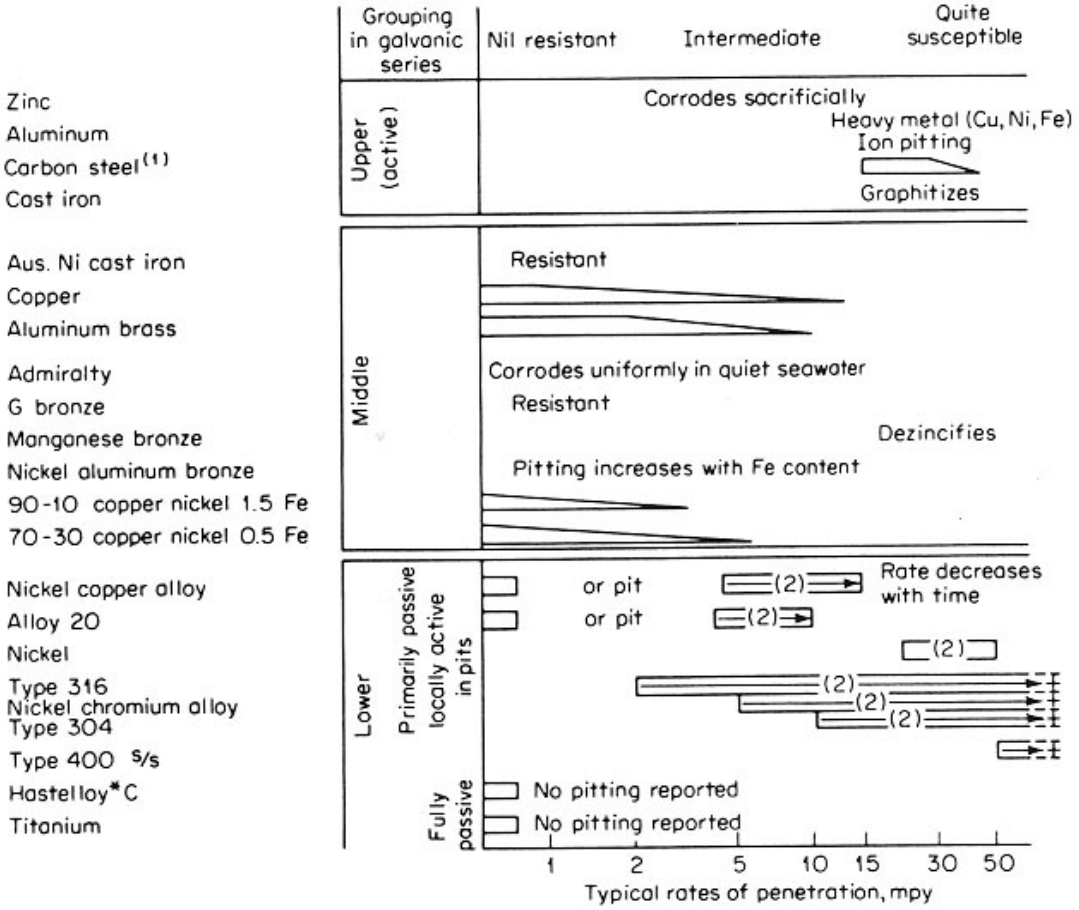

(1) Shallow round-bottom pits

(2) As velocity increases above 3 fps, pitting decreases. When continuously exposed to 5 fps and higher velocities these metals, except series 400 S/s, tend to remain passive without any pitting over the full surface in the absence of crevices.

Figure 47. Pitting in quiet seawater.

Influence of Alloying Elements on Cast Iron Corrosion Behavior

Alloying elements can dramatically affect the corrosion resistance of cast irons:

1. Silicon (Si) is the most important element when added in levels between 3-14%. This range increases the corrosion resistance of the cast iron. However, when the levels are raised above 14% there is a dramatic increase in the corrosion resistance. Over 16% embrittles the cast iron severely.
2. Nickel (Ni) is used to enhance corrosion resistance by the formation of protective oxide layers (as with silicon). Additions of over 12% are needed to enhance the cast iron's resistance to reducing acids and alkalies.

3. Chromium (Cr) is usually added with nickel and/or silicon to increase corrosion resistance. Additions of 15-30% are needed to protect cast iron from oxidizing acids. Chromium additions do not help under reducing conditions.
4. Small additions of copper (Cu) help with atmospheric corrosion.
5. 3-4% molybdenum (Mo) is used to enhance corrosion resistance in high silicon cast irons.

Influence of Microstructure on Cast Iron Corrosion Behavior

The graphite shape and the amount of massive carbides (iron carbide) present are critical to mechanical properties. Additionally, as was discussed earlier, the flake graphite structure of gray iron acts cathodically with regard to the metal matrix and accelerates attack via graphitic corrosion.

The *structure* of the metal *matrix* also has an effect on the corrosion. Generally, the most corrosion resistant is ferrite, while pearlite and cementite show intermediate corrosion resistance [36].

Shrinkage or porosity can degrade the corrosion resistance by allowing corrosive media to enter the casting's body or wall section.

The Effect of Corrosion on Residual Pipe Strength

Adegbite, S., et. al. (2013) [37] investigated cast iron water pipes recovered from service to predict the likelihood of failure, denoted by a factor of safety. The work shows the likelihood of failure as function of input strength value and corrosion pit depth from graphitic corrosion. The relationship between the factor of safety and the corrosion depth and pipe strength is shown in Figure 48.

The factor of safety is defined as the ratio of the failure stress (or resistance capacity) to the imposed stresses, which could be in the axial (σx) or hoop ($\sigma\theta$) directions, see Equation 2 below:

$$\text{Factor of Safety Equivalent: } FS_{equiv} = \text{Failure Stress}/\text{Imposed Stresses} \qquad \text{(Equation 2)}$$

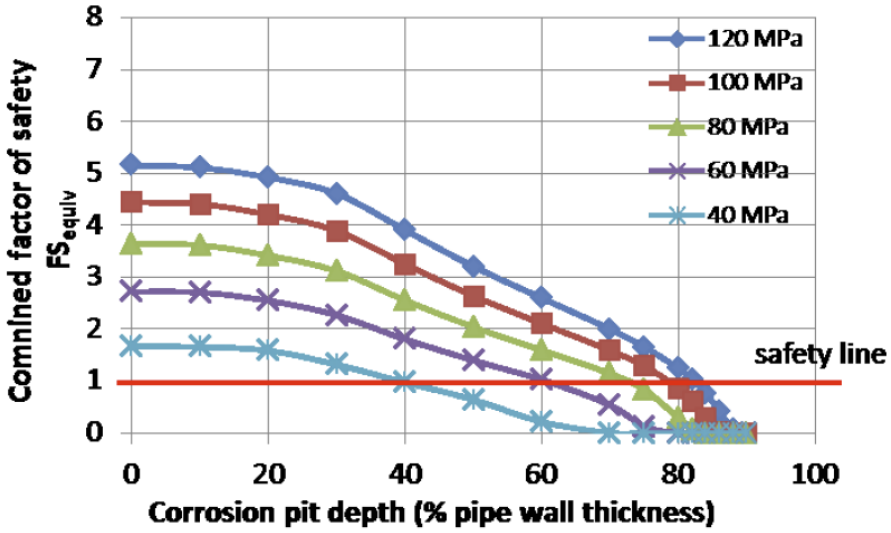

Figure 48. Relationship between the factor of safety and corrosion pit depth at different pipe strengths for combined axial and hoop stress.

The inputting of the lower strength values into the Monte Carlo deterministic model produced a relationship between the equivalent factor of safety FSequiv and the corrosion pit depth, which was properly described by the loss of section analysis approach. Importantly lower FSequiv values were obtained for reduced pipe strength inputs which was in agreement with what should be expected at constant hoop and axial stresses imposed on the main.

It was shown that proactive and targeted strategies for asset management would require choosing a lower limit strength value from the flexural testing of around 40 MPa to determine the maximum pit depth threshold (in this case 40% wall thickness at FSequiv = 1) above which failure is imminent.

Jesson, D.A., et. al. (2013) [38] conducted a study where condition of cast iron samples taken from sections of failure trunk mains was examined. Stress-strain response for the cast irons were determined from testing and correlated with microstructure. The strength variability was modeled with Weibull statistics. A master plot was produced summarizing the strength-pit depth behavior of the pipes and it was shown that the graphitic corrosion influences the remaining strength. Simple strength of materials and fracture mechanics models gave sensible bounds to the observed data. The master plot is shown in Figure 49.

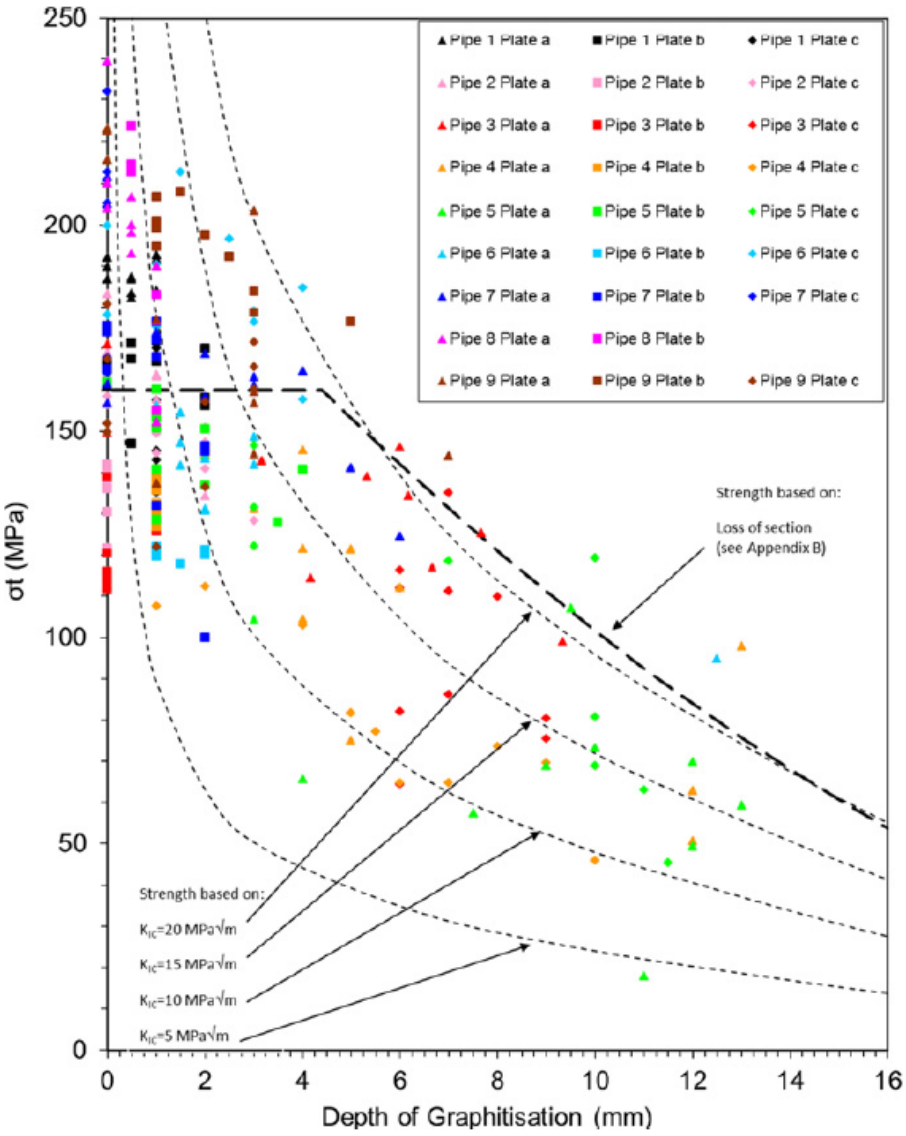

Figure 49. Strength versus depth of graphitization (graphitic corrosion), models for strength based on loss of section and fracture mechanics superimposed.

3. Cast Iron Failure Assessment

This section provides a review of the cast iron failure incidents, and the associated loads and stresses on cast iron pipes due to external loads and environmental conditions.

The first part of this section provides an introduction to the cast iron mains in the natural gas local distribution system and a summary of the associated reported failure incidents.

The second part of this section provides a review of the parameters affecting cast iron corrosion and an analysis of the loads and stresses which the cast iron pipes are subjected to in the field.

The section also provides the background and material properties needed for performing the finite element analysis of corroded pipe sections subjected to external loads which is presented in **Section 5** of the report, *Fitness for Service (FFS) Model of Characterized Graphitic Corrosion*. The calculation of field loads will also be included in Section 5 of this report, along with examples that are based on this section of the report.

Additional details on cast iron and cast iron pipe metallurgy and field corrosion have already been included in the **Section 2** of this report, *Cast Iron Materials Literature Search.*

Cast Iron in the Gas Distribution System

Introduction

Cast iron gas mains have been installed since the 1850's and until the 1960's it was the prime material for natural gas main installations. Since then, steel and plastic PE pipes have been replacing cast iron in natural gas distribution mains and services.

Cast iron pipes are still in service in many U.S. cities. About 27,771 miles of cast iron mains were estimated to be in service in 2015, with about fifty percent of these pipes located within four states: New Jersey, New York, Massachusetts, and Pennsylvania [39].

Cast iron pipes are typically joined by bell and spigot joints with lead-caulked or cement sealants. The joints are typically at every 12 ft sections of the pipe. Typical dimensions of the joints are shown in Figure 50.

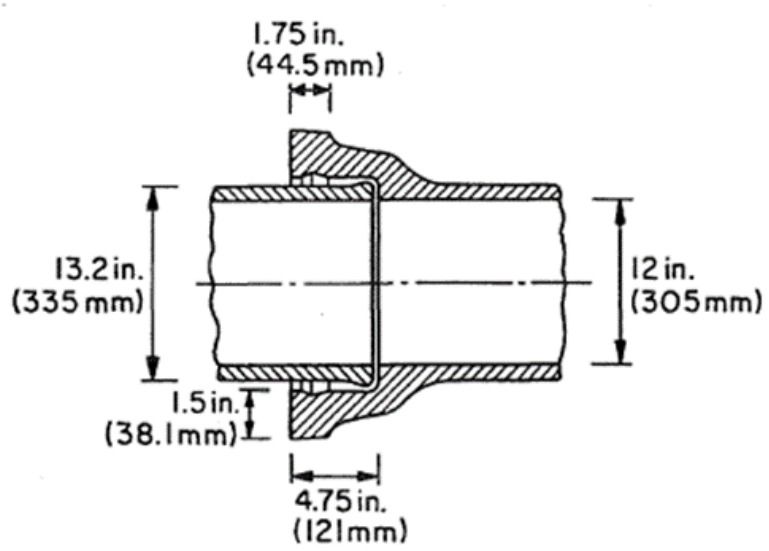

Figure 50. Typical dimensions of the bell and spigot cast iron joint [40]

A typical distribution of the age of CI pipes in the gas distribution system is shown in Figure 51. The figure is compiled from the CI inventory data of natural gas Local Distribution Companies (LDC) in New York City and it shows that the average cast iron age in the area is about 90 years old; with few installations since the 1960's.

From the 1930s to the 1950s most of the cast iron pipes were centrifugal metal mold pipes of lengths 12 ft, 16 ft, and 18 ft and were manufactured according to Federal Specification WW-P-421. After the 1950s, they were manufactured according to

American Standards Association Specification A21.7, except that the metal thickness met WW-P-421.

Table 14 shows the pipe sizes and Figure 52 shows the stress-strain relationship of the class 150 cast iron pipes. Class 150 as noted here refers to 150 psi use, not the material grade/class of the pipe as noted in Section 2 of this report, specifically using ASTM 48 – Standard Specification for Gray Iron Castings. The ASTM "class" is typically between class 20 to class 60, corresponding to the materials approximate tensile strength in ksi.

The cement joint (yarn and cement) was adopted as a standard joining method by the gas industry around 1900. In the 1930s, cement joints were used in small diameter pipes while the 12-inch and larger mains had combination joints (yarn, cement, lead). The maximum pressure used in a cement joint was 15 psig.

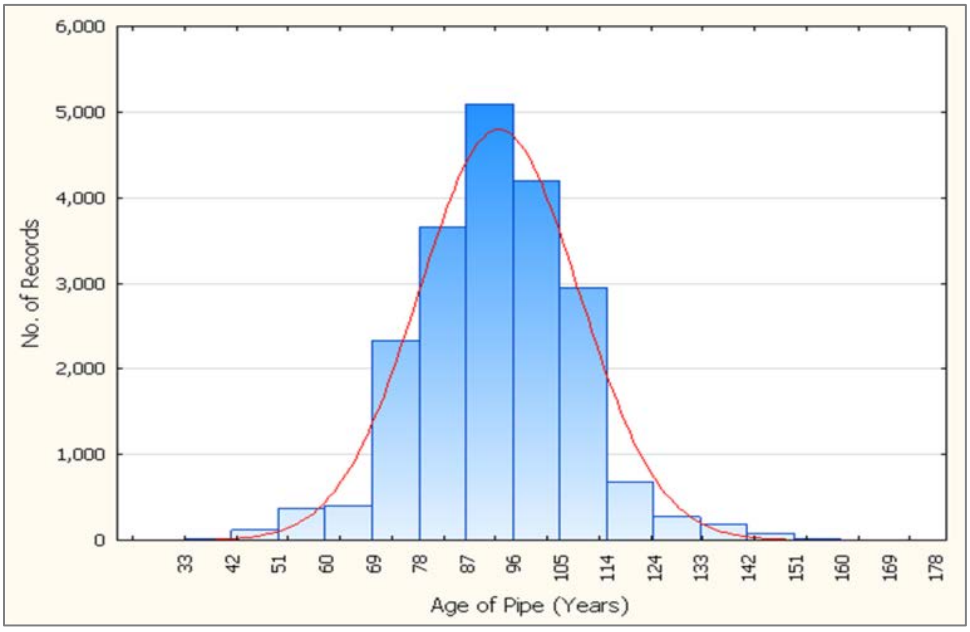

Figure 51. Distribution of CI age in gas distribution system

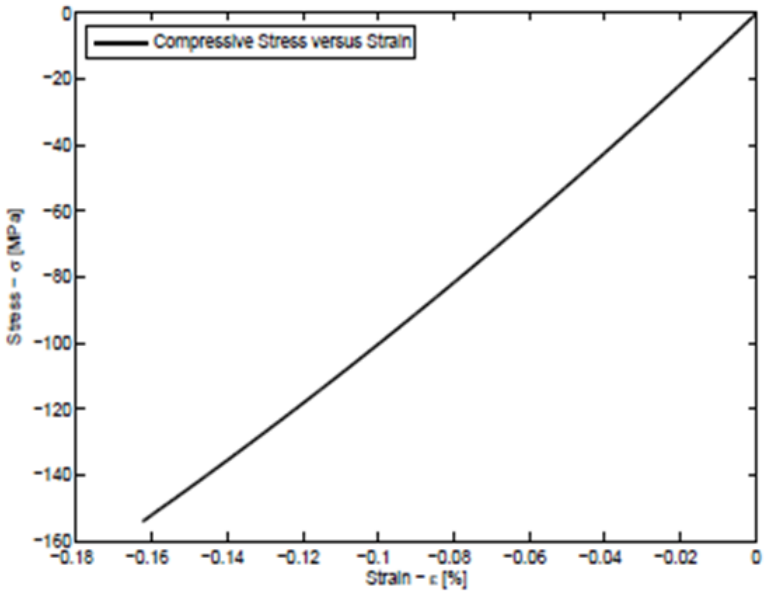

Figure 52. Stress-strain relationship of cast iron in compression [41]

Table 14. Pipe Sizes for Class 150 Cast Iron Pipes

Nominal size	CENTRIFUGALLY CAST PIPE ANSI A21.6 • ANSI A21.8 AWWA C106 • AWWA C108			PIT CAST PIPE ANSI A21.2 AWWA C102		
	O.D.	I.D.	THICKNESS	O.D.	I.D.	THICKNESS
CLASS 150 • 150 PSI • 346 FT. HD.						
3"	3.96	3.32	.32	3.80	3.06	.37
4"	4.80	4.10	.35	4.80	4.00	.40
6"	6.90	6.14	.38	6.90	6.04	.43
8"	9.05	8.23	.41	9.05	8.13	.46
10"	11.10	10.22	.44	11.10	10.02	.54
12"	13.20	12.24	.48	13.20	12.04	.58
14"	15.65	14.63	.51	15.65	14.39	.63
16"	17.80	16.72	.54	17.80	16.44	.68
18"	19.92	18.76	.58	19.92	18.46	.73
20"	22.06	20.82	.62	22.06	20.40	.83
24"	26.32	24.86	.73	26.32	24.46	.93
30"	32.00	30.30	.85	32.40	30.20	1.10
36"	38.30	36.42	.94	38.70	36.26	1.22
42"	44.50	42.40	1.05	45.10	42.40	1.35
48"	50.80	48.52	1.14	51.40	48.44	1.48
54"	-	-	-	57.80	54.54	1.63
60"	-	-	-	64.20	60.42	1.89

In 1991, the National Transportation Safety Board (NTSB) recommended that PHMSA – then called the Research and Special Programs Administration – require pipeline operators to implement a program to identify and replace cast iron pipelines that may threaten public safety [42]. PHMSA issued two Advisory Bulletins related to cast iron replacement programs.

The first advisory bulletin [43] encouraged operators to develop procedures to identify segments of cast iron pipe that may need replacement. It reminded operators that pipeline safety regulations require generally graphitized cast iron pipe to be replaced and protect excavated cast iron pipe from damage.

The second advisory bulletin [44] also indicated that pipeline safety regulations require operators to have a procedure for continuing surveillance of pipeline facilities to identify problems and take appropriate action concerning failures, leakage, corrosion, and other unusual operating and maintenance conditions. This procedure included surveillance of cast iron to identify problems and take appropriate action concerning graphitization.

See **Section 2** of this report for a detailed description of cast iron graphitic corrosion, sometimes termed graphitization.

Cast Iron Reported Incidents

PHMSA collects data from operators on incidents occurring on their gas distribution systems as defined by the Code of Federal Regulations 49 CFR 191.3. Incidents are categorized by pipeline type, size, cause of failure, and other metrics. Figure 53 shows the total number of significant incidents since 1985 in comparison to the cast iron pipe incidents. The figure shows that the number of significant incidents of cast iron pipes ranged from 3 to 22 incidents annually during this period [45].

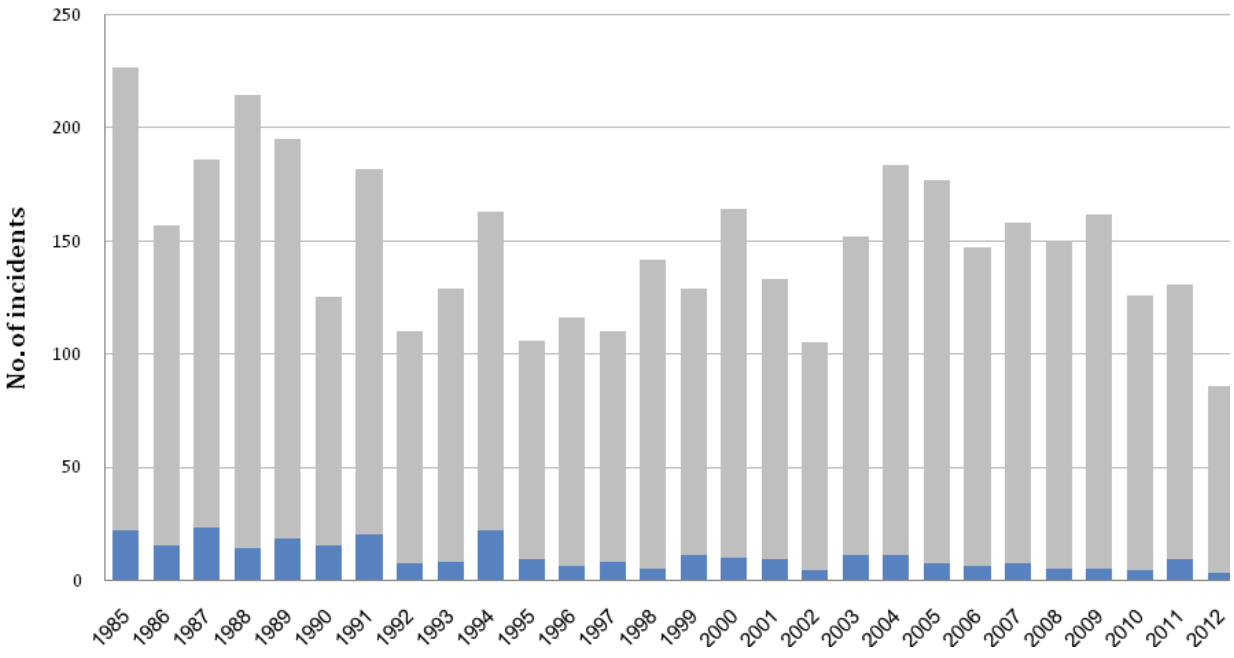

Figure 53. Total incidents vs. Cast iron incidents

Table 15 and Table 16 show a list of the PHMSA reported incidents of the cast iron failures from 2010 to 2016. Table 15 summarizes the system properties and Table 16 shows the causes of failure and characteristics [46]. The data in the table presents the significant incidents which result in fatality, injury, more than $50,000 in total costs, or volatile gas or liquid release.

Table 15. Cast Iron Pipes and System Characteristics in Reported Incidents [2010-2016]

YEAR	CITY_NAME	STATE	FATALITY_	INJURY_IN	INJURE	SHUTDOWN_	IGNITE_IND	EXPLODE_IND	INCIDENT_AREA_SUBTYPE	DEPTH_OF COVER	CROSSING	SYSTEM_PART_INV	INSTALLATION_	PIPE_DIAMETER	LEAK_TYPE
2016	DETROIT	MI	NO	NO	0	NO	YES	YES	INSIDE A BUILDING		NO	MAIN	1931	6	CRACK
2015	NEW YORK	NY	NO	NO	0	YES	YES	NO	UNDER PAVEMENT	33	NO	MAIN	1907	6	
2015	SAINT LOUIS	MO	NO	NO	0	YES	NO	NO	UNDER PAVEMENT	43	NO	MAIN	1902	16	CRACK
2015	DETROIT	MI	NO	YES	1	NO	YES	YES	INSIDE A BUILDING		NO	MAIN	1923	6	CRACK
2015	NORTHBORO	MA	NO	NO	0	NO	YES	YES	INSIDE A BUILDING		NO	MAIN	1929	6	CRACK
2015	PHILADELPHIA	PA	NO	NO	0	NO	YES	YES	UNDER PAVEMENT	30	NO	MAIN	1906	6	CRACK
2015	JACKSON	MI	NO	YES	1	NO	NO	NO	UNDER PAVEMENT	42	NO	MAIN	1932	4	CRACK
2015	CORDOVA	AL	YES	YES	3	YES	YES	YES	UNDER SOIL	60	NO	MAIN	1952	6	
2014	SAINT LOUIS	MO	NO	NO	0	NO	NO	NO	UNDER PAVEMENT	62	NO	MAIN		8	
2014	CHICAGO	IL	NO	NO	0	YES	NO	NO	EXPOSED DUE TO EXCAVATION	60	YES	MAIN	1962	20	CONNECTION FA
2014	PHILADELPHIA	PA	NO	YES	1	YES	YES	YES	UNDER PAVEMENT		NO	MAIN	1939	4	
2014	BROOKLYN	NY	NO	YES	3	NO	YES	YES	INSIDE A BUILDING		NO	MAIN	1926	4	CRACK
2013	BIRMINGHAM	AL	YES	YES	1	NO	YES	YES	UNDER SOIL	36	NO	MAIN	1951	2.25	CRACK
2013	COLUMBUS	OH	NO	YES	1	NO	YES	NO	EXPOSED DUE TO EXCAVATION	36	NO	MAIN		4	OTHER
2013	PITTSBURGH	PA	NO	NO	0	NO	NO	NO	VAULT	36	NO	VALVE 12 INCH	1959		CRACK
2013	FITCHBURG	MA	NO	NO	0	YES	NO	YES	UNDER SOIL	28	NO	MAIN		4	CRACK
2013	JACKSON	MO	NO	NO	0	YES	NO	NO	ABOVEGROUND		NO	REGULATOR/METER	1980		
2012	SAINT LOUIS	MO	NO	NO	0	YES	YES	NO	EXPOSED DUE TO EXCAVATION	48	NO	MAIN	1961	12	
2012	BALTIMORE	MD	NO	NO	0	YES	NO	NO	EXPOSED DUE TO EXCAVATION	38	NO	MAIN	1909	4	
2012	AUSTIN	TX	YES	YES	1	YES	YES	YES	UNDER SOIL	38	NO	MAIN	1950	4	
2011	BALTIMORE	MD	NO	NO	0	YES	NO	NO	EXPOSED DUE TO EXCAVATION		NO	MAIN	1900	12	
2011	DETROIT	MI	YES	NO	0	NO	NO	NO	UNDER SOIL	54	NO	MAIN	1928	6	
2011	BALTIMORE	MD	NO	NO	0	YES	YES	NO	ABOVEGROUND		NO	OUTSIDE METER/RE	2010		
2011	BALTIMORE	MD	NO	NO	0	NO	YES	NO	ABOVEGROUND		NO	OUTSIDE METER/RE	1980		
2011	DETROIT	MI	NO	NO	0	NO	NO	YES	INSIDE A BUILDING		NO	MAIN	1930	4	CRACK
2011	READING	PA	YES	YES	3	YES	YES	YES	UNDER PAVEMENT	52	NO	MAIN	1928	12	CRACK
2011	BALTIMORE	MD	NO	NO	0	YES	YES	NO	ABOVEGROUND		NO	OUTSIDE METER/RE	2000		
2011	SALISBURY	MD	NO	NO	0	NO	YES	NO	ABOVEGROUND		NO	SERVICE RISER	2003		
2011	PHILADELPHIA	PA	YES	YES	3	YES	YES	YES	UNDER PAVEMENT	37	NO	MAIN	1942	12.75	CRACK
2010	ATLANTA	GA	NO	NO	0	YES	NO	NO	UNDER PAVEMENT	48	YES	MAIN	1924	4	
2010	MOBILE	AL	NO	YES	1	NO	NO	NO	VAULT		NO	OTHER	1950		
2010	DENVER	CO	NO	NO	0	YES	YES	YES	UNDER SOIL	18	NO	SERVICE	1940	1.25	
2010	WALTHAM	MA	NO	YES	1	NO	YES	YES	UNDER SOIL	48	NO	MAIN	1930	6	CRACK
2010	NEWARK	NJ	NO	NO	0	NO	YES	YES	INSIDE A BUILDING		NO	MAIN	1959	16	

Table 16. Cast Iron Causes of Failure Characteristics in Reported Incidents [2010-2016]

YEAR	CITY_NAME	STATE	CLASS_LOCATION_T	NORMAL_PSIG	MOP_PSIG	CAUSE	CORROSION_TYP	NATURAL_FORCE_TYPE	NF_EXTREME_WEATHER_DETAI	EX_PARTY_TYPE	OUTSIDE_FORCE_TYPE
2016	DETROIT	MI	CLASS 3 LOCATION	5	5	MATERIAL FAILURE OF PIPE OR WELD					
2015	NEW YORK	NY	CLASS 4 LOCATION	0.25	0.5	OTHER INCIDENT CAUSE					
2015	SAINT LOUIS	MO	CLASS 3 LOCATION	23	25	OTHER INCIDENT CAUSE					
2015	DETROIT	MI	CLASS 3 LOCATION	2	2	NATURAL FORCE DAMAGE		TEMPERATURE			
2015	NORTHBORO	MA	CLASS 3 LOCATION	0.34	0.5	NATURAL FORCE DAMAGE		TEMPERATURE	PIPE WAS IN FROZEN GROUND.		
2015	PHILADELPHIA	PA	CLASS 4 LOCATION	0.25	0.5	NATURAL FORCE DAMAGE		TEMPERATURE			
2015	JACKSON	MI	CLASS 3 LOCATION	0.5	0.97	NATURAL FORCE DAMAGE		TEMPERATURE			
2015	CORDOVA	AL	CLASS 1 LOCATION	22	40	NATURAL FORCE DAMAGE		EARTH MOVEMENT			
2014	SAINT LOUIS	MO	CLASS 3 LOCATION	1.1	2.2	EXCAVATION DAMAGE				EXCAVATION DAMAGE	
2014	CHICAGO	IL	CLASS 4 LOCATION	22	25	INCORRECT OPERATION					
2014	PHILADELPHIA	PA	CLASS 4 LOCATION	0.25	0.5	NATURAL FORCE DAMAGE		TEMPERATURE			
2014	BROOKLYN	NY	CLASS 4 LOCATION	0.33	0.65	OTHER INCIDENT CAUSE					
2013	BIRMINGHAM	AL	CLASS 3 LOCATION	19	25	OTHER INCIDENT CAUSE					
2013	COLUMBUS	OH	CLASS 3 LOCATION	0.45	1	OTHER INCIDENT CAUSE					
2013	PITTSBURGH	PA	CLASS 3 LOCATION	143	150	INCORRECT OPERATION					
2013	FITCHBURG	MA	CLASS 3 LOCATION	0.5	0.5	NATURAL FORCE DAMAGE		EARTH MOVEMENT			
2013	JACKSON	MO	CLASS 3 LOCATION	70	80	EQUIPMENT FAILURE					
2012	SAINT LOUIS	MO	CLASS 3 LOCATION	12.5	25	CORROSION FAILURE	GRAPHITIC				
2012	BALTIMORE	MD	CLASS 2 LOCATION	0.28	0.36	EXCAVATION DAMAGE				EXCAVATION DAMAGE	
2012	AUSTIN	TX	CLASS 3 LOCATION	48	60	NATURAL FORCE DAMAGE		OTHER NATURAL FORCE	DROUGHT AND RAINFALL		
2011	BALTIMORE	MD	CLASS 3 LOCATION	0.3	0.36	EXCAVATION DAMAGE				EXCAVATION DAMAGE	
2011	DETROIT	MI	CLASS 3 LOCATION	5	5	CORROSION FAILURE	GRAPHITIZATION				
2011	BALTIMORE	MD	CLASS 4 LOCATION	93	99	OTHER OUTSIDE FORCE DAMAGE					R OTHER FIRE/EXPLOSION
2011	BALTIMORE	MD	CLASS 4 LOCATION	92	99	OTHER OUTSIDE FORCE DAMAGE					OTHER FIRE/EXPLOSION
2011	DETROIT	MI	CLASS 3 LOCATION	5	5	NATURAL FORCE DAMAGE		TEMPERATURE			
2011	READING	PA	CLASS 3 LOCATION	0.36	1	OTHER INCIDENT CAUSE					
2011	BALTIMORE	MD	CLASS 4 LOCATION	85	99	OTHER OUTSIDE FORCE DAMAGE					DAMAGE BY CAR,
2011	SALISBURY	MD	CLASS 3 LOCATION	32	45	OTHER OUTSIDE FORCE DAMAGE					OTHER FIRE/EXPLOSION
2011	PHILADELPHIA	PA	CLASS 4 LOCATION	18	35	MATERIAL FAILURE OF PIPE OR WELD					
2010	ATLANTA	GA	CLASS 3 LOCATION	13	15	EXCAVATION DAMAGE				EXCAVATION DAMAGE	
2010	MOBILE	AL	CLASS 3 LOCATION	40	60	OTHER INCIDENT CAUSE					
2010	DENVER	CO	CLASS 3 LOCATION	5	15	EXCAVATION DAMAGE				EXCAVATION DAMAGE	
2010	WALTHAM	MA	CLASS 3 LOCATION	1.8	2	NATURAL FORCE DAMAGE		TEMPERATURE			
2010	NEWARK	NJ	CLASS 4 LOCATION	32	35	NATURAL FORCE DAMAGE		EARTH MOVEMENT			

Figure 54 shows the number of incidents from 2010 to 2015 sorted by material type. Incident records of cast iron and wrought iron pipes were 34 out of the total 660 incidents (5.2%) in this five-year period. Figure 55 shows the distribution of the cast iron failures in this reporting period. Cast iron incidents resulting in leaks were about 47% of the incidents, about 18% of the pipes had ruptures, and the remaining percentage was mostly characterized by circular cracking due to external loads. Out of the 34 incidents in cast iron pipes in this period, two incidents were caused by external corrosion of the pipe as shown in Figure 56.

Figure 57 shows the geographical distribution of the cast iron failure incidents in the U.S. The incidents in the figure are categorized by the causes of failure.

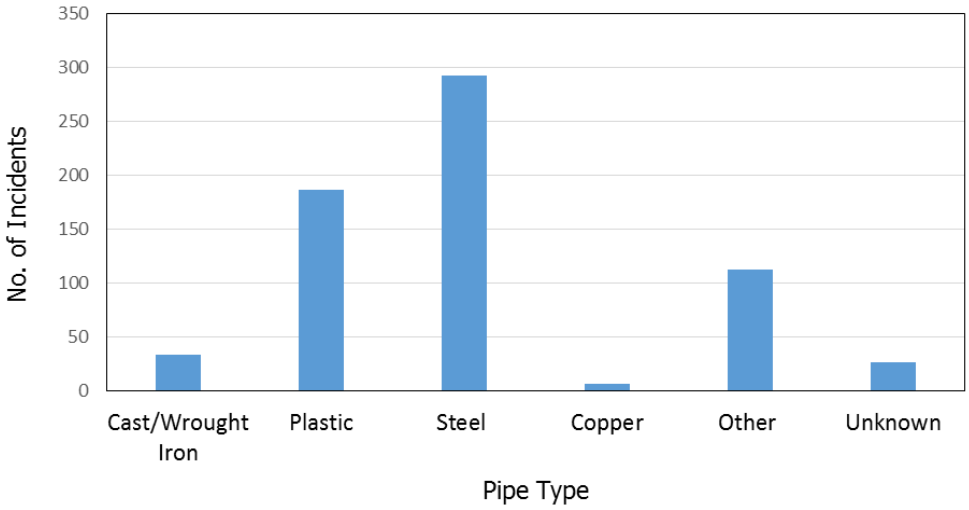

Figure 54. Incidents by pipe material type, from 2010 to present

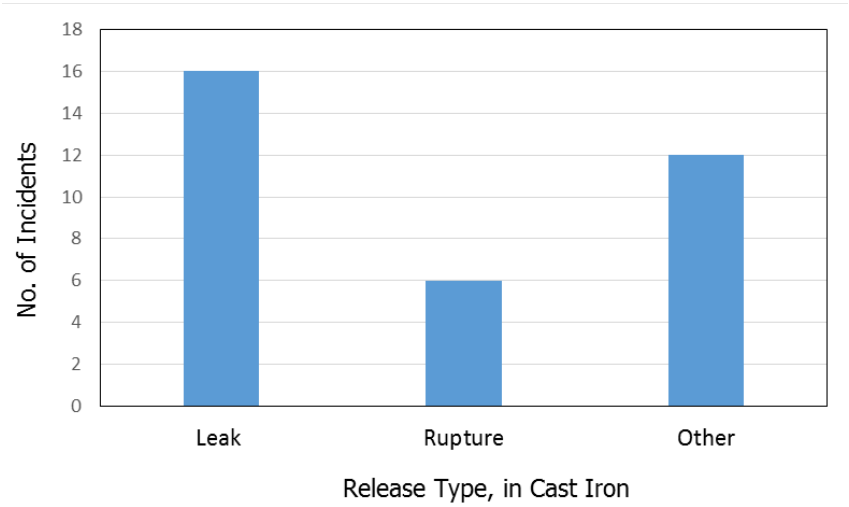

Figure 55. Type of pipe failure in the cast iron incidents

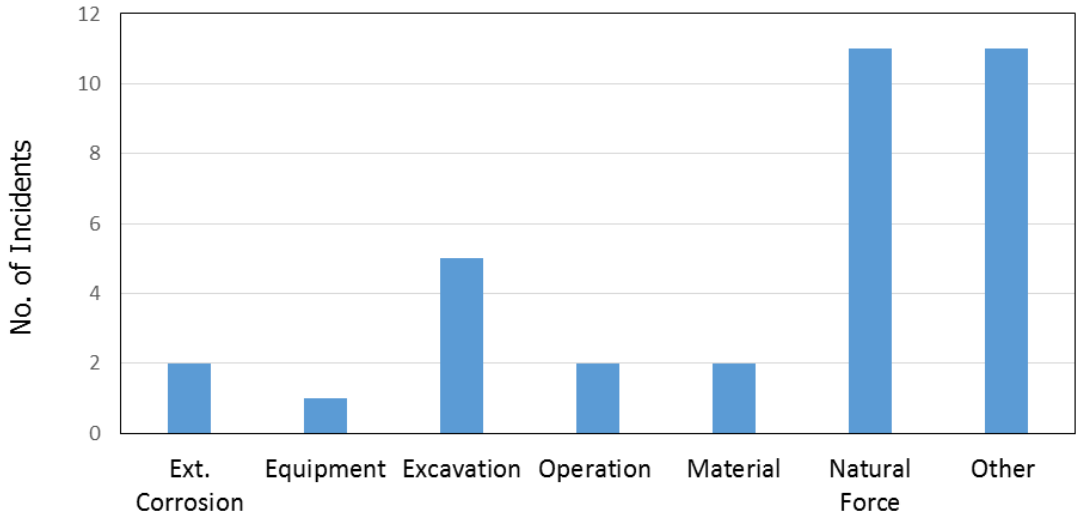

Figure 56. Causes of incidents in cast iron pipes

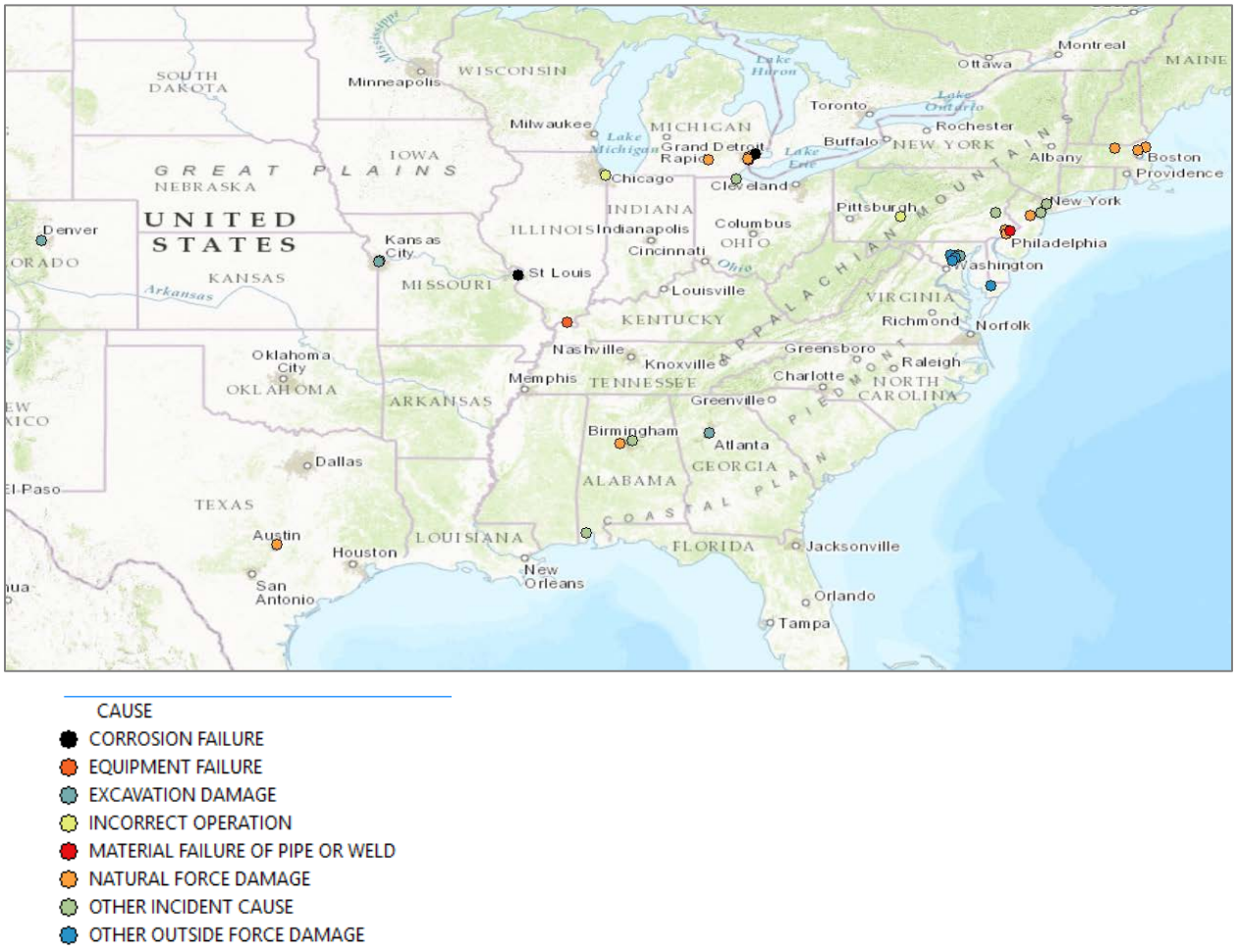

Figure 57. Locations of cast iron incidents [2010-2016]

Parameters Affecting Cast Iron Graphitization

A review of a survey performed by a northeast utility in 2015 on the cast iron sections in their service area is presented in this section. The survey included obtaining local soil samples at locations around random cast iron sections with and without graphitization. A total of 292 soil samples were obtained and tested for resistivity, pH value, chloride, and sulfate.

Out of these samples, only 50 samples were inspected for corrosion and 24 of these samples showed moderate to extensive levels for graphitization. Only these 50 samples were analyzed to evaluate the effect of soil properties on the graphitization potential. The distribution of the soil resistivity measurements (ohm-cm), pH, and chloride and sulfate contents (ppm) are shown in Figure 58 to Figure 61, respectively.

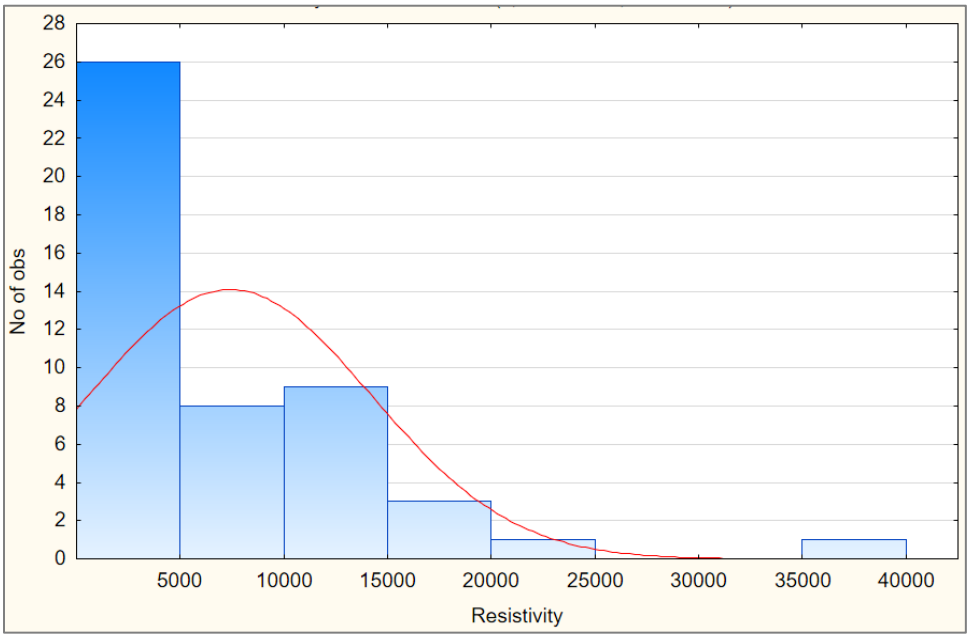

Figure 58. Histogram of the soil resistivity measurements in the samples

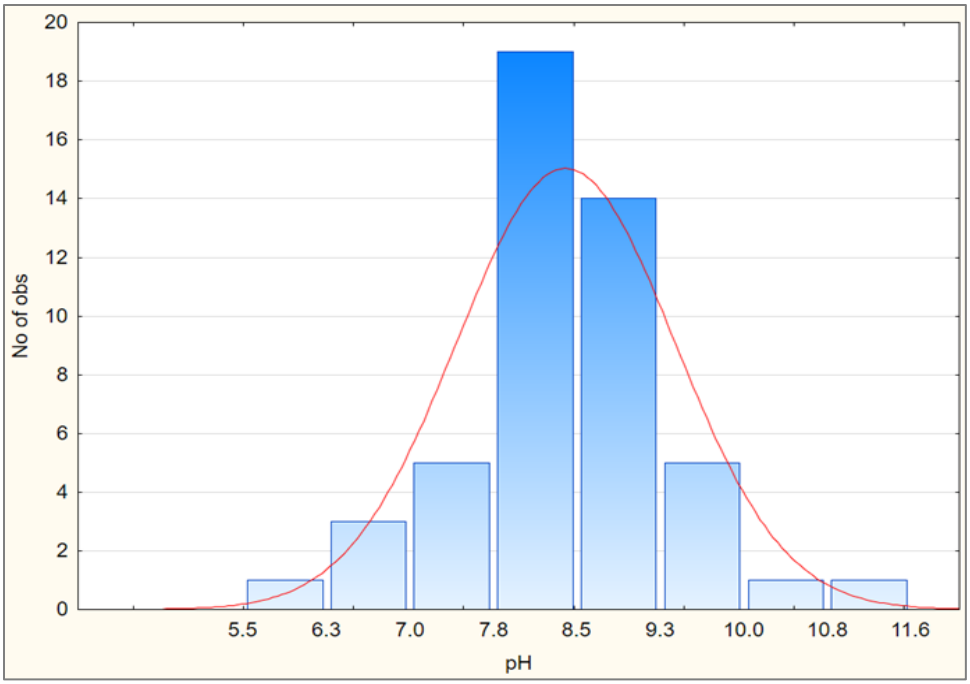

Figure 59. Histogram of the pH measurements in the samples

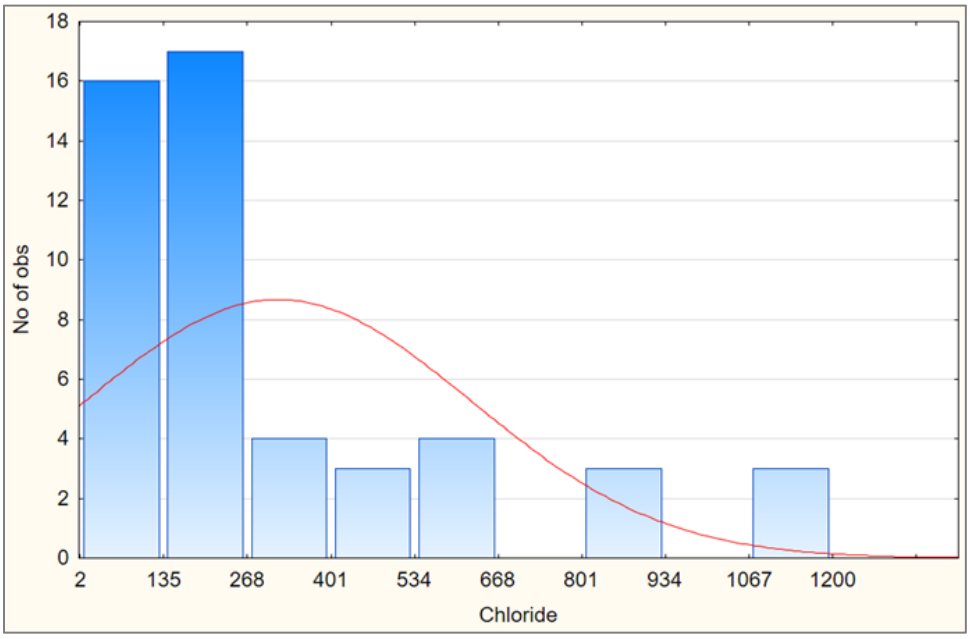

Figure 60. Histogram of the chloride measurements in the samples

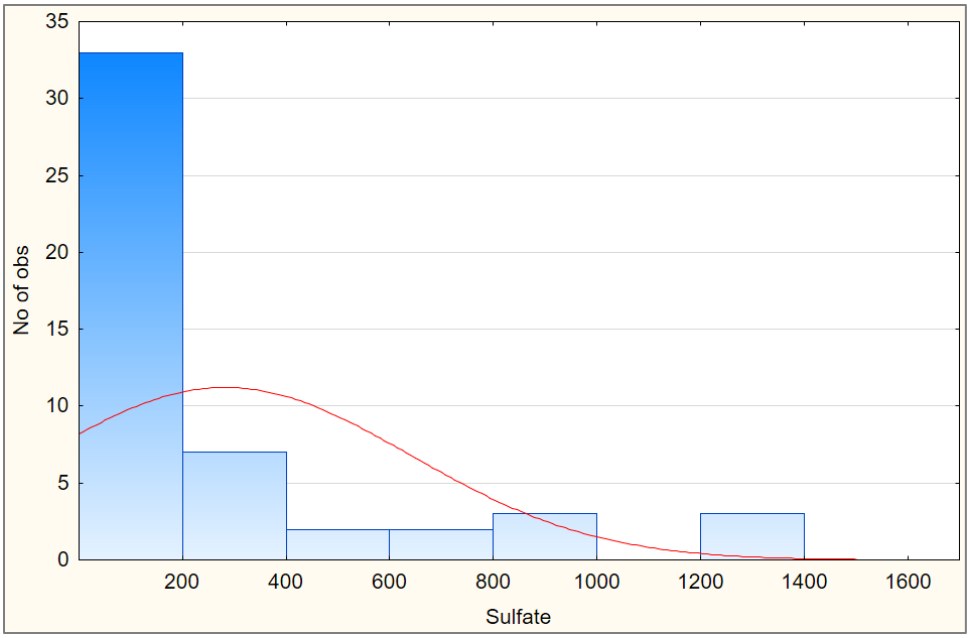

Figure 61. Histogram of sulfate measurements in the samples

The correlations between the soil parameters and observed graphitization was performed using the means (i.e., averages) of the measurements and their statistical distributions. The plots in Figure 62 to Figure 65 show the distributions of the soil parameters in box-whisker plots in relation to the cast iron graphitization. The graphitization in the x-axis of these figures are categorized as 0 = no observed graphitization, 1 = moderate graphitization, and 2 = severe graphitization.

The plots show insignificant changes in the mean values of soil parameters for the three graphitization categories; suggesting no to weak correlations between soil parameters and graphitization in these samples. This could be mainly due to the need to incorporate a larger sample size and additional soil parameters in the analysis.

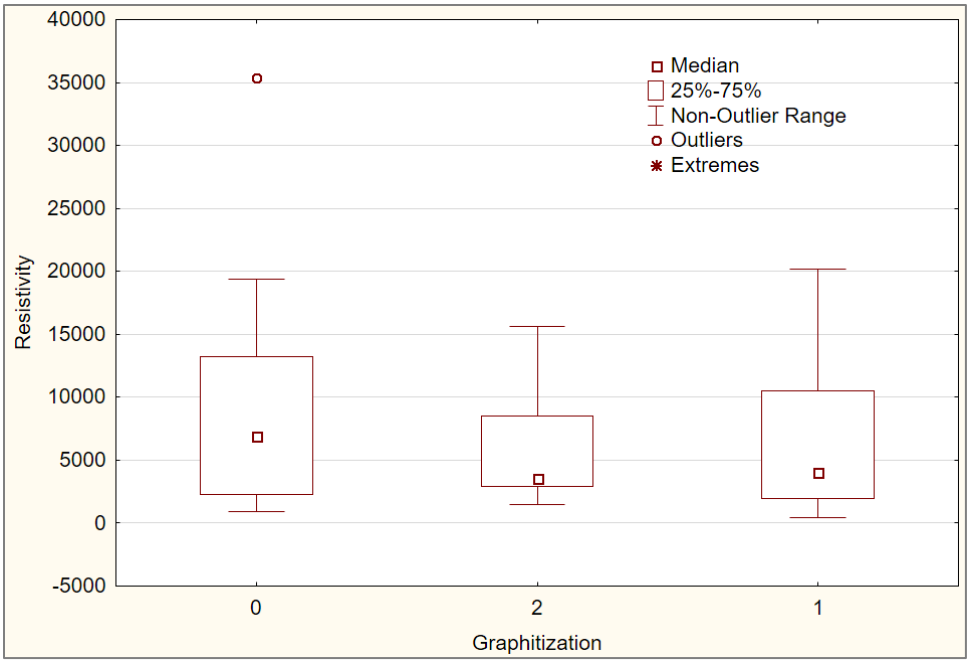

Figure 62. Box-Whiskers plot for graphitization change with soil resistivity

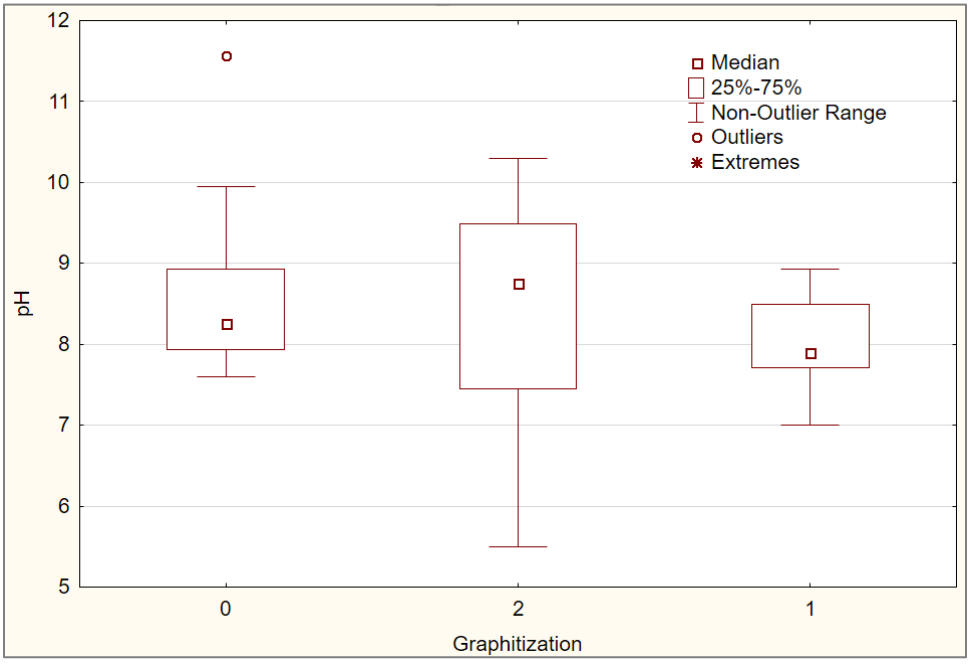

Figure 63. Box-Whiskers plot for graphitization change with pH values

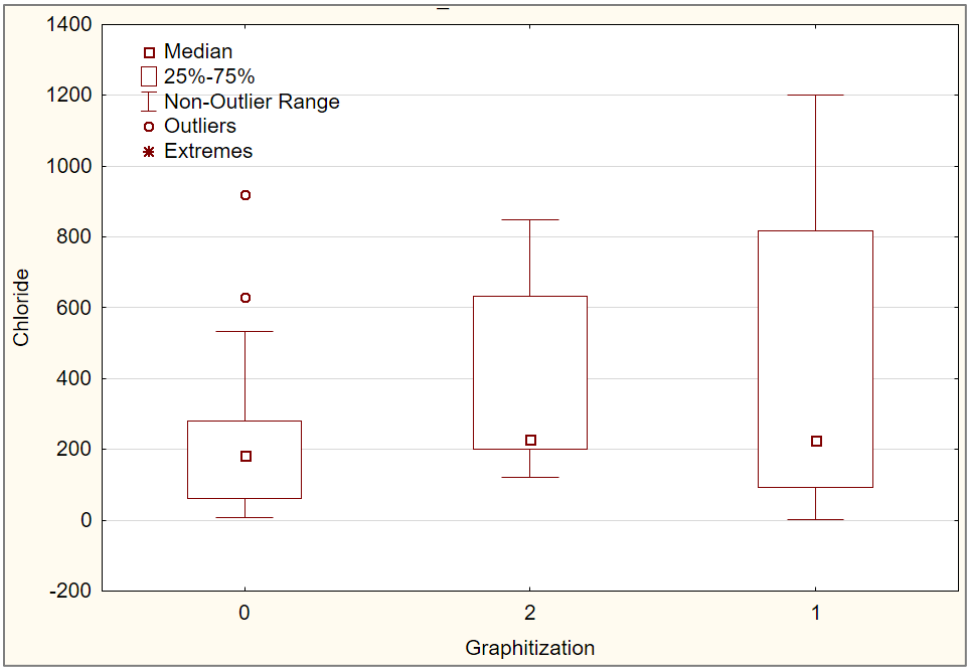

Figure 64. Box-Whiskers plot for graphitization change with chloride

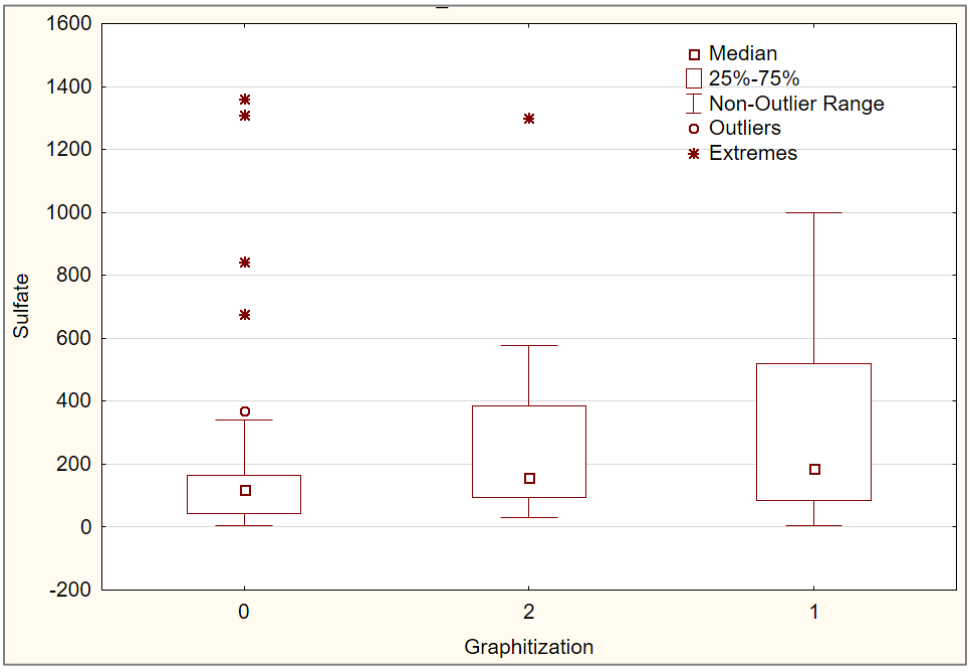

Figure 65. Box-Whiskers plot for graphitization change with sulfate

The data was also analyzed using the Analysis of Variance (ANOVA) of the Design-Expert® Software program. Table 17 shows the input parameters used in the analysis and Table 18 shows the results of the of the graphitization response. The results show

high *model* p values above 0.17; and weak correlations with the soil *parameters*; with mostly p values higher than 0.05 except with chloride; indicating that there is no strong relationship between the graphitization and these parameters to construct a meaningful predictive model.

Table 17. Input Soil Parameters and Response (Graphitization) in the Data Set

Factor	Name	Units	Type	Subtype	Minimum	Maximum
A	Resistivity	ohm-cm	Numeric	Continuous	440	35330
B	pH		Numeric	Continuous	5.5	11.56
C	Chloride	ppm	Numeric	Continuous	2	1200
D	Sulfate	ppm	Numeric	Continuous	5	1360
Response	**Name**	**Units**	**Obs**	**Analysis**	**Minimum**	**Maximum**
R1	Graphitization		50	Polynomial	0	2

Table 18. Results of the ANOVA model analysis

Response 1 Graphitization

ANOVA for Response Surface 2FI model

Analysis of variance table [Partial sum of squares - Type III]

Source	Sum of Squares	df	Mean Square	F Value	p-value Prob > F
Model	9.52	10	0.95	1.51	0.1717
A-Resistivity	*2.63*	*1*	*2.63*	*4.18*	*0.0478*
B-pH	*2.42*	*1*	*2.42*	*3.84*	*0.0572*
C-Chloride	*4.34*	*1*	*4.34*	*6.89*	*0.0123*
D-Sulfate	*0.13*	*1*	*0.13*	*0.21*	*0.6463*
AB	*2.39*	*1*	*2.39*	*3.79*	*0.0588*
AC	*1.70*	*1*	*1.70*	*2.70*	*0.1084*
AD	*0.60*	*1*	*0.60*	*0.96*	*0.3342*
BC	*3.09*	*1*	*3.09*	*4.91*	*0.0326*
BD	*0.084*	*1*	*0.084*	*0.13*	*0.7170*
CD	*1.37*	*1*	*1.37*	*2.17*	*0.1488*

Pipe Stresses under Internal and External Loads

A buried natural gas cast iron pipe is commonly subjected to both internal pressure from the pressurized gas and external pressure from the overburden earth load and highway traffic. The pipe may also be subjected to additional loads associated with ground deformations and environmental factors. The sources of these additional loads include:

- Shrinking and swelling of soil and frost heave,
- Loss of ground support due to undermining by adjacent excavations,
- Dynamic loads due to earthquakes and nearby blasting, and
- Pipe stresses induced by temperature fluctuations.

The pipe may also be subjected to additional initial stresses during installation. These stresses can be caused by carrying and placing the pipe in an open trench installation, which was the common installation procedure for cast iron gas mains. However, these initial installation stresses are not relevant in the purpose of evaluating the aged cast iron pipes.

Stresses Due to Internal Pressure

The internal pressure of the pipe, p (psig) causes circumferential stress on the pipe cross section. The circumferential stress S_i in psi may be calculated using the Barlow formula:

$$S_{i\,(Barlow)} = p\,D/\,2\,t_w \qquad (1)$$

Where,

D Pipe outside diameter, inch

t_w Pipe wall thickness, inch.

Stresses Due to Vertical Earth Load

The earth load applied to the pipe is the weight of the prism of soil with a width equal to that of the pipe and the height of that of the soil above the pipe as shown in Figure 66. For the general condition where the pipe is buried below the water table, the vertical pressure P_e (lb/ft2) due to earth load can be obtained from the simple formula [47]:

$$P_e = \gamma_w\,h_w + R_w\,\gamma_d\,H \qquad (2)$$

Where,

γ_w Unit weight of water (pcf)

h_w Height of water above pipe (ft)

γ_d Unit weight of dry soil (pcf)
H Height of soil above top of pipe (ft)
R_w Water buoyancy factor = $1 - 0.33\ (h_w/H)$.

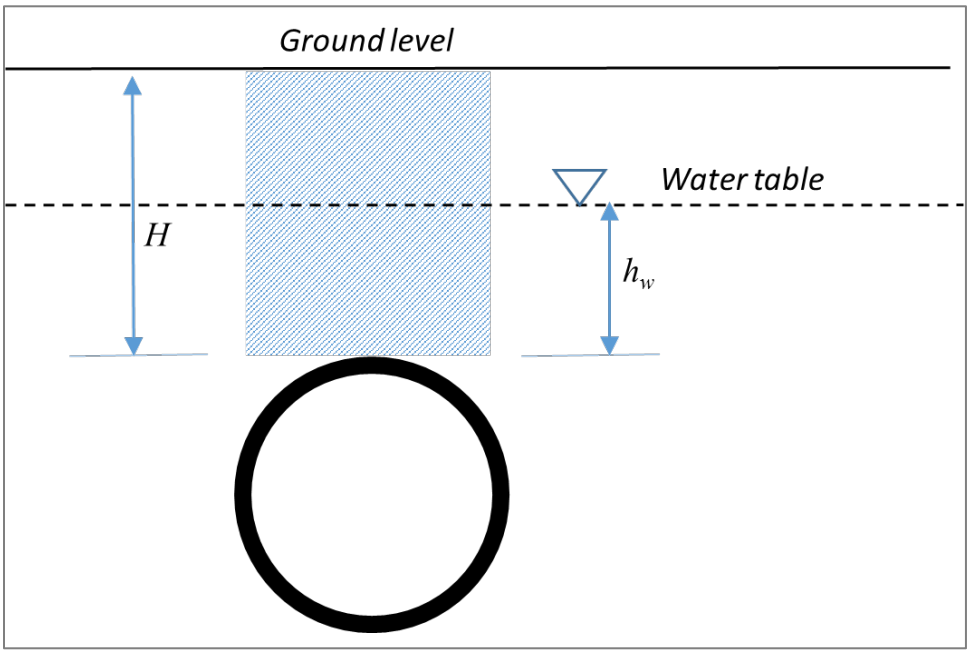

Figure 66. Soil prism above pipe

As an example, for a pipe buried 6 ft in a soil with a dry soil unit weight of 110 pcf and the water table 3 ft above the top of the pipe, the water buoyancy factor R_w is 0.835 and the vertical earth pressure is calculated as:

$P_e = 62.4 \times 3.0 + 110.0 \times 6.0 \times 0.835 = 738.3$ lb/ft^2

The circumferential stress S_{He} (psi) due to earth load, which accounts for the pipe-soil frictional interaction and pipe installation procedure, is calculated as follows [48, 49]:

$$S_{He} = K_e . B_e . E_e . \gamma . D \quad (3)$$

Where,
K_e Stiffness factor from earth load
B_e Burial factor
E_e Excavation factor
γ Soil unit weight (lb/in^3).

Values of $K_e, B_e, and\ E_e$ can be obtained as follows:

- The stiffness factor for earth load, K_e accounts for the interaction between the soil and pipe and depends on pipe diameter, wall thickness, and coefficient of soil reaction E_{soil}. The values of E_{soil} ranges from 0.2 ksi for highly plastic, soft to medium silt and clay to 1.0 ksi for very stiff clay and silt. A value of 2 ksi is commonly taken for very dense sands and gravels. Figure 67 shows values of K_e for various soils and pipe parameters.

- The burial factor B_e depends on pipe diameter and depth of soil cover. Figure 68 shows the burial factors for various depth of cover H over B_d ratios. For trenched construction, which was the common practice for cast iron pipe installations, the value of B_d equals pipe diameter D.

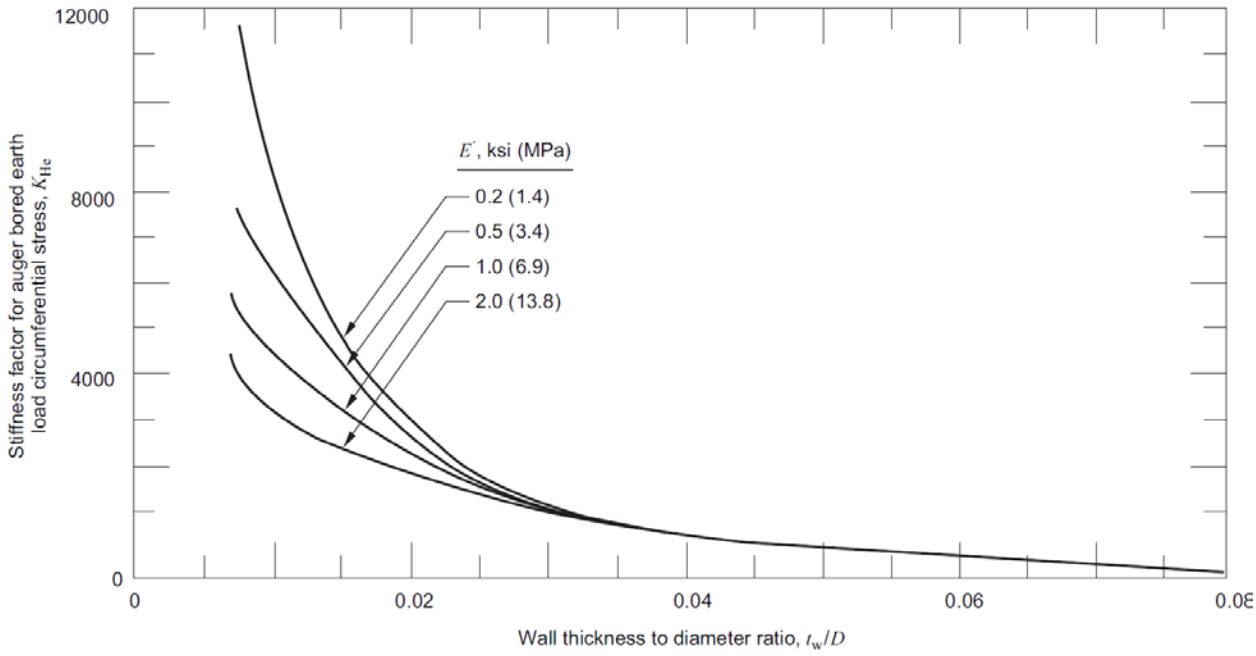

Figure 67. Stiffness factor K_e for stresses due to earth load

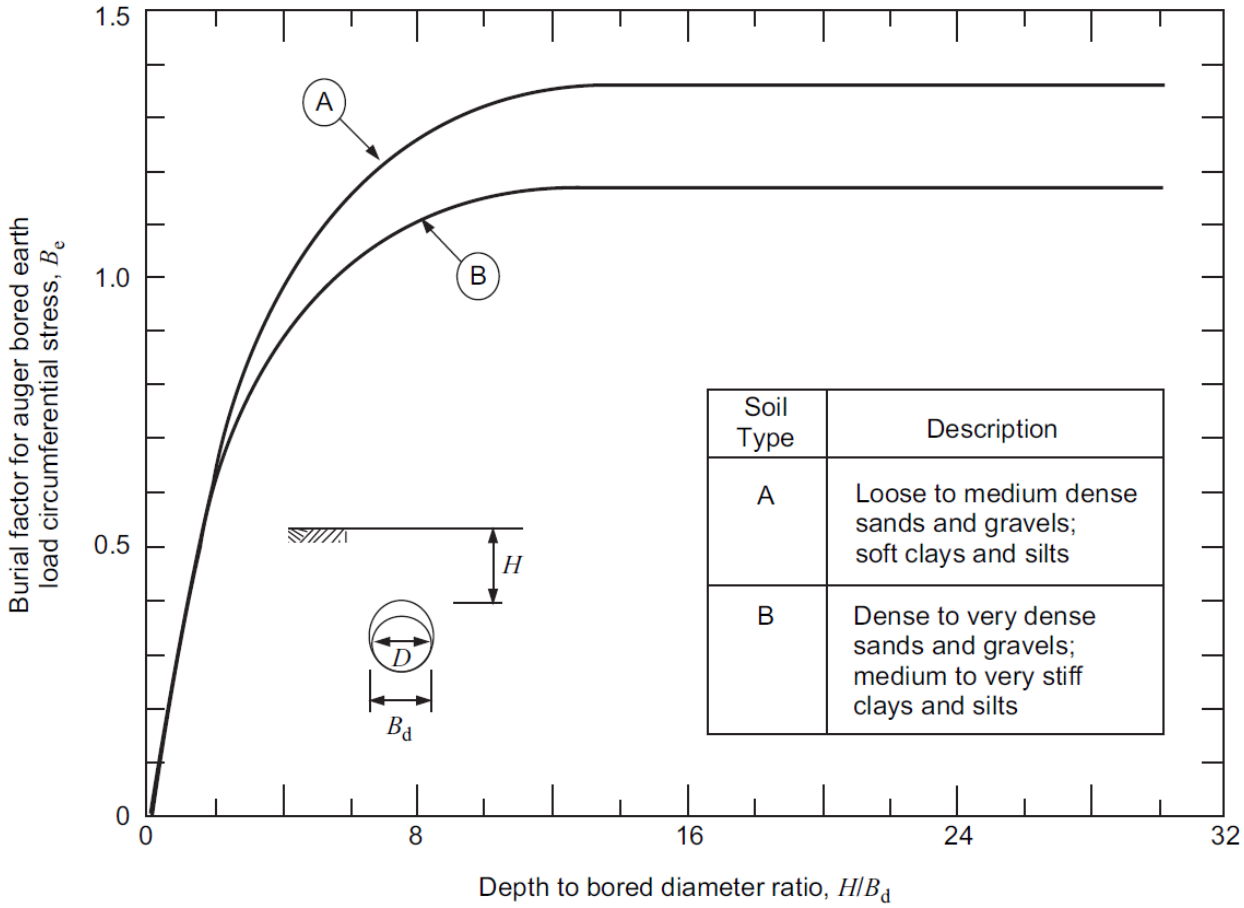

Figure 68. Burial Factor B_e for stresses due to earth load

- The excavation factor E_e is assumed as 1.0 for trenched construction, which was commonly performed in cast iron pipe installations.

- Soil unit weight γ is commonly taken as 120-130 lb/ft^3 for most soil types unless higher values are determined in laboratory or field tests.

Stresses due to Traffic Loads

The highway pressure w due to the traffic wheel load P at the surface of the roadway is calculated as:

$$w = {}^{P}/_{A_p} \qquad (4)$$

Where P is the either the design single wheel load P_s or the design tandem wheel load P_t as shown in Figure 69.

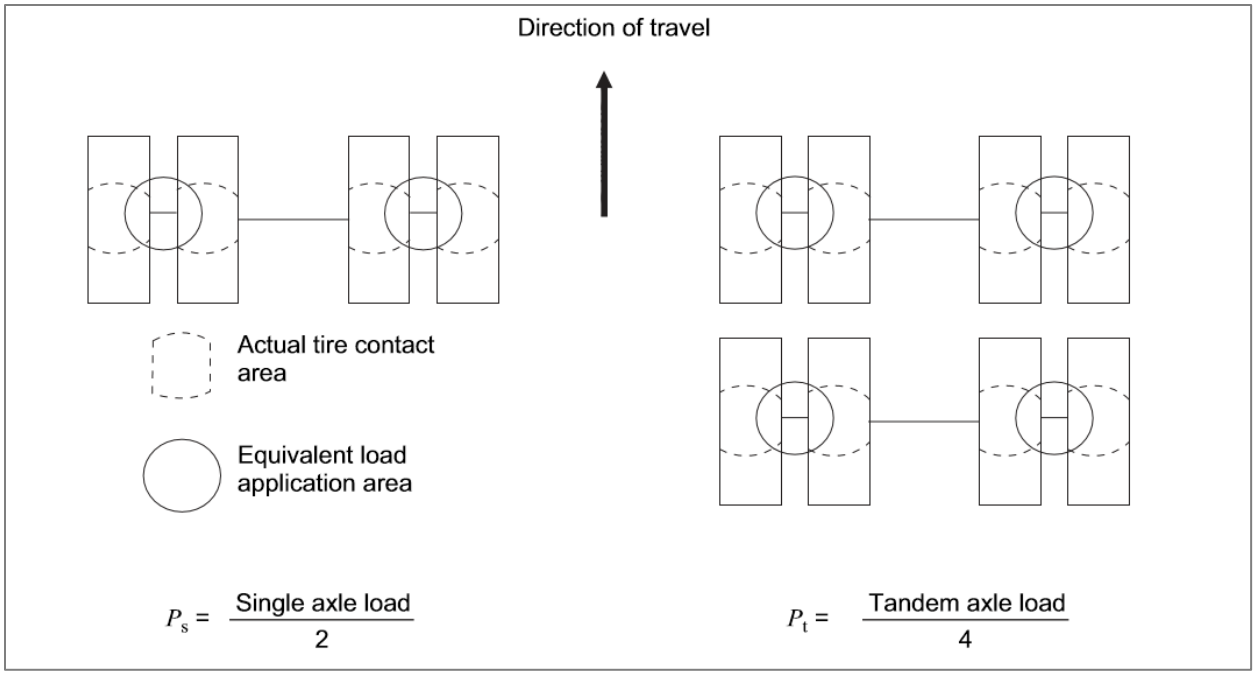

Figure 69. Single and tandem wheel loads

The recommended design load for a single traffic wheel load is 12,000 lb. A_p is the contact area over which the wheel load is applied and it is taken as 144 in^2. For single axle loading, the above equation results in a surface pressure w of 83.3 psi.

The values of the life load are commonly increased by an impact factor of 1.5 on the ground surface to account for the impact of the bumps. However, the impact factor has no effect at depths greater than 3 ft and the vertical pressure due to traffic load drops drastically at this depth. The values in Table 19 show estimates of the life loads (in psi) with the change of depth of cover for a standard HS-20 truck load at the surface [48]. The calculation of the stress resulting from the traffic wheel loads are also presented in the above reference.

Table 19. Live loads with Depth of Cover

Live load transferred to pipe, lb/in^2			
Height of cover, ft	Highway H20*	Railway E80†	Airport‡
1	12.50	--	--
2	5.56	26.39	13.14
3	4.17	23.61	12.28
4	2.78	18.40	11.27
5	1.74	16.67	10.09
6	1.39	15.63	8.79
7	1.22	12.15	7.85
8	0.69	11.11	6.93
10	§	7.64	6.09
12	§	5.56	4.76

Pipe stresses calculated from the internal pressure may not exceed the allowable values set by Title 49 in the Code of Federal Regulations [50] as:

$$S_{i\,(Barlow)} \leq F.E.T.SMYS \qquad (5)$$

Where,

F Class location design factor
E Longitudinal joint factor
T Temperature de-rating factor
SMYS Specified minimum yield strength of the pipe material.

Additionally, the total effective stresses calculated from the internal pressure, soil, and traffic loads may not exceed the specified pipe minimum yield strength divided by a factor of safety. A summary of the federal requirements for the design of the cast iron pipes are presented in a following section.

Additional loads associated with ground deformations and environmental factors should also be taken into account in the calculation of the circumferential and axial pipe stresses. These stresses may result from temperature changes, dynamic loads due to earthquakes and nearby blasting, soil movement and heave, and uplift pressure.

Stresses Due to Uplift Load

The rise of water table in flooded areas can result in a net upward force on the buried pipe when the buoyancy force exceeds the downward weights of the pipe and soil column above the pipe.

The largest upward force on a submerged straight pipe (F_b) per unit length of the pipe can be calculated as [51]:

$$F_b = W_w - [\, W_p + (\gamma_s\, h_s - \gamma_w\, h_w) D \qquad (6)$$

Where,

W_w Weight of water displaced by pipe

W_p Weight of pipe, D = Pipe diameter

γ_s and γ_w Unit weights of soil and water, respectively

h_s and h_w Height of soil and water above the pipe, respectively.

The bending stress induced in the pipe due to buoyancy [σ_b] can be approximated as (neglecting the resisting soil friction and cohesion at the pipe surface):

$$\sigma_b = \frac{F_b\, L^2}{10\, Z} \qquad (7)$$

Where,

L = pipe length in the buoyancy zone, and

Z = Pipe cross section modulus (I/D).

Stresses due to Temperature Change

The axial stress along the buried pipe due to temperature changes can be estimated by assuming the pipe is restrained from expansion at the end points. In this case, the maximum compressive thermal stress σ_t can be calculated as:

$$\sigma_t = E\, \alpha\, (T_2 - T_1) \qquad (8)$$

Where,

E Modulus of elasticity of the pipe (psi)

α Coefficient of thermal expansion (in/in/^{O}F)

$T_2 - T_1$ Maximum and installation temperatures, respectively (^{O}F).

Table 20 shows the coefficient of thermal expansion of the cast iron and other various materials.

Table 20. Coefficient of Thermal Expansion of Various Material

Material	Inches per inch 10^{-6} X per °F	Inches per 100′ of pipe per 100°F.
Cast iron	6.2	0.745
Concrete	5.5	0.66
Steel (mild)	6.5	0.780
Steel (stainless)	7.8	0.940
Copper	9.2	1.11
PVC (high impact)	55.6	6.68
ABS (type 1A)	56.2	6.75
Polyethylene (type 1)	94.5	11.4
Polyethylene (type 2)	83.3	10.0

Bending Stresses on the Cast Iron Pipe

Vertical loads on the pipe may also result in bending stresses along the length of the pipe when the underlying soil below the pipe is weak and allows for the pipe to deform (Figure 70). Flexural stresses in corroded cast iron pipe sections are evaluated in the finite element analysis of this project.

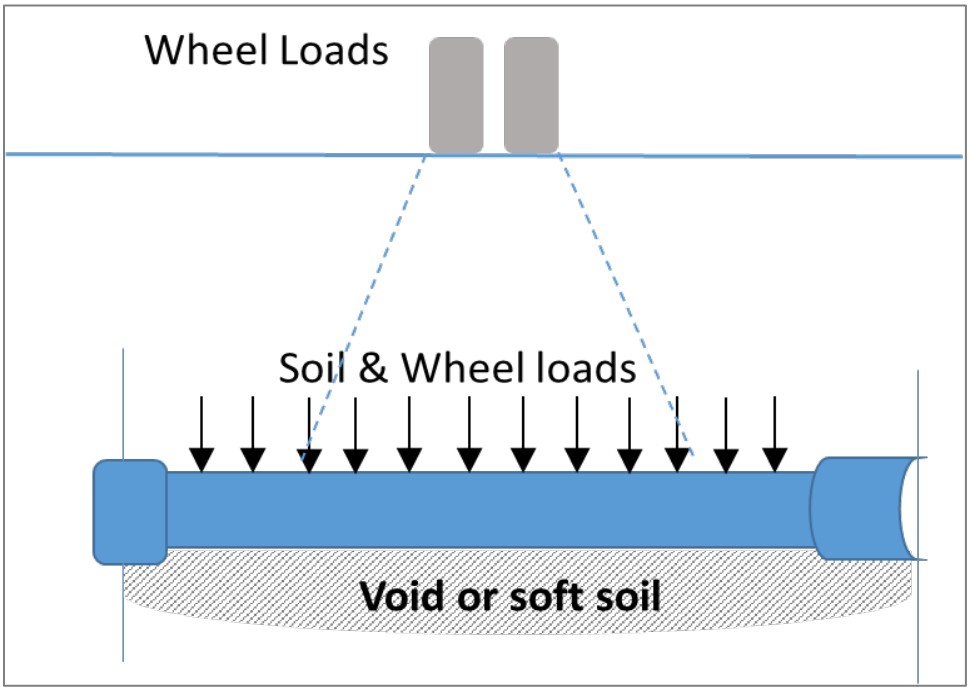

Figure 70. Loads on a pipe segment supported at end joints

Review of Design Codes for Cast Iron Pipes

CFR Title 49 - Part 192 of the Code of Federal Regulations provides additional requirements for the design and installation of cast iron pipes. These requirements are summarized as follows:

§ 192.275 Cast iron pipe:

(a) Each caulked bell and spigot joint in cast iron pipe must be sealed with mechanical leak clamps.
(b) Each mechanical joint in cast iron pipe must have a gasket made of a resilient material as the sealing medium. Each gasket must be suitably confined and retained under compression by a separate gland or follower ring.
(c) Cast iron pipe may not be joined by threaded joints.
(d) Cast iron pipe may not be joined by brazing.

§ 192.369 Service lines: Connections to cast iron or ductile iron mains:

(a) Each service line connected to a cast iron or ductile iron main must be connected by a mechanical clamp, by drilling and tapping the main, or by another method meeting the requirements of §192.273.
(b) If a threaded tap is inserted, the requirements of §192.151 (b) and (c) must also be met.

§ 192.373 Service lines: Cast iron and ductile iron:

(a) Cast or ductile iron pipe less than 6 inches (152 millimeters) in diameter may not be installed for service lines.
(b) If cast iron pipe or ductile iron pipe is installed for use as a service line, the part of the service line which extends through the building wall must be of steel pipe.
(c) A cast iron or ductile iron service line may not be installed in unstable soil or under a building.

§ 192.489 Remedial measures: Cast iron and ductile iron pipelines:

(a) General graphitization. Each segment of cast iron or ductile iron pipe on which general graphitization is found to a degree where a fracture or any leakage might result, must be replaced.
(b) Localized graphitization. Each segment of cast iron or ductile iron pipe on which localized graphitization is found to a degree where any leakage might result, must be replaced or repaired, or sealed by internal sealing methods adequate to prevent or arrest any leakage.

§ 192.557 Uprating:

(d) If records for cast iron or ductile iron pipeline facilities are not complete enough to determine stresses produced by internal pressure, trench loading, rolling loads, beam stresses, and other bending loads, in evaluating the level of safety of the pipeline when operating at the proposed increased pressure, the following procedures must be followed:

(1) In estimating the stresses, if the original laying conditions cannot be ascertained, the operator shall assume that cast iron pipe was supported on blocks with tamped backfill and that ductile iron pipe was laid without blocks with tamped backfill.

(2) Unless the actual maximum cover depth is known, the operator shall measure the actual cover in at least three places where the cover is most likely to be greatest and shall use the greatest cover measured.

(3) Unless the actual nominal wall thickness is known, the operator shall determine the wall thickness by cutting and measuring coupons from at least three separate pipe lengths. The coupons must be cut from pipe lengths in areas where the cover depth is most likely to be the greatest. The average of all measurements taken must be increased by the allowance indicated in Table 21:

Table 21. Pipe Wall Thickness Allowance

	Allowance inches (millimeters)		
	Cast iron pipe		
Pipe size inches (millimeters)	Pit cast pipe	Centrifugally cast pipe	Ductile iron pipe
3 to 8 (76 to 203)	0.075 (1.91)	0.065 (1.65)	0.065 (1.65)
10 to 12 (254 to 305)	0.08 (2.03)	0.07 (1.78)	0.07 (1.78)
14 to 24 (356 to 610)	0.08 (2.03)	0.08 (2.03)	0.075 (1.91)
30 to 42 (762 to 1067)	0.09 (2.29)	0.09 (2.29)	0.075 (1.91)
48 (1219)	0.09 (2.29)	0.09 (2.29)	0.08 (2.03)
54 to 60 (1372 to 1524)	0.09 (2.29)		

(4) For cast iron pipe, unless the pipe manufacturing process is known, the operator shall assume that the pipe is pit cast pipe with a bursting tensile strength of 11,000 psi (76 MPa) gage and a modulus of rupture of 31,000 psi (214 MPa) gage.

§ 192.621 Maximum allowable operating pressure: High-pressure distribution systems:

(3) 25 psi gage in segments of cast iron pipe in which there are unreinforced bell and spigot joints.

§ 192.753 Caulked bell and spigot joints:

(a) Each cast iron caulked bell and spigot joint that is subject to pressures of more than 25 psi gage must be sealed with:

(1) A mechanical leak clamp; or

(2) A material or device which:

(i) Does not reduce the flexibility of the joint;

(ii) Permanently bonds, either chemically or mechanically, or both, with the bell and spigot metal surfaces or adjacent pipe metal surfaces; and

(iii) Seals and bonds in a manner that meets the strength, environmental, and chemical compatibility requirements of §§192.53 (a) and (b) and 192.143.

(b) Each cast iron caulked bell and spigot joint that is subject to pressures of 25 psi (172kPa) gage or less and is exposed for any reason must be sealed by a means other than caulking.

§ 192.755 Protecting cast-iron pipelines:

When an operator has knowledge that the support for a segment of a buried cast-iron pipeline is disturbed:

(a) That segment of the pipeline must be protected, as necessary, against damage during the disturbance by:

(1) Vibrations from heavy construction equipment, trains, trucks, buses, or blasting;

(2) Impact forces by vehicles;

(3) Earth movement;

(4) Apparent future excavations near the pipeline; or

(5) Other foreseeable outside forces which may subject that segment of the pipeline to bending stress.

(b) As soon as feasible, appropriate steps must be taken to provide permanent protection for the disturbed segment from damage that might result from external loads, including compliance with applicable requirements of §§192.317(a), 192.319, and 192.361(b)–(d).

4. Characterization of Graphitic Corrosion Severity

This section of the report provides a general set of guidelines an operator will use to characterize the type and severity of graphitic corrosion on a cast iron pipeline in the field.

This will allow the operator to consistently and reliably develop part of the input data needed to run the FFS cast iron model.

Addition details on cast iron and cast iron pipe metallurgy and field corrosion have already been included in **Section 2** of this report and these details have not been repeated in this section.

General Approach

The first thing that must be emphasized in any discussion of the detection of graphitic corrosion is that cast iron (CI) pipes with severe graphitic corrosion are often not readily obvious after excavation. The original pipe diameter and contour are often still present.

Graphitic corrosion is light gray in color (see Figure 71), not reddish like rust. As a general rule if any CI pipe is excavated, it should be tested with a dull knife to see if the surface is hard or can be chipped out like clay. When a corrosion assessment is to be performed it is usually desirable to grit blast to get down to clean metal, see Figure 72. Because blasting is not being done to produce a surface profile lower than normal blasting air pressure can be used.

If grit blasting is not an option, then a stiff wire brush on an angle grinder can be used. Care must be taken here because too aggressive of an abrasive on a power tool will remove sound metal which should be avoided.

An exception to the need for surface preparation would be pulsed eddy current testing, or some other electromagnetic method that can measure sound metal thickness and not count the graphite sponge that results from graphitic corrosion.

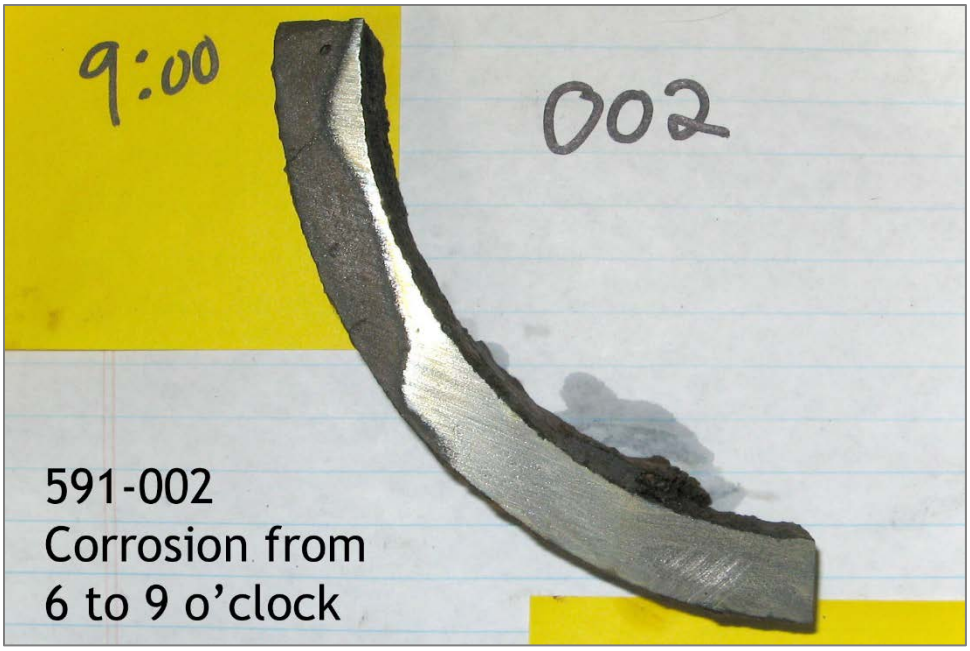

Figure 71. Original pipe contour and thickness is maintained in region of graphitic corrosion (darker color wall)

Figure 72. Severely corroded CI pipe after grit blasting

Possible methods for the measurement of graphitic corrosion are described below.

Pit Gauges

A pit gauge of the simplest type is shown below in Figure 73. This type of instrument does not provide as accurate a reading as a dial gauge with a bridge bar.

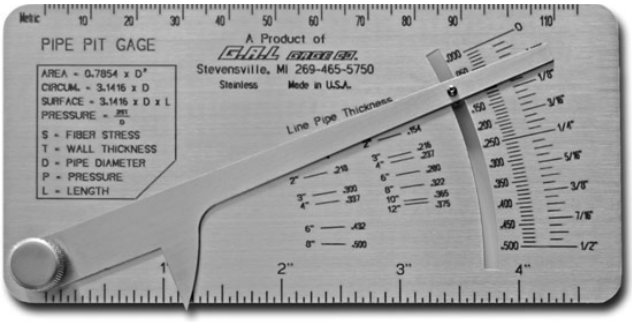

Figure 73. Basic Pit Gauge

The measured pit must be bridged over with the straight edge flush against a non-pitted surface and oriented along the pipes axis. The pointer is then depressed into the deepest part of the pit and the depth read from the scale. Where large pitted areas are present this type of gauge is unusable. A more sophisticated variation is the bridging pit gauge shown in Figure 74.

Figure 74. Bridging Pit Gauge

This type of pit gauge is preferred when use is possible. It is held to the pipe by magnets and can be rotated around the pipe's circumference at any chosen interval. Similarly, the rail has ruler marks to position the dial indicator. Bridge rail lengths of over 2 feet are

available. A disadvantage of this type of device compared to a hand-held gauge is that some of the deeper pits may not be measured depending on the rails positioning.

Ultrasonic Thickness Testing

Ultrasonic thickness (UT) testing is commonplace in measuring the wall thickness of steel pipe but its use is problematic for cast iron pipe, especially the common gray iron pipe.

If the velocity of sound is known for the tested material, then a pipe's wall thickness can simply be calculated by the travel time of a UT signal. However, while the velocity of sound is nearly invariant in practical terms for all steel grades it is highly variable among cast irons, a composite material. The percent graphite and the graphite shape both strongly affect velocity. These two properties are both highly variable in the CI pipe population.

It has been suggested that prior to thickness measurement a particular pipes velocity could be measured along the surface by sending a signal across a known distance [52]. This does not take into consideration that graphite flake size and distribution are usually much different (finer) near a pipe's surface than towards mid wall.

Pulsed Eddy Current Broadband Electromagnetic Testing (PEC-BEM)

BEM is a variation of pulsed eddy current testing where an external pulsed electromagnetic field is used to induce eddy currents in a pipe. The detected eddy currents and their decay is compared to a reference model based on the pipe's dimensions and composition. On this basis wall thickness can be estimated. The advantages of the BEM technique are that no direct contact with the pipe is necessary, coatings and corrosion products do not have to be removed, and several instrument configurations are available, full encirclement, in-line pigs, hand held, and a keyhole inspection device.

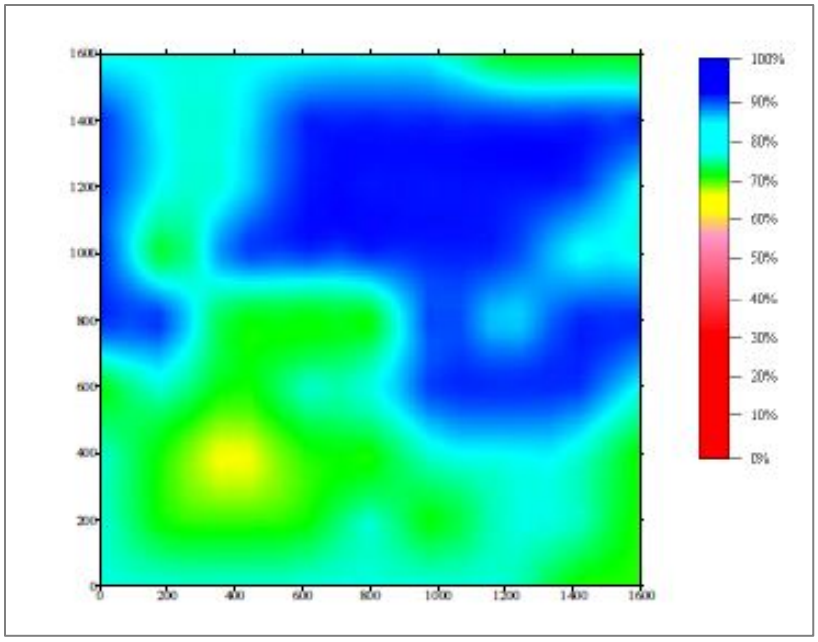

Figure 75. BEM signal intensity color contour plot, X-axis longitudinal location Y-axis circumferential location. % thickness by color...

Optical Methods

Two very similar optical methods for determining corrosion pitting are laser 3D scanning (e.g., Handyscan 3D, Creaform 3D) and structured light scanning (e.g. Seikowave). Both techniques have been steadily improving in recent years and are now reported to be capable of automatic image stitching along and around a pipe. Figure 76 is an example output from a laser scan of a pipe surface.

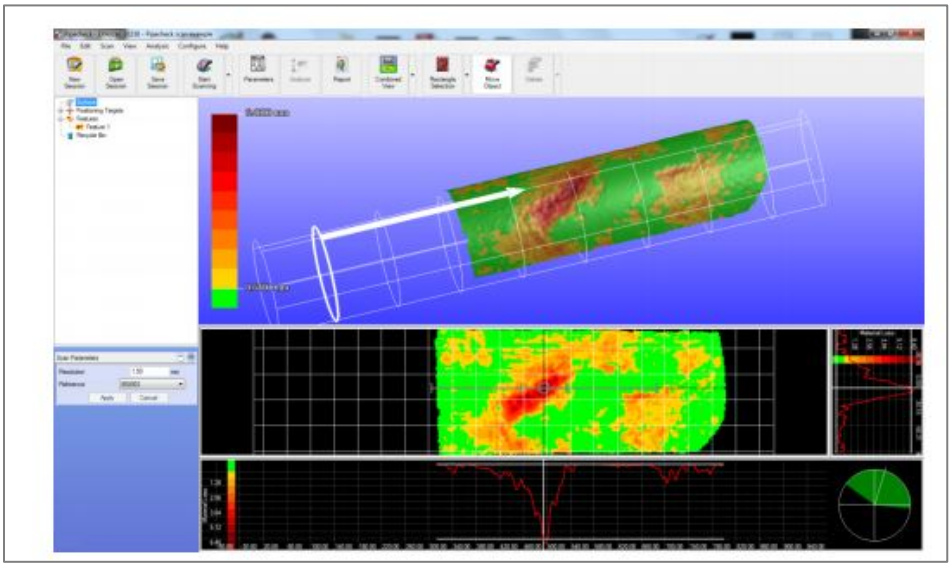

Figure 76. 2D to 3D laser scan produced by Creaform laser scanner and software

Both systems are available with software that can import the mesh data and interpret it per B31G or RSTRENG rules, including procedures on when to combine defects. Operators should be aware that optical methods require a clean, grit blasted surface in order to produce good results.

It is not the objective of this section to fully report on all the specific technical options to measure corrosion defects. These technologies progress and change over time. Rather, the remainder of the section will focus on what needs to be measured and how adjacent corrosion defects should be measured and interpreted. The objective is to get a reproducible and reliable measurement of graphitic corrosion wall loss in a form that can be input into the developed Fitness For Service (FFS) model.

Data Reporting Requirements

API 579-1/ASME FFS-1

API 579-1/ASME FFS-1 [53] provides detailed descriptions of how local thinned areas are to be measured, when separated defects should be combined, and how defect length is to be measured.

Not all of this procedure is applicable to cast iron distribution pipes because it is focused on use with internal pressures where the maximum stress is the hoop stress. In addition, steel differs from cast iron in that it is equally strong in tension and compression where CI is markedly lower in strength in tension than compression, as explained in Section 2 of this report.

While its treatment of longitudinal defects is very conservative, it may not be the case of bending stresses on CI pipe. For these reasons the procedure for reporting thickness readings may differ in some respects from API 579/ASME FFS-1.

API 579/ASME FFS-1 describes three general methods for assessing metal loss: Part 4 is to be used for the assessment of general loss, Part 5 for local metal loss and Part 6 for the assessment of pitting corrosion.

The standard recommends that the procedure in part 4 be used for most evaluations and part 5 only to reduce the conservatism in the analysis.

Part 6 on pitting corrosion is not applicable to graphitic corrosion.

The method to be recommended for use with the Cast Iron FFS model then is based on Part 4.

Measurement Considerations

The data collection process for the graphitic corrosion length, width, and depth as well as pipe thickness is an important step. Repeatable methods should be used, and when appropriate is to be conducted by a trained/certified technician.

Inspection Guidelines

Per paragraph 4.3.3.1 of the API/ASME standard, two options for obtaining thickness data are presented:

- Point thickness readings only, and
- Thickness profiles which should be used if there is significant variation in the thickness readings.

Per the standard, thickness profiles must be used unless the Coefficient of Variation (CV) is proved to be 10% or less.

This procedure will therefore use thickness profiles on a dimensional grid to characterize the remaining thickness and size of the region of metal loss due to graphitic corrosion. The procedure can be used on the outside or inside of the pipe surface since the effect of metal loss on the inside and outside is the same [54].

Per the standard the following procedure shall be used to determine the required inspection locations and the Critical Thickness Profiles (CTP).

1. **STEP 1** - Locate the region of metal loss and determine the location, orientation and length of the inspection planes.
2. **STEP 2** - Determine the critical inspection planes. For cast iron pipe both longitudinal and circumferential planes are critical.
3. **STEP 3** - Mark the inspection planes on the pipe surface.
4. **STEP 4** - Determine the uniform thickness away from the local metal loss t_{rd}.
5. **STEP 5** - Measure and record thickness readings along each inspection plane and determine the minimum measured wall thickness t_{mm}, see Figure 77 (figure 4.6a from API 579-1/ASME FFS-1).

a. The spacing distance for thickness readings (the grid) should allow for an accurate characterization of the thickness profile.

b. A guideline is that the spacing should be done in a manner that the path of minimum measured thickness (t_{mm}) can be determined in both the longitudinal and circumferential directions (explained in STEP 6 below).

6. **STEP 6** - Determine the Critical Thickness Profile (**CTP**) in the longitudinal and circumferential directions.

   a. The CTP in each direction is determined by projecting the minimum remaining thickness for each position along all parallel inspection planes onto a common plane as shown in Figure 78 (figure 4.6a from API 579-1/ASME FFS-1) and Figure 79 (figure 4.6c from API 579-1/ASME FFS-1). These also show the corroded wall thickness, t_c.

   b. One can see in these two figures that there are two planes of minimum thickness, one for the circumferential (dotted line C) and one for the longitudinal (solid line M) direction.

   c. The length of the profile is established by determining the end point locations where the remaining wall thickness is greater than the uniform thickness away from local metal loss, t_{rd}, in both the longitudinal and circumferential directions. Note, t_{rd}, can be less than the nominal, t_{nom}, (non-corroded) wall thickness away from the local areas of metal loss. This is a determination that must be made in the field with careful measurements made in and around areas of metal loss.

   d. If there are multiple flaws in close proximity to one another, then the size of the flaw to be used in the assessment is established considering the effects of neighboring flaws using the *intersecting box methodology* shown in Figure 80 (figure 4.7 in API 579-1/ASME FFS-1).

   e. The final CTP can be established as shown in Figure 81 (figure 4.8 in API 579-1/FFS-1).

   f. The thickness profile for both the longitudinal and circumferential planes should be evaluated in this manner.

7. **Step 7** – The operator will also record the measurements in a way to determine the axial direction of the pipe relative to the measurements.

   a. This can be a simple annotation on the drawing of the pipe's center line as shown in Figure 77.

b. This information will be needed to determine the angle of the overall wall loss measurement relative to the pipe's axial direction, in degrees.

The above process will provide the graphitic corrosion defect (wall loss): length, depth, and width and orientation of the wall loss relative to the pipe's axial directions. These measurements along with the pipe's diameter, nominal thickness, and class (strength/grade) are the inputs to the CI FFS model.

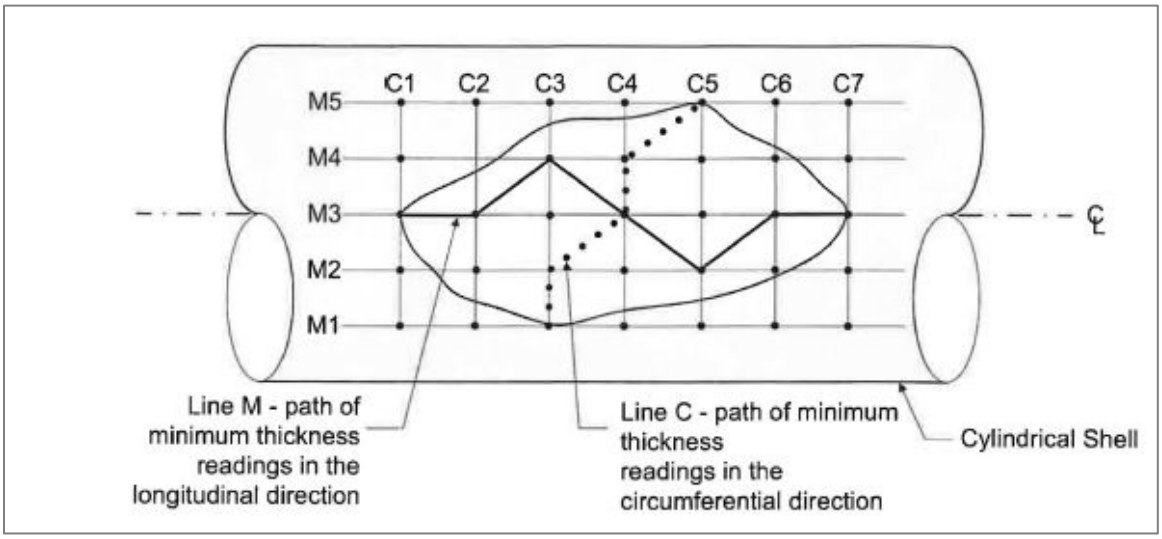

Figure 77. Inspection planes per API 579-1/FFS-1 fig 4.6a and the critical thickness profiles

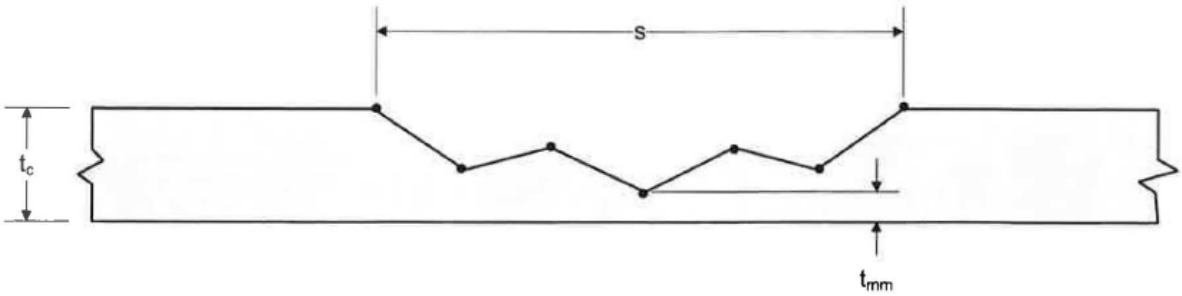

Figure 78. Critical Thickness Profile (CTP) – Longitudinal Plane (Projection of Line M) API 579-1/FFS-1 fig 4.6b

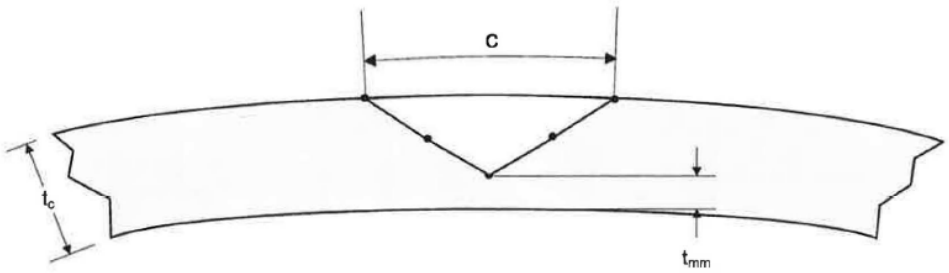

Figure 79. Critical Thickness Profile (CTP) – Circumferential Plane (Projection of Line C) API 579-1/FFS-1 fig 4.6c

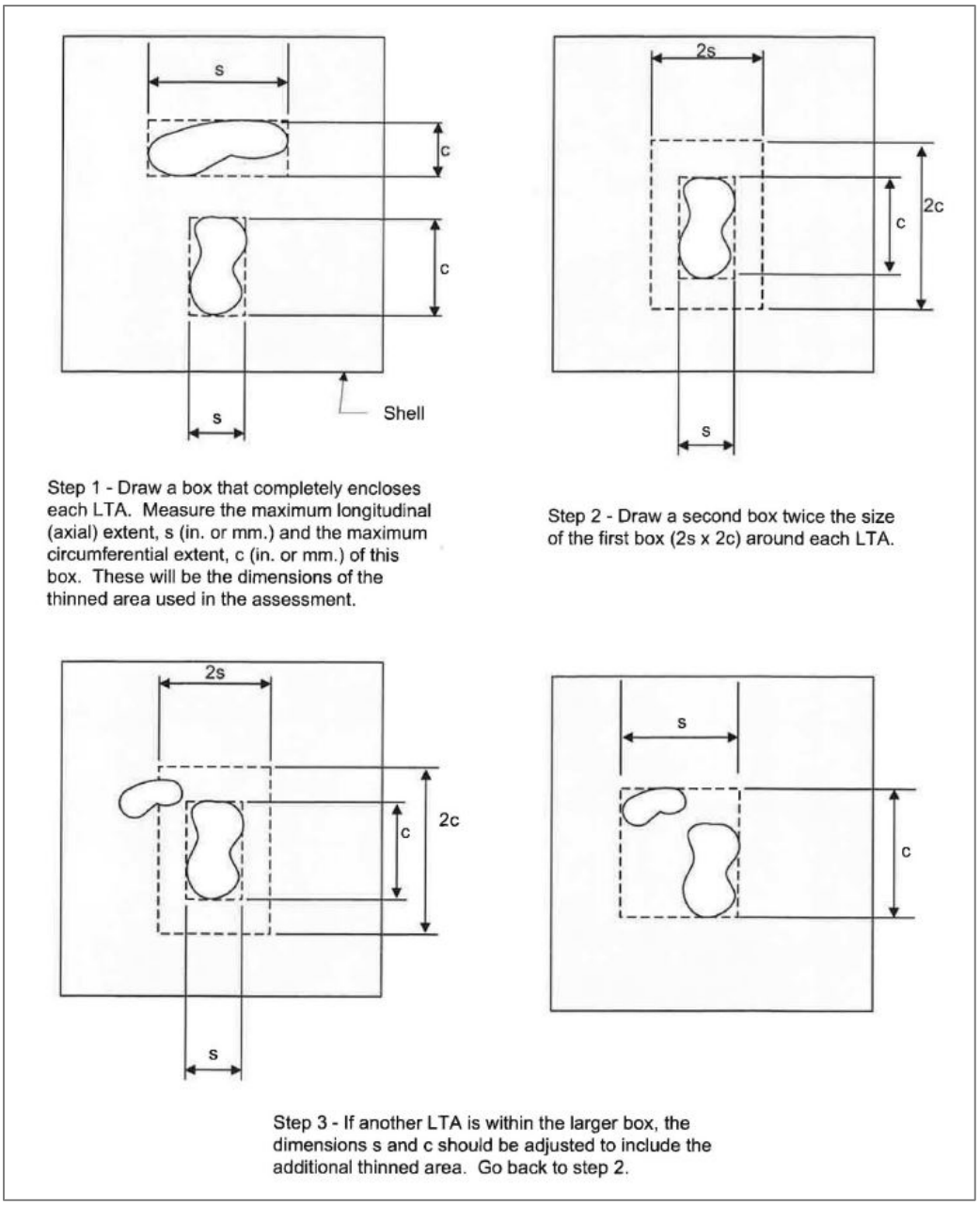

Figure 80. Combining and resizing flaws per API 579-1/ASME FFS-1 fig 4.7

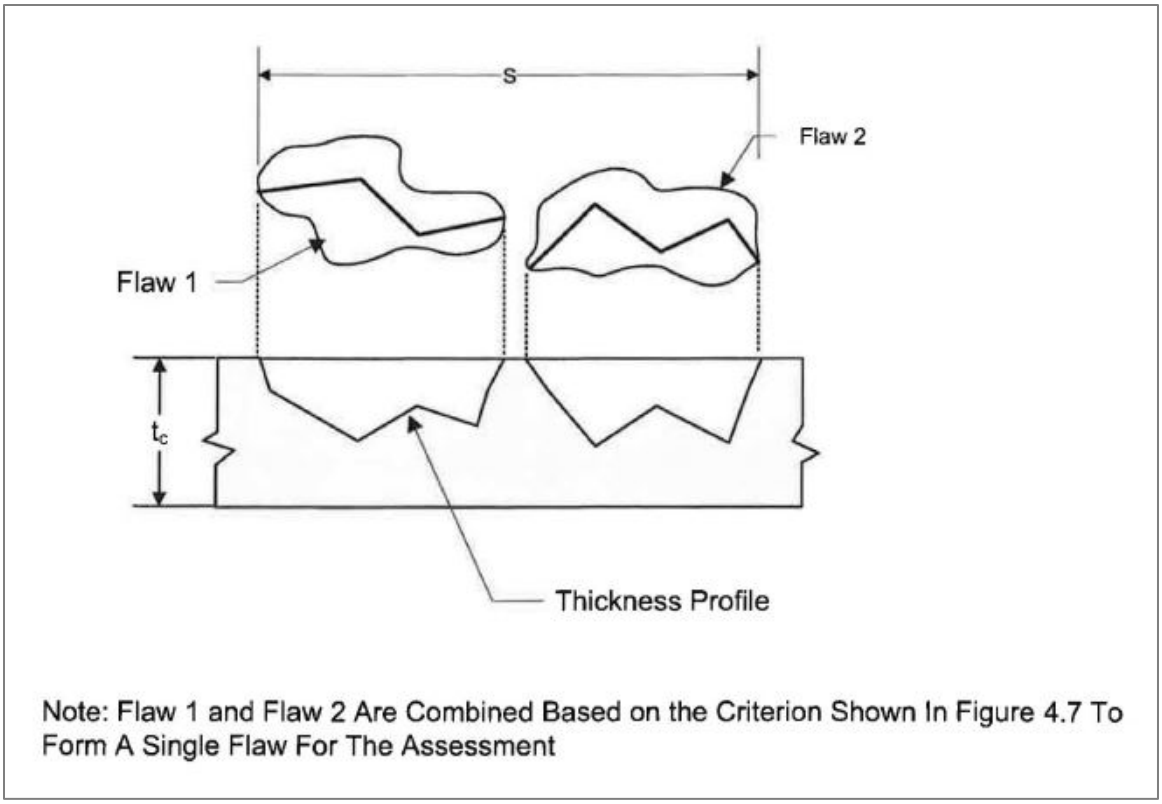

Figure 81. Sizing of a network of flaws from API 579-1/ASME FFS-1 fig 4.8

5. Fitness for Service (FFS) Model of Characterized Graphitic Corrosion

This section reports the development of a Fitness-For-Service (FFS) model for cast iron piping systems with graphitic corrosion defects. This FFS model can be used to determine the critical defect size and characteristics that could lead to premature piping failure.

A nonlinear, 3D finite element (FE) model, simulating a single pipe span was utilized as the basis for the Fitness-For-Service (FFS) model. A Design of Experiment (DoE) method was used to produce response surfaces from the FE simulation results that can predict the maximum ligament stress in pipes with and without wall loss.

Two simulation spaces were evaluated – Simulation Space 1 (SS1) for a pipe segment without a flaw, and Simulation Space 2 (SS2) for a pipe segment with a flaw. Eight response surfaces were generated from the two simulation spaces, covering different combination of flaw geometry and axial restraint conditions.

An Excel-based, user calculator produced utilizes the 97.5% upper prediction limit (UPL) of the response surfaces described in this report. The user manual for this calculator is provided in **Appendix B**.

General Approach

A nonlinear, 3D finite element (FE) model, simulating a single pipe span was utilized as the basis for the Fitness-For-Service (FFS) model. A Design of Experiment (DoE) method was used to produce response surfaces from the FE simulation results that can predict the maximum ligament stress in pipes with and without wall loss. The final simulation approach had two simulation spaces:

1. Simulation of a pipe span without wall loss.
2. Simulation of a pipe span with wall loss.

The simulation spaces described above are herein referred to as Simulation Space 1 (SS1) and Simulation Space 2 (SS2). Further details of these simulation spaces are provided in this section.

A Microsoft Excel based calculator utilizing 97.5% upper prediction limit (UPL) of the response surfaces described in this report was produced during this project. The calculator takes user inputs of pipe geometry, flaw geometry, and loading conditions and outputs the maximum stress. The user manual for this calculator is provided in **Appendix B**.

Experiment Design

The Design of Experiment (DoE) method was used to generate the appropriate combination of geometric input variables in order to fit a cubic response surface to the results from the FEAs. For every geometric configuration, the boundary conditions (e.g. bearing load and temperature change) were swept through several combinations covering their specified ranges. All DoE matrixes were based on a face-centered cubic design with no replicates (due to the deterministic nature of FEA results).

The relatively large number of parameters defining the geometry, load cases, and material properties of a single span of pipe leads to a very large design-of-experiment (DoE) design, well in excess of 2,000 simulations. The experiment designs under this project were limited in scope in order to meet budget limitations, however, the designs can be readily augmented at a later stage.

The input parameters, parameter ranges, and number of results per response surface are detailed in this section.

Boundary Conditions

Figure 82 illustrates the boundary conditions defined in the FE model. The pipe ends have a "rigid connector" constraint that allows the end face to rotate about the virtual centroid of the pipe cross-section, while limiting the x-y-z displacement of that centroid to zero. In the case of no axial restrain, the centroid of one of the ends is free to move in the direction of the pipe's longitudinal axis. In cases where thermal contraction was evaluated, the centroids at both ends had fixed displacements.

External bearing load and temperature change (in axially restrained cases) were swept in each simulation run to get all load combinations. The external bearing load was applied as a uniform pressure on the entire length of the pipe, on the opposite side of the flaw.

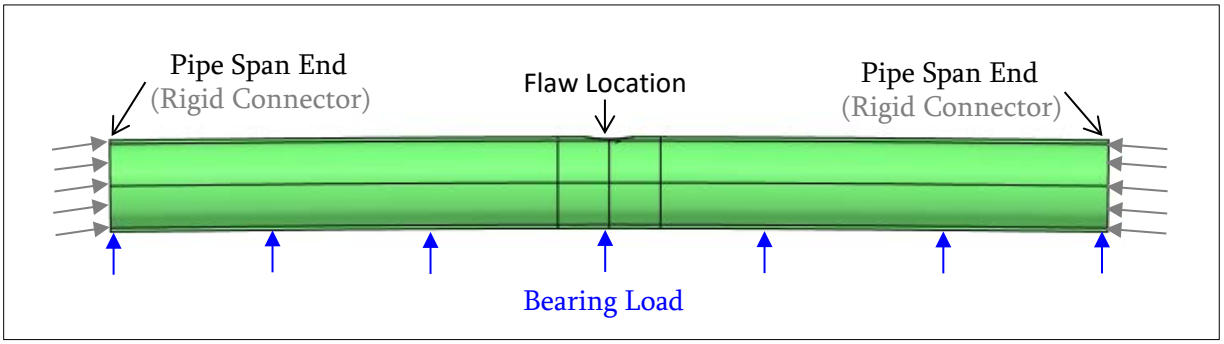

Figure 82. FE model boundary conditions

Modeling of Material Loss

The FE model has a parametrically defined volume of material loss. The flaw had a rectangular cross-section and was adjustable by three parameters: depth, width, and length, as shown in Figure 83. The rectangular cross-section was defined by the depth and length was revolved around the circumference with an arc length defined by the width. A rectangular cross-section was used since it creates the highest stress concentrations and, therefore, represents the most conservative geometric assumption. Defining the wall loss in terms of depth, width and length also aligns with the API 579-1/ASME FFS-1 approach for measuring wall loss.

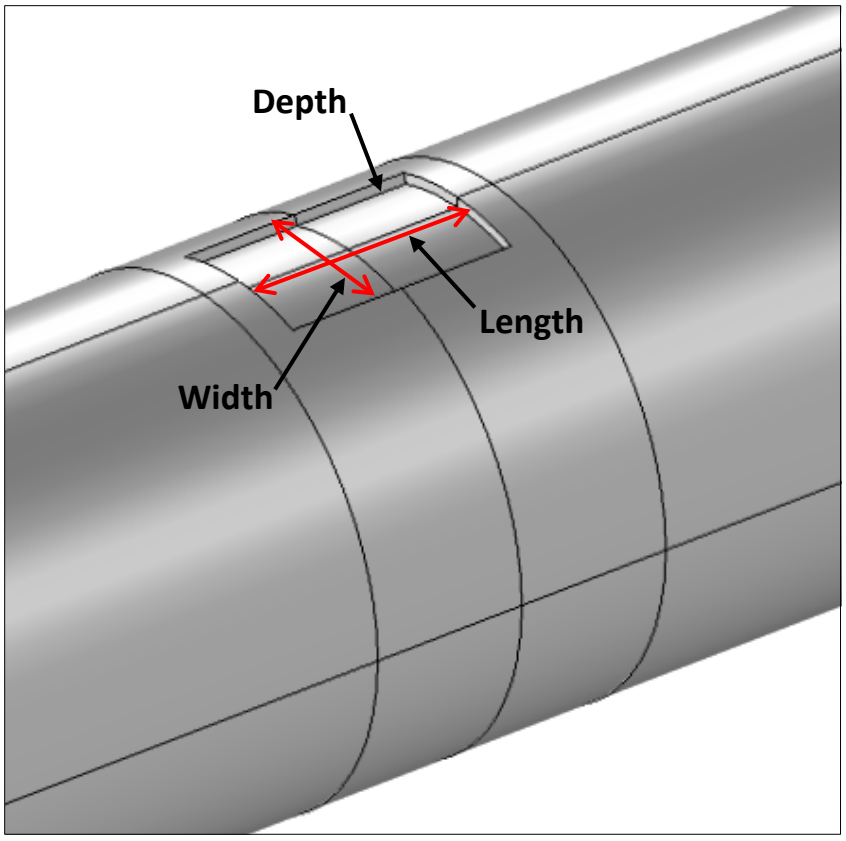

Figure 83. Schematic of flaw geometry and its defining parameters

The flaw geometry parameters were defined in the analyses as follows:

- Flaw depth as percent of pipe wall thickness
- Flaw length as a normalized parameter based on pipe diameter and wall thickness
- Flaw width as percent of pipe outer circumference

The units and ranges of the flaw parameters used in the FE analyses are shown in Table 22.

Table 22. Flaw geometry parameters and ranges used in FEA

	Units	Lower Value	Upper Value
Outer Diameter	in	4.8	13.2
Flaw Depth	% of WT	5	80
Flaw Length	C	0.1	3
Flaw Width	% of Pipe Circumference	5	49

Flaw length was defined by a normalization parameter C so that the length scales with pipe diameter and wall thickness, which is better suited for fitting a response surface that covers a wide range of geometries. The flaw length normalization parameter is defined below:

$$L = C\sqrt{Dt} \rightarrow C = \frac{L}{\sqrt{Dt}}$$

Where,
L = flaw length [in],
C = normalization parameter,
D = outer diameter of pipe [in],
t = pipe wall thickness [in].

For general reference, Figure 84 through Figure 87 show various flaw configurations and their respective meshes.

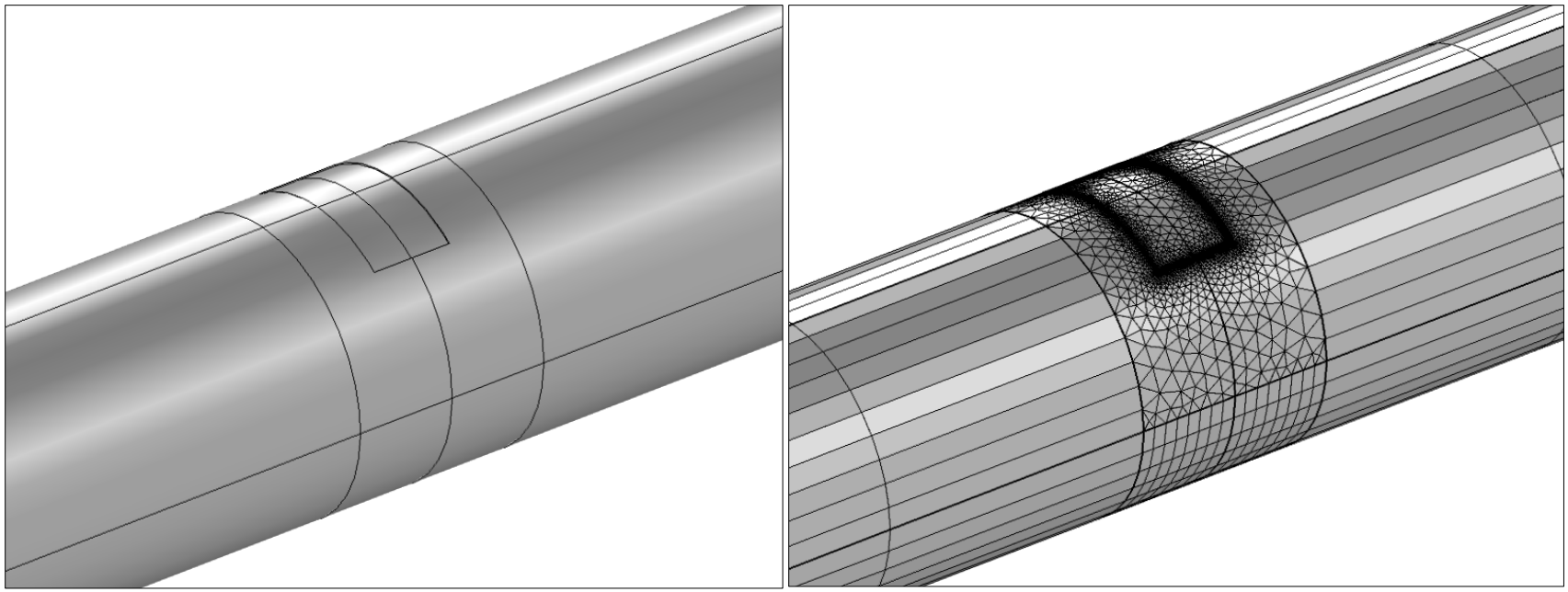

Figure 84. Geometry and mesh for Depth=5%, Length=1, Width=20%

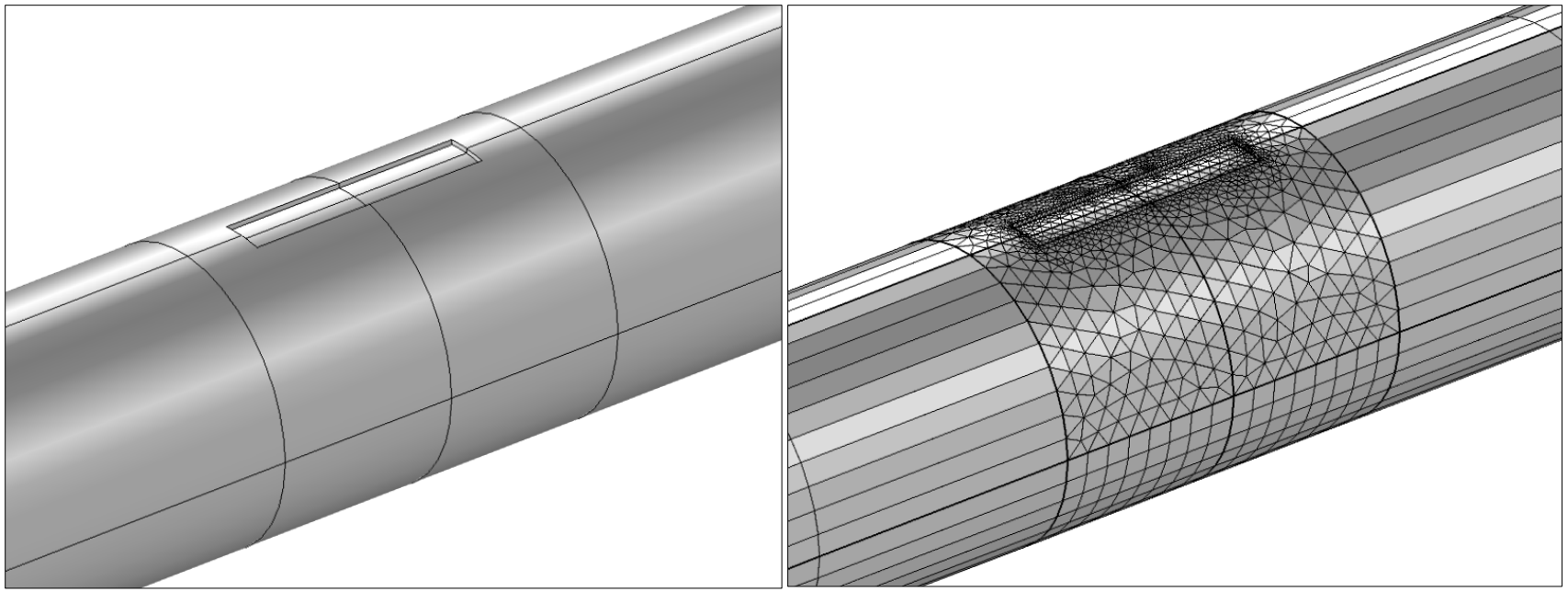

Figure 85. Geometry and mesh for Depth=20%, Length=3, Width=5%

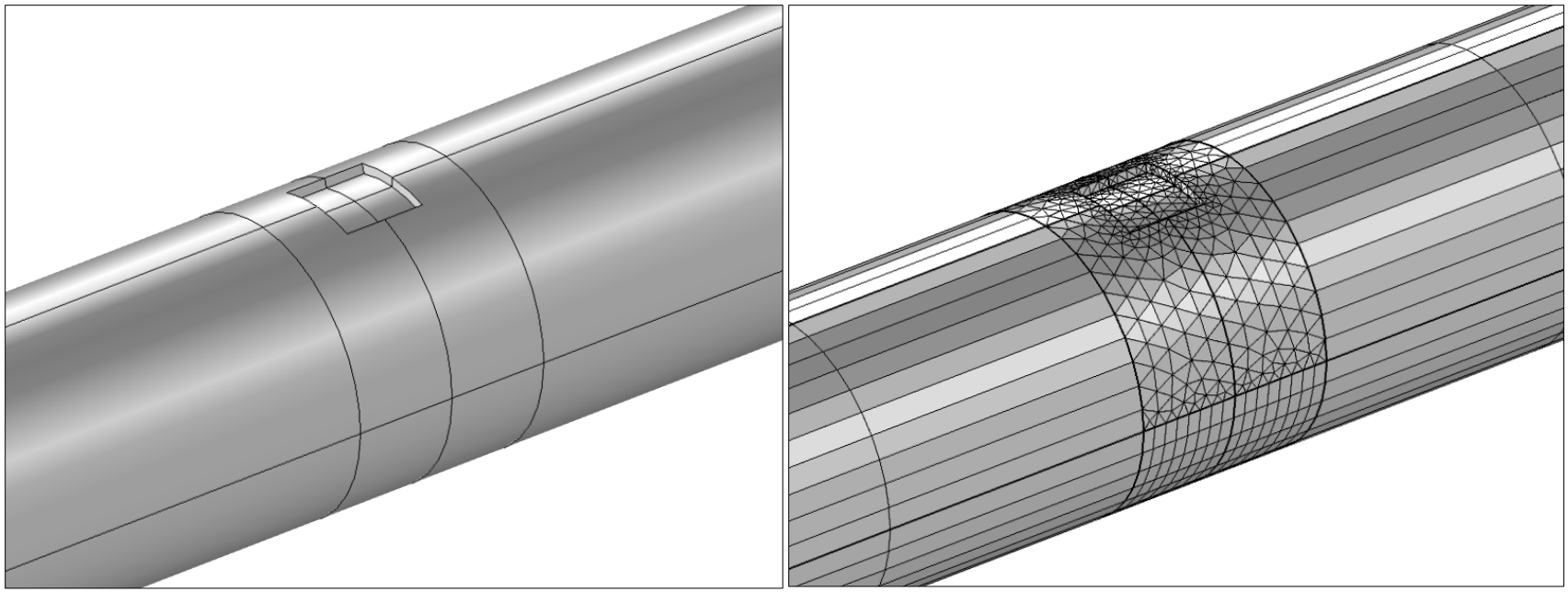

Figure 86. Geometry and mesh for Depth=40%, Length=1, Width=10%

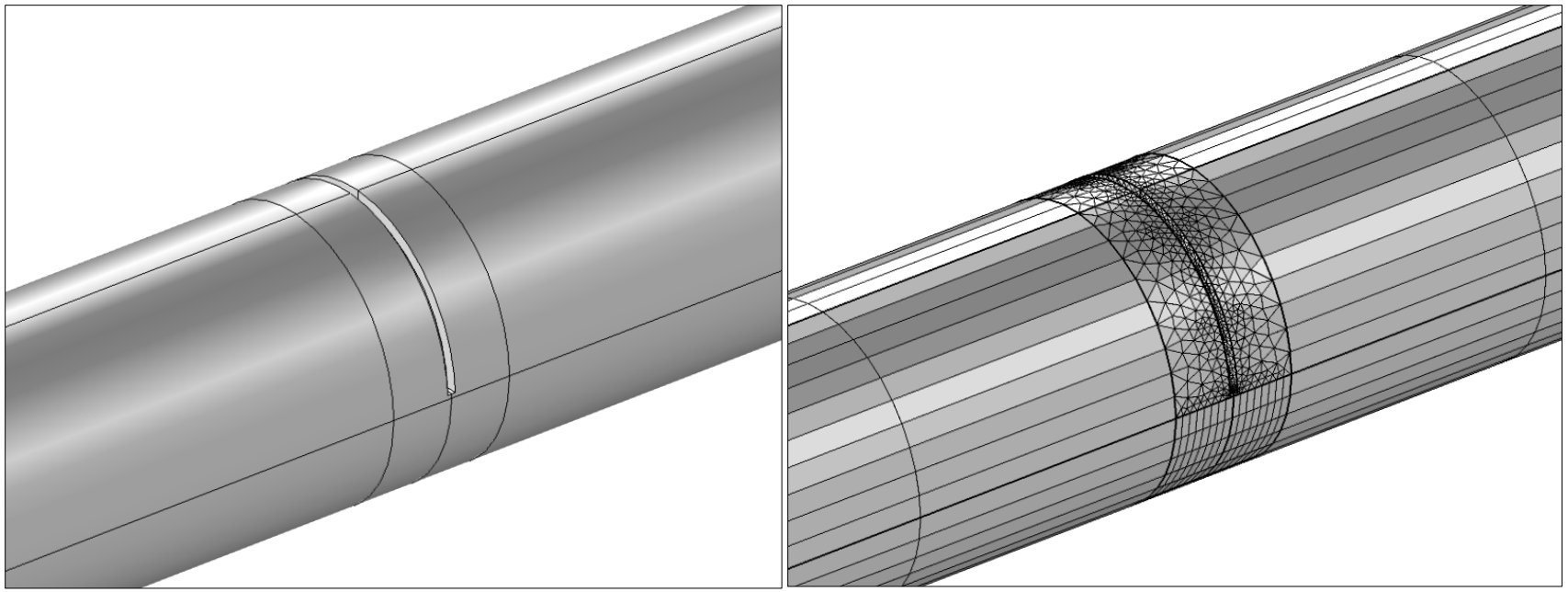

Figure 87. Geometry and mesh for Depth=50%, Length=0.1, Width=49%

Material Properties

Previous works regarding the material properties of cast iron have included discussions of the applicability of a linear material model [55, 56]. Since cast iron has a nonlinear stress-strain response, as well as different responses in tension and compression, the FE model developed here uses nonlinear stress-strain data or analytical curve fits. Furthermore, different curves for tension and compression can be input, which is relevant in bending loads where both tensile and compressive stresses are present.

Figure 88 shows an example of a nonlinear stress-strain curve that includes the different responses in tension and compression.

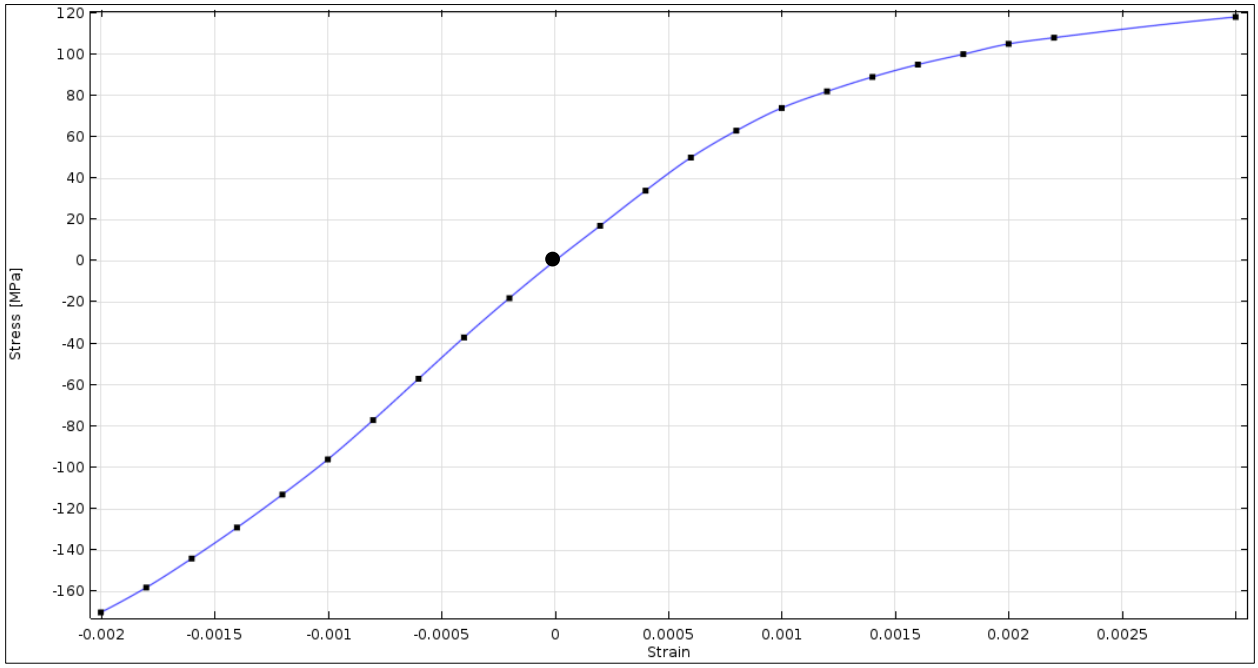

Figure 88. Nonlinear true stress-strain curve, with different responses in tension and compression

The ability of the simulation to utilize the stress-strain curve in Figure 88 was verified by simulating simple pipe bending. Figure 89 shows a first principal stress plot of this simulation, which illustrates the portions of the pipe and tension and compression, and Figure 90 shows the stress-strain results at two different probe locations. As can be seen in Figure 90, the simulated stress-strain response at different bending strains matches the input stress-strain curve, as expected.

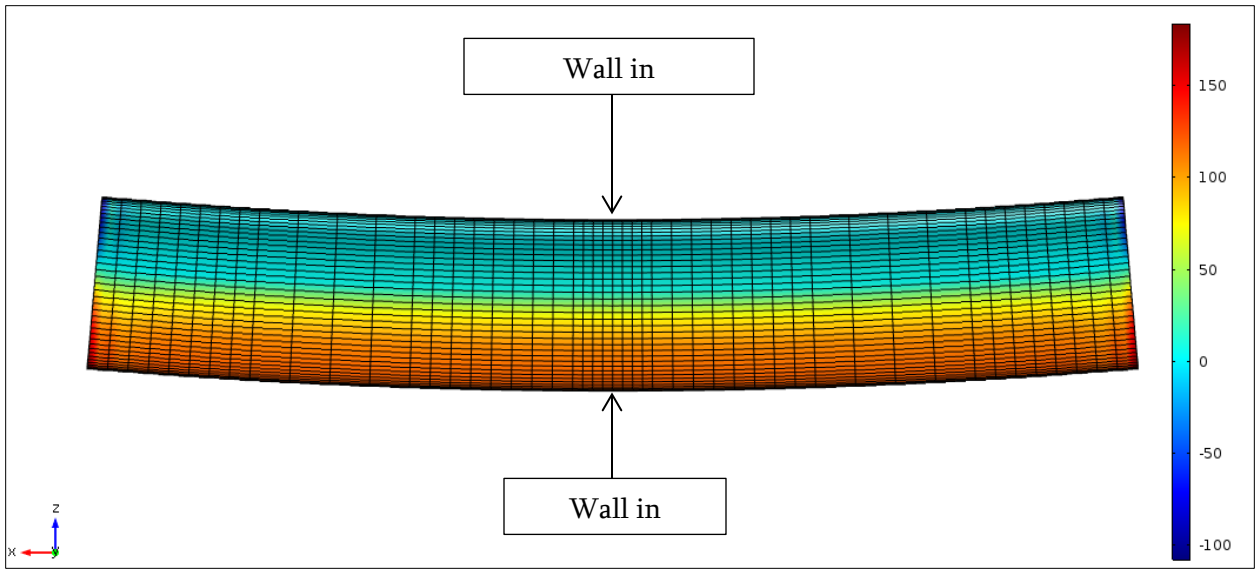

Figure 89. First principal stress plot showing a pipe span under simple bending

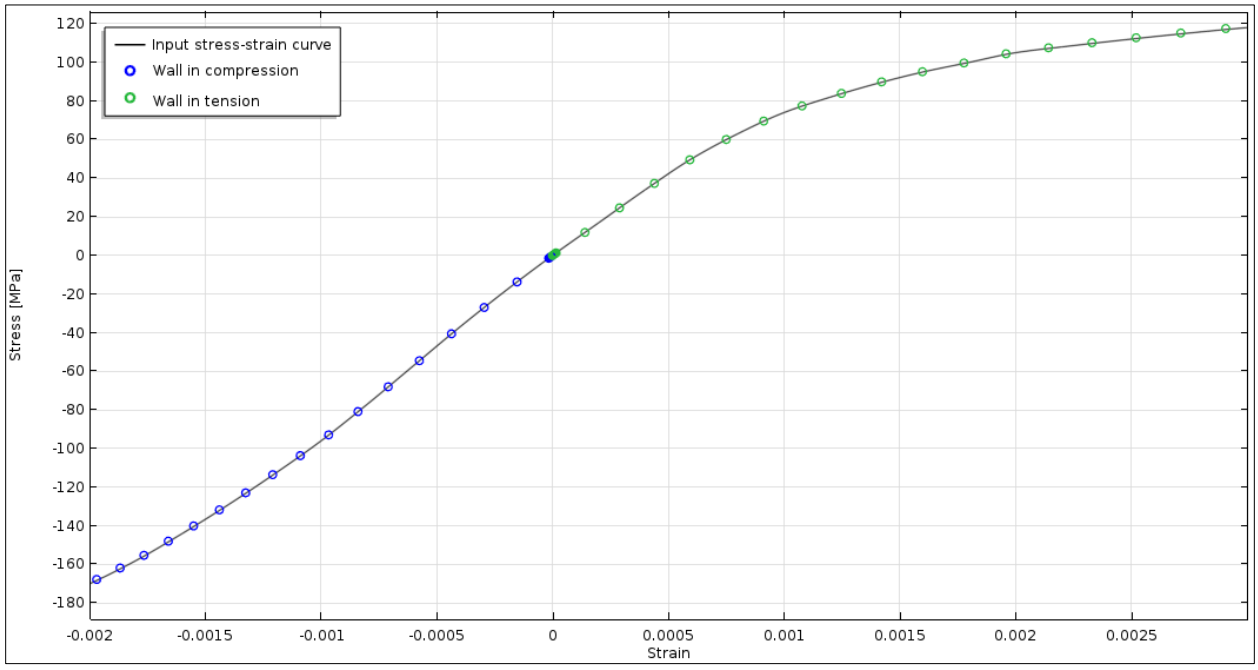

Figure 90. Simulation stress values following the input stress-strain curves at different tension and compression strains

The analysis results used in the final calculator response surfaces are based on the stress-strain curves shown in Figure 91. Because stress-strain curves for cast-iron are uncommon, extrapolation from the two available curves (class 20 and class 40) was necessary, given that the scope of this project covers cast-iron classes 10, 20, 30, 40, 50, and 60. An extrapolation method using Ramberg-Osgood curve fitting was initially envisioned, however, a direct linear interpolation/extrapolation from the available class 20 and class 40 curves was ultimately used.

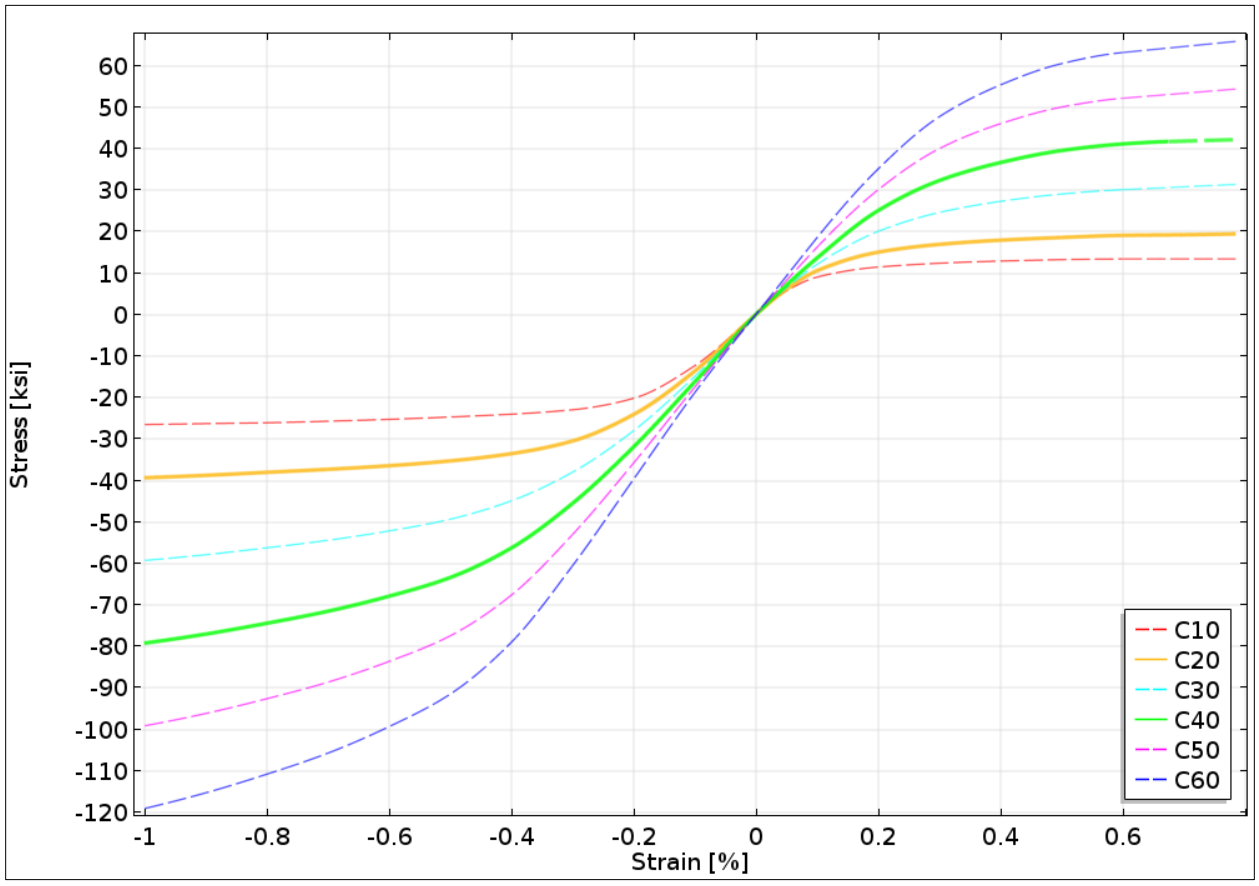

Figure 91. True stress-strain curves for classes 10 through 60, as used in FEA. Dashed curves are extrapolated or interpolated.

Overview of FEA Results and Selected Responses

For general reference, Figure 92 through Figure 97 show typical first principal stress plots under different loading conditions. The first principal stress is an accepted stress criterion for brittle materials and has been used in previous work where cast-iron was simulated in FEA. The selected responses for all design spaces was the maximum first principal stress in the area of the flaw and average first principal stress on a radial line at the center of the pipe (see Figure 98). The radial line at the center of the pipe span was selected for the following reasons:

- The center of the pipe undergoes the greatest strain,
- The probe is located at the center of the modeled flaw and therefore,
    - Gives a measurement at the point of minimum wall thickness,
    - Gives a consistent location for probing the stress regardless of flaw geometry.

In the context of the simulated geometry, the location of absolute maximum first principal stress varies according to flaw geometry and will typically be at the edge of the flaw where stress intensification occurs due to the (artificially) sharp change in wall thickness.

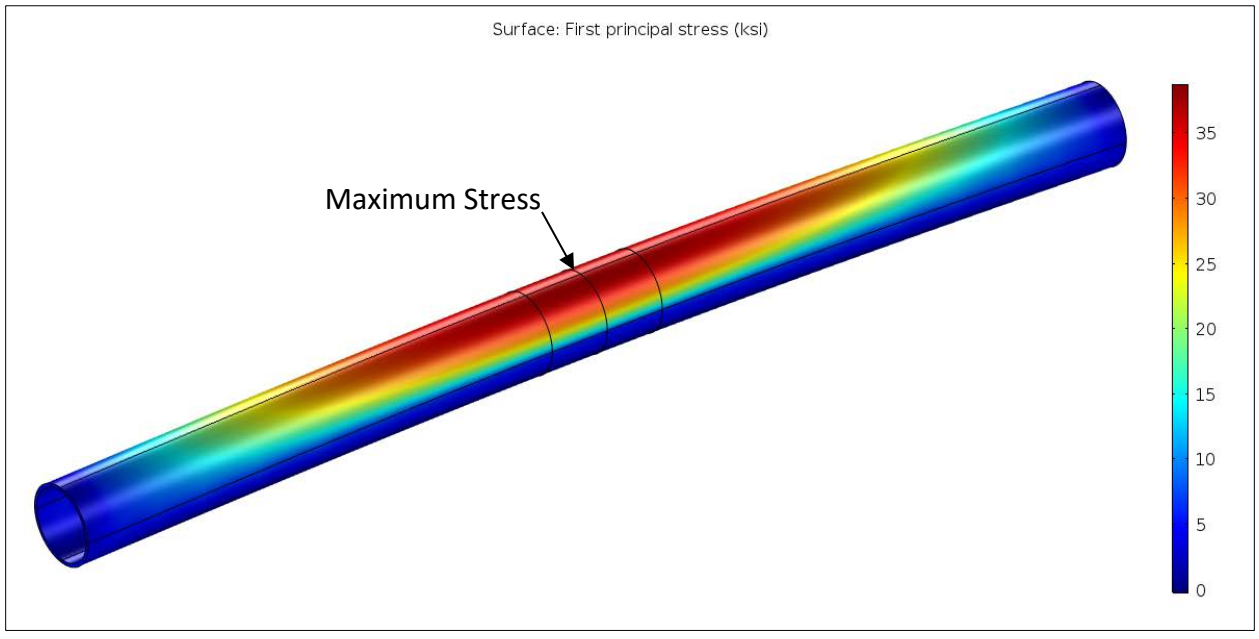

Figure 92. Pipe under bending, axially unrestrained end

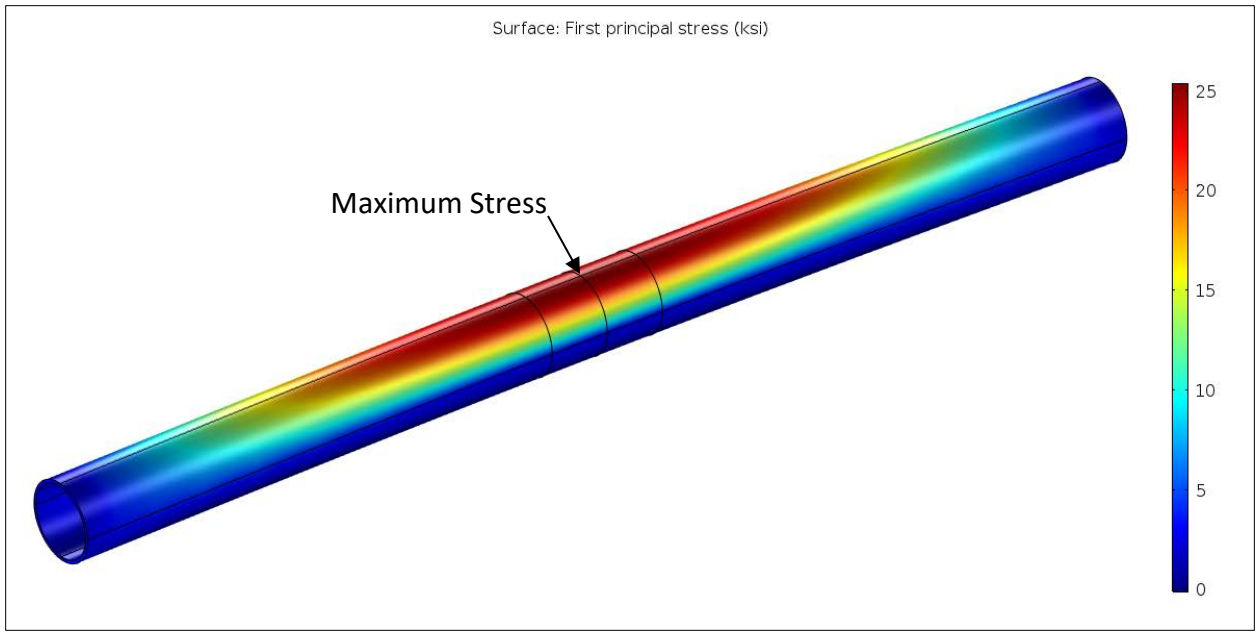

Figure 93. Pipe under bending, axially restrained ends

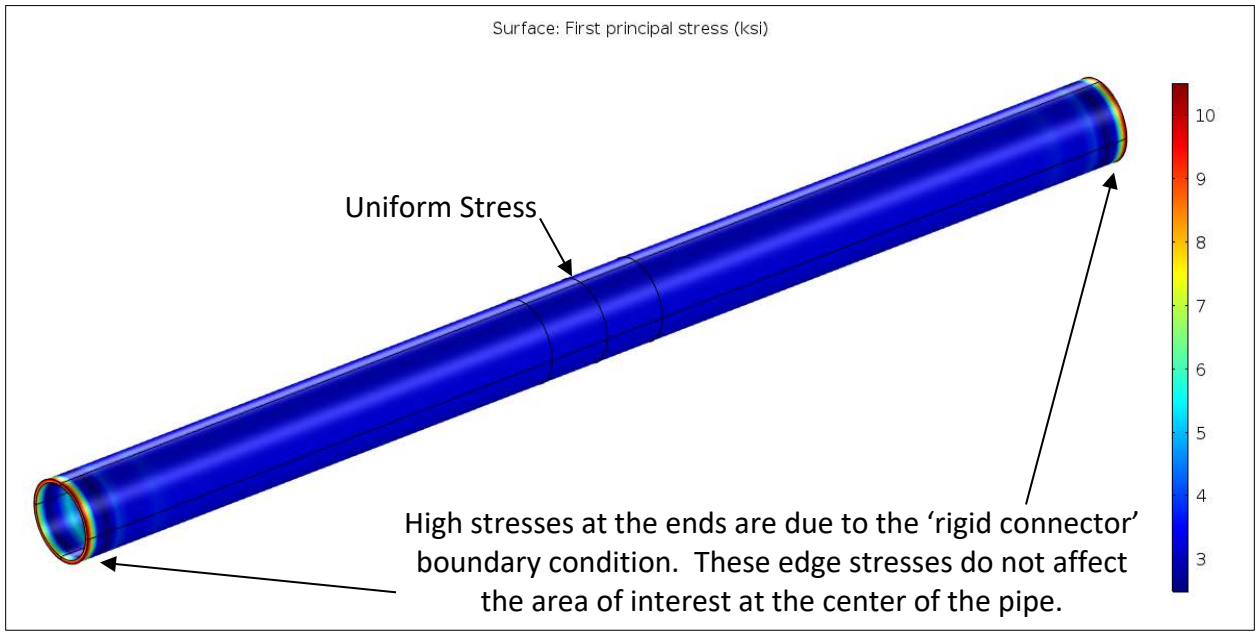

Figure 94. Pipe under thermal contraction, no bending

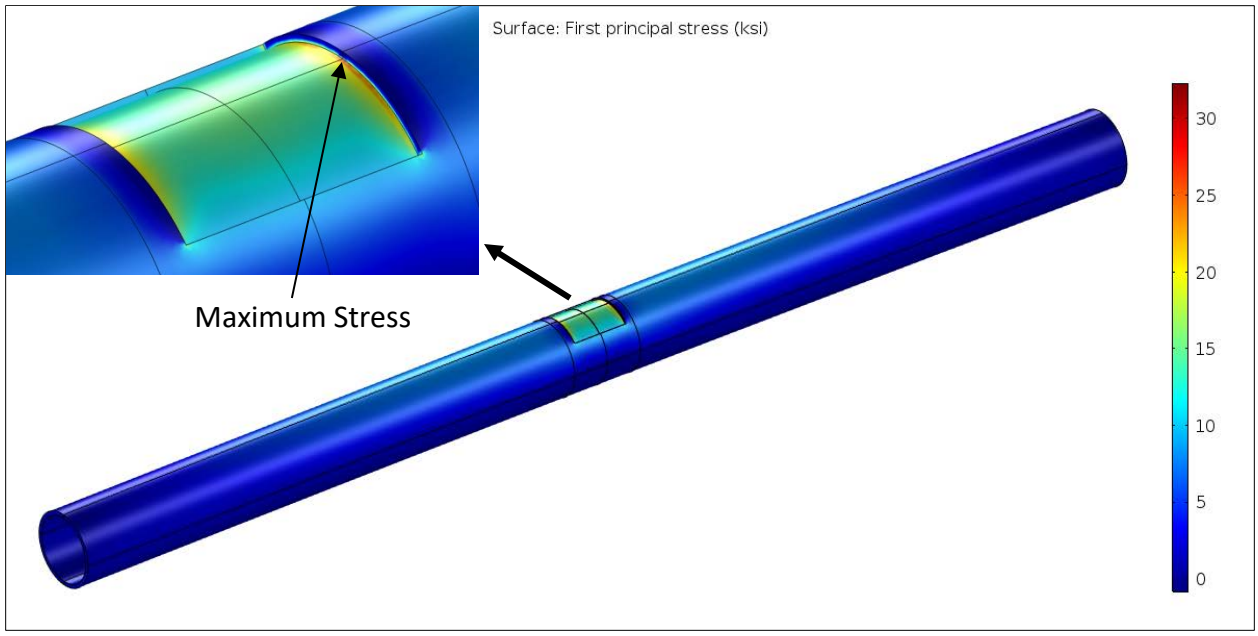

Figure 95. Pipe with wall loss under bending

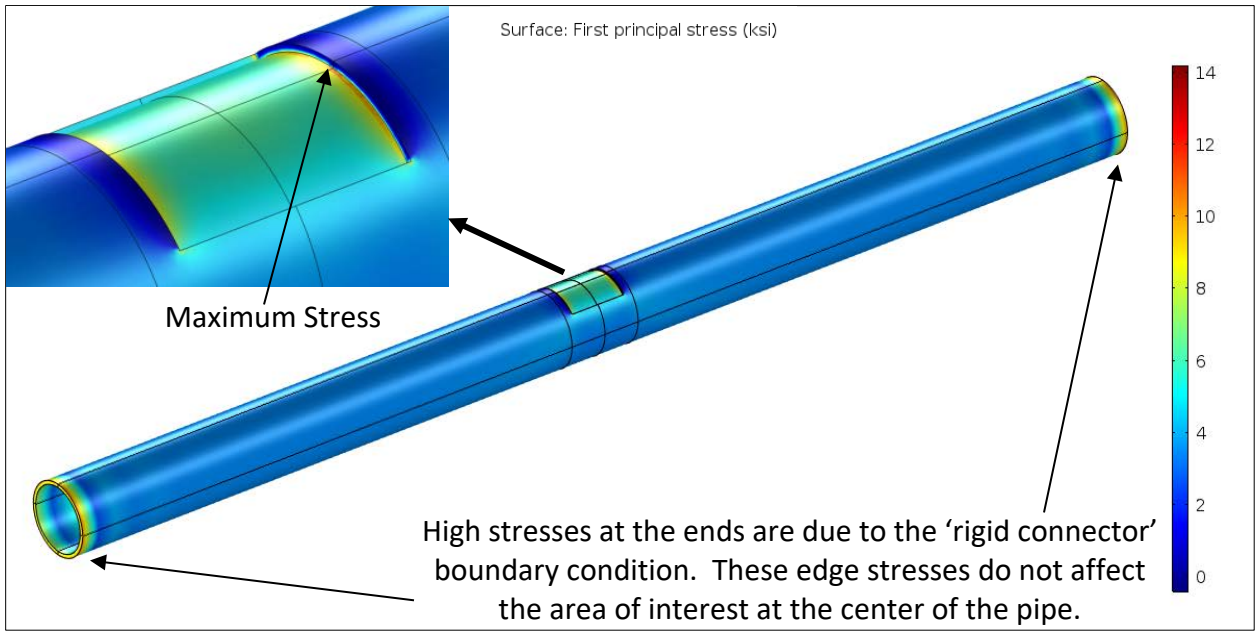

Figure 96. Pipe with wall loss under thermal contraction, no bending

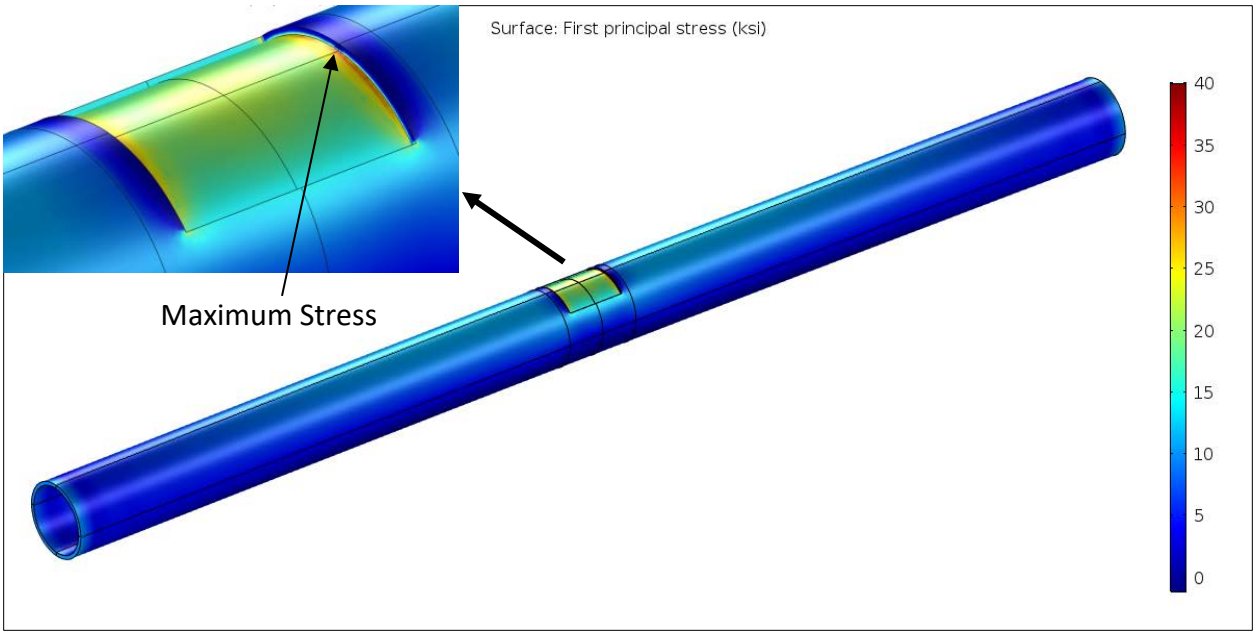

Figure 97. Pipe with wall loss under bending and thermal contraction

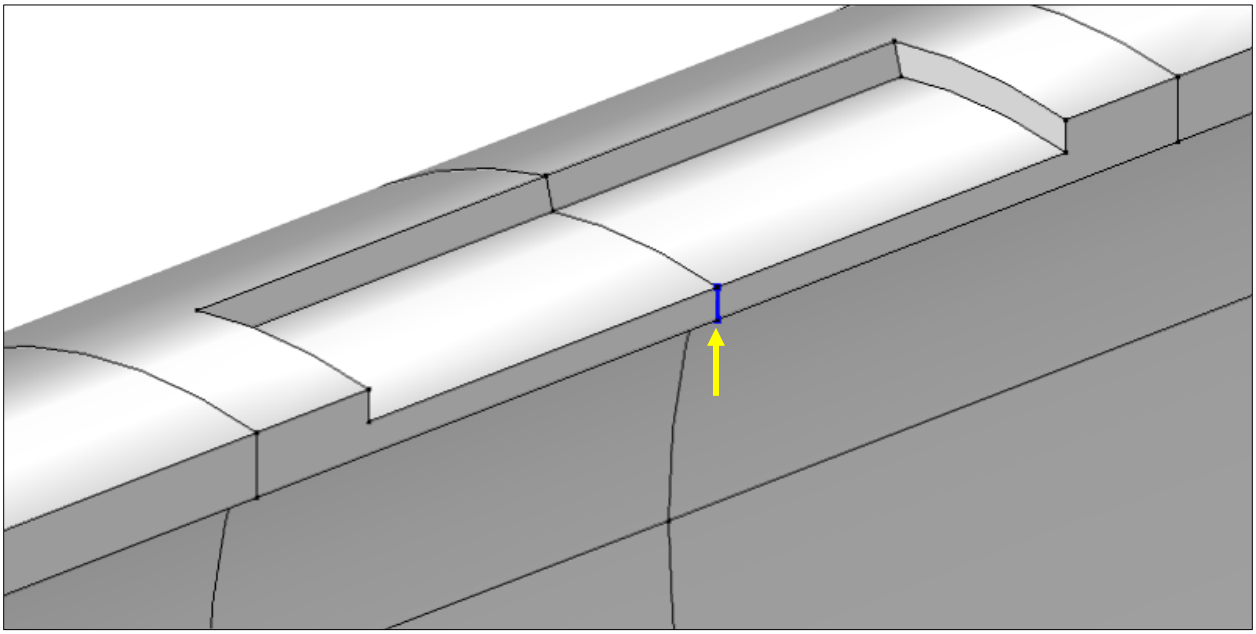

Figure 98. Radial line (highlighted in blue) at center of flaw for average stress probe (model cross-section shown for illustration)

General observations from the analyses include:

- In pure bending, a pipe with axially restrain ends will have a lower stress than a pipe with one axially free end,
- Stresses from internal pressure (at least up to 25 psig, which is considered to be the upper bound of cast iron pipe operating pressures) are negligible,
- Bending stresses are significantly higher than thermal stresses.

Response Surfaces

The response surfaces in both SS1 and SS2 needed to be separated by axial restraints. These separations necessitate the evaluation of the all response surfaces on a case-by-case basis using a calculator. Such a calculator will use one set of input variable and output the result from all response surfaces with an indication of the most conservative result.

SS1 (pipe without flaw) is comprised of two response surfaces as follows:

- SS1-1: axially free end
- SS1-2: axially restrained ends

SS2 (pipe with flaw) is comprised of two response surfaces as follows:

- SS2-1: axially free end
- SS2-2: axially restrained ends

The SS1 and SS2 response surfaces presented in this report do not include internal pressure since it was found to be negligible at least up to 25 psig, which is considered to be the upper bound of cast iron pipe operating pressures, and thus pressure was eliminated as a variable to reduce analysis time. The simulation models developed under this project do accept an internal pressure input such that response surfaces that include internal pressure can be generated.

All of the response surfaces based are on a reduced cubic model where insignificant terms were eliminated using a stepwise selection with p-value criteria of 0.0001.
The following figures show the perturbation and predicted versus actual graphs for each of the design spaces.

Response Surface SS1-1 – pipe without flaw, axially free end

Response surface SS1-1 applies to a non-axially restrained pipe segment without wall loss.

The response surfaces for the maximum and average first principal stresses are based on 936 data points and have the input variables given in Table 23:

Table 23. Design Variables for SS1-1

	Units	Lower Value	Upper Value
Class	-	10	60
Outer Diameter	in	4.8	15.65
Pipe Span	ft	12	18
Vertical Load Pressure	psi	2	80

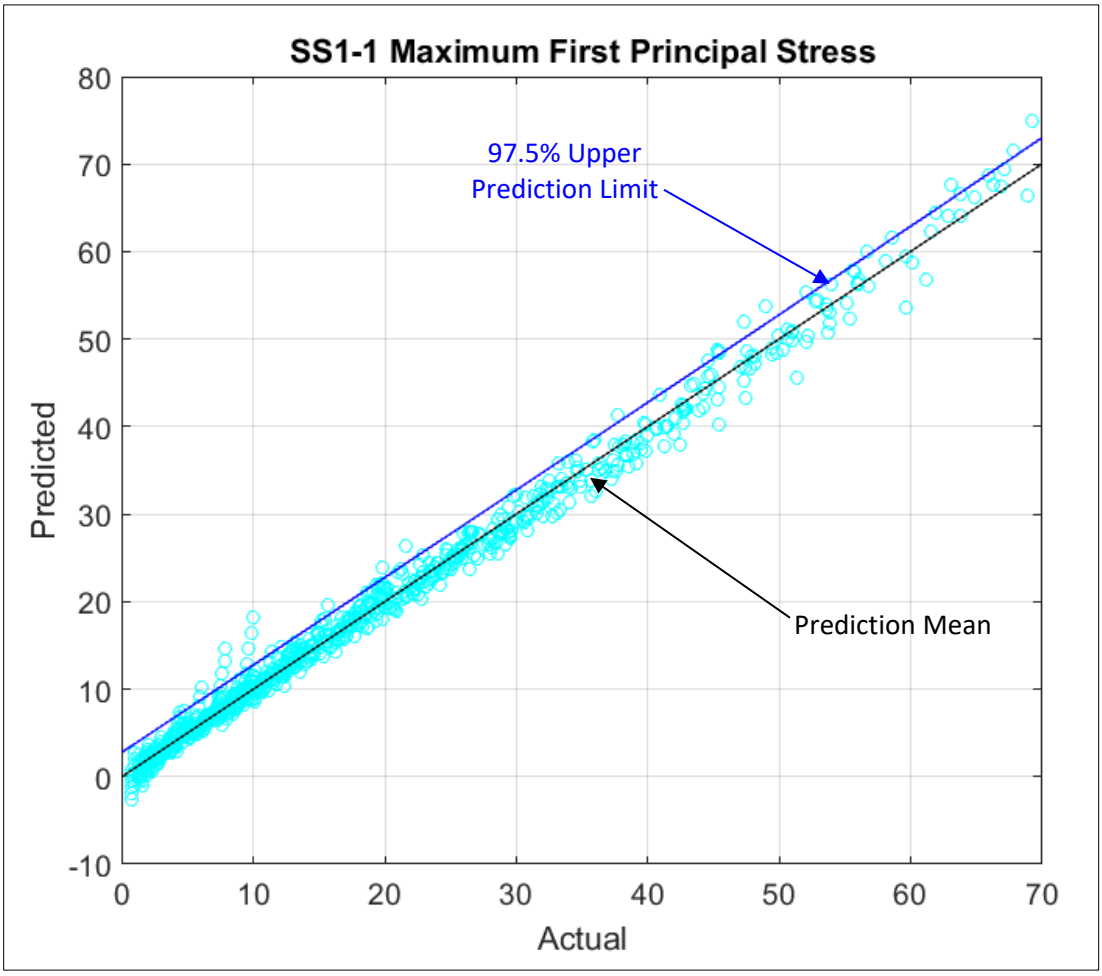

Figure 99. SS1-1 Maximum First Principal Stress, Predicted versus Actual, predicted R2=0.9917, with 97.5% upper confidence bound

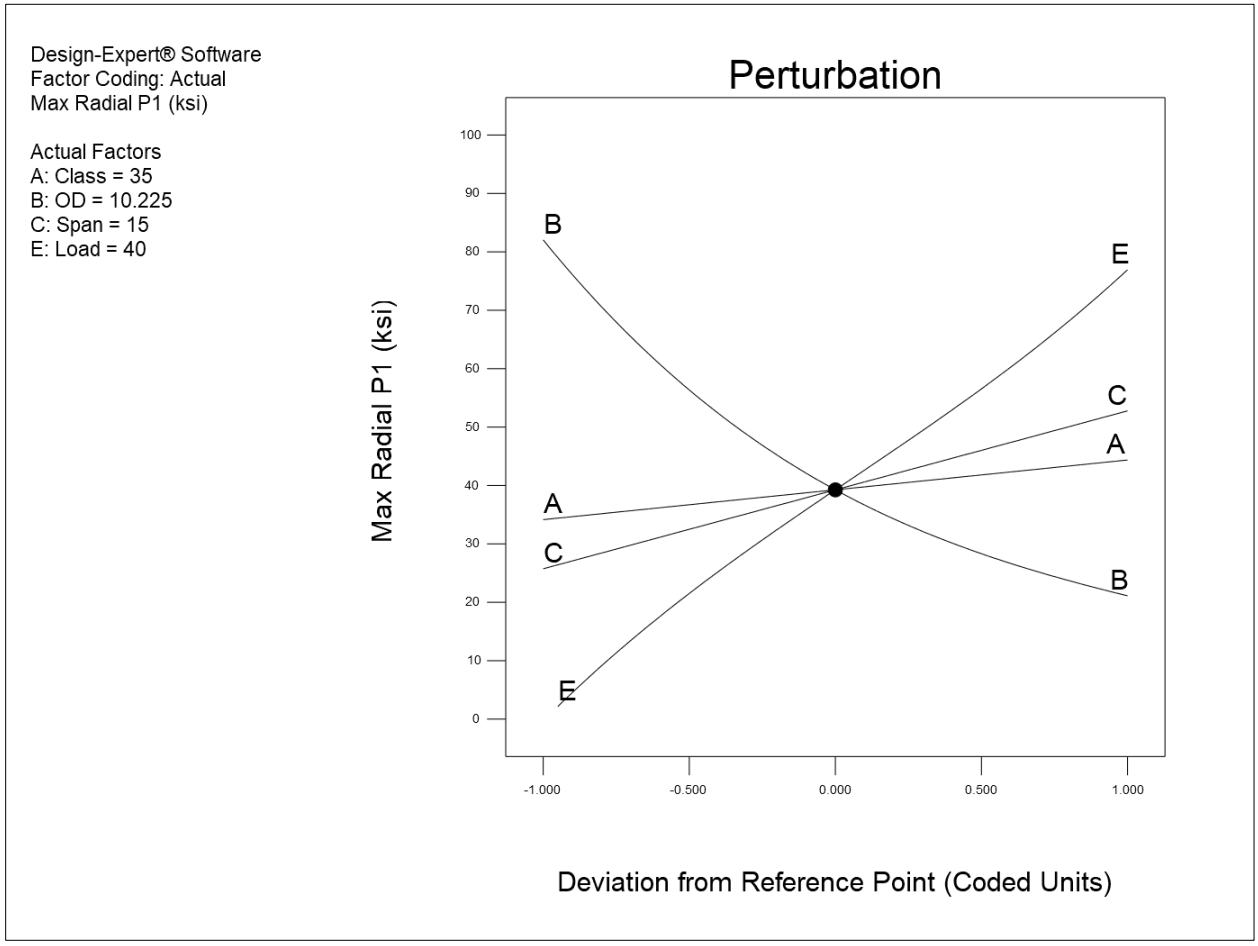

Figure 100. SS1-1 Maximum First Principal Stress, perturbation graph

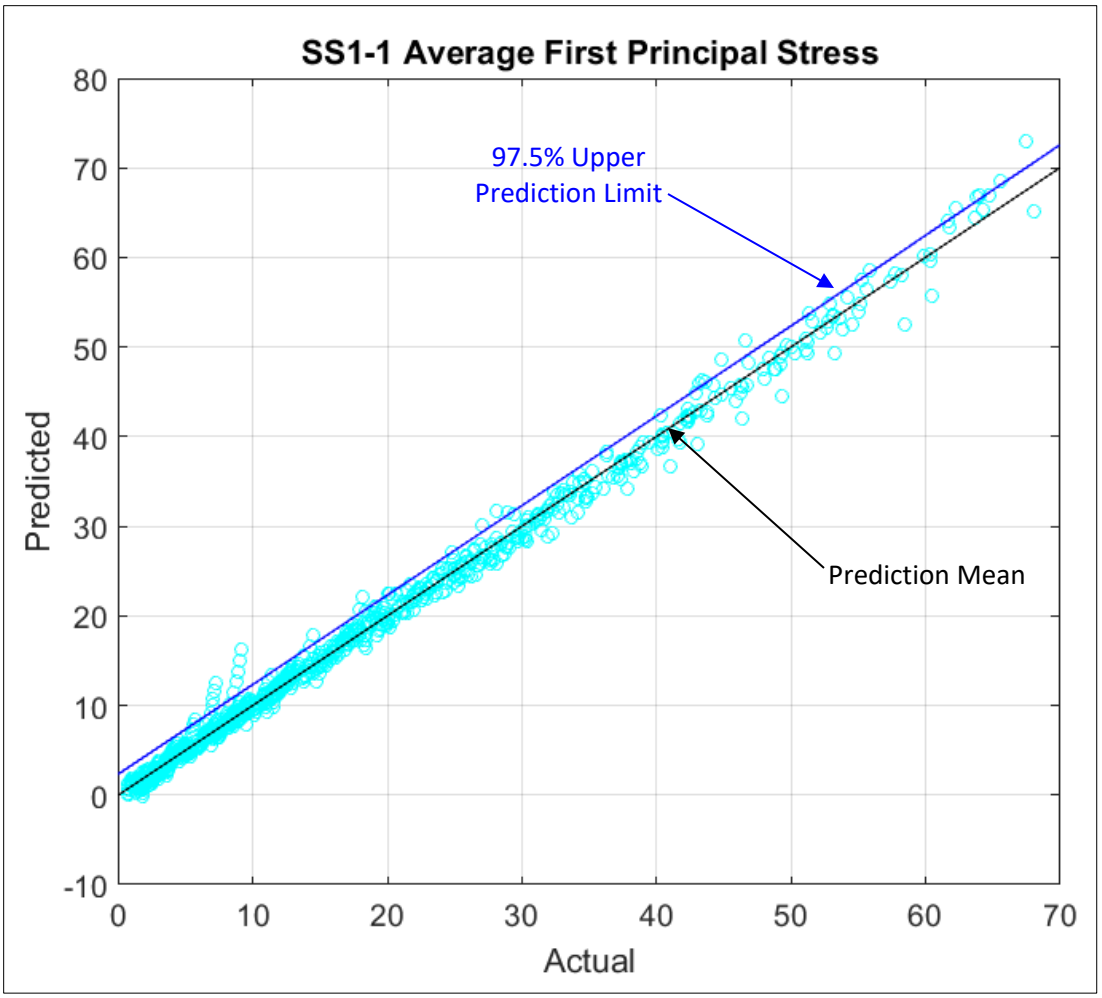

Figure 101. SS1-1 Average Radial First Principal Stress, Predicted versus Actual, predicted R2=0.9937, with 97.5% upper confidence bound

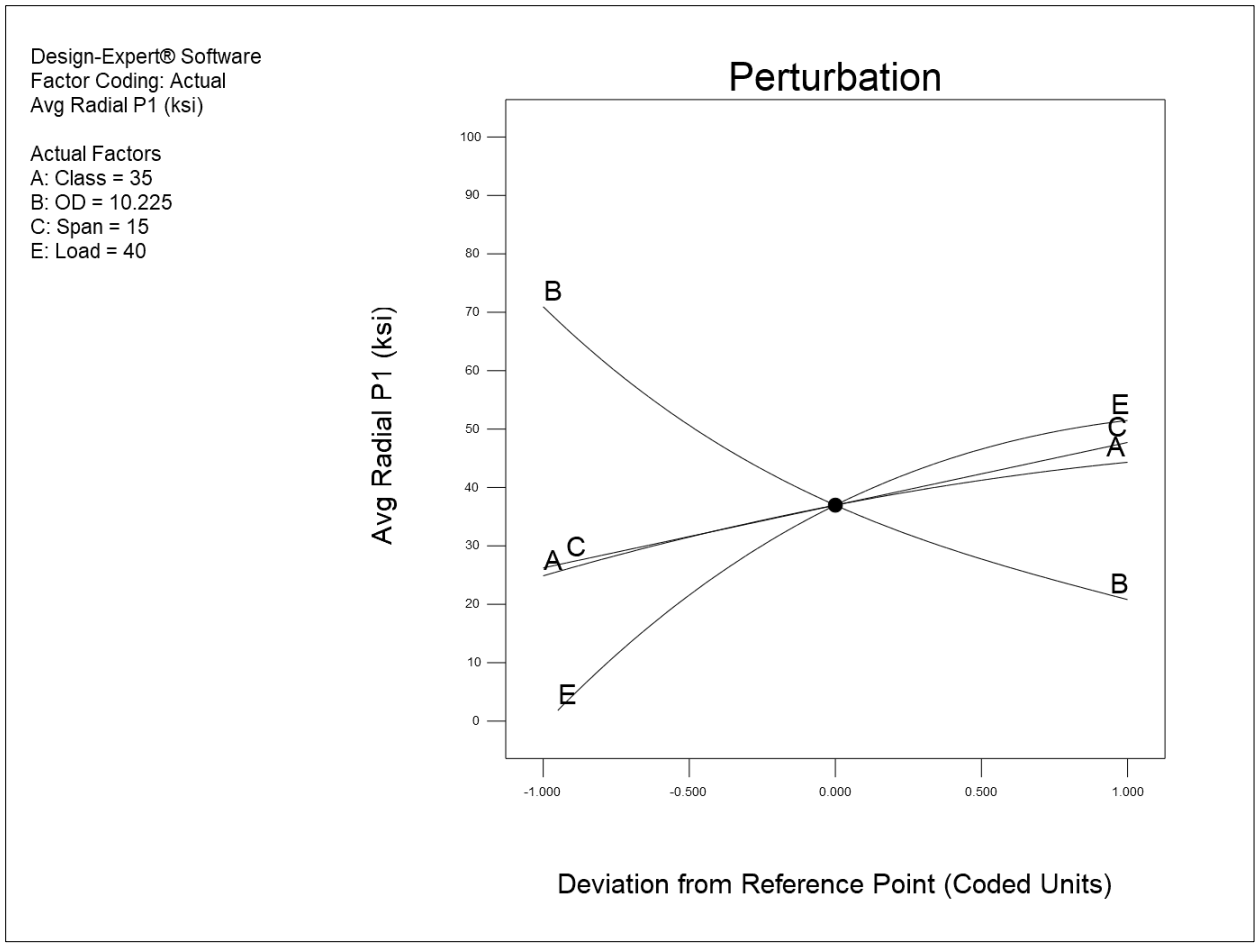

Figure 102. SS1-1 Average Radial First Principal Stress, perturbation graph

Response Surface SS1-2 – pipe without flaw axially restrained ends

Response surface SS1-2 applies to an axially restrained pipe segment without wall loss.

The response surfaces for the maximum and average first principal stresses are based on 3008 data points and have the input variables given in Table 24:

Table 24. Design Variables for SS1-2

	Units	Lower Value	Upper Value
Class	-	10	60
Outer Diameter	in	4.8	15.65
Pipe Span	ft	12	18
Temperature Change	degC	-20	0
Vertical Load Pressure	psi	0	80

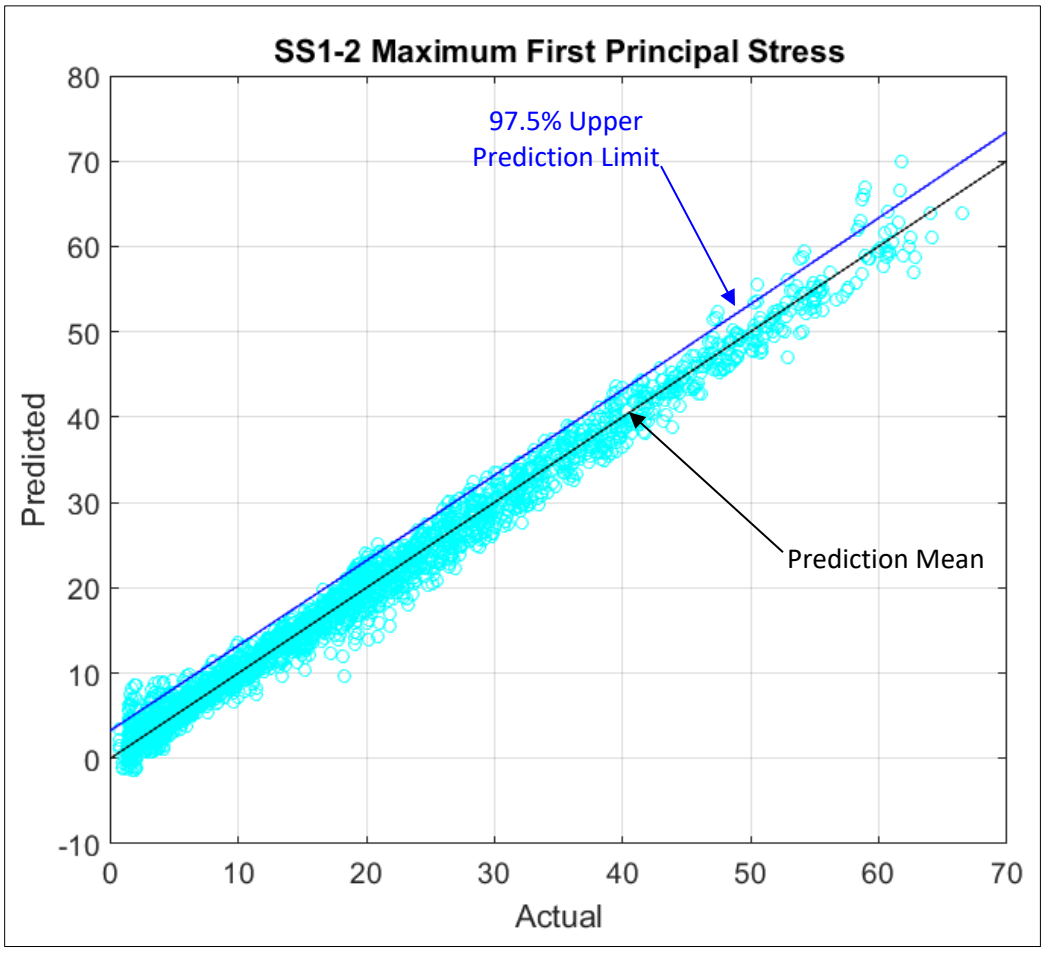

Figure 103. SS1-2 Maximum First Principal Stress, Predicted versus Actual, predicted R2=0.9868, with 97.5% upper confidence bound

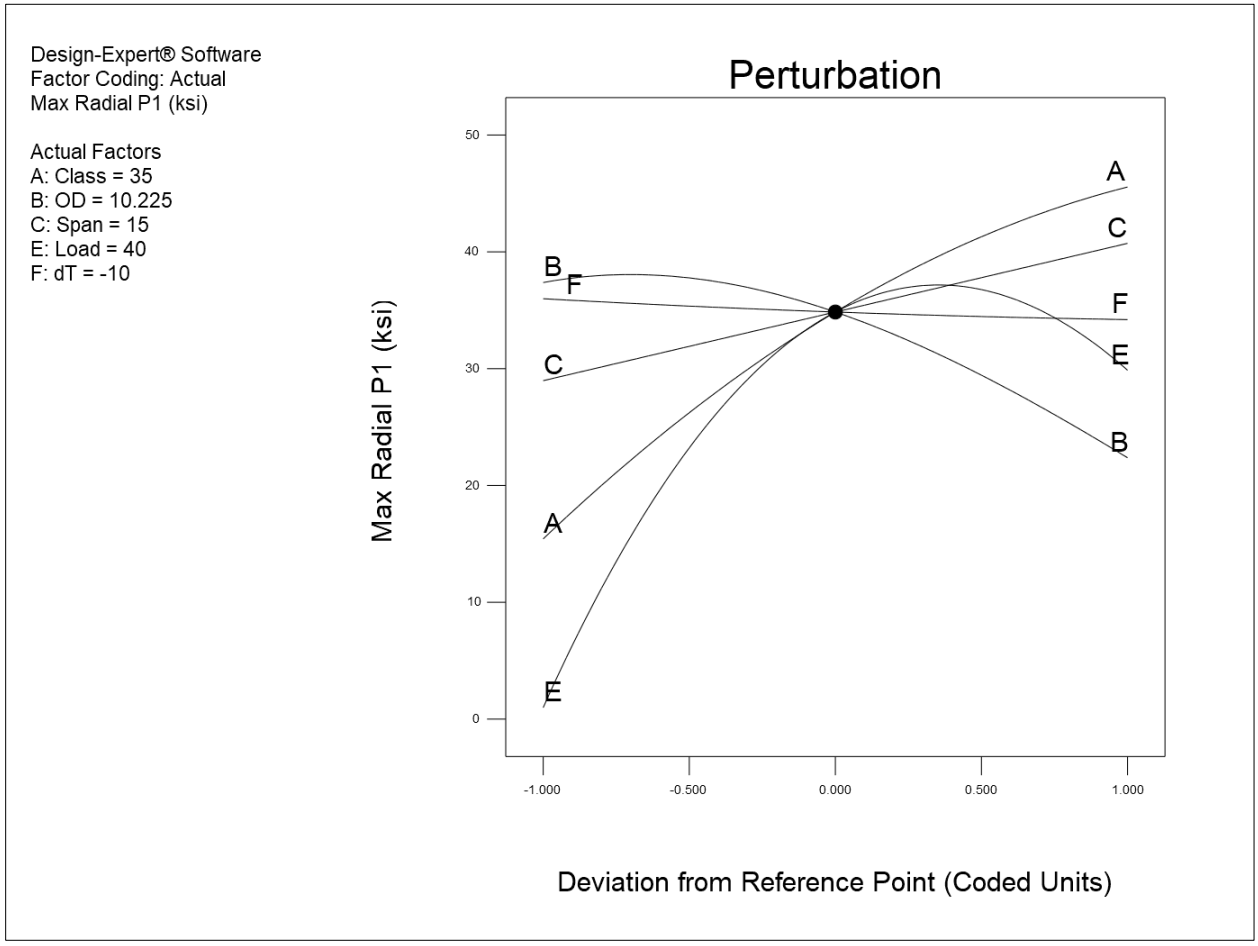

Figure 104. SS1-2 Maximum First Principal Stress, perturbation graph

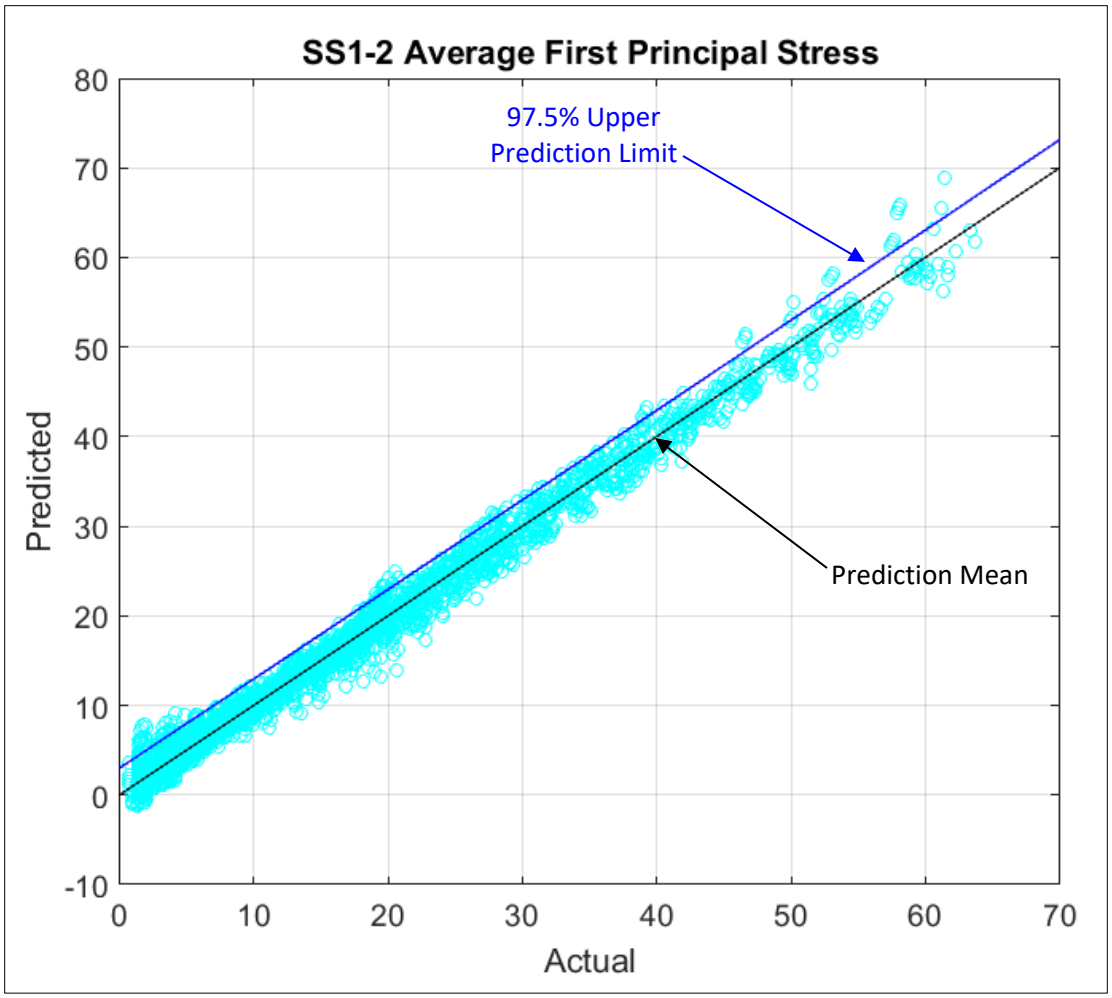

Figure 105. SS1-2 Average First Principal Stress, Predicted versus Actual, predicted R2=0.9882, with 97.5% upper confidence bound

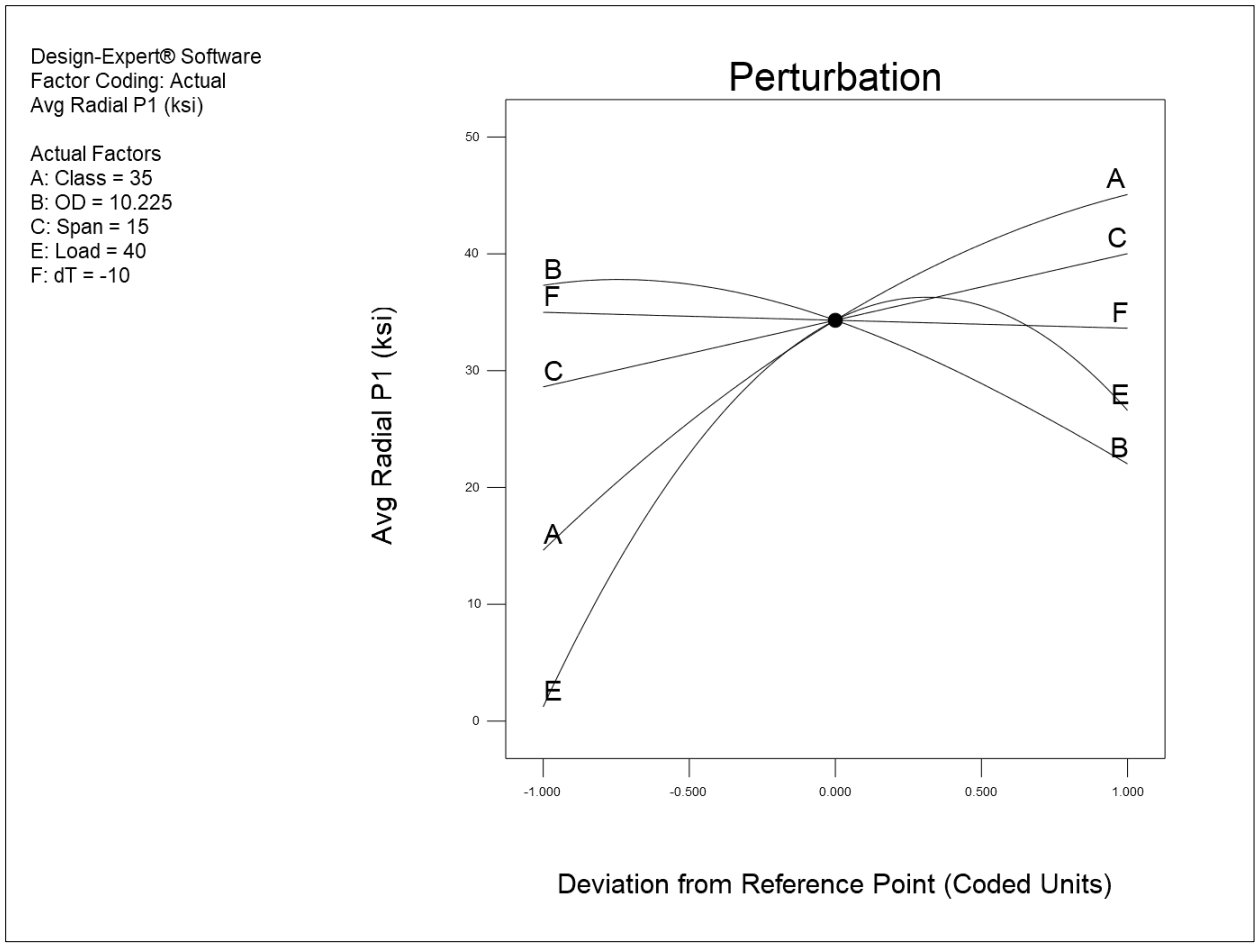

Figure 106. SS1-2 Average Radial First Principal Stress, perturbation graph

Response Surface SS2-1 – pipe with flaw, axially free end

Response surface SS2-1 applies to a non-axially restrained pipe segment with wall loss.

The response surfaces for the maximum and average first principal stresses are based on 7390 data points and have the input variables given in Table 25:

Table 25. Design Variables for SS2-1

	Units	Lower Value	Upper Value
Class	-	10	60
Outer Diameter	in	4.8	13.2
Span	ft	12	18
Flaw Depth	% of WT	5	80
Flaw Length	C	0.1	3
Flaw Width	% of Pipe Circumference	5	49
Vertical Load Pressure	psi	0	80

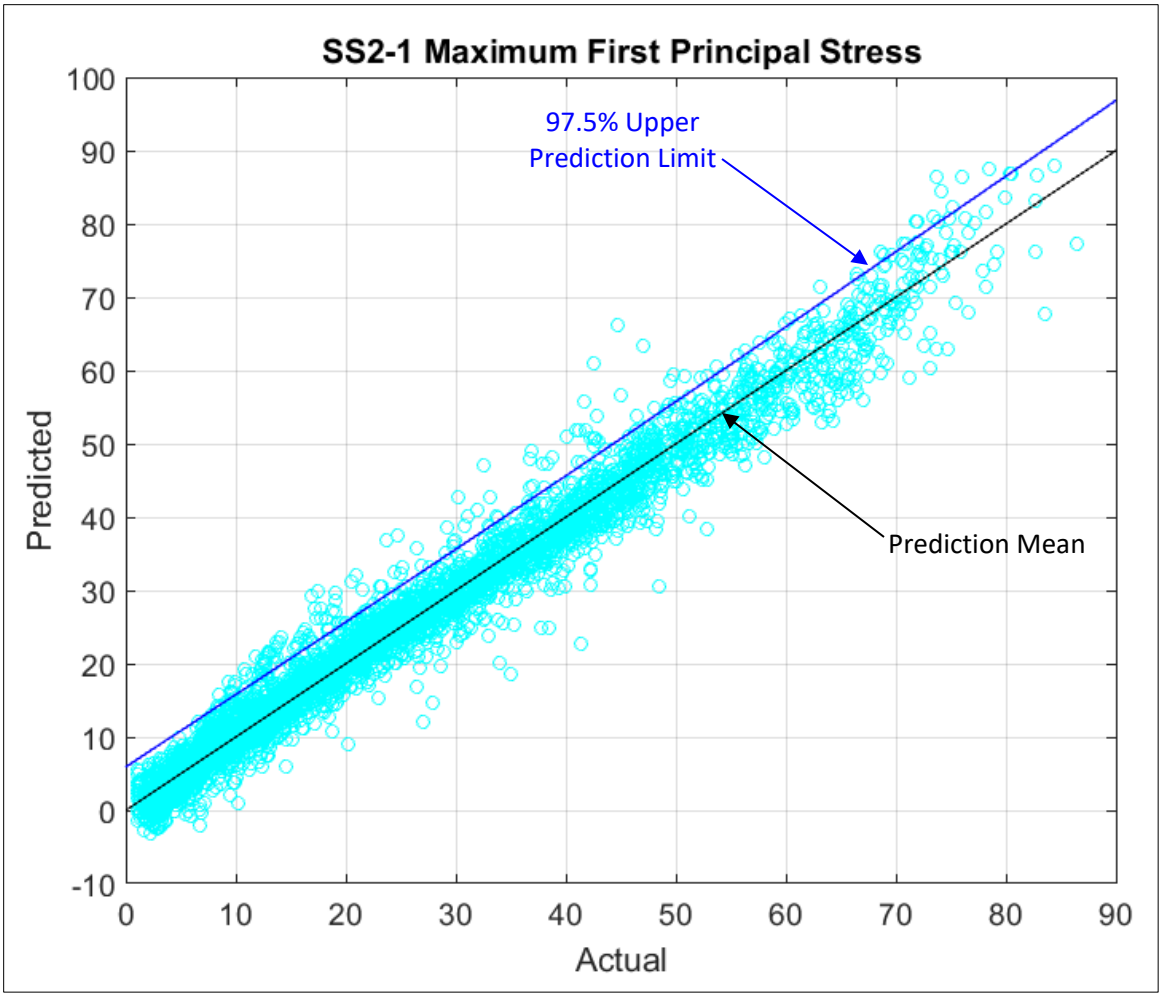

Figure 107. SS2-1 Maximum First Principal Stress, Predicted versus Actual, predicted R2=0.9749, with 97.5% upper confidence bound

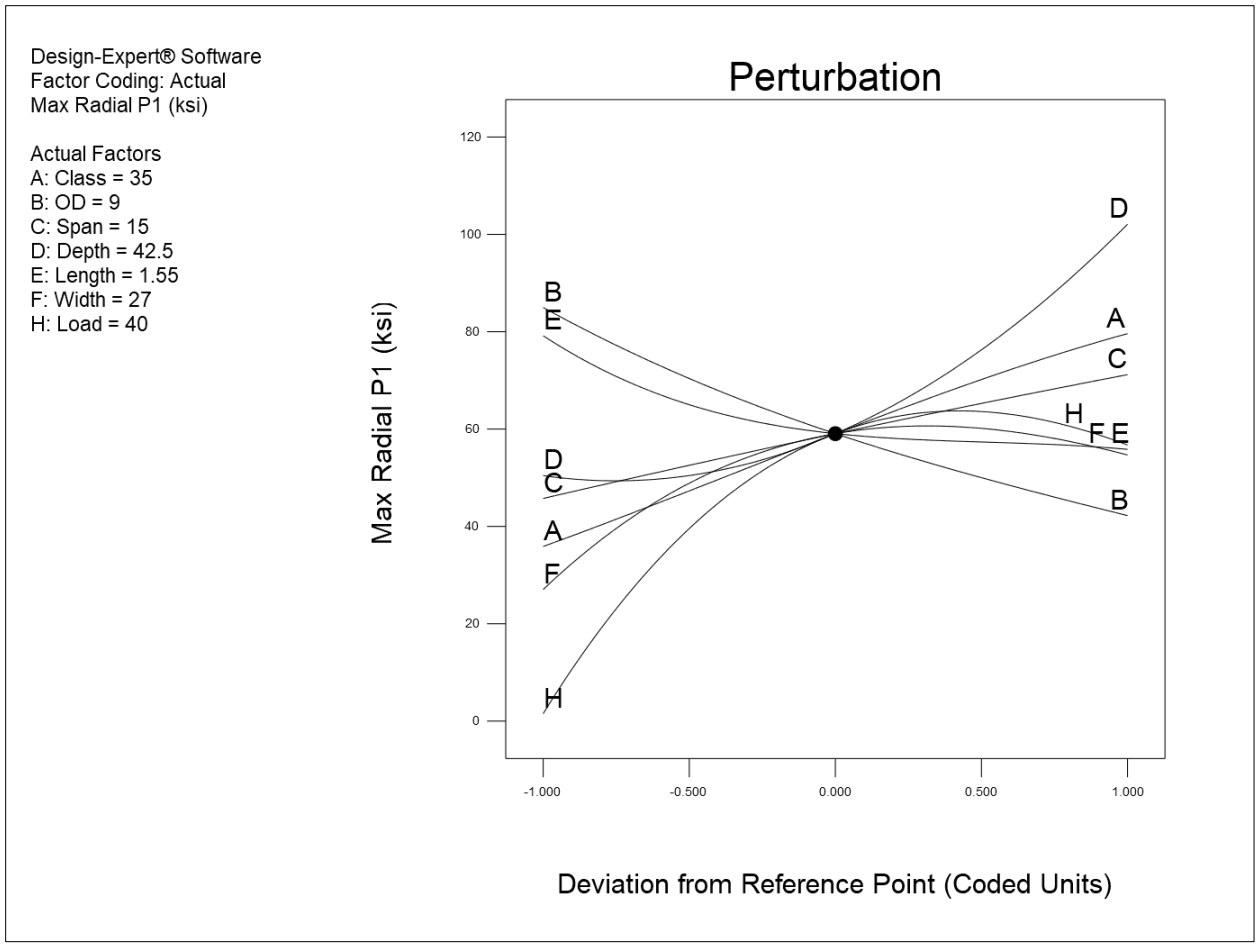

Figure 108. SS2-1 Maximum First Principal Stress, perturbation graph

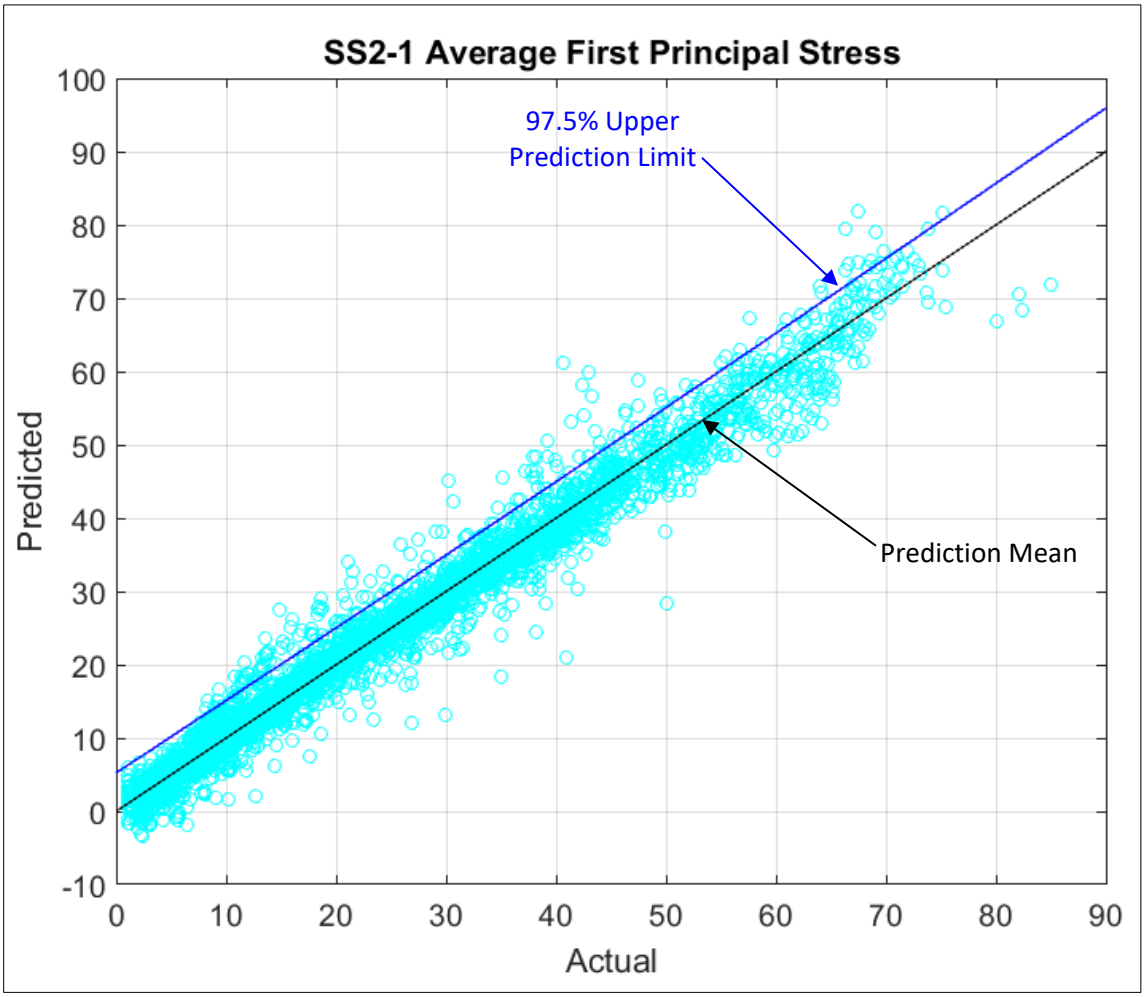

Figure 109. SS2-1 Average Radial First Principal Stress, Predicted versus Actual, predicted R2=0.9765, with 97.5% upper confidence bound

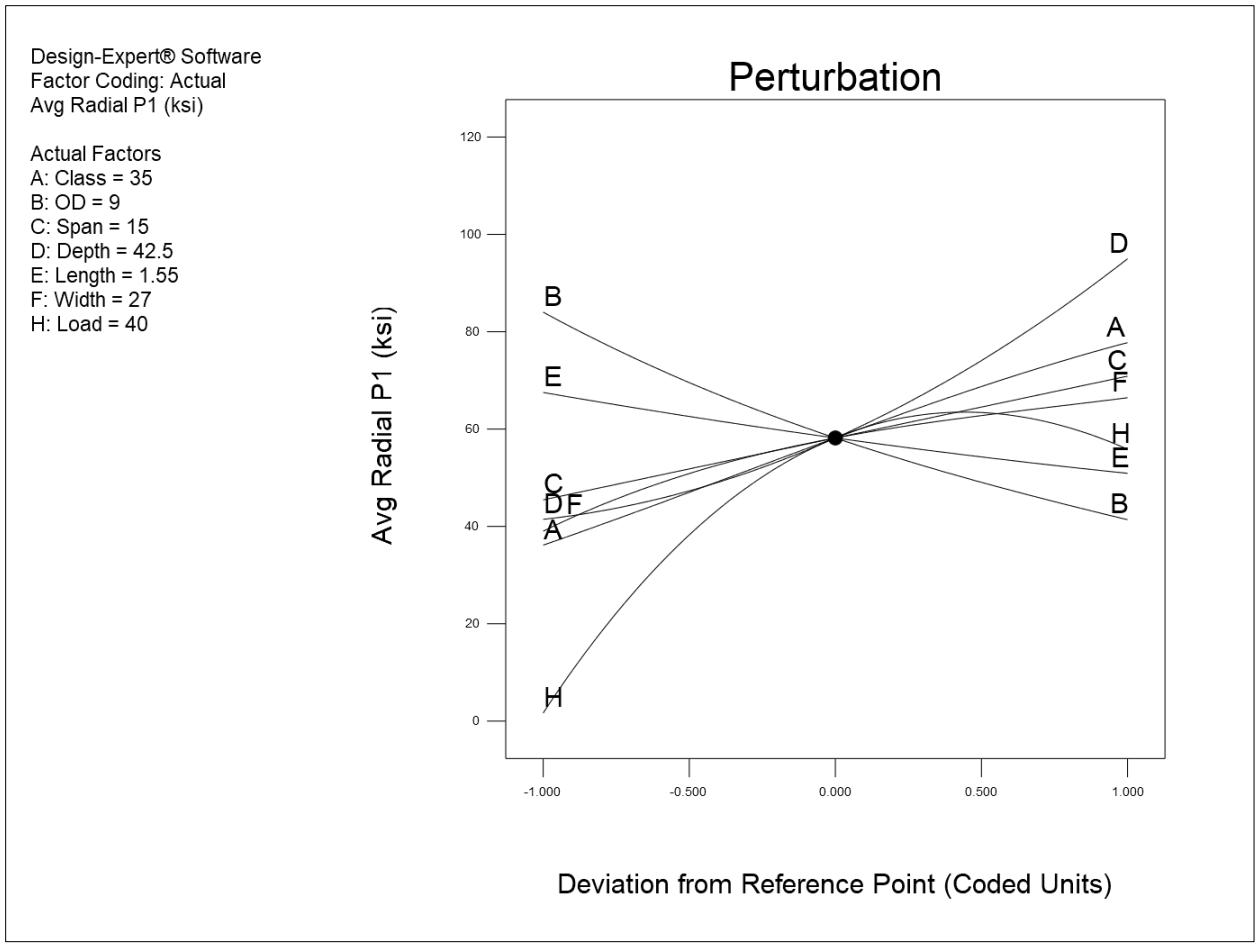

Figure 110. SS2-1 Average Radial First Principal Stress, perturbation graph

Response Surface SS2-2 – pipe with flaw, axially restrained ends

Response surface SS2-2 applies to an axially restrained pipe segment with wall loss.

The response surfaces for the maximum and average first principal stresses are based on 11314 data points and have the input variables given in Table 26:

Table 26. Design Variables for SS2-2

	Units	Lower Value	Upper Value
Class	-	10	60
Outer Diameter	in	4.8	13.2
Span	ft	12	18
Flaw Depth	% of WT	5	80
Flaw Length	C	0.1	3
Flaw Width	% of Pipe Circumference	5	49
Vertical Load Pressure	psi	0	80
Temperature Change	degC	-30	0

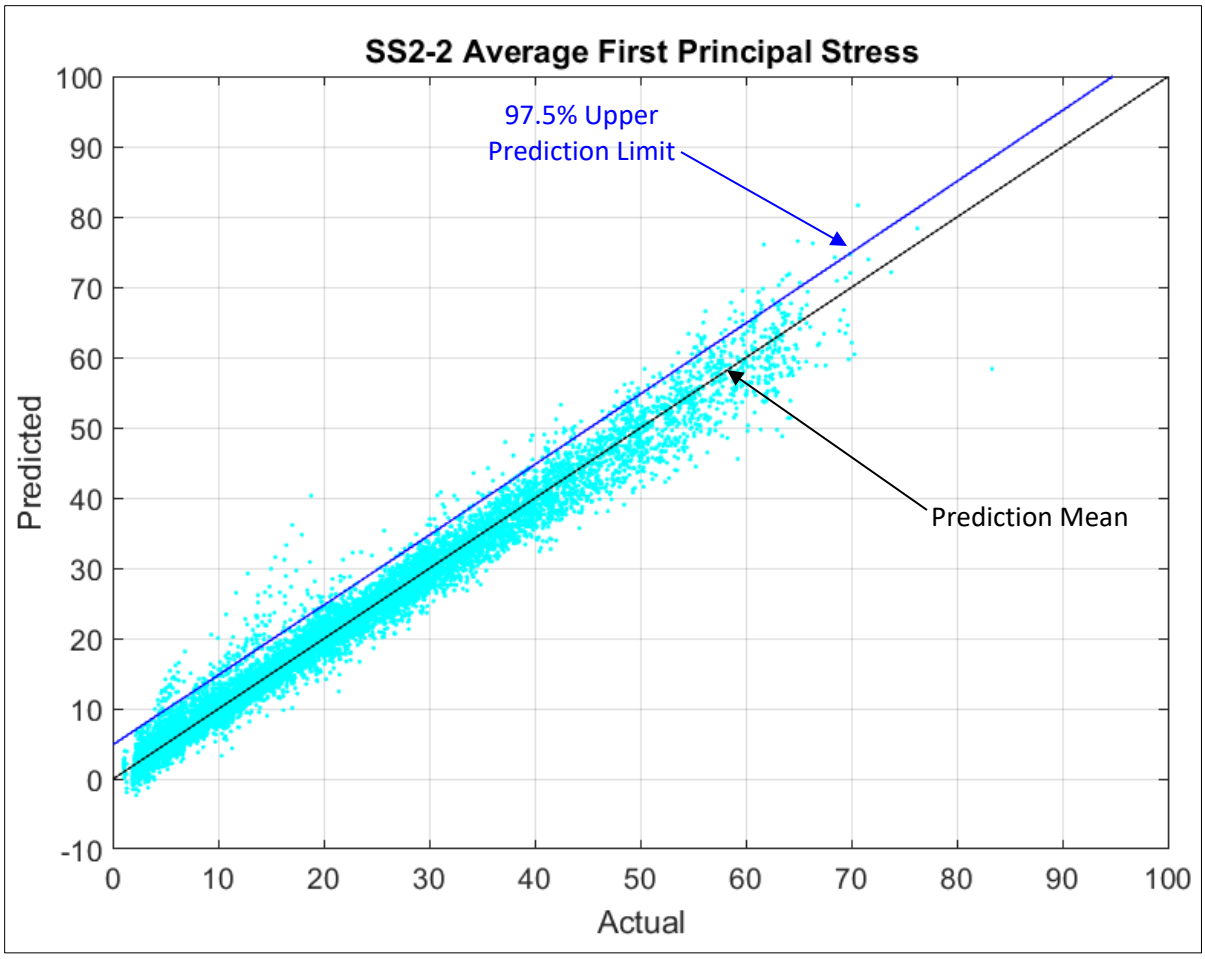

Figure 111. SS2-2 Maximum First Principal Stress, Predicted versus Actual, predicted R2=0.9725, with 97.5% upper prediction limit

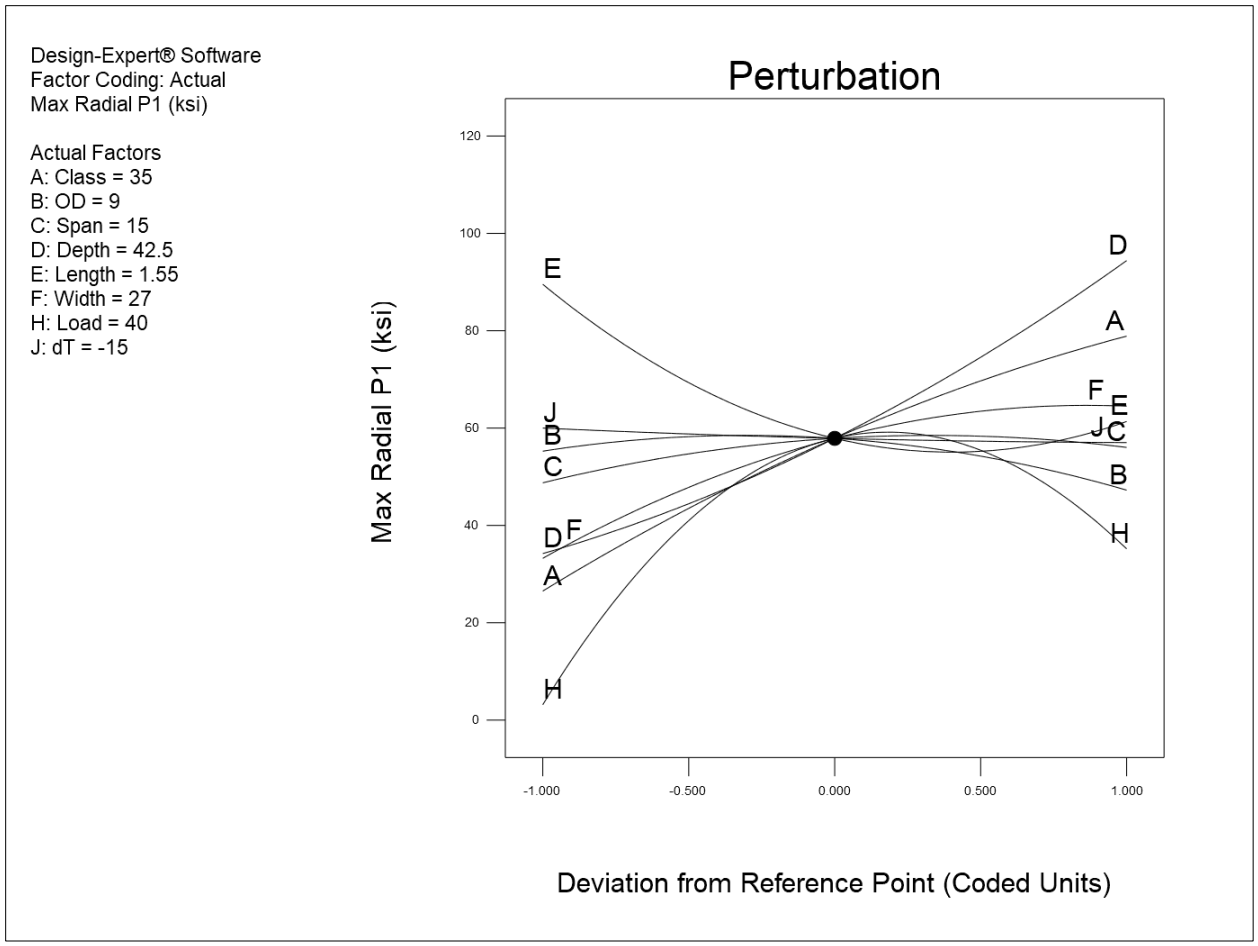

Figure 112. SS2-2 Maximum First Principal Stress, perturbation graph

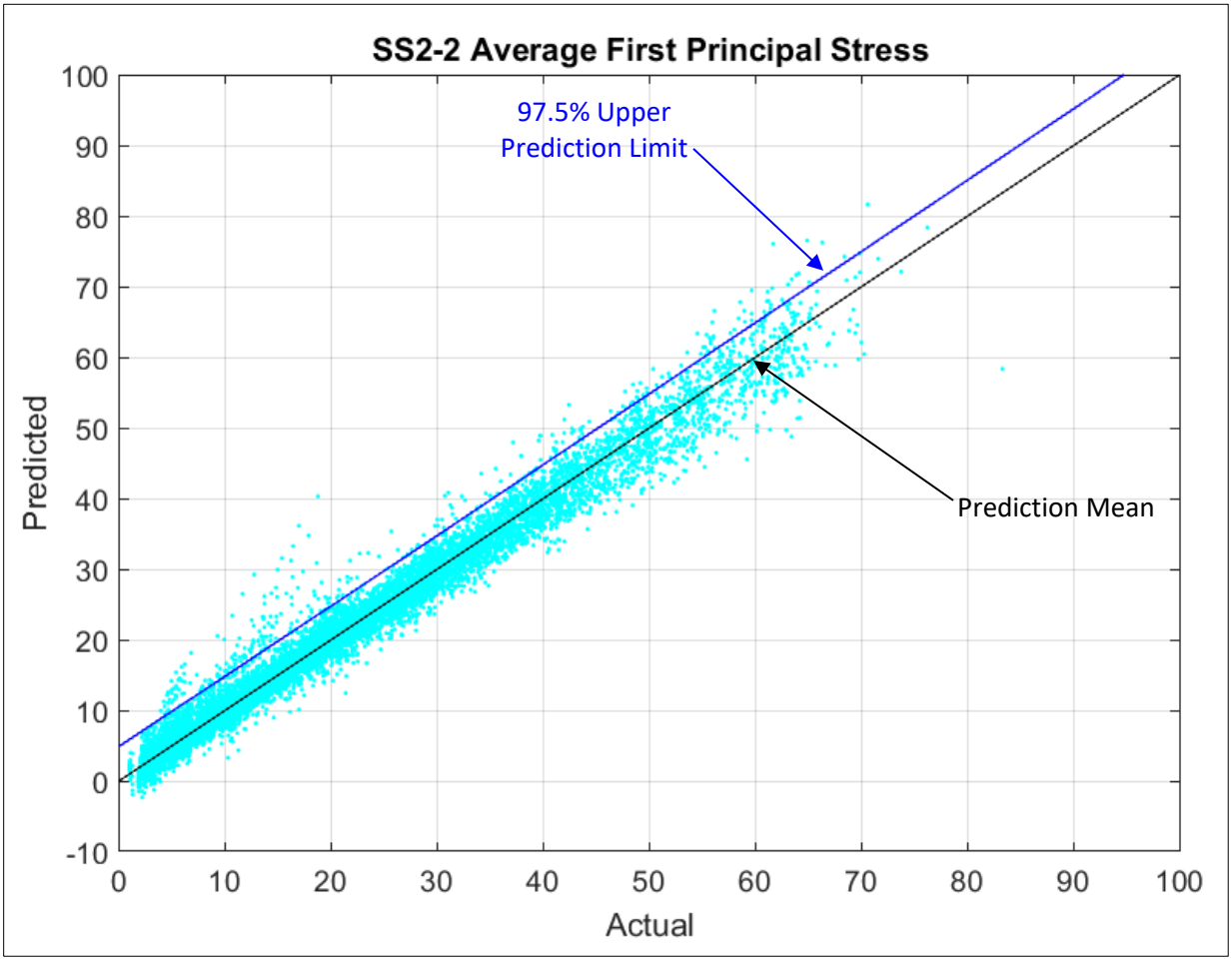

Figure 113. SS2-2 Average Radial First Principal Stress, Predicted versus Actual, predicted R2=0.8617, with 97.5% upper confidence bound

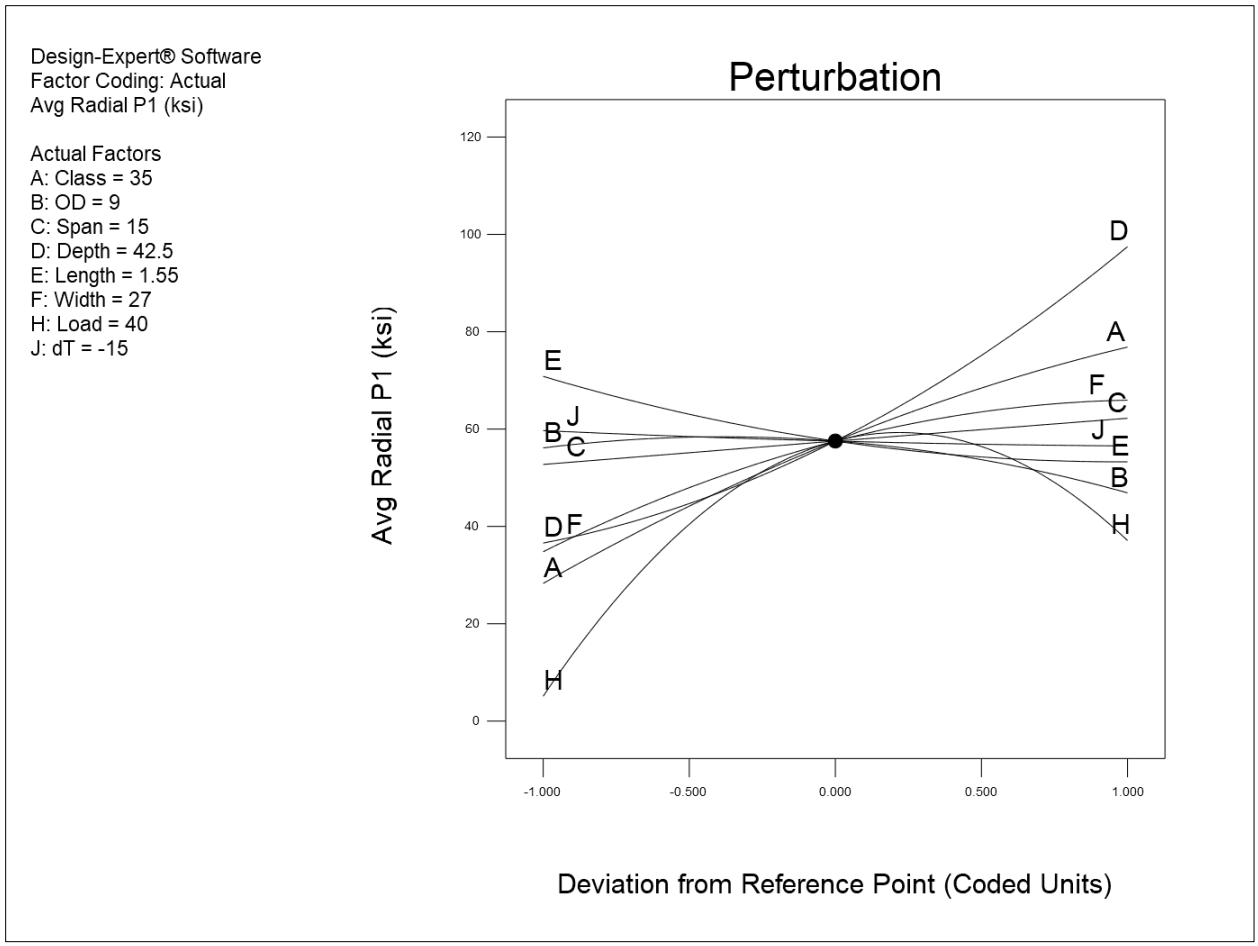

Figure 114. SS2-2 Average Radial First Principal Stress, perturbation graph

6. Comparison of FFS Model with Field Failure Data and Uncertainty Analysis

This section of the report provides analysis of cast iron field failures summarized in **Section 3.** The failure data were compared against the FFS model results applied to the same situations. This is considered a first pass validation of the FFS model. Gaps and discrepancies are noted in each of the case studies.

An analysis was also conducted on the effect that the uncertainty of input values would have on the model results. This was done through Monte Carlo simulations of tens of thousands of model runs where input variables like diameter, thickness, material strength, corrosion defect geometry, etc. were perturbated within a band of uncertainty and then model results were compared vs. non-perturbated input values.

Cast Iron Reported Incidents

PHMSA collects annual data from operators on incidents occurring on their gas distribution and transmission systems as defined by the Code of Federal Regulations 49 CFR 191.3 [45]. Incidents reports include relevant data on pipeline and site characteristics, cause of failure, and other metrics.

Figure 115 shows the cast iron pipe incidents in comparison to total number of significant incidents since 1985. The figure shows that the number of significant incidents of cast iron pipes ranged from 3 to 22 annual incidents during this period [46].

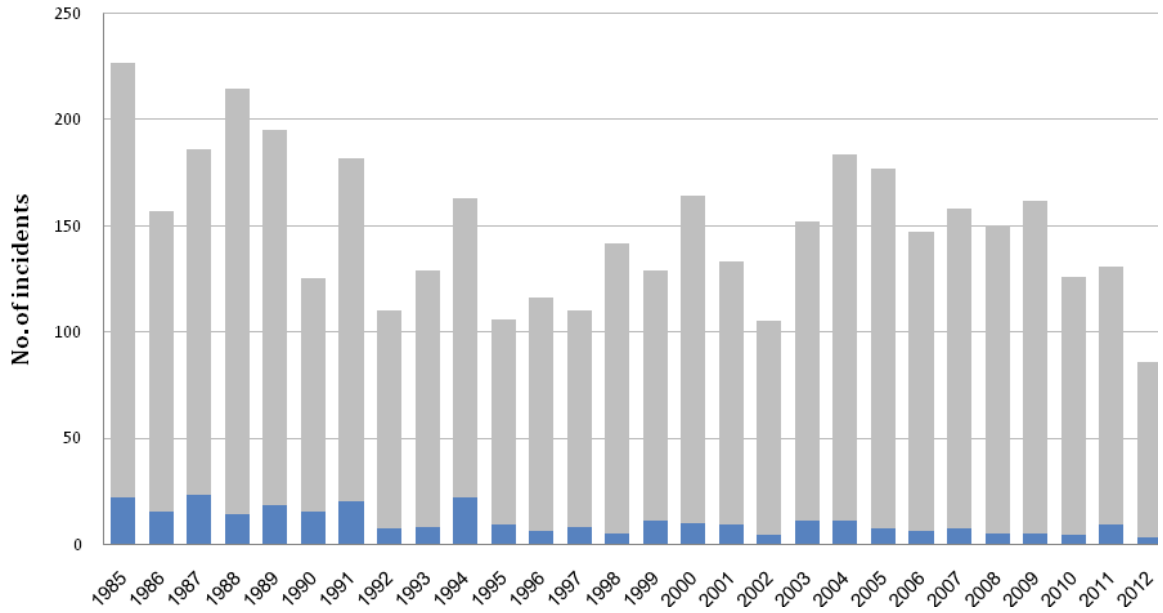

Figure 115. Total incidents vs. Cast iron incidents

Table 27 shows a list of the PHMSA reported significant cast iron failures from 2010 to 2017. The data in the table presents the significant incidents which resulted in fatality, injury, more than $50,000 in total costs, or volatile gas or liquid release. Two of the incidents were caused by localized graphitic corrosion. The pipe characteristics and associated site conditions of these two incidents were analyzed in the FFS program, developed for this project, to investigate the program estimated pipes Factors of Safety (F.S.) against circumferential stress failure.

Additionally, stress analysis using the FFS program was performed on selected incidents where circumferential crack failures occurred in the cast iron pipes due to temperature change and frost heave. Since these incidents did not specify metal loss, the analysis was performed to evaluate pipe stresses due to soil freeze, with no metal loss parameters. It should be noted that pipe failures due to frost commonly accumulates along extended freeze-thaw cycles and the program will only give an approximate estimate of F.S. of a single freeze cycle.

Table 27. Cast Iron Pipes and System Characteristics in Reported Incidents [2010-2016]

NAME	CITY_NAME	STATE	YEAR	FATALITY	INJURY	SHUTDOWN	IGNITE	EXPLODE	DEPTH_OF_COVER	CROSSING	INSTALLATION_YEAR	PIPE_DIAMETER	RUPTURE_ORIENT	CAUSE
PUBLIC SERVICE ELECTRIC & GAS CO	NEWARK	NJ	2010	NO	NO	NO	YES	YES		NO	1959	16	CIRCUMFERENT	NATURAL FORCE DAMAGE
ATLANTA GAS LIGHT CO	ATLANTA	GA	2010	NO	NO	YES	NO	NO	48	YES	1924	4		EXCAVATION DAMAGE
MOBILE GAS SERVICE CORP	MOBILE	AL	2010	NO	YES	NO	NO	NO		NO	1950		CIRCUMFERENT	OTHER INCIDENT CAUSE
BOSTON GAS CO	WALTHAM	MA	2010	NO	YES	NO	YES	YES	48	NO	1930	6		NATURAL FORCE DAMAGE
PUBLIC SERVICE CO OF COLORADO	DENVER	CO	2010	NO	NO	YES	YES	YES	18	NO	1940	1.25	CIRCUMFERENT	EXCAVATION DAMAGE
PHILADELPHIA GAS WORKS	PHILADELPHIA	PA	2011	YES	YES	YES	YES	YES	37	NO	1942	12.75		MATERIAL FAILURE OF PIPE OR WELD
BALTIMORE GAS & ELECTRIC CO	BALTIMORE	MD	2011	NO	NO	YES	YES	NO		NO	2000			OTHER OUTSIDE FORCE DAMAGE
UGI UTILITIES, INC	READING	PA	2011	YES	YES	YES	YES	YES	52	NO	1928	12		NATURAL FORCE DAMAGE
MICHIGAN CONSOLIDATED GAS CO	DETROIT	MI	2011	NO	NO	NO	NO	YES		NO	1930	4		NATURAL FORCE DAMAGE
MICHIGAN CONSOLIDATED GAS CO	DETROIT	MI	2011	YES	NO	NO	NO	NO	54	NO	1928	6	OTHER	CORROSION FAILURE
BALTIMORE GAS & ELECTRIC CO	BALTIMORE	MD	2011	NO	NO	YES	NO	NO		NO	1900	12		EXCAVATION DAMAGE
TEXAS GAS SERVICE COMPANY	AUSTIN	TX	2012	YES	YES	YES	YES	YES	38	NO	1950	4		NATURAL FORCE DAMAGE
BALTIMORE GAS & ELECTRIC CO	BALTIMORE	MD	2012	NO	NO	YES	NO	NO	38	NO	1909	4		EXCAVATION DAMAGE
LACLEDE GAS CO	SAINT LOUIS	MO	2012	NO	NO	YES	YES	NO	48	NO	1961	12	LONGITUDINAL	CORROSION FAILURE
LIBERTY ENERGY	JACKSON	MO	2013	NO	NO	YES	NO	NO		NO	1980			EQUIPMENT FAILURE
PEOPLES NATURAL GAS COMPANY LLC	PITTSBURGH	PA	2013	NO	NO	NO	NO	NO	36	NO	1959			INCORRECT OPERATION
FITCHBURG GAS & ELECTRIC LIGHT CO	FITCHBURG	MA	2013	NO	NO	YES	NO	YES	28	NO		4		NATURAL FORCE DAMAGE
COLUMBIA GAS OF OHIO INC	COLUMBUS	OH	2013	NO	YES	NO	YES	NO	36	NO		4		OTHER INCIDENT CAUSE
CONSOLIDATED EDISON CO OF NY	NEW YORK	NY	2013	NO	NO	YES	NO	NO		NO	1952	6		MATERIAL FAILURE OF PIPE OR WELD
ALABAMA GAS CORPORATION	BIRMINGHAM	AL	2013	YES	YES	NO	YES	YES	36	NO	1951	2.25		OTHER INCIDENT CAUSE
KEYSPAN ENERGY DELIVERY - NY CITY	BROOKLYN	NY	2014	NO	YES	NO	YES	YES		NO	1926	4		OTHER INCIDENT CAUSE
PHILADELPHIA GAS WORKS	PHILADELPHIA	PA	2014	NO	YES	YES	YES	YES		NO	1939	4	CIRCUMFERENT	NATURAL FORCE DAMAGE
MISSOURI GAS ENERGY	SAINT LOUIS	MO	2014	NO	NO	NO	NO	NO	62	NO		8		EXCAVATION DAMAGE
PEOPLES GAS LIGHT & COKE CO	CHICAGO	IL	2014	NO	NO	YES	NO	NO	60	YES	1962	20		INCORRECT OPERATION
CORDOVA, WATER WORKS & GAS	CORDOVA	AL	2015	YES	YES	YES	YES	YES	60	NO	1952	6		NATURAL FORCE DAMAGE
PHILADELPHIA GAS WORKS	PHILADELPHIA	PA	2015	NO	NO	NO	YES	YES	30	NO	1906	6		NATURAL FORCE DAMAGE
CONSUMERS ENERGY CO	JACKSON	MI	2015	NO	YES	NO	NO	NO	42	NO	1932	4		NATURAL FORCE DAMAGE
NIAGARA MOHAWK POWER CORP	NORTHBORO	MA	2015	NO	NO	NO	YES	YES		NO	1929	6		NATURAL FORCE DAMAGE
DTE GAS COMPANY	DETROIT	MI	2015	YES	YES	NO	YES	YES		NO	1923	6		NATURAL FORCE DAMAGE
CONSOLIDATED EDISON CO OF NY	NEW YORK	NY	2015	NO	YES	NO	NO	YES	UNKNOWN	NO		16		EQUIPMENT FAILURE
MISSOURI GAS ENERGY	SAINT LOUIS	MO	2015	NO	NO	YES	NO	NO	43	NO	1902	16		OTHER INCIDENT CAUSE
CONSOLIDATED EDISON CO OF NY	NEW YORK	NY	2015	NO	NO	YES	YES	NO	33	NO	1907	6		OTHER OUTSIDE FORCE DAMAGE
DTE GAS COMPANY	DETROIT	MI	2016	NO	NO	NO	YES	YES		NO	1931	6		MATERIAL FAILURE OF PIPE OR WELD
CONSOLIDATED EDISON CO OF NY	NEW YORK	NY	2016	NO	NO	YES	NO	NO	36	NO	1900	12		OTHER OUTSIDE FORCE DAMAGE
LACLEDE GAS CO	SAINT LOUIS	MO	2016	NO	NO	NO	NO	NO	84	NO	1903	24		MATERIAL FAILURE OF PIPE OR WELD
CENTERPOINT ENERGY	HOUSTON	TX	2016	YES	YES	YES	YES	NO	54	NO	1911	4		OTHER INCIDENT CAUSE
KEYSPAN ENERGY DELIVERY - NY CITY	WALTHAM	MA	2016	NO	NO	YES	NO	NO	48	NO		30		EXCAVATION DAMAGE
PHILADELPHIA GAS WORKS	PHILADELPHIA	PA	2016	NO	YES	NO	NO	NO		NO		4		OTHER OUTSIDE FORCE DAMAGE
DTE GAS COMPANY	DETROIT	MI	2017	NO	NO	YES	NO	NO	60	NO	1901	12		EXCAVATION DAMAGE
KEYSPAN ENERGY DELIVERY - NY CITY	WALTHAM	MA	2017	NO	NO	YES	NO	NO	24	NO	2000	24		EXCAVATION DAMAGE

Figure 54 shows the number of incidents from 2010 to 2015 sorted by material type and Figure 117 shows the causes of the cast iron failure in this reporting period. Figure 116 shows cast iron incidents resulting in a leak were about 47% of the incidents, about 18% of the pipes had a rupture, and the remaining percentage was mostly characterized by circular cracking due to external loads. Out of the cast iron pipe incidents in this period, two incidents were caused by external corrosion of the pipe.

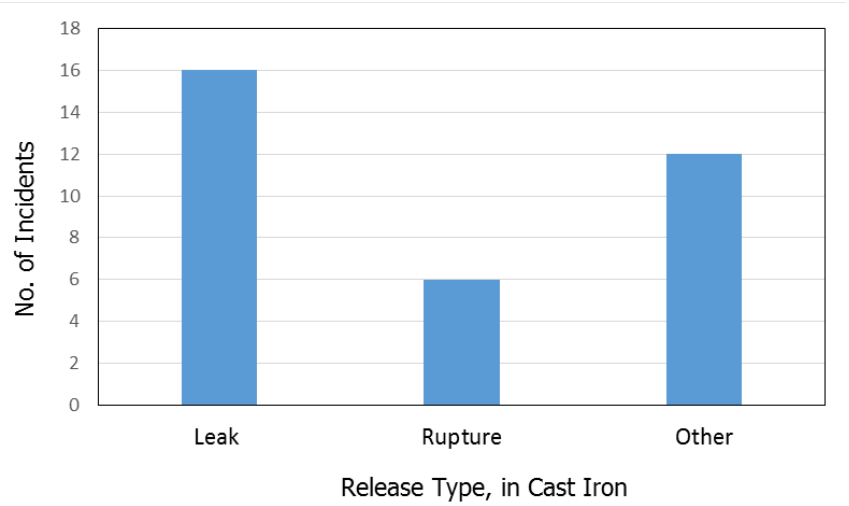

Figure 116. Type of pipe failure in the cast iron incidents

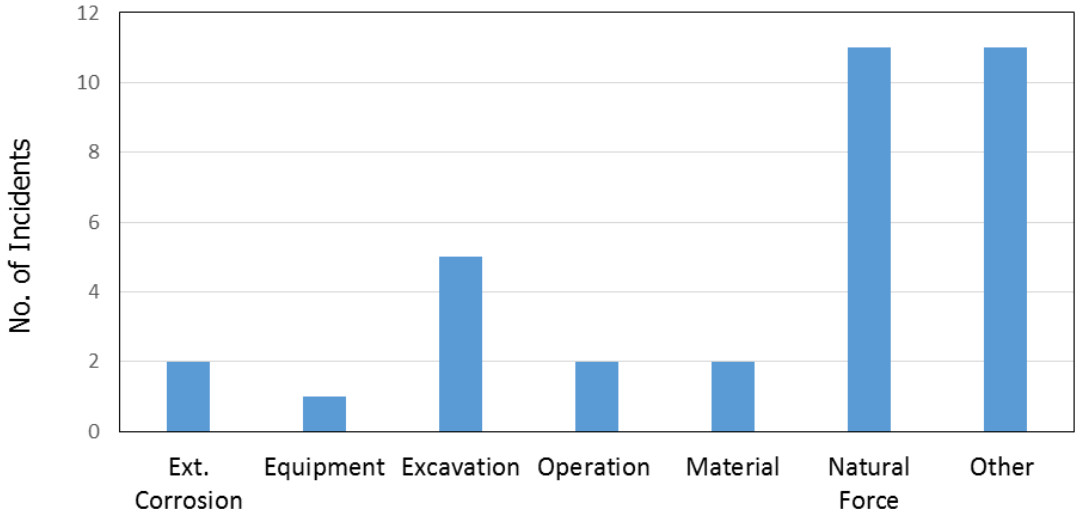

Figure 117. Causes of incidents in cast iron pipes

Modeling of Cast Iron Failures Using the FFS Program

The two incidents caused by localized graphitic corrosion and resulted in circumferential crack failures are shown below. Pipe attributes and failure parameters are shown in each case based on PHMSA failure records.

Case 1 - Corrosion Effects

Table 28 below shows pipe properties and incident characteristics of Case 1. The incident record did not specify the material class (i.e., tensile strength) of the cast iron pipes. The FFS analyses were accordingly performed using three cast iron classes of 20, 30, and 40 to evaluate the effect of their change on the overall strength of pipe and corresponding F.S. Incidents records indicated an old pipe material from 1928 with no road crossing. Soil temperature was taken at normal operating conditions. The pipe was severely corroded at the bottom and the maximum corroded depth was assumed in the data analysis.

Table 29 shows a sample run of the FFS program with cast iron class 40. The corroded pipe F.S. with the pipe parameters was 0.70. The change of the corroded pipe F.S. with pipe class is shown in Figure 118.

Table 28. Incident Characteristics of Case 1

Pipe Characteristics	
Pipe material	NA
Pipe diameter (inch)	6
Internal Pressure (psi)	5
Crossing	No
Depth of Cover (inch)	54
Installation year	1928
Location	Class 3
Incident	
City, State	Detroit, MI
Incident Year	Oct 2011
Damage Width	2 holes at bottom of pipes about 4 inch diam.
Damage Length	
Cause	External Graphitic Localized Corrosion
Consequences	Pipe rupture, fatality, release of gas

Table 29. Model Output of Case 1 with Cast Iron Class 40

Inputs:

Pipe Dimensions

Parameter	Units	Description	Value	Minimum	Maximum
class	ksi	Material class (tensile strength)	40	10	60
D	in	Pipe outer diameter	6	4.8	13.2
span	ft	Pipe span	12	12	18
t	in	Pipe wall thickness (if known)			<-- *If a value is entered h*
t.pred	in	Pipe wall thickness predicted by OD	**0.413**		

Corrosion Flaw Dimensions

Parameter	Units	Description	Value	Minimum	Maximum
flaw.d	in	Maximum corrosion flaw depth	0.33	0.021	0.330
flaw.l	in	Maximum corrosion flaw length (along pipe axis)	4	0.157	4.723
flaw.w	in	Maximum corrosion flaw width (around circumference)	4	0.942	9.236

Operating Conditions

Parameter	Units	Description	Value	Minimum
P	psig	Pressure	5	0
T.max	°F	Maximum buried operating temperature	75	
T.min	°F	Minimum buried operating temperature	55	

Soil and Traffic Loads

Parameter	Units	Description	Value	
soil.type		Soil type	Gravel/Base	
soil.weight	pcf	Soil wet weight per cubic foot	**153**	
soil.weight.user	pcf	Soil weight per cubic foot, user defined		<-- *If a value is entered h*
soil.depth	ft	Soil depth	4.5	
traffic.type		Traffic type (road,rail,none)	None	

Outputs:

Pipe stresses with corrosion defect

Parameter	Units	Description	Value
UTS	ksi	Material class (tensile strength)	**40**
P1.max	ksi	Maximum resolved tensile stress	**56.9**
SF.corroded	ratio	Tensile strength safety factor	**0.70**

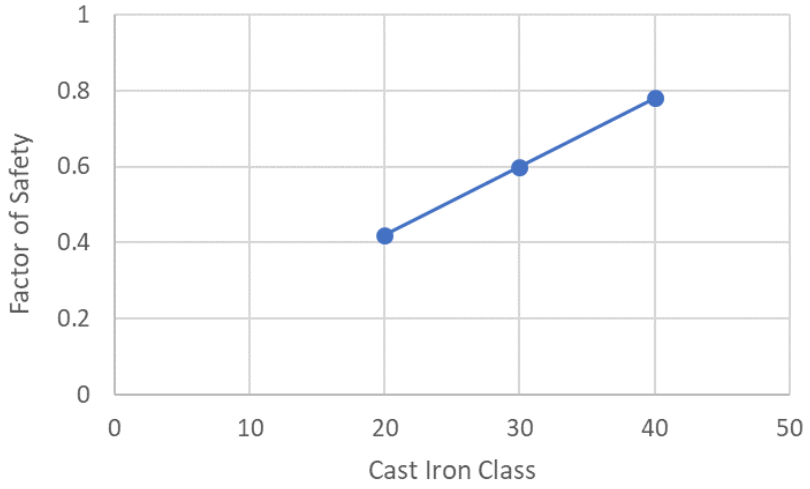

Figure 118. Case 1, Change of F.S. with Pipe Class

Case 2 - Corrosion and Crossing Effects

Table 30 below shows pipe properties and incident characteristics. Similar to Case 1, the FFS analyses were performed using three cast iron classes of 20, 30, and 40 to evaluate the effect of their change on the overall strength of pipe and corresponding factor of safety.

Incidents records indicated a relatively newer pipe material. Soil temperature was taken at normal operating conditions. The pipe was severely corroded with the size shown in Table 30, the maximum corroded depth was assumed in the analysis. As per the accident report, a segment of the graphitized main dislodged at the 6-O'clock position during clamp repair. A spark occurred which ignited the gas.

Table 31 shows a sample run of the FFS program with cast iron class 20. Modeling was performed with and without highway crossing conditions. The changes of the corroded pipe F.S. with pipe class and highway load are shown in Figure 119.

Table 30. Incident Characteristics of Case 2

Pipe Characteristics	
Pipe material	ASA A21.1
Pipe diameter (inch)	12
Internal Pressure, MOP (psi)	25
Crossing	No
Depth of Cover (inch)	48
Installation year	1961
Location	Class 3
Incident Characteristics	
City, State	Saint Louis, MO
Incident Year	2012
Damage Width (inch)	2.5
Damage Length (inch)	6.5
Cause	External Graphitic Localized Corrosion
Consequences	Shut down, ignition, evacuation, no explosion

Table 31. Model Output of Case 2 with Cast Iron Class 20

Inputs:

Pipe Dimensions

Parameter	Units	Description	Value	Minimum	Maximum
class	ksi	Material class (tensile strength)	20	10	60
D	in	Pipe outer diameter	12	4.8	13.2
span	ft	Pipe span	12	12	18
t	in	Pipe wall thickness (if known)			<-- If a value is entered h
t.pred	in	Pipe wall thickness predicted by OD	0.513		

Corrosion Flaw Dimensions

Parameter	Units	Description	Value	Minimum	Maximum
flaw.d	in	Maximum corrosion flaw depth	0.5	0.026	0.411
flaw.l	in	Maximum corrosion flaw length (along pipe axis)	2.5	0.248	7.446
flaw.w	in	Maximum corrosion flaw width (around circumference)	6.5	1.885	18.473

Operating Conditions

Parameter	Units	Description	Value	Minimum
P	psig	Pressure	25	0
T.max	°F	Maximum buried operating temperature	75	
T.min	°F	Minimum buried operating temperature	55	

Soil and Traffic Loads

Parameter	Units	Description	Value	
soil.type		Soil type	Gravel/Base	
soil.weight	pcf	Soil wet weight per cubic foot	153	
soil.weight.user	pcf	Soil weight per cubic foot, user defined		<-- If a value is entered h
soil.depth	ft	Soil depth	4	
traffic.type		Traffic type (road,rail,none)	Highway	

Outputs:

Pipe stresses with corrosion defect

Parameter	Units	Description	Value
UTS	ksi	Material class (tensile strength)	20
P1.max	ksi	Maximum resolved tensile stress	22.5
SF.corroded	ratio	Tensile strength safety factor	0.89

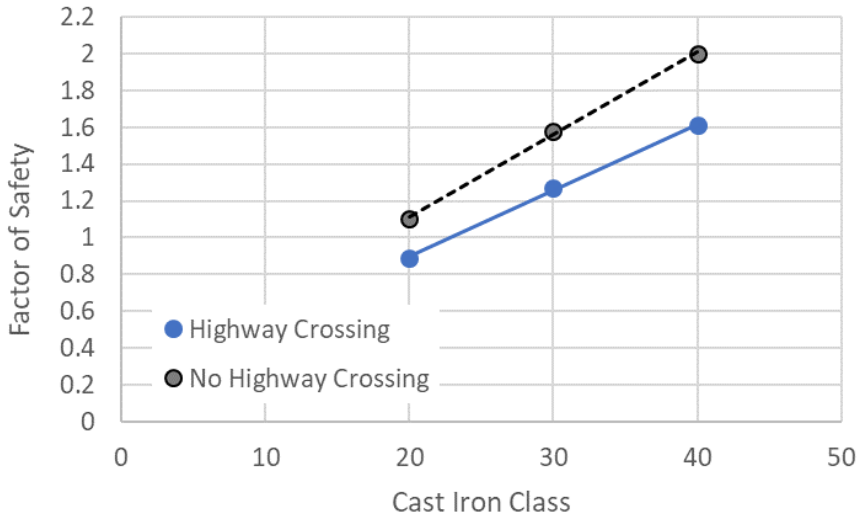

Figure 119. Case 2, Change of F.S. with Pipe Class and Crossing

Modeling of Cast Iron Failures Caused by Freeze

The FFS model was used to evaluate the circumferential stresses and corresponding factors of safety of the pipe when subjected to temperature changes and soil freeze. Since the reported significant incidents cause by this outside force did not have recorded metal loss, the analysis was performed with the minimal metal loss parameters in the program.

The estimated temperature changes where taken as typical one-cycle of soil temperature change from 75^{O}F to 30^{O}F. The results would show low F.S. values but it should be noted that pipe failures due to soil freeze commonly occurs as a results of accumulated cycles of extended freeze-thaw which are not modeled in the program.

Case 3 - Crossing Effects

Table 32 shows pipe properties and incident characteristics. The incident record did not specify metal loss or the material class of the cast iron pipes. Accordingly, the analysis was performed for three cast iron classes of 20, 30, and 40. The factor of safety was calculated for non-corroded pipe.

Table 33 shows a sample run of the FFS program with cast iron class 20. The change of the non-corroded pipe F.S. with pipe class is shown in Figure 120.

Table 32. Incident Characteristics of Case 3

Pipe Characteristics	
Pipe material	NA
Pipe diameter (inch)	6
Internal Pressure, MOP (psi)	2
Crossing	No
Depth of Cover (inch)	48
Installation year	1930
Location	Class 3
Incident Characteristics	
City, State	Waltham, MA
Incident Year	2010
Damage Width (inch)	NA
Damage Length (inch)	NA
Cause	Crack due to frost heave
Consequences	Injury, Ignition, Explosion

Table 33. Model Output of Case 3 with Cast Iron Class 20

Inputs:

Pipe Dimensions

Parameter	Units	Description	Value	Minimum	Maximum	
class	ksi	Material class (tensile strength)	20	10	60	
D	in	Pipe outer diameter	6	4.8	13.2	
span	ft	Pipe span	12	12	18	
t	in	Pipe wall thickness (if known)				*<-- If a value is entered h*
t.pred	in	Pipe wall thickness predicted by OD	**0.413**			

Corrosion Flaw Dimensions

Parameter	Units	Description	Value	Minimum	Maximum	
flaw.d	in	Maximum corrosion flaw depth	**0**	0.021	0.330	N
flaw.l	in	Maximum corrosion flaw length (along pipe axis)	**0**	0.157	4.723	N
flaw.w	in	Maximum corrosion flaw width (around circumference)	**0**	0.942	9.236	N

Operating Conditions

Parameter	Units	Description	Value	Minimum
P	psig	Pressure	2	0
T.max	°F	Maximum buried operating temperature	75	
T.min	°F	Minimum buried operating temperature	30	

Soil and Traffic Loads

Parameter	Units	Description	Value	
soil.type		Soil type	Gravel/Base	
soil.weight	pcf	Soil wet weight per cubic foot	**153**	
soil.weight.user	pcf	Soil weight per cubic foot, user defined		*<-- If a value is entered h*
soil.depth	ft	Soil depth	4	
traffic.type		Traffic type (road,rail,none)	Highway	

Outputs:

Pipe stresses with corrosion defect

Parameter	Units	Description	Value
UTS	ksi	Material class (tensile strength)	**20**
P1.max	ksi	Maximum resolved tensile stress	**21.4**
SF.corroded	ratio	Tensile strength safety factor	**0.93**

Pipe stresses with no defect

Parameter	Units	Description	Value
UTS	ksi	Material class (tensile strength)	**20**
P1.max.flawless	ksi	Maximum resolved radial stress, without flaw	**15.6**
SF.flawless	ratio	Tensile strength safety factor of flawless pipe	**1.28**
P.hoop	ksi	Hoop stress due to internal pressure (Barlow's Formula)	**0.01**

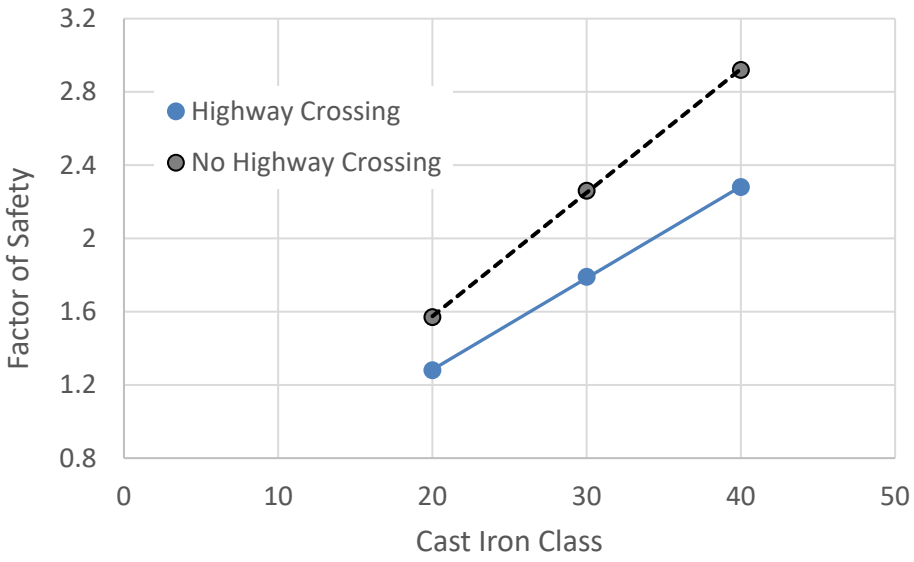

Figure 120. Case 3, Non-Corroded Pipe F.S. with Pipe Class and Crossing

Case 4 - Non- Corroded Pipe

Table 34 shows pipe properties and incident characteristics of Case 4. The incident record did not specify meta loss or the material class of the cast iron pipes. The analysis was performed with no-metal loss and the factor of safety was calculated for a 4 inch diameter non-corroded pipe.

Table 35 shows a sample run of the FFS program. The F.S. for the non-corroded pipe is shown in Figure 121.

Table 34. Incident Characteristics of Case 4

Pipe Characteristics	
Pipe material	ANSI/AWWA
Pipe diameter (inch)	4
Internal Pressure, MOP (psi)	35
Crossing	No
Depth of Cover (inch)	NA
Installation year	1959
Location	Class 4
Incident Characteristics	
City, State	Newark, NJ
Incident Year	2010
Damage Width (inch)	0.3
Damage Length (inch)	50.2
Cause	Circumferential rupture due to earth movement

Table 35. Model Output of Case 4 with Cast Iron Class 20

Inputs:

Pipe Dimensions

Parameter	Units	Description	Value	Minimum	Maximum	
class	ksi	Material class (tensile strength)	20	10	60	
D	in	Pipe outer diameter	4	4.8	13.2	I
span	ft	Pipe span	12	12	18	
t	in	Pipe wall thickness (if known)				*<-- If a value is entered h*
t.pred	in	Pipe wall thickness predicted by OD	0.401			

Corrosion Flaw Dimensions

Parameter	Units	Description	Value	Minimum	Maximum	
flaw.d	in	Maximum corrosion flaw depth	0	0.020	0.320	I
flaw.l	in	Maximum corrosion flaw length (along pipe axis)	0	0.127	3.797	I
flaw.w	in	Maximum corrosion flaw width (around circumference)	0	0.628	6.158	I

Operating Conditions

Parameter	Units	Description	Value	Minimum
P	psig	Pressure	35	0
T.max	°F	Maximum buried operating temperature	75	
T.min	°F	Minimum buried operating temperature	25	

Soil and Traffic Loads

Parameter	Units	Description	Value	
soil.type		Soil type	Sand/Silt	
soil.weight	pcf	Soil wet weight per cubic foot	127	
soil.weight.user	pcf	Soil weight per cubic foot, user defined		*<-- If a value is entered h*
soil.depth	ft	Soil depth	3	
traffic.type		Traffic type (road,rail,none)	Highway	

Outputs:

Pipe stresses with corrosion defect

Parameter	Units	Description	Value
UTS	ksi	Material class (tensile strength)	20
P1.max	ksi	Maximum resolved tensile stress	23.6
SF.corroded	ratio	Tensile strength safety factor	0.85

Pipe stresses with no defect

Parameter	Units	Description	Value
UTS	ksi	Material class (tensile strength)	20
P1.max.flawless	ksi	Maximum resolved radial stress, without flaw	17.4
SF.flawless	ratio	Tensile strength safety factor of flawless pipe	1.15
P.hoop	ksi	Hoop stress due to internal pressure (Barlow's Formula)	0.17

Figure 121. Case 4, Non-Corroded Pipe F.S. with Pipe Class

Case 5 - Corrosion Severity

Table 36 shows pipe properties and incident characteristics of Case 5. Similar to earlier cases with soil freeze, the incident record did not specify meta loss. The analysis was performed with the factor of safety calculated for non-corroded pipe and for the case of minimum metal loss to evaluate their combined effect. Table 37 shows a sample run of the FFS program. The F.S. for corroded and non-corroded pipes is shown in Figure 122.

Table 36. Incident Characteristics of Case 5

Pipe Characteristics	
Pipe material	NA
Pipe diameter (inch)	4
Internal Pressure, MOP (psi)	5
Crossing	No
Depth of Cover (inch)	48
Installation year	1930
Location	Class 3
Incident Characteristics	
City, State	Detroit, MI
Incident Year	March 2011
Damage Width (inch)	NA
Damage Length (inch)	NA
Cause	Circumferential crack due to frost heave
Consequences	Explosion

Table 37. Model Output of Case 5 with Cast Iron Class 20

Inputs:

Pipe Dimensions

Parameter	Units	Description	Value	Minimum	Maximum	
class	ksi	Material class (tensile strength)	20	10	60	
D	in	Pipe outer diameter	4	4.8	13.2	I
span	ft	Pipe span	12	12	18	
t	in	Pipe wall thickness (if known)				*<-- If a value is entered h*
t.pred	in	Pipe wall thickness predicted by OD	0.401			

Corrosion Flaw Dimensions

Parameter	Units	Description	Value	Minimum	Maximum	
flaw.d	in	Maximum corrosion flaw depth	0	0.020	0.320	I
flaw.l	in	Maximum corrosion flaw length (along pipe axis)	0	0.127	3.797	I
flaw.w	in	Maximum corrosion flaw width (around circumference)	0	0.628	6.158	I

Operating Conditions

Parameter	Units	Description	Value	Minimum
P	psig	Pressure	35	0
T.max	°F	Maximum buried operating temperature	75	
T.min	°F	Minimum buried operating temperature	25	

Soil and Traffic Loads

Parameter	Units	Description	Value	
soil.type		Soil type	Sand/Silt	
soil.weight	pcf	Soil wet weight per cubic foot	127	
soil.weight.user	pcf	Soil weight per cubic foot, user defined		*<-- If a value is entered h*
soil.depth	ft	Soil depth	3	
traffic.type		Traffic type (road,rail,none)	Highway	

Outputs:

Pipe stresses with corrosion defect

Parameter	Units	Description	Value
UTS	ksi	Material class (tensile strength)	20
P1.max	ksi	Maximum resolved tensile stress	23.6
SF.corroded	ratio	Tensile strength safety factor	0.85

Pipe stresses with no defect

Parameter	Units	Description	Value
UTS	ksi	Material class (tensile strength)	20
P1.max.flawless	ksi	Maximum resolved radial stress, without flaw	17.4
SF.flawless	ratio	Tensile strength safety factor of flawless pipe	1.15
P.hoop	ksi	Hoop stress due to internal pressure (Barlow's Formula)	0.17

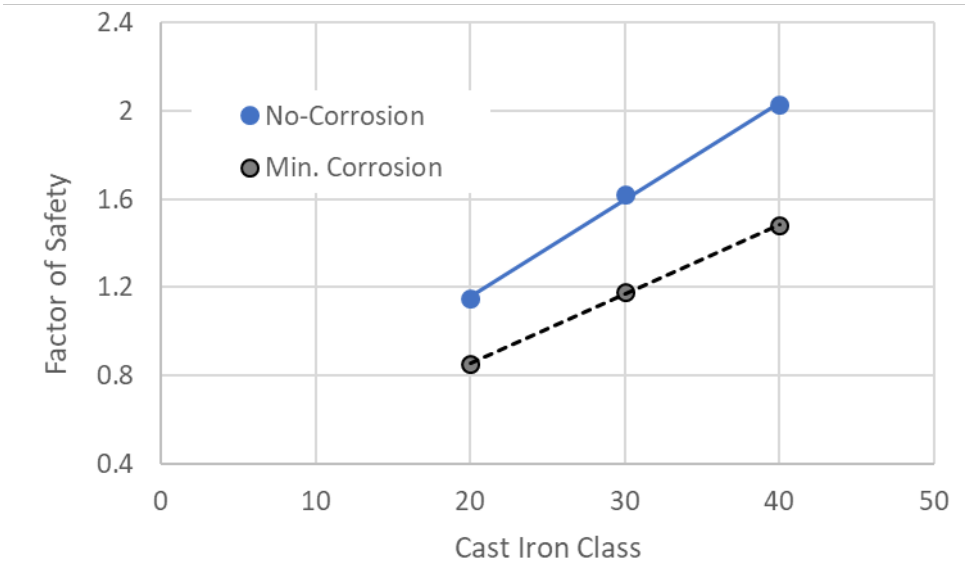

Figure 122. Case 5, Corroded and Non-Corroded Pipe F.S.

Case 6 - Soil Effects

Table 38 shows pipe properties and incident characteristics of Case 6. Two incidents in this case had similar characteristics. The analysis was performed with the factor of safety calculated for non-corroded pipe. Table 39 shows a sample run of the FFS program. The F.S. for the non-corroded pipes is shown in Figure 123 for clay and sandy soil. Small change in the F.S. is shown for these soil types.

Table 38. Incident Characteristics of Case 6

Pipe Characteristics	Incident 6-A	Incident 6-B
Pipe material	NA	NA
Pipe diameter (inch)	6	6
Internal Pressure, MOP (psi)	0.5	0.5
Crossing	No	No
Depth of Cover (inch)	30	NA
Installation year	1906	1929
Location	Class 4	Class 3
Incident Characteristics		
City, State	Philadelphia, PA	Northborough, MA
Incident Year	2015	2015
Damage Width (inch)	NA	NA
Damage Length (inch)	NA	NA
Cause	Crack due to frost heave	Crack due to frost heave
Consequences	Ignition, Explosion	Ignition, Explosion

Table 39. Model Output of Case 6

Inputs:

Pipe Dimensions

Parameter	Units	Description	Value	Minimum	Maximum	
class	ksi	Material class (tensile strength)	20	10	60	
D	in	Pipe outer diameter	6	4.8	13.2	
span	ft	Pipe span	12	12	18	
t	in	Pipe wall thickness (if known)				*<-- If a value is entered he*
t.pred	in	Pipe wall thickness predicted by OD	**0.413**			

Corrosion Flaw Dimensions

Parameter	Units	Description	Value	Minimum	Maximum	
flaw.d	in	Maximum corrosion flaw depth	**0**	0.021	0.330	N
flaw.l	in	Maximum corrosion flaw length (along pipe axis)	**0**	0.157	4.723	N
flaw.w	in	Maximum corrosion flaw width (around circumference)	**0**	0.942	9.236	N

Operating Conditions

Parameter	Units	Description	Value	Minimum
P	psig	Pressure	0.5	0
T.max	°F	Maximum buried operating temperature	75	
T.min	°F	Minimum buried operating temperature	25	

Soil and Traffic Loads

Parameter	Units	Description	Value	
soil.type		Soil type	Sand/Silt	
soil.weight	pcf	Soil wet weight per cubic foot	**127**	
soil.weight.user	pcf	Soil weight per cubic foot, user defined		*<-- If a value is entered he*
soil.depth	ft	Soil depth	3	
traffic.type		Traffic type (road,rail,none)	Highway	

Outputs:

Pipe stresses with corrosion defect

Parameter	Units	Description	Value
UTS	ksi	Material class (tensile strength)	**20**
P1.max	ksi	Maximum resolved tensile stress	**21.8**
SF.corroded	ratio	Tensile strength safety factor	**0.92**

Pipe stresses with no defect

Parameter	Units	Description	Value
UTS	ksi	Material class (tensile strength)	**20**
P1.max.flawless	ksi	Maximum resolved radial stress, without flaw	**15.4**
SF.flawless	ratio	Tensile strength safety factor of flawless pipe	**1.30**
P.hoop	ksi	Hoop stress due to internal pressure (Barlow's Formula)	**0.00**

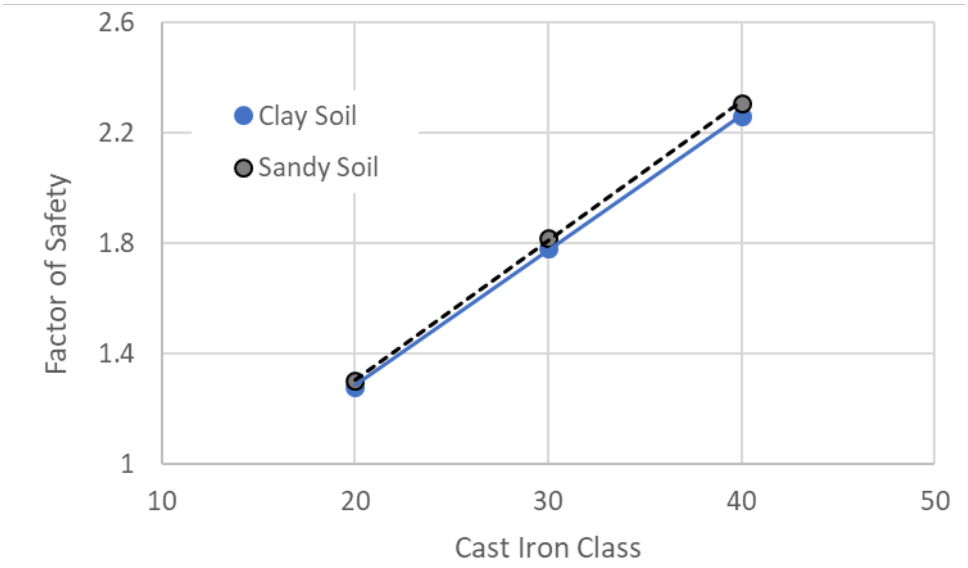

Figure 123. Case 6, Non-Corroded Pipe F.S. for Different Soils

Effect of Input Uncertainty on Model Output

To quantify the extent that typical input (measurement) uncertainty might have on model output the input values were modeled with a normal distribution of measurement error. The maximum and minimum error were also bounded and a standard deviation of three was used for the distribution shape. The distribution was normal, hence symmetric with no skew or long tails.

Input Variable Uncertainty

These assumptions are sound based on well-established measurement statistics and process control. Based on prior research and direct observations of error, the bounded conditions for the uncertainty distributions are shown in Table 40 below.

Table 40. Input Variable Uncertainty Bounds

Input Variable	Units	Min/Max Bounds of Measurement
Pipe Tensile Strength (Class)	KSI	+/- 10%
Pipe Outer Diameter (OD)	Inches	+/- 1%
Flaw Depth (Flaw D)	Inches	+/- 5%
Flaw Length (Flaw L)	Inches	+/- 5%
Flaw Width (Flaw W)	Inches	+/- 5%
Burial Depth (Soil D)	Feet	+/- 10%

Five Monte Carlo simulations were conducted to gauge the effect the input uncertainty would have on the model output vs. a measurement with no uncertainty taken into consideration.

It should be noted again that the model output is the 97.5% Upper Prediction Limit (UPL) of the prediction surface for both average and maximum stress solutions. This is a very conservative approach and has a built in conservative factor in the solution. For the Monte Carlo simulations we used both the average and maximum stress solutions from the model for the flawed pipe with free ends.

Monte Carlo Simulation Set Up

The simulations each included 20,000 samples using a decoupled and random selection of variable uncertainty from distributions. The average and maximum stresses were calculated for both the standard solution and then for the solution with the uncertainty perturbations. The % Difference was plotted on a combined Histogram/Pareto diagram with upper prediction limits for the difference set at 90%.

Simulation Results

Two of the six failure cases discussed in this section above were selected for simulation runs: Case 1 and Case 5 - these were both field failures. An additional three cases (near, but not failures) were run to round out the ranges of input variables: Example #1, #2, and #3.

A summary of the simulations and the % Difference for Maximum Stress for both the Ave. and Max. cases are shown in Table 41 below. This table also lists the most likely value (MVL) for the factor of safety for each case. Note the two field failures had F.S. < 1.0 as one would expect.

The plots are displayed after the table.

Table 41. Input Variable Uncertainty Bounds

Simulation Name	Class (ksi)	OD (in)	Span (ft)	Flaw D (in)	Flaw L (in)	Flaw W (in)	Soil Dep (ft)	%Diff Ave UPL	%Diff Max UPL	Factor of Safety (F.S.)
Failure Case #1	40	6	12	0.33	4.0	4.0	4.5	3.95%	3.6%	0.70
Failure Case #5	20	4	12	0.020	0.127	0.628	3	1.76%	1.88%	0.85
Example #1	30	10	18	0.25	4	8	6	4.26%	5.13	1.06
Example #2	20	6	12	0.05	1	4	6	4.38	5.15	1.17
Example #3	50	8	18	0.2	1	5	6	4.26	4.03	1.14

The % Differences between the expected values of average and maximum stresses and the same when variability due to uncertainty in input values are included are very reasonable and between approximately 2%-5% across the board. This is a reasonable amount of variability and shows the model is robust as related to input variability. Additionally, since both the average and maximum solutions are the 97.5% UPL, the variability due to measurement uncertainty is more than offset by the conservatism of using the UPL for the solutions and not the expected values.

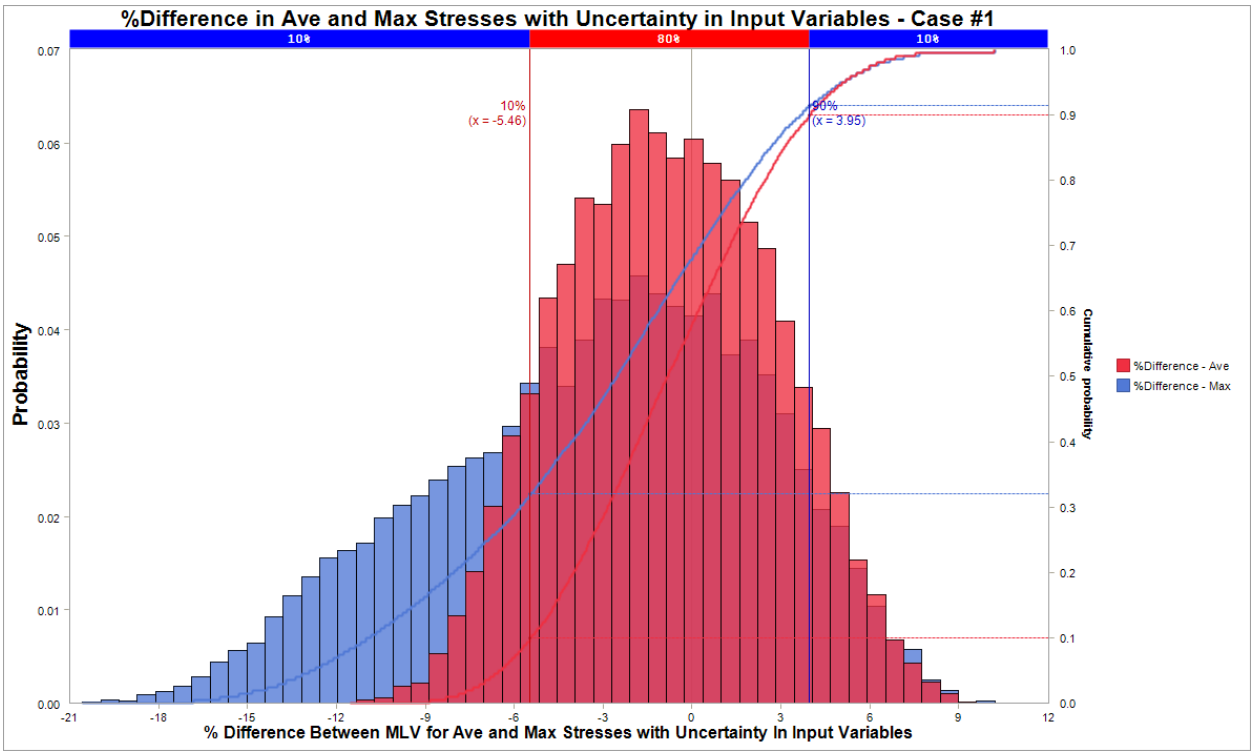

Figure 124. Monte Carlo Simulation Results for % Difference in Stresses - Failure Case #1

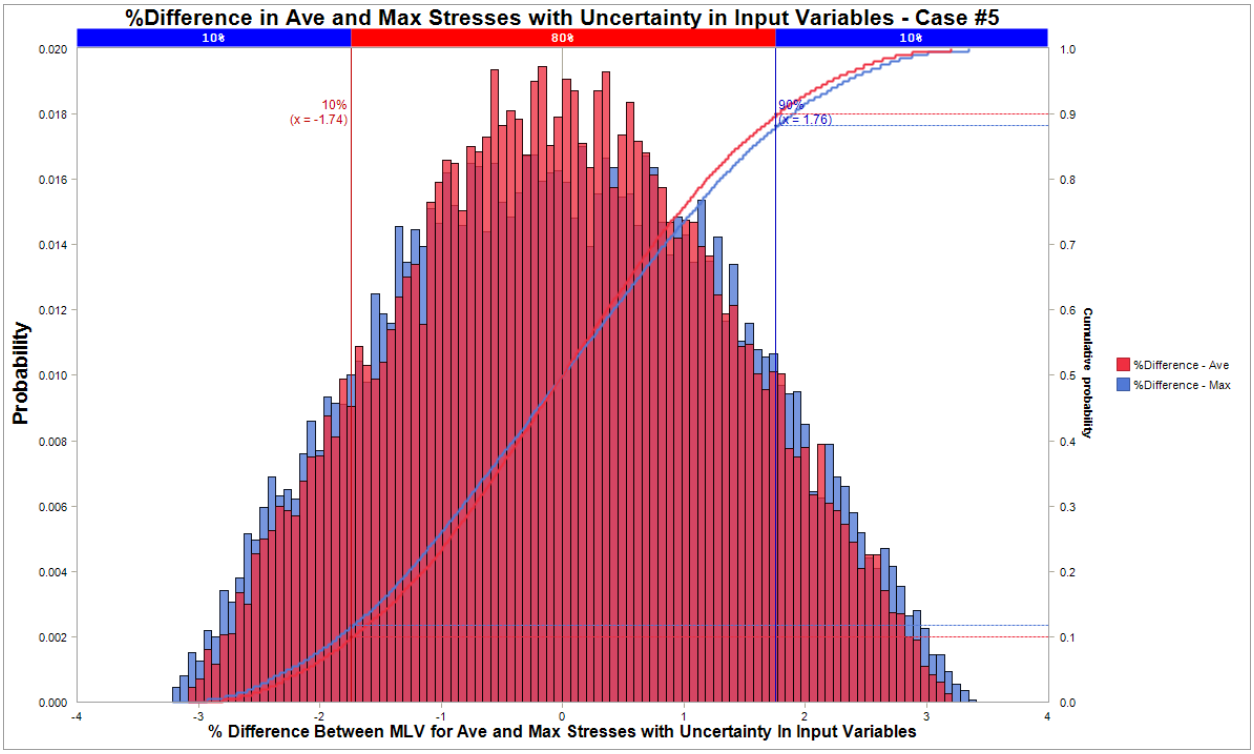

Figure 125. Monte Carlo Simulation Results for % Difference in Stresses - Failure Case #5

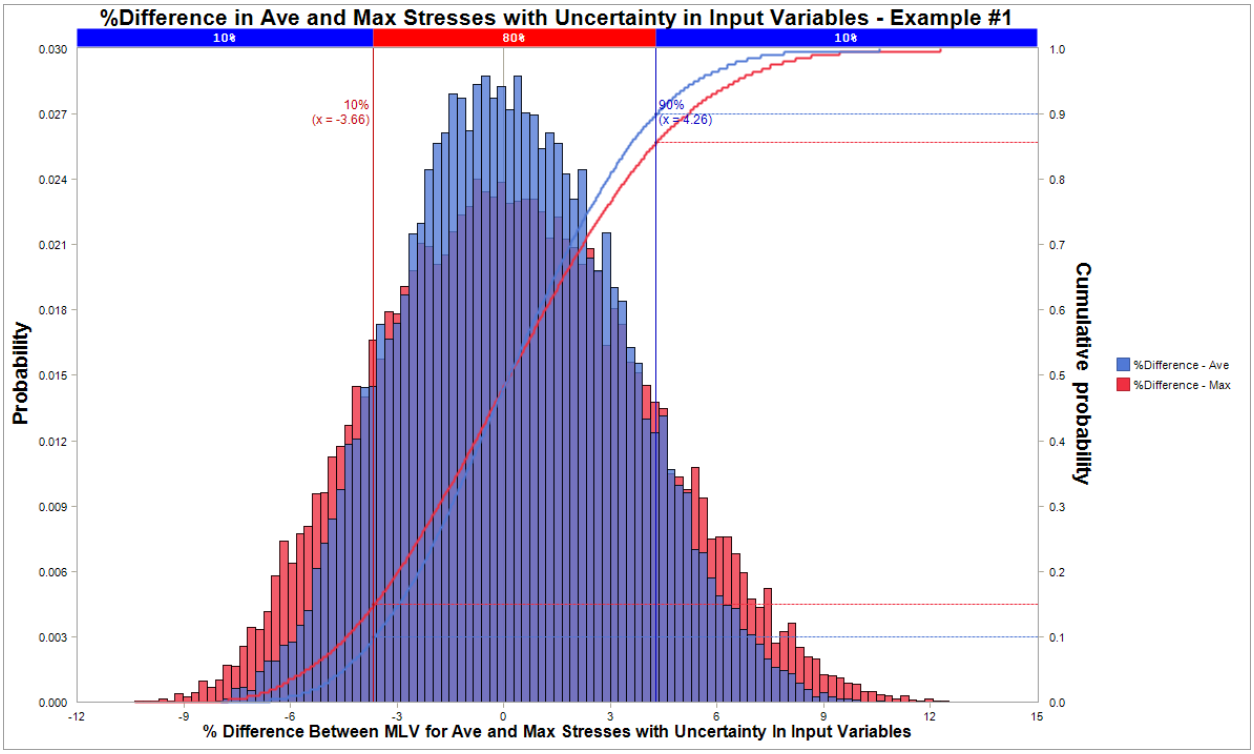

Figure 126. Monte Carlo Simulation Results for % Difference in Stresses - Example #1

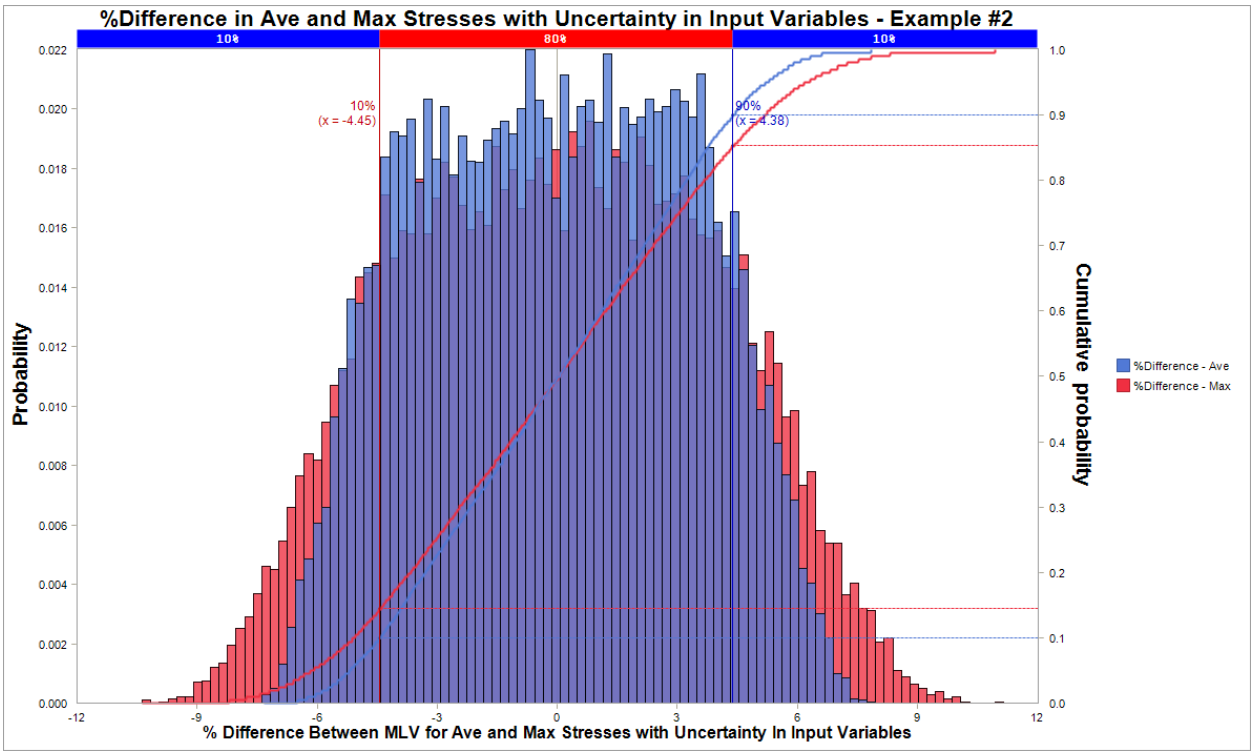

Figure 127. Monte Carlo Simulation Results for % Difference in Stresses - Example #2

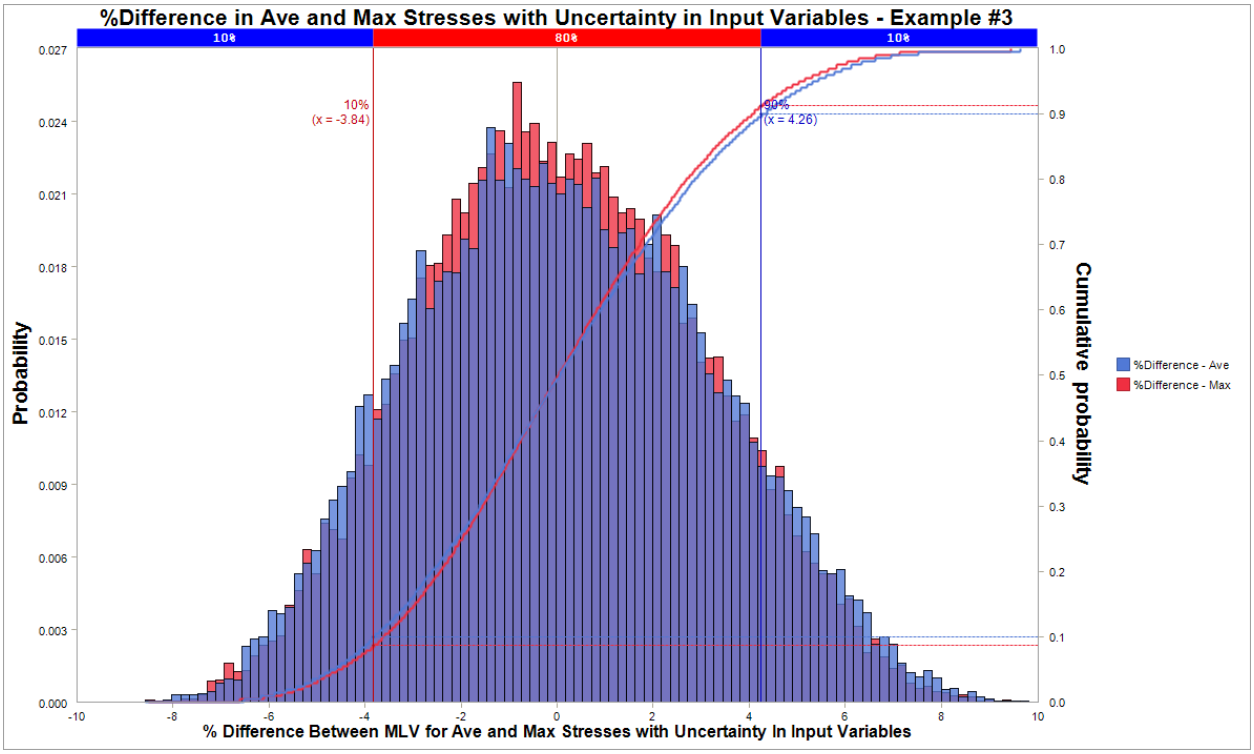

Figure 128. Monte Carlo Simulation Results for % Difference in Stresses - Example #3

7. Physical Testing Validation Program Concept

This section provides the basis for and the specific recommendations for a comprehensive, testing-based validation program for the developed FFS model. The program considers and lists the gray iron materials testing specifications, consensus standards for mechanical testing, currently available (new) gray cast iron materials, vintage piping samples to consider, and how many testing replicates are recommended for each material type.

Gray Iron Material Test Specifications

Any program to develop mechanical test data on gray irons must first consider the wide variety of microstructures and material properties that are found in these historical pipe materials. **Section 2** of this report discusses the metallurgy of gray iron in some detail. The table below lists historical and modern gray iron mechanical specifications.

Table 42. Gray Iron Test Specifications

Specification	Year	Class	UTS	Modulus of Rupture	Comments
AWWA Cast Iron Pipe Specification	1908	NA	20 ksi	NA	UTS by tensile bar
ASA A21.1 Cast Iron Pit Cast Pipe	1939	NA	11 ksi	40 ksi	UTS by burst test
ASA A21.7 Cast Iron Centrifugally Cast Pipe	1952	NA	18 ksi	40 ksi	UTS by burst test
ANSI/AWWA C101 Thickness Design of Cast Iron Pipe	1957	NA	21 ksi	45 ksi	Specimens Machined from Cast test Bars
ASTM A74 Standard Specification for Cast Iron Soil Pipe and Fittings	2016	NA	21 ksi	NA	
ASTM A48 Standard Specification for Gray Iron Castings	2016	class 20	20 ksi	NA	
		class 25	25 ksi		
		class 30	30 ksi		
		class 35	35 ksi		
		class 40	40 ksi		
		class 45	45 ksi		
		class 50	50 ksi		
		class 55	55 ksi		
		class 60	60 ksi		

It is noteworthy that the tensile strength specification for pit cast pipe was changed substantially between 1908 and 1939, from 20ksi on tensile bars to 11ksi on pipe burst tests. This was done after extensive testing indicated casting defects from the pit casting process introduced strength lowering defects that were not detected in cast tensile bars.

Per the ANSI A21.1 standard introduced in 1939 and the later 1952 A21.7 standard for centrifugally cast pipe, it was intended that the day to day production testing was to be done with Talbot strip bend tests. Ring and pipe burst tests were to be performed once a month. Modulus of Rupture was determined by conducting 4-point bend tests on strip samples and a 3-edge bend test on a pipe ring specimen.

Gray Iron Mechanical Tests

Specifics of some the most common gray iron mechanical tests are listed below. Included in the table are both tests specified by standards organizations and some used by previous investigators of cast iron pipe failures.

Table 43. Gray Iron Mechanical Tests

Standards Organization	Test Type	Specification	Test Specimen approx dimensions	Comments	
ASTM	Compression Test	E-9 Standard Test Methods of Compression Testing	1" x 0.5"dia.	Standard ASTM compression test of machined cylindrical specimens, demanding requirements for test fixturing, specimen preparation.	
ANSI-AWWA	Talbot Strip Test of Modulus of Rupture	ANSI C106 Gray Iron Pipe Centrifugally Cast Pipe	10.5" x 0.5" x pipe wall thickness longitudinal from pipe specimen, parallel machined sides	4 point bend test, 10" between supports, loads applied at two points 3.33" in from supports.	Modulus of Rupture $R = Wl/td^2$ where W is the breaking load, l is the span between supports, t is the wall thickness and d is the machined width.
ANSI-AWWA	Pipe Ring Test for Modulus of Rupture	ANSI C106 Gray Iron Pipe Centrifugally Cast Pipe	for pipe $\leq$ 12" ring length = 1/2 the nominal dia., for pipe sizes $\geq$ 14", 10.5" ring length	3 edge ring compression test, U-channel in bottom hardwood block, single top hardwood block. This test is designed to produce longitudinal cracks.	$R = 0.954(W(d+t)/bt^2)$ where R is modulus of rupture, W is the breaking load, d is the inside diameter, t= thickness and b= ring length.
ASTM	Bend Test	A438 Standard Test Method for Transverse Testing Of Gray Cast Iron	15" x 1" round bar	3 point bend test with tables that allow estimates of UTS based on the breaking load of a test bar.	
ASTM	Tensile Test	A74 Standard Specification for Cast Iron Soil Pipe and Fittings , ASTM A48 and E8	4" long, 0.5" dia. in gauge length	Standard tensile test per ASTM A48 and E8m, specimen machined from cast bar.	
N/A	Strip Flexure Test	4 point bend test	120mm x 10mm x WT strip samples	Bend test used by Belmonte et al . 2008 to produce failure strength data and Weibull modulus. N = 10-15/pipe.	
N/A	Longitudinal Bend test	4 point bend test	1.4 m pipe specimen	Pipe bend test used by Seica *et al* 2004 to produce circumferential failures.	

Gray Iron Materials Currently Available

To develop a comprehensive database of mechanical properties of gray iron it will be necessary to test both new production gray iron materials and vintage pipe. Table 3 below describes gray iron materials that are currently available in the marketplace.

Table 44. New production gray iron materials

Configuration	Manufacturer	Product	UTS spec	ASTM A247 Flake type	ASTM A247 Flake size	Matrix	Comments
Bars and Machined Tubes	Dura-Bar	G2	40 ksi min	A and D	4-6	pearlite, with ferrite/pearlite rim	This grade also produced in trepanned tubes, e.g. 7" OD with 5" ID
	Dura-Bar	G2S	40 ksi min	A and D	4-6	pearlite, rim 80% pearlite	This grade also produced in trepanned tubes, e.g. 7" OD with 5" ID
	Dura-Bar	G2P	40 ksi min	A and D	4-6	pearlite, rim 80% pearlite	
	Dura-Bar	G2A	40 ksi min	D	6-8	pearlite	
	Dura-Bar	G1A	25 ksi min	D	6-8	ferrite	Dura-Bar states that this grade is not a stock item but "can be ordered in volume quantities"
New Pipe	Charlotte Pipe	ASTM A74 Cast Iron Soil Pipe	21 ksi min	unspecified	unspecified	unspecified	(n.b. per the mfr's literature the pipes are spun cast, therefore the actual tensile is probably closer to the range of 30 to 40ksi than to 21ksi, see Makar & McDonald 2007)
Pipe Fittings	Charlotte Pipe	ASTM A74 Cast Iron Soil Pipe	21 ksi min	unspecified	unspecified	unspecified	(n.b. per the mfr's literature fittings are cast in static molds this should create a coarser graphite structure and lower UTS than spun cast pipe)

Gray Iron Vintage Materials

A large fraction of the cast iron pipes currently in service were produced by the pit casting process prevalent before the 1920s. Pit casting produced a coarser graphitic microstructure and a lower UTS pipe with more frequent casting defects. Because pit cast iron pipes are no longer manufactured GTI has made plans to acquire vintage pit cast pipes from local gas distribution companies. GTI has on hand sufficient vintage pipe specimens to conduct some tensile, compression and strip bend/flexural tests but not pipe bend tests. The table below lists some of these specimens on hand.

Table 45. Cast Gray Iron Coupons in GTI Pipe Library

Coupon Size	Installation Year	UTS Spec	ASTM A247 Flake Type	ASTM A247 Flake Size	Matrix	Comments
Approx. 10"x10" coupon from 20" pipe	N/A	N/A	A/B	2/3	ferrite /pearlite	Pit cast pipe. Based on its microstructure, this is probably the lowest strength vintage sample in GTI's library, coarse large flake graphite and mostly ferritic matrix.
6" x 11.5"	N/A	N/A	A/B	3	pearlitic	
6" x 20"	N/A	N/A	A	3	pearlitic	
4" x 14"	1948	N/A	D	7	ferrite /pearlite	Spun cast pipe. Fine graphite microstructure.
6" x 14"	N/A	N/A	A/B	3	pearlitic	
6" x 13.5"	N/A	N/A	A/B	3	pearlitic	

Planned Testing Scope Considerations

GTI has not as of yet conducted any mechanical testing but based on the variations seen in microstructures as shown in the table above, and on the papers published by previous investigators we expect them to be large.

Tensile and Compression Testing

In order to comprehensively model the mechanical properties of gray iron pipe it will be necessary to perform both tensile (ASTM A48) and compression tests (ASTM E9) with a video extensometer to establish the true stress strain properties of various gray iron materials.

Form and Vintage of Test Specimens

The materials to be tested will include vintage pit cast pipe, vintage spun cast pipe, modern spun cast pipe and modern static cast fittings. Based on their microstructures and reported tensile strengths the available continuous cast bar material does not appear as a suitable material for testing.

Bend Testing

Both 3 point and 4 point bend tests will also be performed to establish Weibull distributions on both corroded and non-corroded specimens.

Corroded Specimens - Natural and Machined

Where corroded specimens are not available machined defects will be introduced. After the properties of a given pipe have been determined they will be input to the finite element analysis model.

The exact dimensions of the pipes and their defects and the defect locations will be measured by structured light or laser scanning to produce a precise specimen geometry. The model will then be used to simulate a bend test to failure.

FEA Modeling and Analysis

The FEA model predictions will subsequently be evaluated against the actual bend test results. Additionally, true stress strain curve(s) will be created through testing to validate the interpolated and/or extrapolated curves for the current model.

Planned Testing Matrix

The table below describes the planned test matrix.

Table 46. Test Replicate Table

Material	TEST REPLICATES							
	Form	A48/E8 Tensile	E9 Compression	ASTM A247 Microstructure	4 point bend of longitudinal strip	4 point bend of pipe	3 point ring bearing	Hydrostatic Pressure Test
Vintage Pit Cast Iron Pipe	pipe 1	3	3	1	5	1	1	
	pipe 2	3	3	1	5	1	1	
	pipe 3	3	3	1				1
Vintage Spun Cast Iron Pipe	pipe 4	3	3	1	5	1	1	
	pipe 5	3	3	1	5	1	1	
	pipe 6	3	3	1				1
2018 A74 spun cast soil pipe (new production)	as received	5	5	1	15	3	3	1
	w. artificial defects				15	3	3	
2018 A74 static cast soil pipe fitting (new production)	as received	5	5	1	15	3	3	
	w. artificial defects				15	3	3	

End of Report Body

Recommendations

The Technical Advisory Panel (TAP) suggested that the project expand the applicability of the calculator solution to include larger diameter pipe, 20 inch and larger, which several of them are currently using.

Another suggestion is to provide a full geo-spatial implementation example showing the solution applied to a cast iron network with rankings for an accelerated mains replacement program.

Based on these suggestions, the project team will augment the FFS solution for the larger diameter cast iron pipes and provide a geo-spatial example of the FFS solution applied to a pipe network.

These additional features will be distributed by an addendum report and revised calculator by December 31, 2018.

Appendix A – Field Testing and Sampling Considerations

The determination of a cast iron pipe's properties requires both in the field measurements and laboratory testing. Both the pipe diameter and length should be measured in the field.

Length of Pipe Section

The pipe length has been found to be an important variable in failure rates because of its effect on a pipe's beam stiffness.

Hardness Testing for Tensile Relationships

Hardness testing can also be performed in the field with a portable Brinell hardness tester though with reduced precision from a laboratory setting. This can be used to estimate tensile strength from known relationships.

Wall Thickness

Wall thickness can be easily and accurately measured on steel pipes with ultrasonic gages. These instruments however cannot be readily used on cast iron pipes in the field. Cast irons exhibit highly variable reflection and absorption characteristics depending on their particular graphite microstructures. When these conditions are unknown, accurate calibration is not possible.

Metallography

Metallography of steel structures is likewise a useful tool but field metallography of cast iron is not a realistic possibility. Because of the dramatic differences between the surface and mid-wall microstructures, surface examination would not reveal any useful information.

Test Coupons

In order to obtain sufficient material for laboratory testing, test coupons should be cut from the pipe wall. A saddle shaped coupon cut by a 6" nominal hole saw (4.720" actual dia.) would be sufficient to provide four tensile specimens and sufficient material for chemistry and microstructural testing. The coupon could also be evaluated for the depth of graphitic corrosion.

ASTM/ASM Specifications

A list of ASTM/ASM specifications and other references applicable to testing cast iron specimens obtained from the field is shown in Table 47.

Table 47. ASTM/ASM specifications and references for field testing of cast iron

ASTM Specifications and Other References Applicable to Testing Cast Iron Specimens Obtained from the Field	Comments
E10 Standard Test Method for Brinell Hardness of Metallic Materials	The standard lab hardness test used by foundries, Brinell hardness can be used to estimate tensile strength
E110 Standard Test Method for Rockwell and Brinell Hardness of Metallic Materials by Portable Hardness Testers	The standards describe procedures to be followed and conducted in performing portable hardness testing and its inherent limitations
A247 Standard Test Method for Evaluating the Microstructure of Graphite in Iron Castings	Graphite structure strongly affects mechanical properties. This standard is used together with the adjunct wall chart to classify graphite microstructures based on size, shape and distribution.
E1999 Standard Test Method for Analysis of Cast Iron by Spark Atomic Emission Spectrometry	The standard spectrometric analysis method for unalloyed and low alloyed cast iron
E351 Standard Test Methods for Chemical Analysis of Cast Iron—All Types	Includes test methods for the analysis of high alloy cast irons.
E1019 Standard Test Methods for Determination of Carbon, Sulfur, Nitrogen, and Oxygen in Steel, Iron, Nickel, and Cobalt Alloys by Various Combustion and Fusion Techniques	The standard method for C and S analysis of cast iron
A370 Standard Test Methods and Definitions for Mechanical Testing of Steel Products	This specification would be used for cutting and machining tensile test specimens from pipe walls. The standard cast iron specimens cannot be used because they must be cast at the foundry.
E3 Standard Guide for Preparation of Metallographic Specimens	Standard on metallographic polishing. Does not include a specific procedure for cast iron.
ASM Handbook Vol. 9 Chapter 6 Metallography and Microstructures of Cast Iron	Describes specific procedures for metallographic polishing of cast iron.
E407 Standard Practice for Micro-etching Metals and Alloys	Recommended etchants for revealing microstructure of the metallic matrix of cast iron

Appendix B – Cast-Iron FFS Calculator Training Manual

1. Background

This is the training manual for the Excel-based cast-iron FFS calculator developed under DOT PHMSA project DTPH56-15-T-00006 *Characterization and Fitness for Service of Corroded Cast Iron Pipe*. For more detailed information see this project's final report.

2. Navigating the Calculator

The calculator contains the following sheets:

- Calculator – used to calculate the maximum stress and factor of safety given the user's inputs.
- Corrosion Measurement Guideline – Contains the *Graphitic Corrosion Field Measurement Guideline* that is provided in this manual in Section 4.

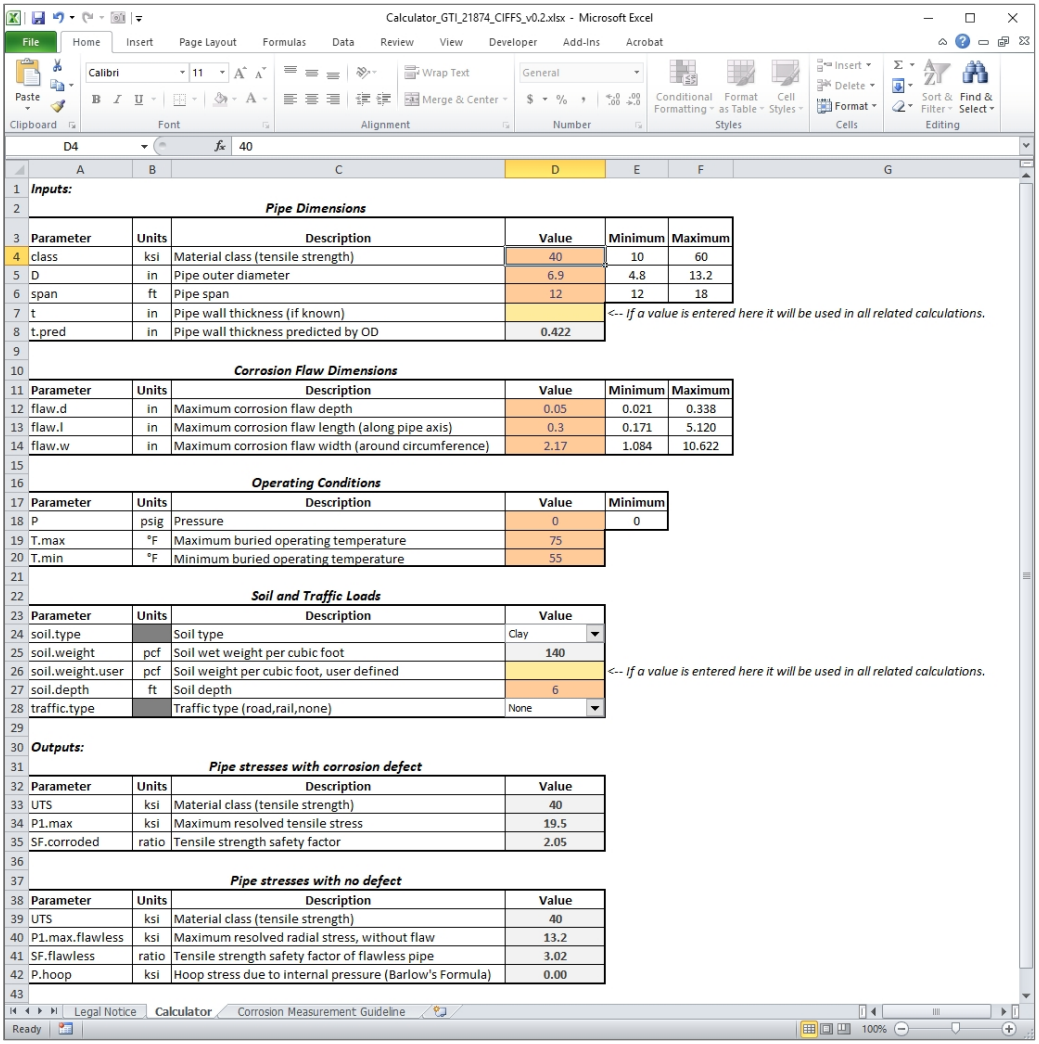

Figure 129. Calculator sheet with input and output fields

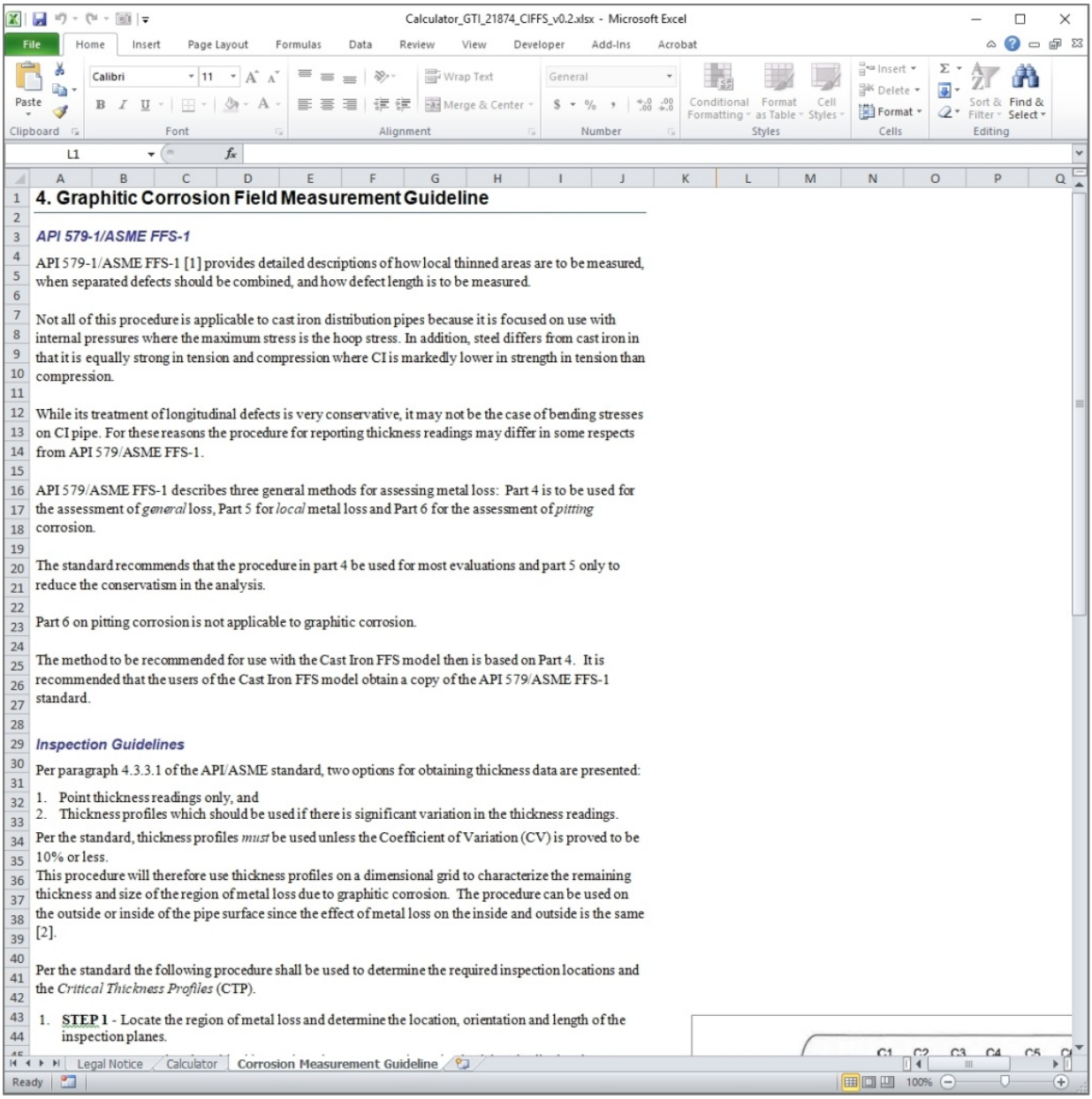

Figure 130. Corrosion Measurement Guideline

3. Using the Calculator

Pipe Dimensions Inputs

There are three required inputs that define the pipe in the calculator:

1. **Material class** (ksi) - range: 10 to 60 ksi
2. **Pipe diameter** (inches) - range: 4.8 to 13.2 inches
3. **Pipe span (feet)** - range: 12 to 18 ft

The calculator user enters these three data inputs into their respective cells. The three cells are circled in red in Figure 131. The respective ranges are shown on the right of the input cells.

An optional input for defining the pipe geometry is pipe wall thickness, which is used for calculating the percent of wall thickness depth of a flaw. If a wall thickness is not entered, the calculator will use a predicted wall thickness based on the outer diameter of the pipe. This wall thickness input cell is shown in Figure 131, highlighted in yellow, and the predicted wall thickness is highlighted in gray.

Inputs:

Pipe Dimensions

Parameter	Units	Description	Value	Minimum	Maximum
class	ksi	Material class (tensile strength)	40	10	60
D	in	Pipe outer diameter	6.9	4.8	13.2
span	ft	Pipe span	12	12	18
t	in	Pipe wall thickness (if known)		*<-- If a value is entered*	
t.pred	in	Pipe wall thickness predicted by OD	0.422		

Figure 131. Pipe dimensions input cells (circled in red).

Corrosion Flaw Dimensions Inputs

There are three inputs that define the corrosion flaw size:

1. **Flaw depth** (inches) - range: depends on wall thickness
2. **Flaw length** (inches) - range: depends on wall thickness and outer diameter
3. **Flaw width** (inches) - range: depends on outer diameter

The flaw dimensions are entered in the cells highlighted in red in Figure 132. The minimum and maximum values that can be input are shown to the right of the input cells.

Corrosion Flaw Dimensions

Parameter	Units	Description	Value	Minimum	Maximum
flaw.d	in	Maximum corrosion flaw depth	0.05	0.021	0.338
flaw.l	in	Maximum corrosion flaw length (along pipe axis)	0.3	0.171	5.120
flaw.w	in	Maximum corrosion flaw width (around circumference)	2.17	1.084	10.622

Figure 132. Corrosion flaw dimensions input cells (circled in red).

Operating Conditions Inputs

There are three inputs that define the operating conditions:

1. **Pressure** (psig) - range: 0 to unlimited
2. **Maximum operating temperature** (°F) - range: unlimited
3. **Minimum operating temperature** (°F) - range: unlimited

The pressure input does not affect the response surface based stress calculation, but is provided for a complimentary hoop stress calculation that uses Barlow's equation. The absolute values of the minimum and maximum operating temperature inputs do not matter, as the calculator only uses the difference between these inputs. Should the difference between these temperatures exceed the calculator's input range, a warning will appear and the calculator will use the maximum temperature difference it can.

Operating Conditions				
Parameter	**Units**	**Description**	**Value**	**Minimum**
P	psig	Pressure	0	0
T.max	°F	Maximum buried operating temperature	75	
T.min	°F	Minimum buried operating temperature	55	

Figure 133. Operating conditions input cells (circled in red).

Soil and Traffic Loads Inputs

Three inputs define the vertical loading on the pipe:

1. **Soil type** - selection from list
2. **Soil depth (ft)** - range: 0 to unlimited
3. **Traffic type** - selection from list

These inputs are circled in red in Figure 134.
Soil types are given in a drop-down list, each defined with a specific wet weight per cubic foot. The soil loading is calculated from the soil weight density and soil depth input. The user may also enter a custom value for soil weight, which will automatically override the selection from the drop-down list. The custom value input cell is highlighted in yellow, as shown in Figure 134.

Traffic types are given in a drop-down list. This list contains industry standard traffic loads and uses the soil depth input to calculate the applied traffic load on the pipe.

Soil and Traffic Loads			
Parameter	**Units**	**Description**	**Value**
soil.type		Soil type	Clay
soil.weight	pcf	Soil wet weight per cubic foot	140
soil.weight.user	pcf	Soil weight per cubic foot, user defined	
soil.depth	ft	Soil depth	6
traffic.type		Traffic type (road,rail,none)	None

Figure 134. Soil and traffic loads input cells (circled in red).

Calculator Outputs

The calculator sheet displays the results from the FFS model calculations in a tabulated format. The outputs are described in the sheet (see Figure 135).

Outputs:

Pipe stresses with corrosion defect

Parameter	Units	Description	Value
UTS	ksi	Material class (tensile strength)	40
P1.max	ksi	Maximum resolved tensile stress	19.5
SF.corroded	ratio	Tensile strength safety factor	2.05

Pipe stresses with no defect

Parameter	Units	Description	Value
UTS	ksi	Material class (tensile strength)	40
P1.max.flawless	ksi	Maximum resolved radial stress, without flaw	13.2
SF.flawless	ratio	Tensile strength safety factor of flawless pipe	3.02
P.hoop	ksi	Hoop stress due to internal pressure (Barlow's Formula)	0.00

Figure 135. Tabulated calculator outputs.

The maximum resolved tensile stress is the maximum stress calculated by the applicable response surfaces (pipe with corrosion defect, pipe with no defect).

The tensile strength factor of safety results are based on the maximum resolved tensile strength and material class. If a factor of safety is less than 1.5, it will display in red. The hoop stress of a pipe with no defect is provided for reference and is calculated according to Barlow's equation.

4. Graphitic Corrosion Field Measurement Guideline

API 579-1/ASME FFS-1

API 579-1/ASME FFS-1 [1] provides detailed descriptions of how local thinned areas are to be measured, when separated defects should be combined, and how defect length is to be measured.

Not all of this procedure is applicable to cast iron distribution pipes because it is focused on use with internal pressures where the maximum stress is the hoop stress. In addition, steel differs from cast iron in that it is equally strong in tension and compression where CI is markedly lower in strength in tension than compression.

While its treatment of longitudinal defects is very conservative, it may not be the case of bending stresses on CI pipe. For these reasons the procedure for reporting thickness readings may differ in some respects from API 579/ASME FFS-1.

API 579/ASME FFS-1 describes three general methods for assessing metal loss: Part 4 is to be used for the assessment of *general* loss, Part 5 for *local* metal loss and Part 6 for the assessment of *pitting* corrosion.

The standard recommends that the procedure in part 4 be used for most evaluations and part 5 only to reduce the conservatism in the analysis.

Part 6 on pitting corrosion is not applicable to graphitic corrosion.

The method to be recommended for use with the Cast Iron FFS model then is based on Part 4. It is recommended that the users of the Cast Iron FFS model obtain a copy of the API 579/ASME FFS-1 standard.

Measurement Considerations

The data collection process for the graphitic corrosion length, width, and depth as well as pipe thickness is an important step. Repeatable methods should be used, and when appropriate, trained/certified NDE or ASNT technicians can be used.

Inspection Guidelines

Per paragraph 4.3.3.1 of the API/ASME standard, two options for obtaining thickness data are presented:

1. Point thickness readings only, and
2. Thickness profiles which should be used if there is significant variation in the thickness readings.

Per the standard, thickness profiles *must* be used unless the Coefficient of Variation (CV) is proved to be 10% or less.
This procedure will therefore use thickness profiles on a dimensional grid to characterize the remaining thickness and size of the region of metal loss due to graphitic corrosion. The procedure can be used on the outside or inside of the pipe surface since the effect of metal loss on the inside and outside is the same [2].

Per the standard the following procedure shall be used to determine the required inspection locations and the *Critical Thickness Profiles* (CTP).

8. **STEP 1** - Locate the region of metal loss and determine the location, orientation and length of the inspection planes.
9. **STEP 2** - Determine the critical inspection planes. For cast iron pipe both longitudinal and circumferential planes are critical.

10. **STEP 3** - Mark the inspection planes on the pipe surface.
11. **STEP 4** - Determine the uniform thickness away from the local metal loss t_{rd}.
12. **STEP 5** - Measure and record thickness readings along each inspection plane and determine the minimum measured wall thickness t_{mm}, see Figure 77 (figure 4.6a from API 579-1/ASME FFS-1).
    a. The spacing distance for thickness readings (the grid) should allow for an accurate characterization of the thickness profile.
    b. A guideline is that the spacing should be done in a manner that the path of minimum measured thickness (t_{mm}) can be determined in both the longitudinal and circumferential directions (explained in STEP 6 below).
13. **STEP 6** - Determine the Critical Thickness Profile (**CTP**) in the longitudinal and circumferential directions.
    a. The CTP in each direction is determined by projecting the minimum remaining thickness for each position along all parallel inspection planes onto a common plane as shown in Figure 78 (figure 4.6a from API 579-1/ASME FFS-1) and Figure 79 (figure 4.6c from API 579-1/ASME FFS-1). These also show the corroded wall thickness, t_c.
    b. One can see in these two figures that there are two planes of minimum thickness, one for the circumferential (dotted line C) and one for the longitudinal (solid line M) direction.
    c. The length of the profile is established by determining the end point locations where the remaining wall thickness is greater than the uniform thickness away from local metal loss, t_{rd}, in both the longitudinal and circumferential directions. Note, t_{rd}, can be less than the nominal, t_{nom}, (non-corroded) wall thickness away from the local areas of metal loss. This is a determination that must be made in the field with careful measurements made in and around areas of metal loss.
    d. If there are multiple flaws in close proximity to one another, then the size of the flaw to be used in the assessment is established considering the effects of neighboring flaws using the *intersecting box methodology* shown in Figure 80 (figure 4.7 in API 579-1/ASME FFS-1).
    e. The final CTP can be established as shown in Figure 81 (figure 4.8 in API 579-1/FFS-1).

f. The thickness profile for both the longitudinal and circumferential planes should be evaluated in this manner.

14. **Step 7** – The operator will also record the measurements in a way to determine the axial direction of the pipe relative to the measurements.

a. This can be a simple annotation on the drawing of the pipe's center line as shown in Figure 77.

b. This information will be needed to determine the angle of the overall wall loss measurement relative to the pipe's axial direction, in degrees.

The above process will provide the graphitic corrosion defect (wall loss): length, depth, and width of the wall loss. These measurements are inputs to the CI FFS model calculator.

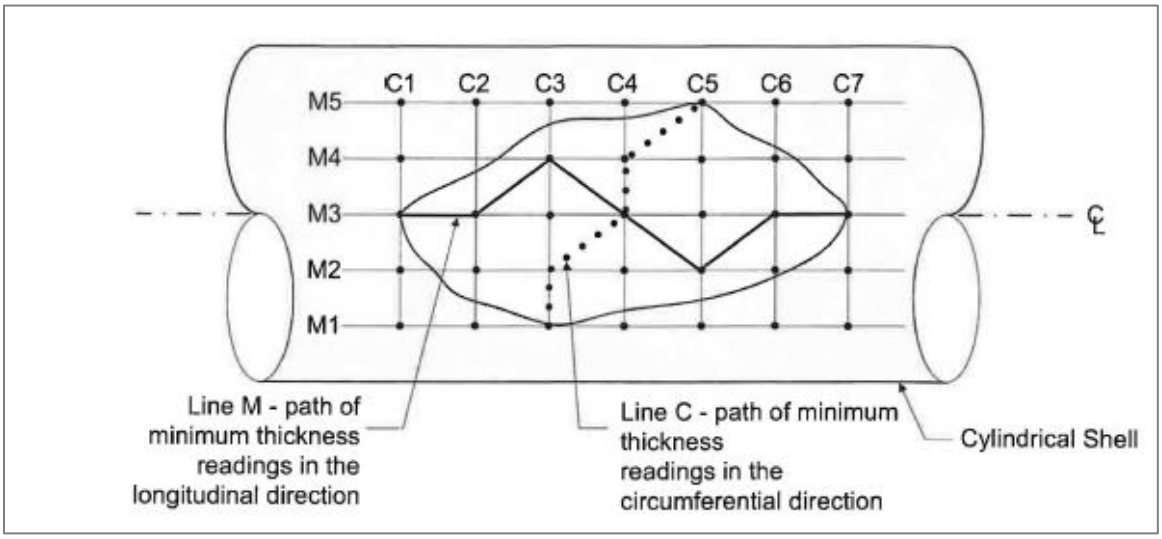

Figure 136. Inspection planes per API 579-1/FFS-1 fig 4.6a and the critical thickness profiles

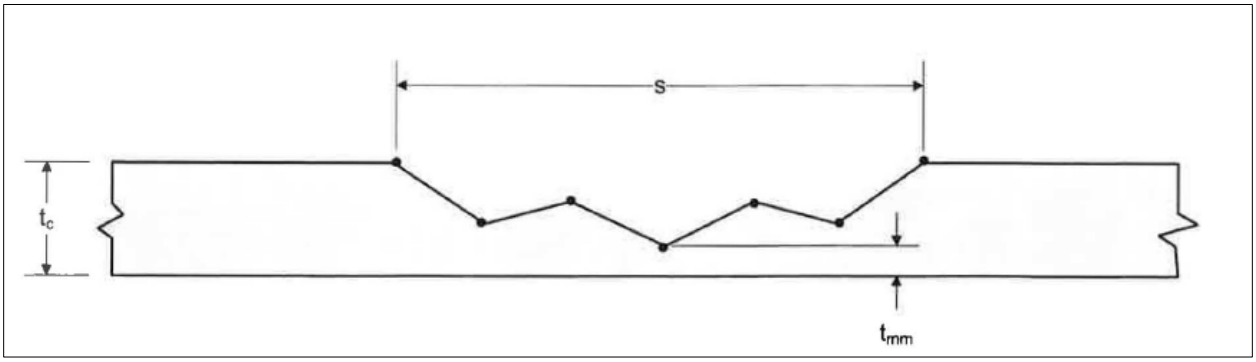

Figure 137. Critical Thickness Profile (CTP) – Longitudinal Plane (Projection of Line M) API 579-1/FFS-1 fig 4.6b

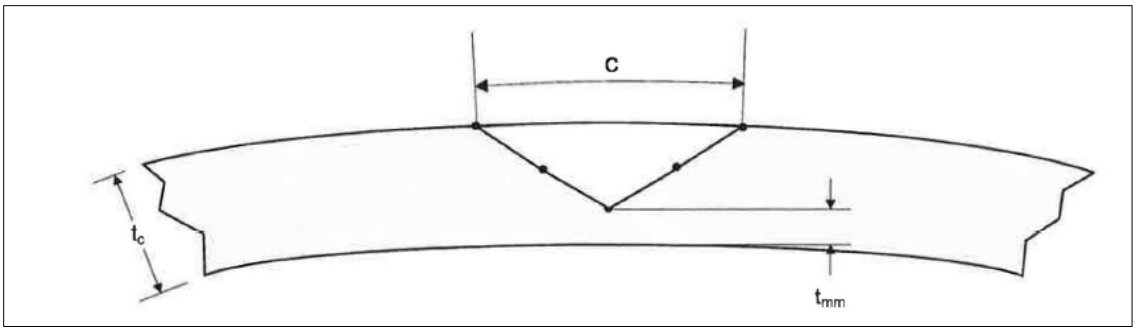

Figure 138. Critical Thickness Profile (CTP) – Circumferential Plane (Projection of Line C) API 579-1/FFS-1 fig 4.6c

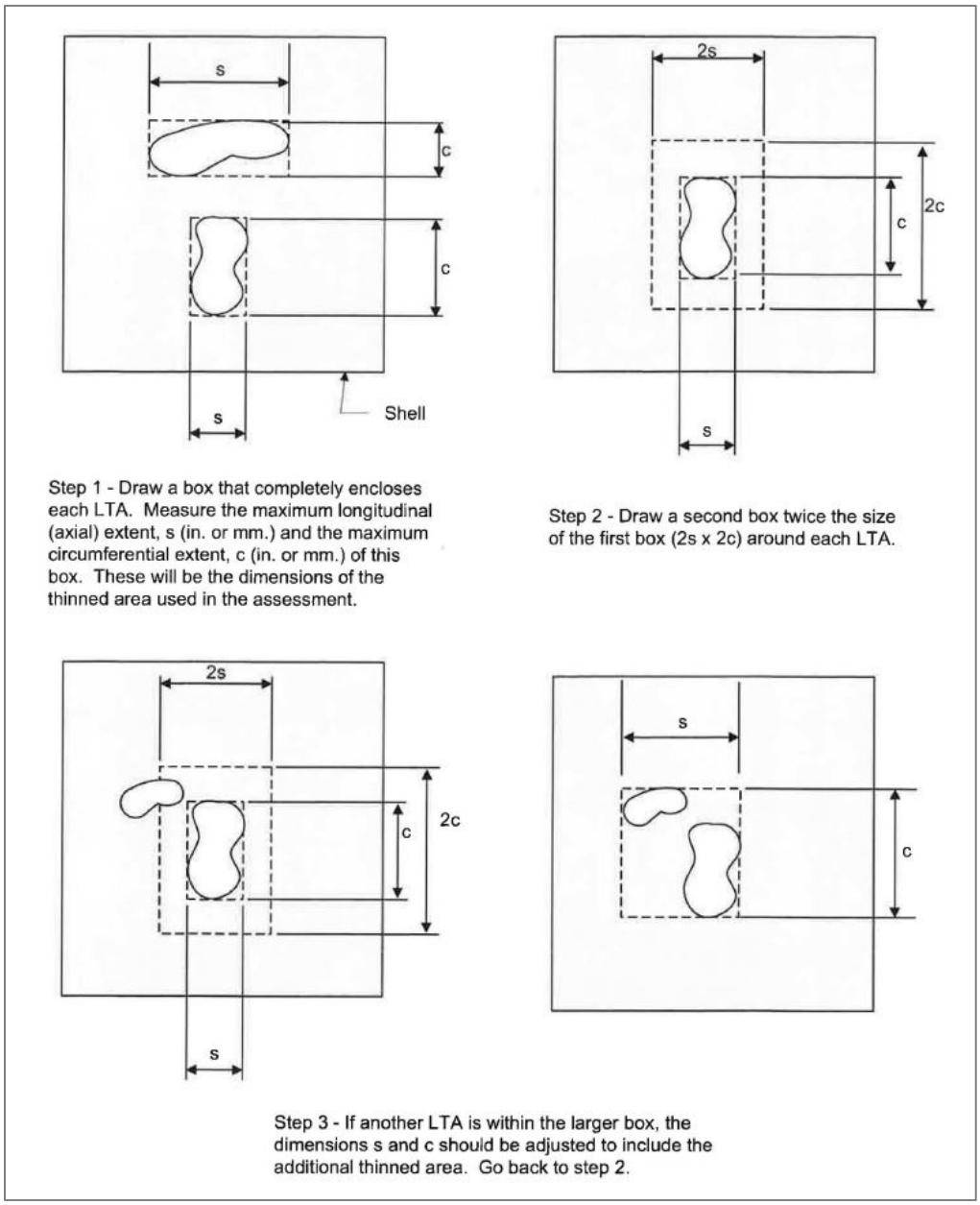

Figure 139. Combining and resizing flaws per API 579-1/ASME FFS-1 fig 4.7

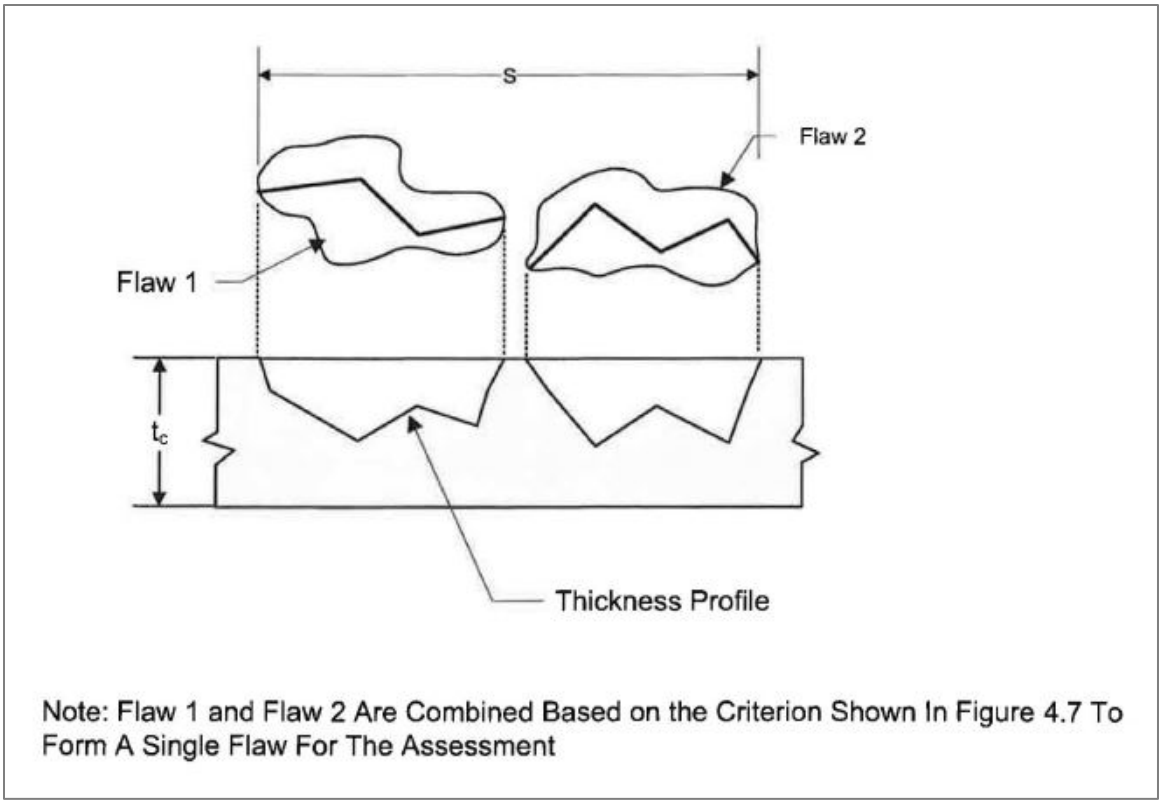

Figure 140. Sizing of a network of flaws from API 579-1/ASME FFS-1 fig 4.8

5. Training Manual References

1. API 579-1/ASME FFS-1 Fitness for Service, The American Society of Mechanical Engineers and the American Petroleum Institute, 2nd Edition, June 5, 2007, Washington D.C.
2. Escoe, K. A., Piping and Pipeline Assessment Guide, Elsevier Publishing, New York, 2006.

End of Training Manual

REFERENCES

[1] Allen, D.K., Metallurgy Theory and Practice, Further References Gray and Ductile Iron Founders' Society, American Technical Publishers, Alsip, Illinois, 1969.

[2] Walton, C.F. and Opar, T.J., Ed., Iron Castings Handbook, Iron Castings Society, 1981.

[3] Allen, D.K., Metallurgy Theory and Practice, American Technical Publishers, Alsip, Illinois, 1969.

[4] Allen, D.K., Metallurgy Theory and Practice, Further reference American Society for Testing and Materials and American Foundryman's Society, American Technical Publishers, Alsip, Illinois, 1969.

[5] Allen, D.K., Metallurgy Theory and Practice, Further references Gray and Ductile Iron Founders' Society, American Technical Publishers, Alsip, Illinois, 1969.

[6] Walton, C.F. and Opar, T.J., Ed., Iron Castings Handbook, Iron Castings Society, 1981.

[7] Cast Irons, ASM Specialty Handbook, Davis, J.R., editor, ASM International, Metals Park, Ohio, 1996.

[8] Bates, C.M., AFS Trans., Vol. 94, 1986, p. 889.

[9] Schneidewind, R. and McElwee, R.G., Composition and Properties of Gary Irons, Parts I and II, Trans. AFS, Vol. 58, 1950, p. 312-330.

[10] Walton, C.F. and Opar, T.J., Ed., Iron Castings Handbook, Iron Castings Society, 1981, page 235.

[11] Seica, M.V. and Packer, J.A., Mechanical Properties and Strength of Aged Cast Iron Water Pipes, Journal of Materials in Civil Engineering, ASCE, v16(1), Jan/Feb 2004, pages 69-77.

[12] Krause, D.E., Gray Iron - A Unique Engineering Material, Gray, Ductile, and Malleable Iron Castings - Current Capabilities, STP 455, American Society for Testing and Materials, 1969, page 3-28.

[13] Cast Iron Pipe Research Association, Handbook of Cast Iron Pipe for Water, Gas, Sewage, and Industrial Services, Chicago, 1952

[14] Makar, J.M., Rogge, R., and McDonald, S.E., and Tefamariam, S., The Effect of Corrosion Pitting on Circumferential Failures In Grey Cast Iron Pipes, AWWA Research Foundation, Denver, 2005

[15] Makar, J.M. and McDonald, S.E., Mechanical Behavior of Spun-Cast Gray Iron Pipe, J Mat Civil Eng, V.19(10), 826-33, Oct. 2007.

[16] Seica, M.V. and Packer, J.A., Mechanical Properties and Strength of Aged Cast Iron Water Pipes, Journal of Materials in Civil Engineering, ASCE, v16(1), Jan/Feb 2004, pages 69-77.

[17] Conlin, R.M. and Baker, T.J., Application of Fracture Mechanics to the Failure Behavior of Buried Cast Iron Mains, Contract Rep., No. 266, Transport and Road Research Laboratory, London, 1991.

[18] Caproco Corrosion Prevention Ltd., Underground Corrosion of Water Pipes in Canadian Cities, Rep. Prepared for CANMET, Ottawa, 1985.

[19] Ma, Z. and Yamada, K., Durability Evaluation of Cast Iron Water Supply Pipes by Sampling Tests, Proc. Structural Engineering, Japan Society of Civil engineers, Tokyo, 40A, 1994.

[20] Yamamoto, K., Mizoguti, S., and Yoshimitusu, K., Relation Between Graphitic Corrosion and Strength Degradation of Cast Iron Pipe, Corr. Eng., 32(3), 157,1983.

[21] Fontana, M.G., Corrosion Engineering, 3rd ed., McGraw-Hill, New York, 1986.

[22] Uhlig's Corrosion Handbook, 3rd ed., Revie, W.R. editor, John Wiley and Sons, Hoboken, New Jersey, 2011.

[23] Bradford, S.A., Corrosion Control, 2nd ed., CASTI Publishing, Edmonton, Alberta, Canada, 2001.

[24] Bradford, S.A., Practical Handbook of Corrosion Control in Soils, CASTI Publishing, Edmonton, Alberta, Canada, 2000.

[25] NACE Corrosion Engineer's Reference Book, 3rd ed., Baboian, R. editor, NACE International, Houston, TX, 2002.

[26] Roberge, P.R., Corrosion Engineering – Principles and Practice, McGraw Hill, New York, 2008.

[27] ASM specialty handbook, "Cast Irons", 1996.

[28] P.M. Unterwieser, Ed., Case Histories in Failure Analysis, ASM, 1979.

[29] Ahmad, Z., Principles of Corrosion Engineering and Corrosion Control, Elsevier, London, 2006.

[30] R.I. Higgins, Corrosion of Cast Iron, J. Res., Feb 1956.

[31] R. Mehra and A. Soni, Cast Iron Deterioration with Time In Various Aqueous Salt Solutions, Bull. Mater. Sci., Vol 25, No. 1, Feb. 2002, pp. 53-58.

[32] G.A. Nelson, ed., Corrosion Data Survey, Shell Development Company, Emeryville, CA, 1954.

[33] Handbook of Corrosion Data, B.D. Craig, and D.S. Anderson, eds., ASM International, Materials Park, OH 1995.

[34] Nickel Development Institute, Eng. Prop. and Applications of Ni-Resists and Ductile Ni-Resists, Paper 1231, 1991.

[35] A.H. Tuthill and C.M. Schillmoller, Useful Guidelines in the Selection of Corrosion Resistant Materials for Marine Service, Marine Tech. Trans., 3 (1965).

[36] Mohebbi, H. and Li, C.Q., Experimental investigation on corrosion of cast iron pipes, Hindawi Publishing Corporation, International Journal of Corrosion, Volume 2011, Article ID 506501, 17 pagers, 2011.

[37] Adegbite, SA, Fahimi, A, Evans, T, Farrow, J, Jesson, DA, Mulheron, MJ and Smith, PA (2013) Trunk Mains Failures: The Effect of Corrosion on Residual Pipe Strength, In: 4th International Conference on Integrity, Reliability and Failure, 2013-06-23 - 2013-06-27, Funchal, Portugal.

[38] D.A.Jesson, H.Mohebbi, J.Farrow, M.J.Mulheron, P.A.Smith, On the Condition Assessment of Cast Iron Trunk Main: The Effect of Microstructure and In-Service Graphitisation on Mechanical Properties In Flexure, Materials Science and Engineering, A 576, pages 192-201, 2013.

[39] Pipeline and Hazardous Materials Safety Administration (PHMSA), 2011 http://opsweb.phmsa.dot.gov/pipeline_replacement/cast_iron_inventory.asp

[40] Evaluating Service Life of Anaerobic, Joint Sealing Products and Techniques, Cornell University, Gas Technology Institute, Report GRI-96/0318, 1996.

[41] ASM Specialty Handbook, Cast Irons, ASM International, 1999.

[42] National Transportation Safety Board, NTSB, Safety Recommendation P-91-12, July 1992.

[43] PHMSA, RSPA Alert Notice 91-02, 1991.

[44] PHMSA, RSPA Alert Notice 92-02, 1992.

[45] PHMSA, Distribution, Transmission & Gathering, LNG, and Liquid Accident and Incident Data, Natural Gas Distribution Incident Data 2010 to present, http://phmsa.dot.gov/pipeline/library/data-stats/flagged-data-files/

[46] PHMSA, Distribution, Transmission & Gathering, LNG, and Liquid Accident and Incident Data, Natural Gas Distribution Incident Data 2010 to present, http://phmsa.dot.gov/portal/site/PHMSA/

[47] Guidelines for the Design of Buried Steel Pipe, American Lifelines Alliance, ASCE, July 2001.

[48] API, American Petroleum Institute, Steel Pipelines Crossing Railroads and Highways, API Recommended Practice 1102, 2007.

[49] Steward, H.E., O'Rourke, T.D., and Ingraffea, A.R., Guidelines for Pipelines Crossing Highways, Cornell University, Report No, GRI-91/0284, Gas Research Institute, December 1991.

[50] Code of Federal Regulations, CFR Title 49 - Part 192, Transportation of Natural Gas and Other Hazardous liquids by Pipeline, 2008.

[51] Preventing Pipeline Failures In Areas of Soil Movement – Part 1, State of The Art, Pipeline Research Council International Inc. (PRCI), Catalog No. L51516e, 1986.

[52] Carodiskey, Thomas et al Thickness Measurement in Materials of Unknown Acoustic Velocity NDT.net October 1997, Vol.2, no.10.

[53] API 579-1/ASME FFS-1 Fitness for Service, The American Society of Mechanical Engineers and the American Petroleum Institute, 2nd Edition, June 5, 2007, Washington D.C.

[54] Escoe, K. A., Piping and Pipeline Assessment Guide, Elsevier Publishing, New York, 2006.

[55] Seica, M.V., Jeffrey, A.P., "Finite Element Evaluation of the Remaining Mechanical Strength of Deteriorated Cast Iron Pipes", Journal of Engineering Materials and Technology, January 2004.

[56] Seica, M.V., Jeffrey, A.P., "Simplified Numerical Method to Evaluate the Mechanical Strength of Cast Iron Water Pipes", Journal of Infrastructure Systems, March 2006.

End of Report

the Energy to Lead

gti

ADDENDUM REPORT NUMBER 1
GTI PROJECT NUMBER 21874
Contract Number: DTPH56-15-T-00006

Characterization and Fitness for Service of Corroded Cast Iron Pipe

Addendum Report #1 – Large Diameter Pipe Modelling

Report Issued
December 31, 2018

Prepared For
U.S. Department of Transportation
Pipeline and Hazardous Materials Safety Administration
Office of Pipeline Safety
Chris McLaren
chris.mclaren@dot.gov

Technical Team
Daniel Ersoy
Oren Lever
Khalid Farrag
Brian Miller

Project Manager
Kristine Wiley
R&D Director, GTI
kristine.wiley@gastechnology.org

Technical Contact
Daniel Ersoy
R&D Executive Director, GTI
daniel.ersoy@gastechnology.org

Gas Technology Institute
1700 S. Mount Prospect Rd.
Des Plaines, Illinois 60018

Signature Page

			Date
Principal Investigator			
Daniel A. Ersoy	*Title:*	Daniel Ersoy//S// R&D Exec. Dir. and PI	12/31/2018
Author			
Oren Lever	*Title:*	Oren Lever//S// Principal Engineer	12/31/2018
Reviewed by			
Kristine Wiley	*Title:*	Kristine Wiley//S// R&D Director and PM	12/31/2018

Legal Notice

This information was prepared by Gas Technology Institute ("GTI") for U.S. DOT/PHMSA under agreement DTPH56-15-T-00006.

Neither GTI, the members of GTI, the Sponsor(s), nor any person acting on behalf of any of them:

Makes any warranty or representation, express or implied with respect to the accuracy, completeness, or usefulness of the information contained in this report, or that the use of any information, apparatus, method, or process disclosed in this report may not infringe privately-owned rights. Inasmuch as this project is experimental in nature, the technical information, results, or conclusions cannot be predicted. Conclusions and analysis of results by GTI represent GTI's opinion based on inferences from measurements and empirical relationships, which inferences and assumptions are not infallible, and with respect to which competent specialists may differ.

Assumes any liability with respect to the use of, or for any and all damages resulting from the use of, any information, apparatus, method, or process disclosed in this report; any other use of, or reliance on, this report by any third party is at the third party's sole risk.

The results within this report relate only to the items reviewed.

Table of Contents

Table of Figures

Page

List of Tables

Page

Executive Summary

The project final report, "Characterization and Fitness for Service of Corroded Cast Iron Pipe" dated February 15, 2018 provided a Cast Iron (CI) Fitness-For-Service (FFS) model and method for operators to characterize and grade graphitic corrosion defects on cast iron natural gas pipe. The project deliverables will help make monitoring, repair, and replacement decisions, as well as prioritize their replacement program decisions leading to improved safety and supply stability.

The Technical Advisory Panel (TAP) suggested that the project expand the applicability of the calculator solution to include larger diameter pipe, 20-inch and larger, which several of them are currently using. Another suggestion was to provide a full geo-spatial implementation example showing the solution applied to a cast iron network with rankings for an accelerated mains replacement program.

These revised and new project deliverables are provided in four additional files in addition to the previously distributed project Final Report:

1. DTPH56-15-T-00006_**FinalReport**_2018-02-15, original final report.
2. **[THIS REPORT]** DTPH56-15-T-00006_**Addendum-01**_2018-12-31, which describes the expanded (larger diameter pipe inclusion) model development.
3. DTPH56-15-T-00006_**Addendum-02**_2018-12-31, which uses the model solution and applies it to a geo-spatial scenario for accelerated mains replacement.
4. DTPH56-15-T-00006_**Model_Calculator_v0.3**_2018-12-31, which includes the expanded model use case range for larger diameters. The v0.3 is the first version released under the project.
5. DTPH56-15-T-00006_**Calculator_Training_Manual_v0.3**_2018-12-31, which explains how to use the calculator.

The objective of this Addendum #1 report was to expand the calculator developed under Task 6 to include large pipe diameters: 14-inch through 48-inch nominal diameter. This expansion was accomplished by running the previously developed nonlinear 3D finite element (FE) model with identical boundary conditions and flaw geometry (normalized) as used for the smaller diameters, albeit with the large pipe diameters and their corresponding wall thicknesses. The results of this expansion were additional response surfaces for the large diameter pipe range (14-inch though 48-inch).

The user calculator produced under Task 6 was updated with the large-diameter response surface, utilizing the 97.5% upper prediction limit (UPL) of the response surfaces described in this report.

Errata Note:
During execution of this addendum work, an error in the MATLAB script that was used to calculate the upper prediction bounds was discovered. The error resulted in tighter upper prediction bounds, thus giving a less conservative calculation of stress. This error was corrected, and the correction was verified against Stat-Ease's Design-Expert 11, a commercial Design-of-Experiment and response surface fitting software. The response surfaces previously detailed in Task 6, have been updated using the corrected MATLAB script and are detailed in this addendum. The parameters of the SS1 and SS2 response surfaces in this addendum supersede those developed in Task 6. The Excel Calculator (v0.3) uses these updated response surfaces as well. Excel Calculator v0.3 is the only version of the solution distributed so this is an informational note only.

General Approach

A nonlinear, 3D finite element (FE) model, simulating a single pipe span was utilized as the basis for the Fitness-For-Service (FFS) model. The details of the FE simulations have been provided in the Final Report. A Design of Experiment (DoE) method was used to produce response surfaces from the FE simulation results that can predict the maximum ligament stress in pipes with and without wall loss. The final simulation approach had four simulation spaces:

1. Simulation of a small-diameter pipe span without wall loss. (Final Report)
2. Simulation of a small-diameter pipe span with wall loss. (Final Report)
3. Simulation of a large-diameter pipe span without wall loss. (This Report Addendum #1)
4. Simulation of a large-diameter pipe span with wall loss. (This Report Addendum #1)

Where small-diameter covers 4” through 12” nominal diameter pipes, and large-diameter covers 14” through 48” diameter pipes.

The simulation spaces described above are herein referred to as Simulation Space 1 (SS1), Simulation Space 2 (SS2), Simulation Space 3 (SS3), and Simulation Space 4 (SS4).

Response Surfaces

The response surfaces in all Simulation Spaces needed to be separated by axial restraints. These separations necessitate the evaluation of the all response surfaces on a case-by-case basis using a calculator. Such a calculator will use one set of input variable and output the result from all response surfaces with an indication of the most conservative result.

SS1 (small diameter pipe without flaw) is comprised of two response surfaces as follows:

- SS1-1: axially free end
- SS1-2: axially restrained ends

SS2 (small pipe with flaw) is comprised of two response surfaces as follows:

- SS2-1: axially free end
- SS2-2: axially restrained ends

SS3 (large diameter pipe without flaw) is comprised of two response surfaces as follows:

- SS3-1: axially free end
- SS3-2: axially restrained ends

SS4 (large diameter pipe with flaw) is comprised of two response surfaces as follows:

- SS4-1: axially free end
- SS4-2: axially restrained ends

All of the response surfaces presented in this report do not include internal pressure since it was found to be negligible at least up to 25 pig, which is considered to be the upper bound of cast iron pipe operating pressures, and thus pressure was eliminated as a variable to reduce analysis time. The simulation models developed under this project do accept an internal pressure input such that response surfaces that include internal pressure can be generated.

All of the response surfaces based are on a reduced cubic model where insignificant terms were eliminated using a stepwise selection with p-value criteria of 0.0001.

Errata Note:

During execution of this addendum work, an error in the MATLAB script that was used to calculate the upper prediction bounds was discovered. The error resulted in tighter upper prediction bounds, thus giving a less conservative calculation of stress. This error was corrected, and the correction was verified against Stat-Ease's Design-Expert 11, a commercial Design-of-Experiment and response surface fitting software. The response surfaces previously detailed in the Final Report, have been updated using the corrected MATLAB script and are detailed in this addendum. The parameters of the SS1 and SS2 response surfaces in this addendum supersede those in the Final Report. The Excel Calculator (v0.3) uses these

updated response surfaces as well and this v0.3 is the first version of the calculator to be released.

The following figures show the perturbation and predicted versus actual graphs for each of the design spaces.

Response Surface SS1-1 – Small diameter pipe without flaw, axially free end

Response surface SS1-1 applies to a non-axially restrained, small-diameter pipe segment without wall loss.

The response surfaces for the maximum and average first principal stresses are based on 1044 data points and have the input variables given in Table 1:

Table 1. Design Variables for SS1-1

	Units	Lower Value	Upper Value
Class	-	10	60
Outer Diameter	in	4.8	15.65
Pipe Span	ft	12	18
Vertical Load Pressure	psi	0	80

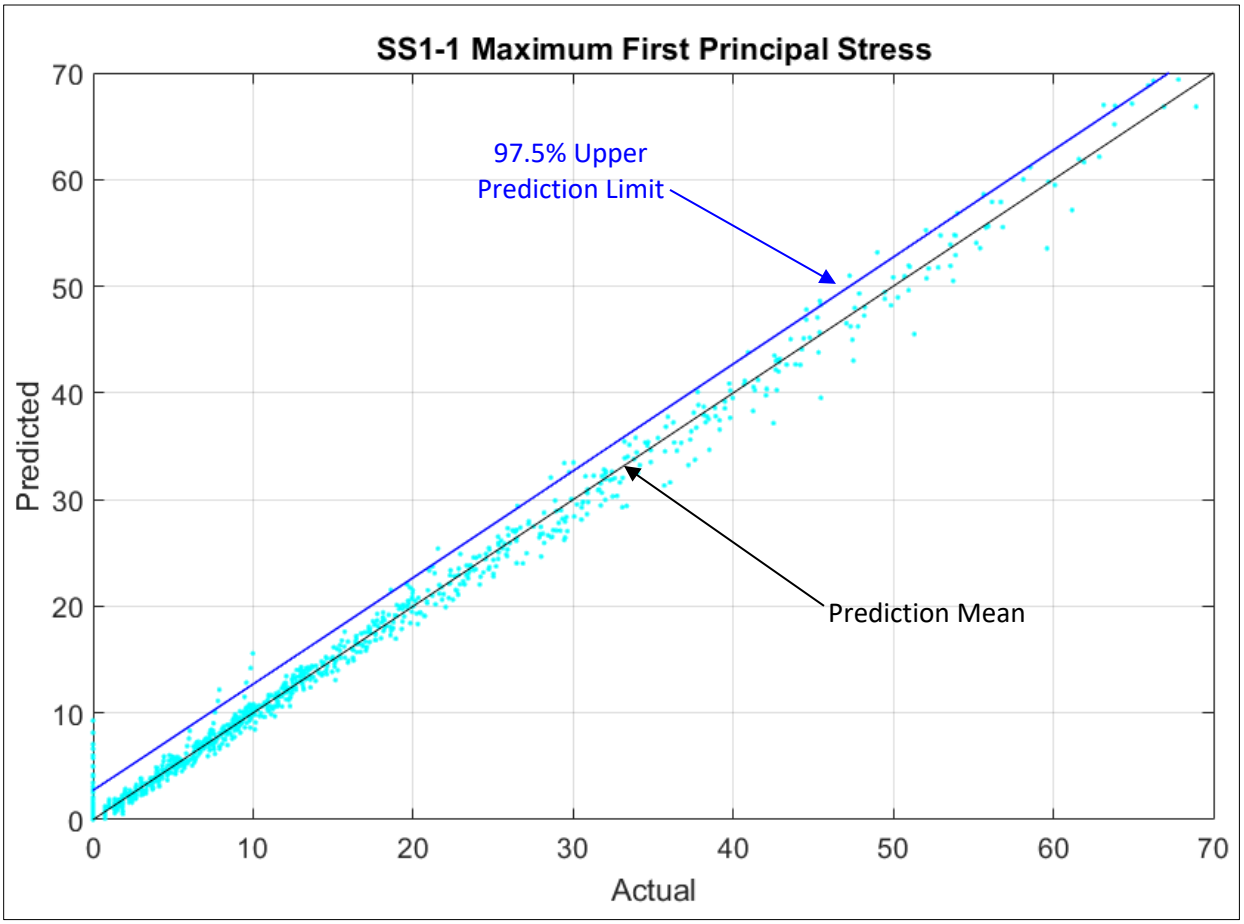

Figure 1. SS1-1 Maximum First Principal Stress, Predicted versus Actual, adjusted R^2=0.9925, with 97.5% upper confidence bound

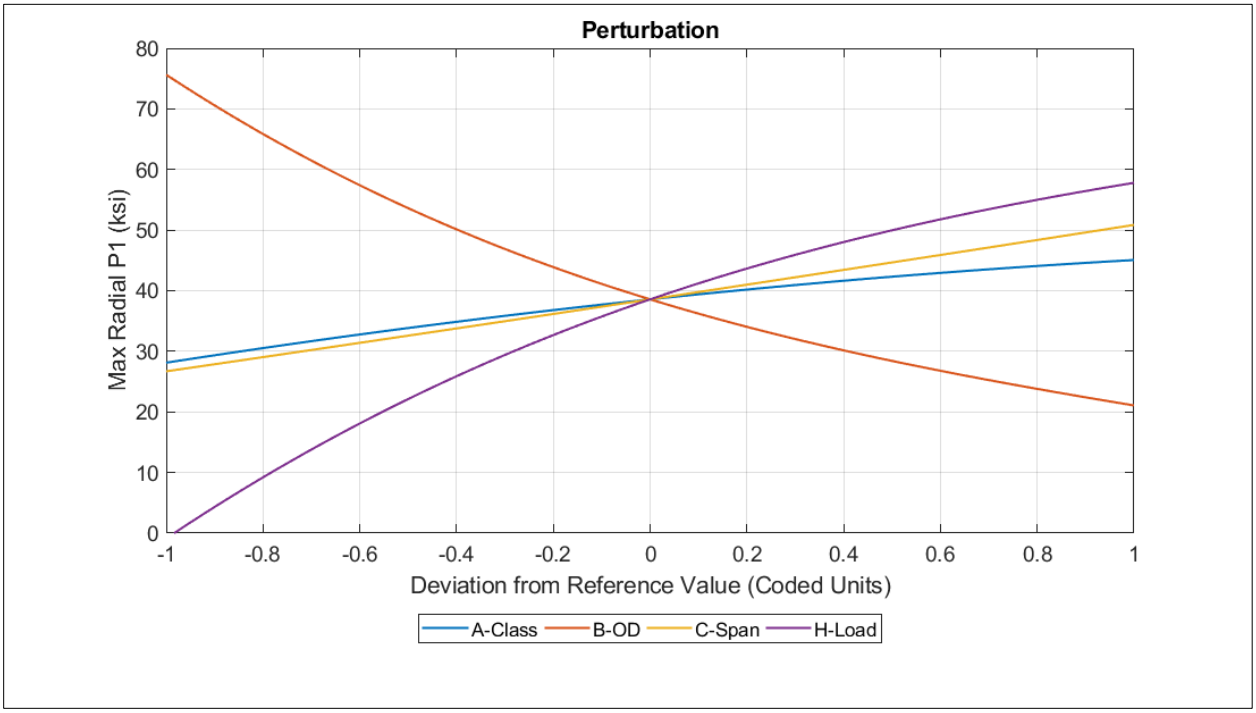

Figure 2. SS1-1 Maximum First Principal Stress, perturbation graph

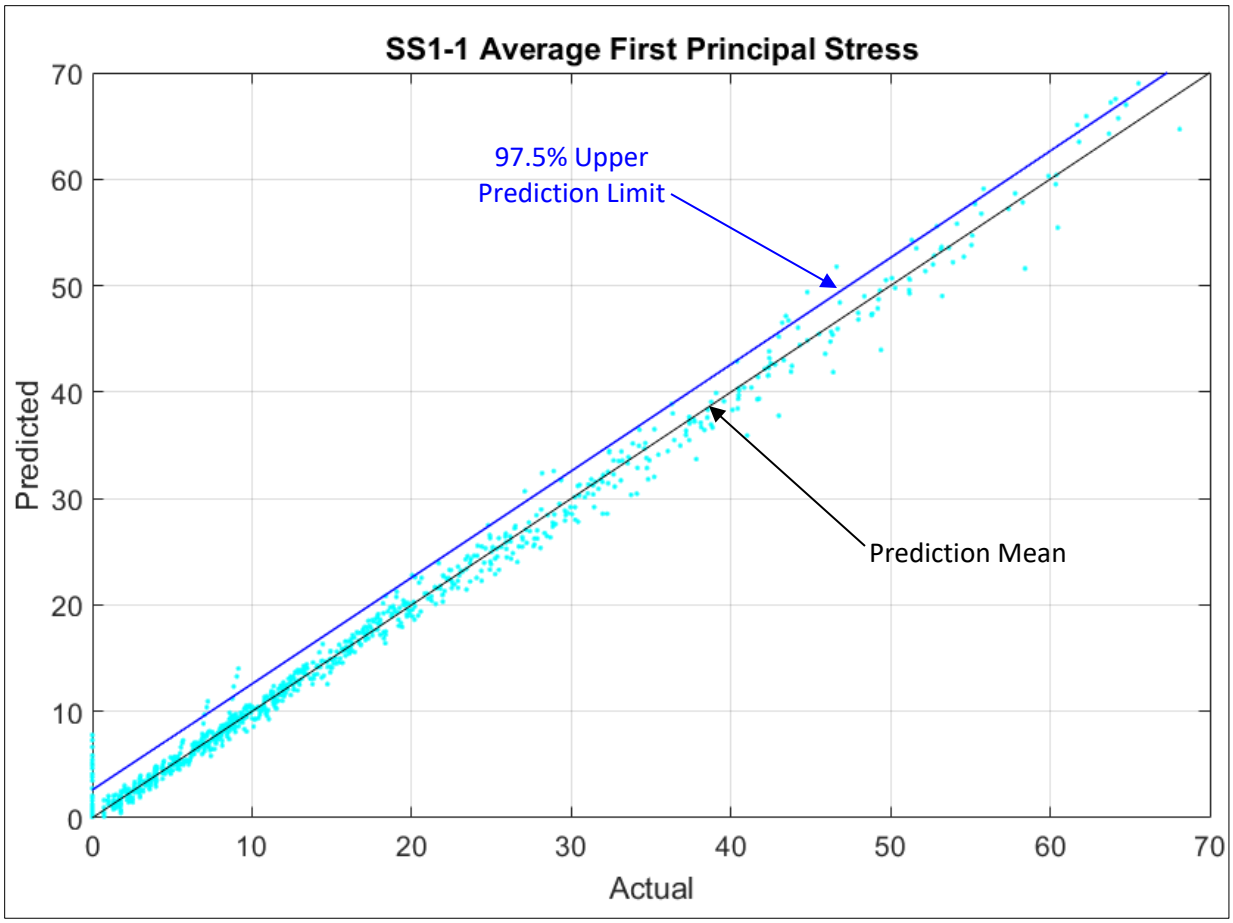

Figure 3. SS1-1 Average Radial First Principal Stress, Predicted versus Actual, adjusted R^2=0.9923, with 97.5% upper confidence bound

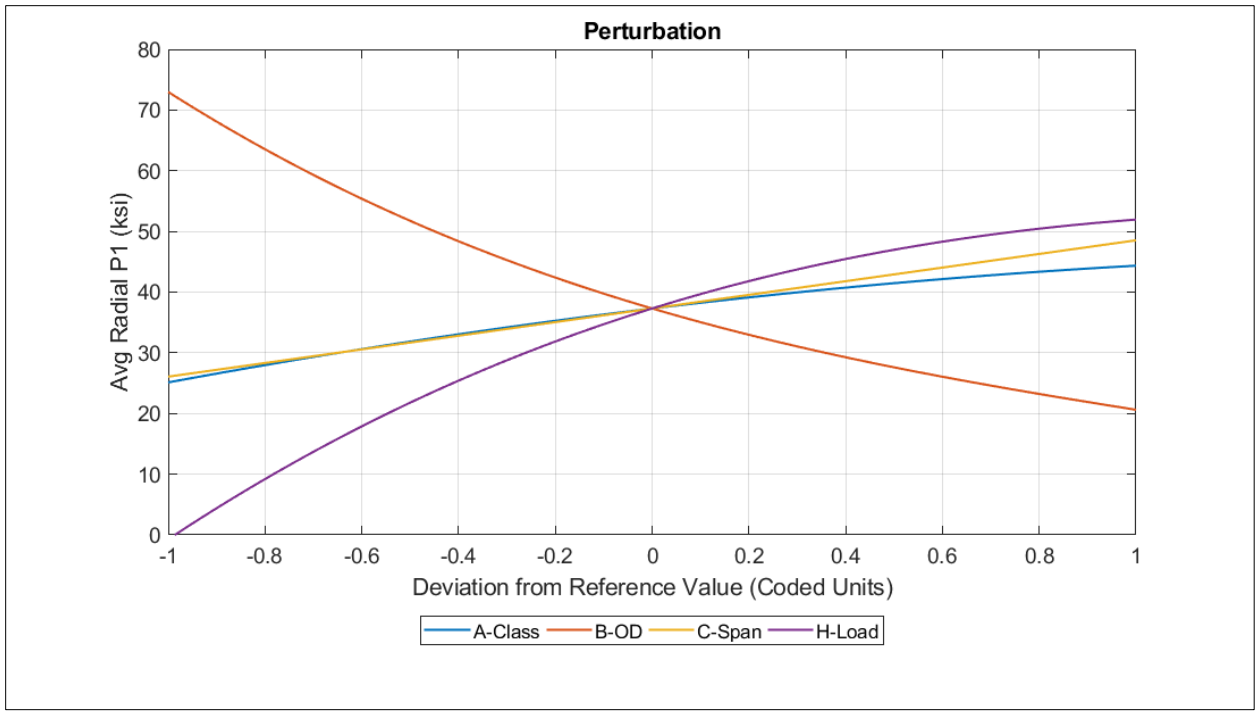

Figure 4. SS1-1 Average Radial First Principal Stress, perturbation graph

Response Surface SS1-2 – Large diameter pipe without flaw axially restrained ends

Response surface SS1-2 applies to an axially restrained, small-diameter pipe segment without wall loss.

The response surfaces for the maximum and average first principal stresses are based on 3116 data points and have the input variables given in Table 2:

Table 2. Design Variables for SS1-2

	Units	Lower Value	Upper Value
Class	-	10	60
Outer Diameter	in	4.8	15.65
Pipe Span	ft	12	18
Temperature Change	degC	-20	0
Vertical Load Pressure	psi	0	80

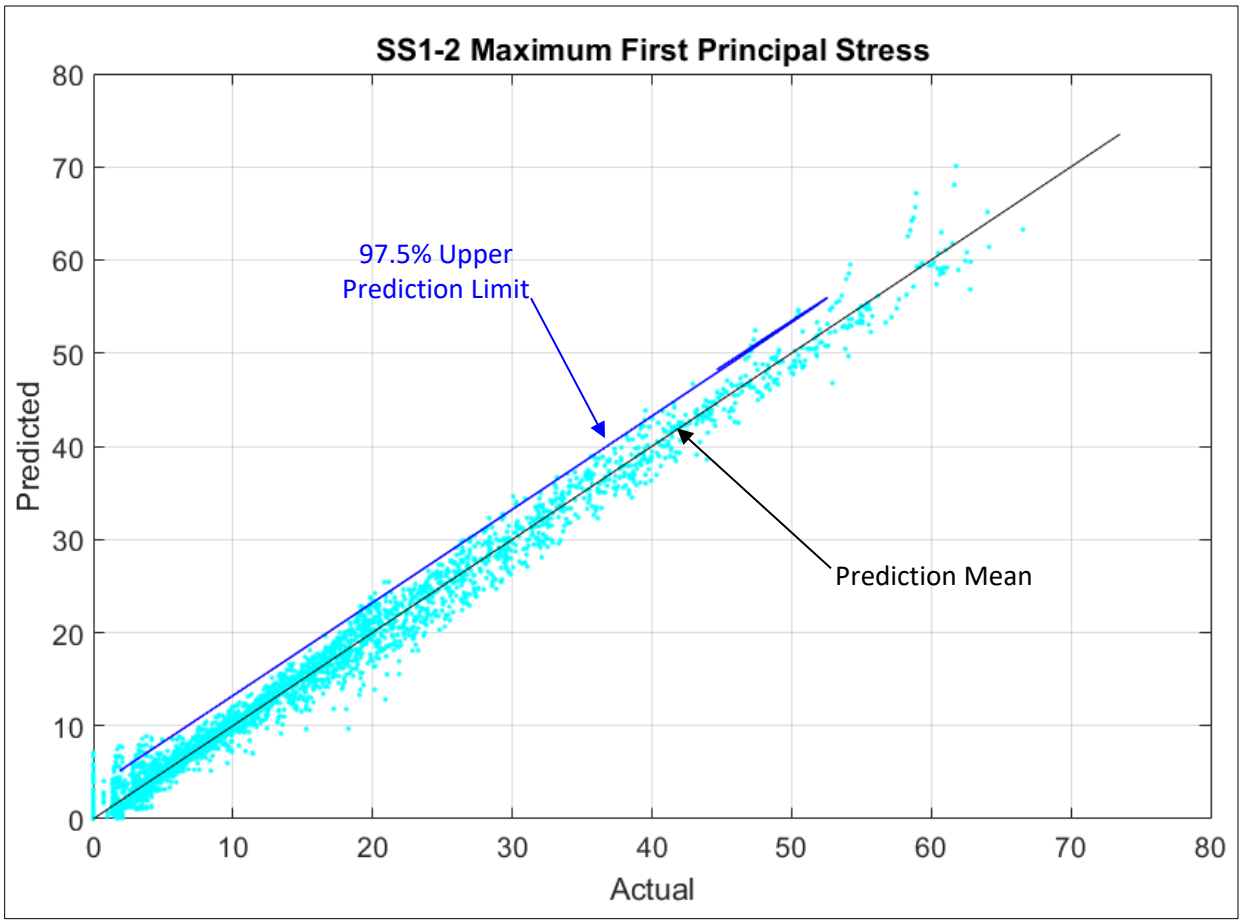

Figure 5. SS1-2 Maximum First Principal Stress, Predicted versus Actual, adjusted R^2=0.9866, with 97.5% upper confidence bound

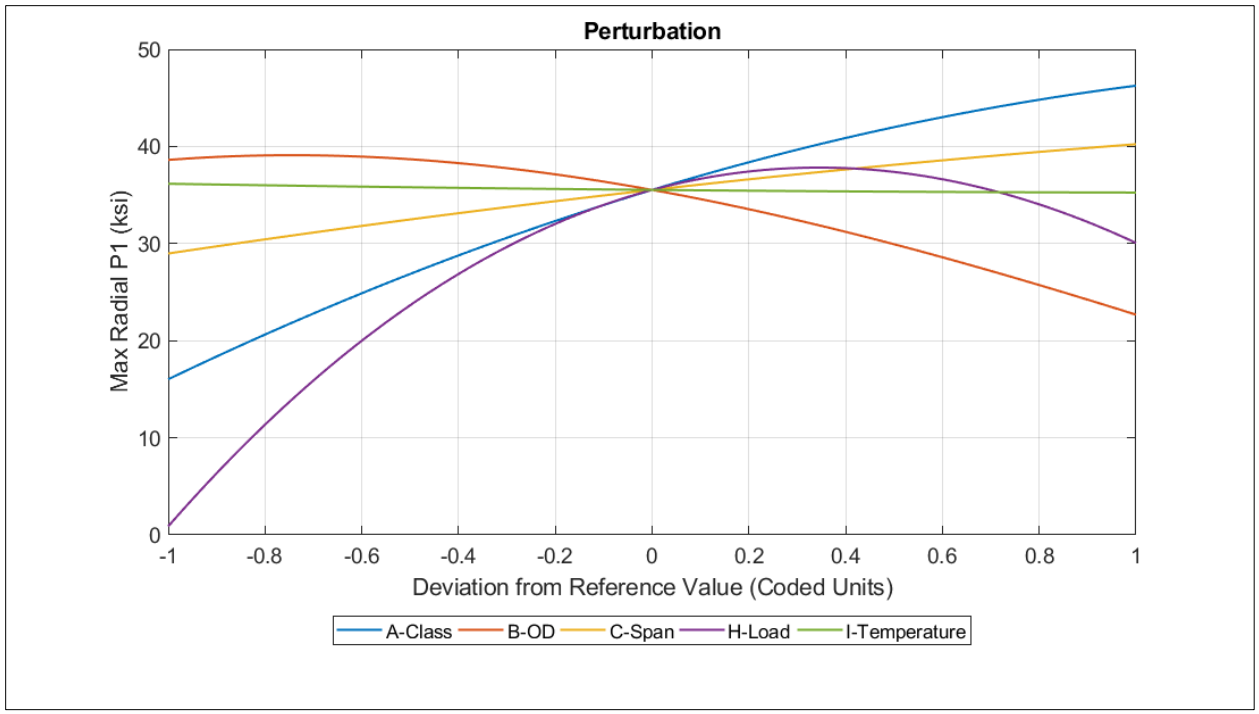

Figure 6. SS1-2 Maximum First Principal Stress, perturbation graph

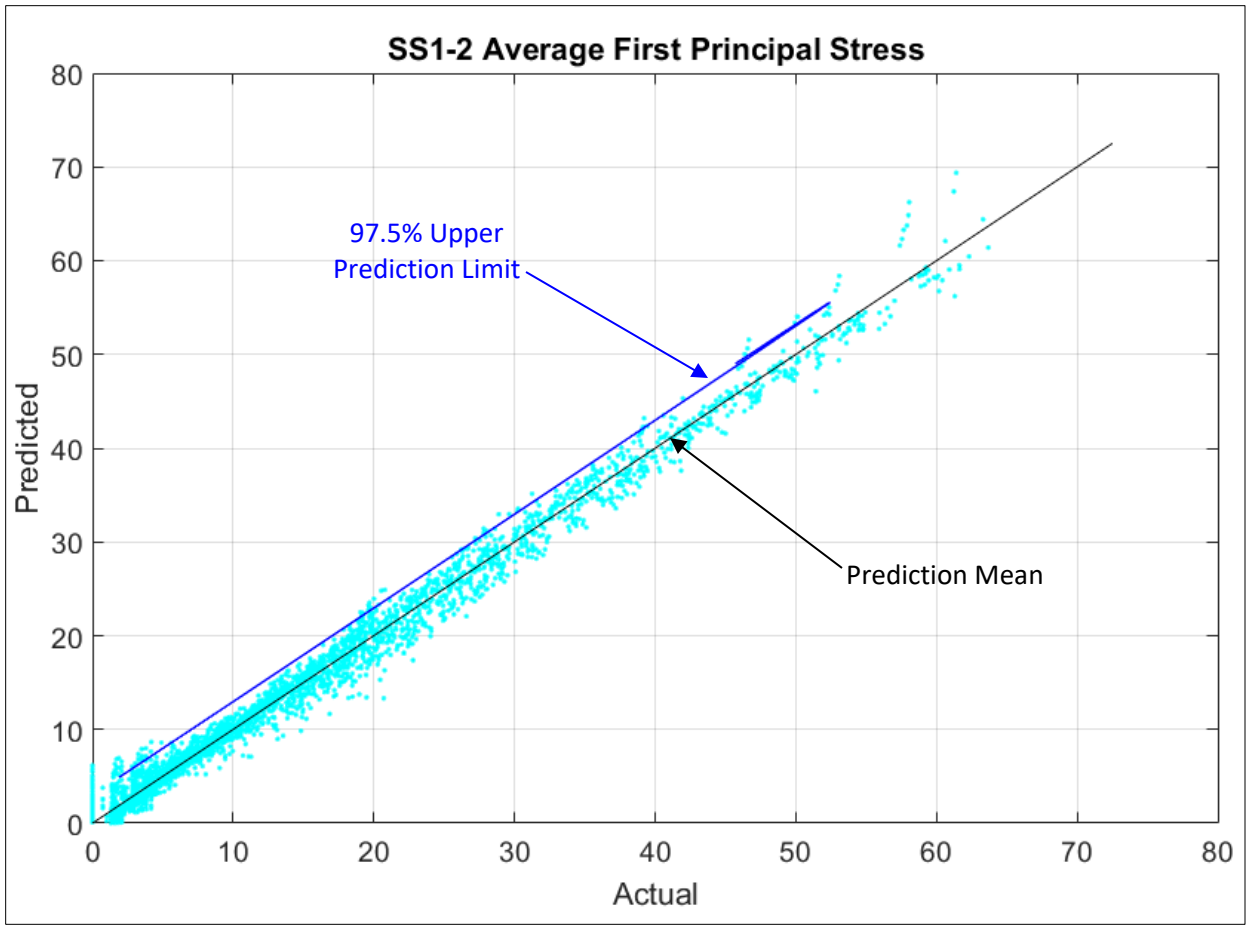

Figure 7. SS1-2 Average First Principal Stress, Predicted versus Actual, adjusted R^2=0.9882, with 97.5% upper confidence bound

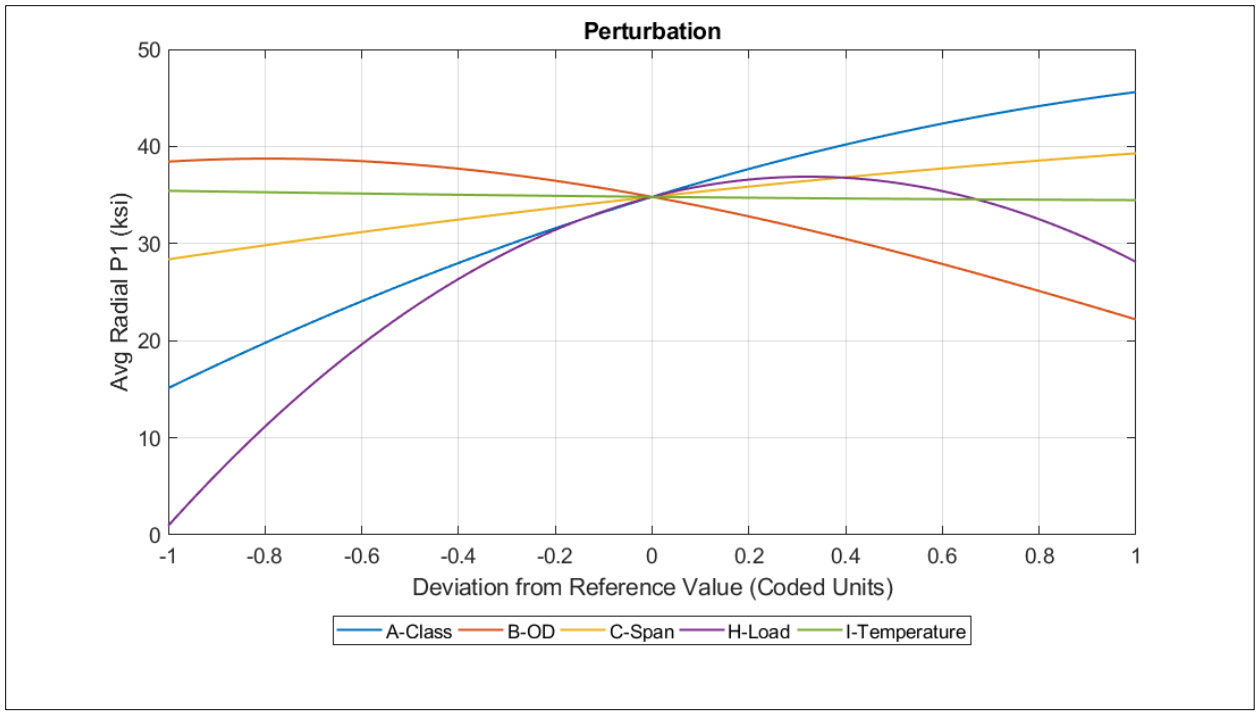

Figure 8. SS1-2 Average Radial First Principal Stress, perturbation graph

Response Surface SS2-1 – Pipe with flaw, axially free end

Response surface SS2-1 applies to a non-axially restrained small-diameter pipe segment with wall loss.

The response surfaces for the maximum and average first principal stresses are based on 8029 data points and have the input variables given in Table 3:

Table 3. Design Variables for SS2-1

	Units	Lower Value	Upper Value
Class	-	10	60
Outer Diameter	in	4.8	13.2
Span	ft	12	18
Flaw Depth	% of WT	5	80
Flaw Length	C	0.1	3
Flaw Width	% of Pipe Circumference	5	49
Vertical Load Pressure	psi	0	80

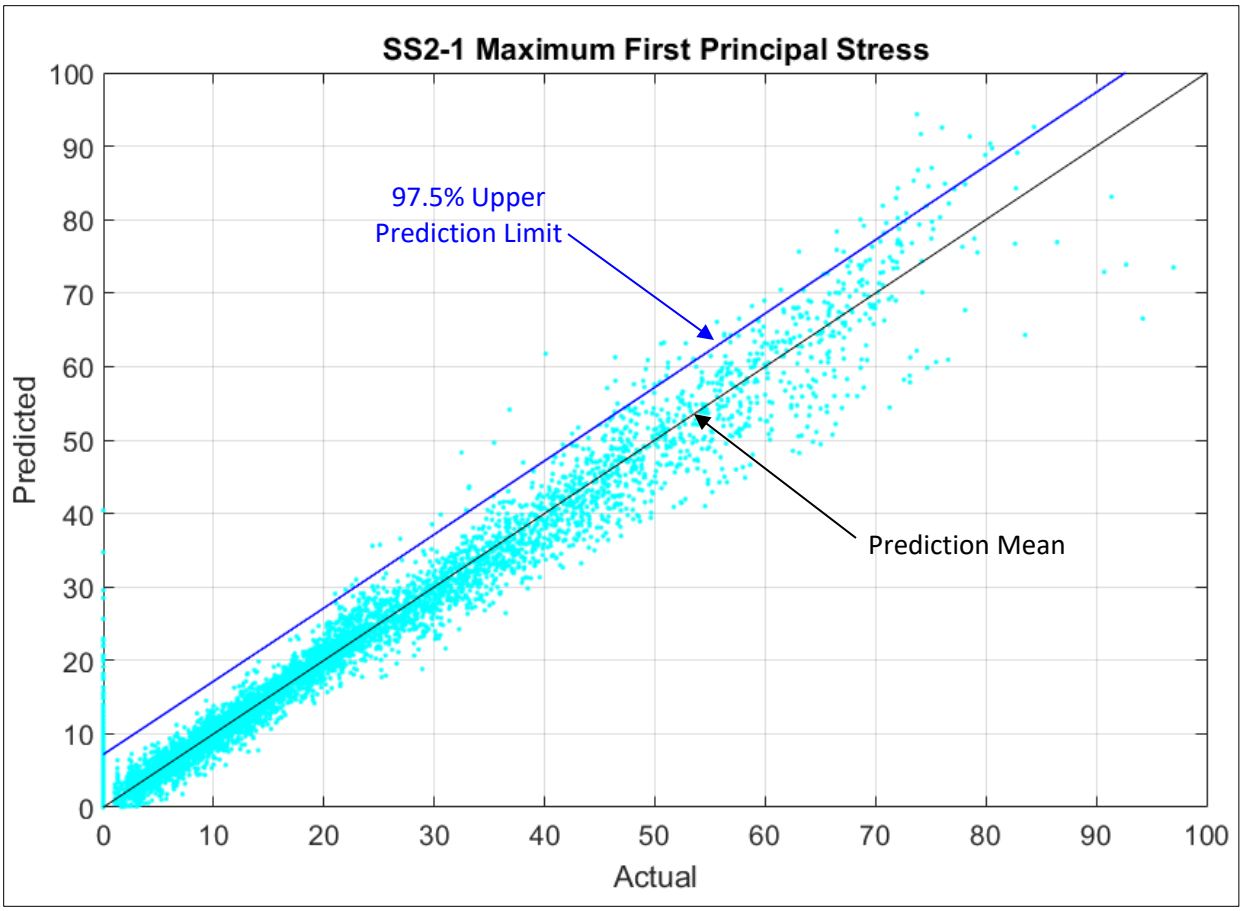

Figure 9. SS2-1 Maximum First Principal Stress, Predicted versus Actual, adjusted R^2=0.9627, with 97.5% upper confidence bound

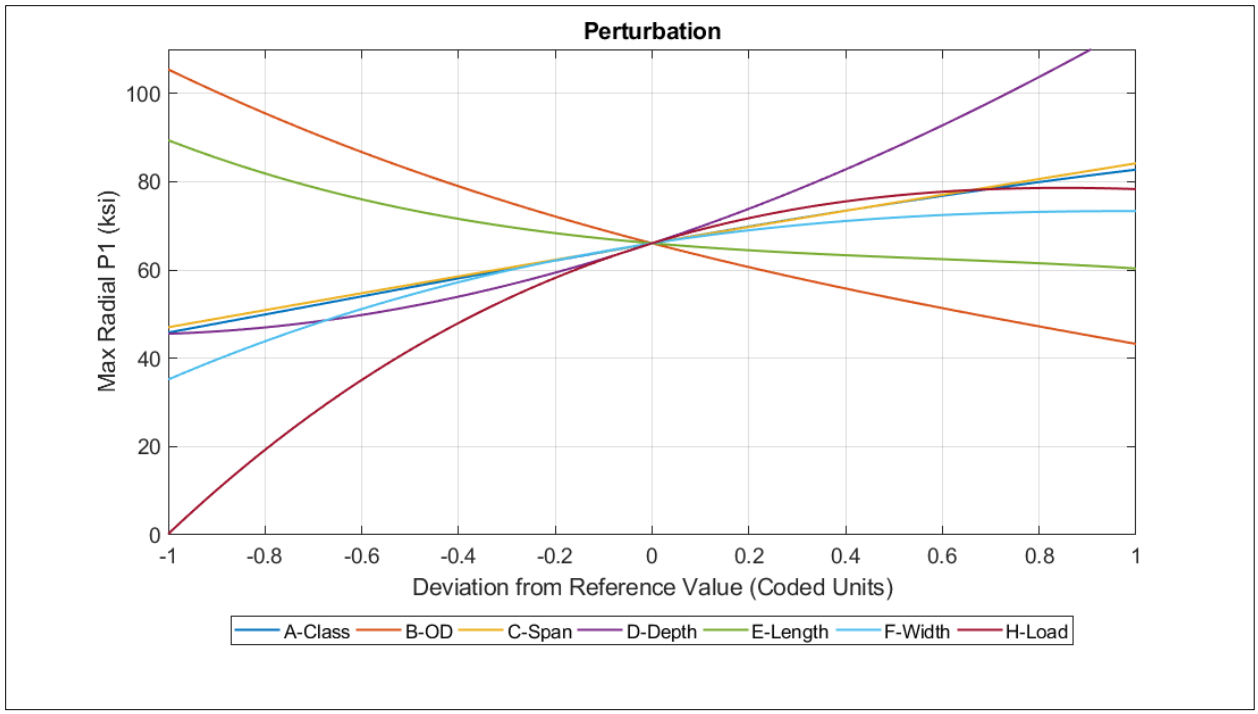

Figure 10. SS2-1 Maximum First Principal Stress, perturbation graph

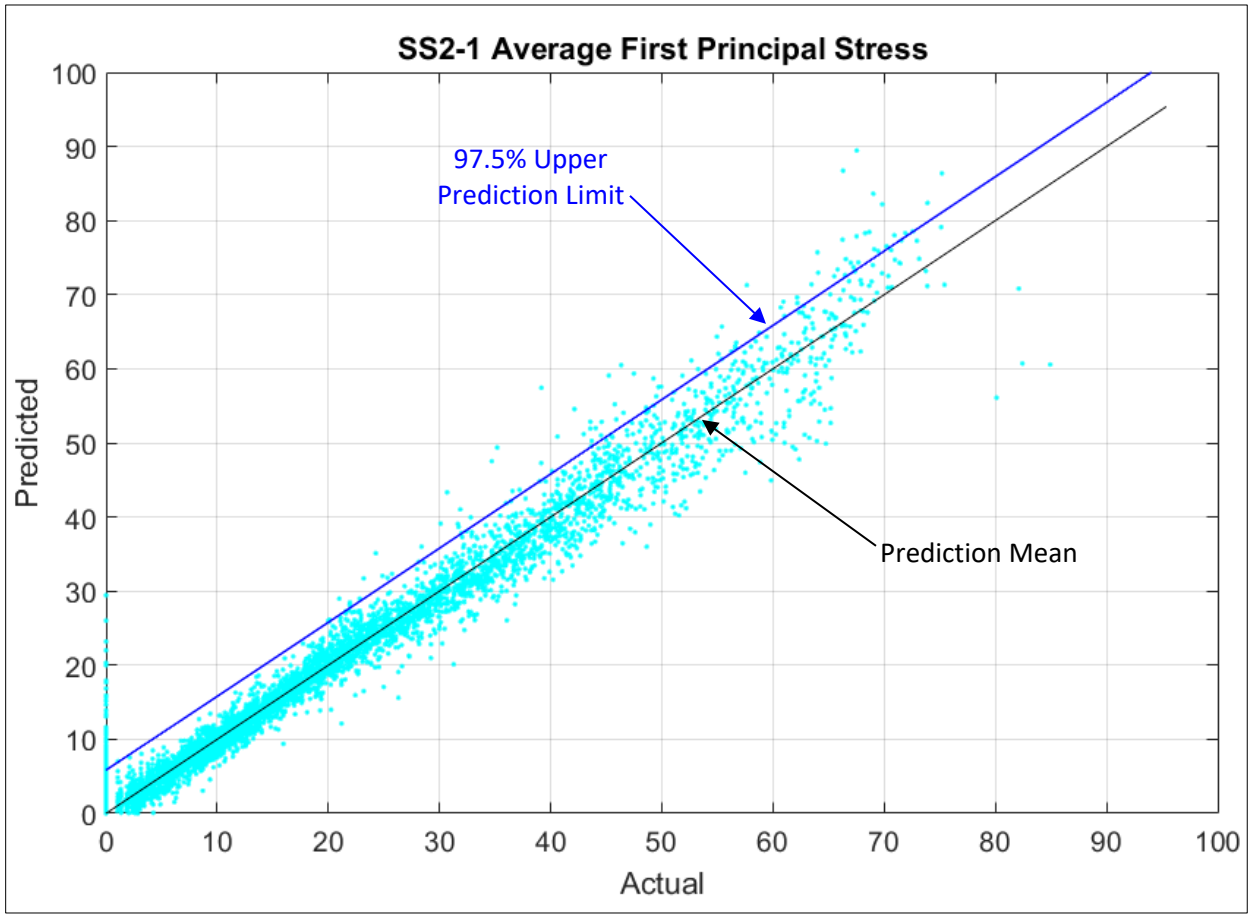

Figure 11. SS2-1 Average Radial First Principal Stress, Predicted versus Actual, adjusted R^2=0.9713, with 97.5% upper confidence bound

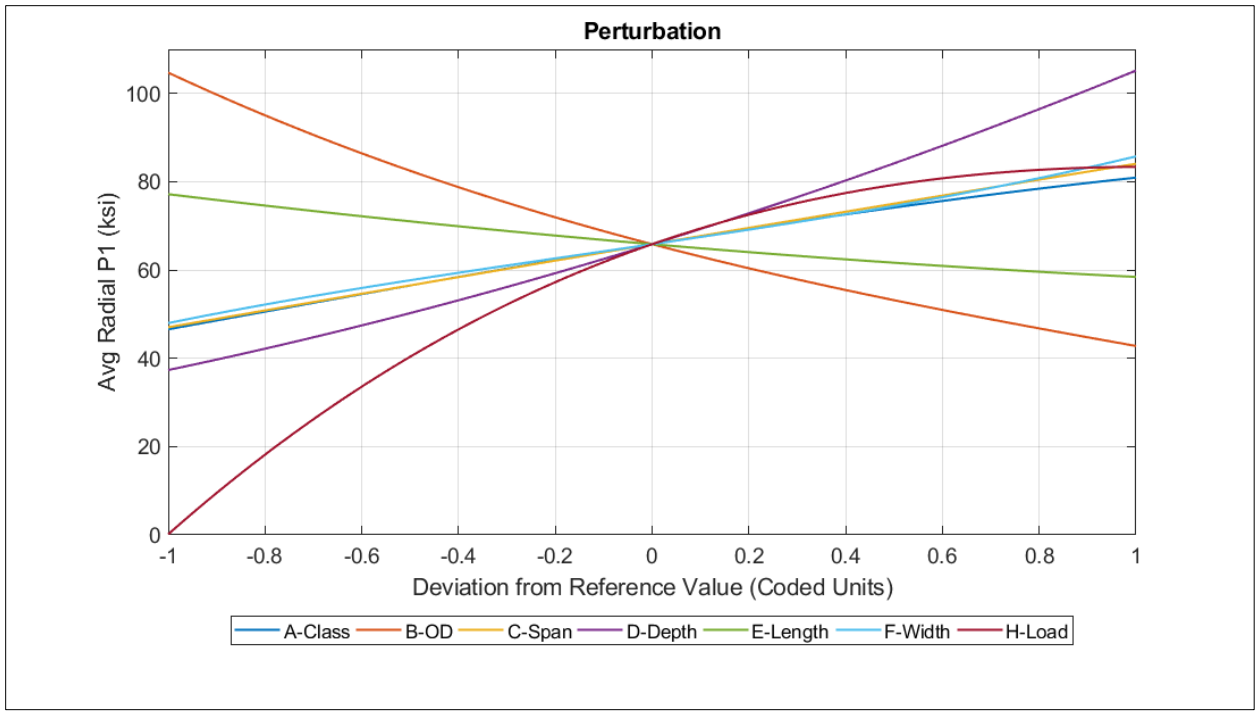

Figure 12. SS2-1 Average Radial First Principal Stress, perturbation graph

Response Surface SS2-2 – Pipe with flaw, axially restrained ends

Response surface SS2-2 applies to an axially restrained small-diameter pipe segment with wall loss.

The response surfaces for the maximum and average first principal stresses are based on 11914 data points and have the input variables given in Table 4:

Table 4. Design Variables for SS2-2

	Units	Lower Value	Upper Value
Class	-	10	60
Outer Diameter	in	4.8	13.2
Span	ft	12	18
Flaw Depth	% of WT	5	80
Flaw Length	C	0.1	3
Flaw Width	% of Pipe Circumference	5	49
Vertical Load Pressure	psi	0	80
Temperature Change	degC	-30	0

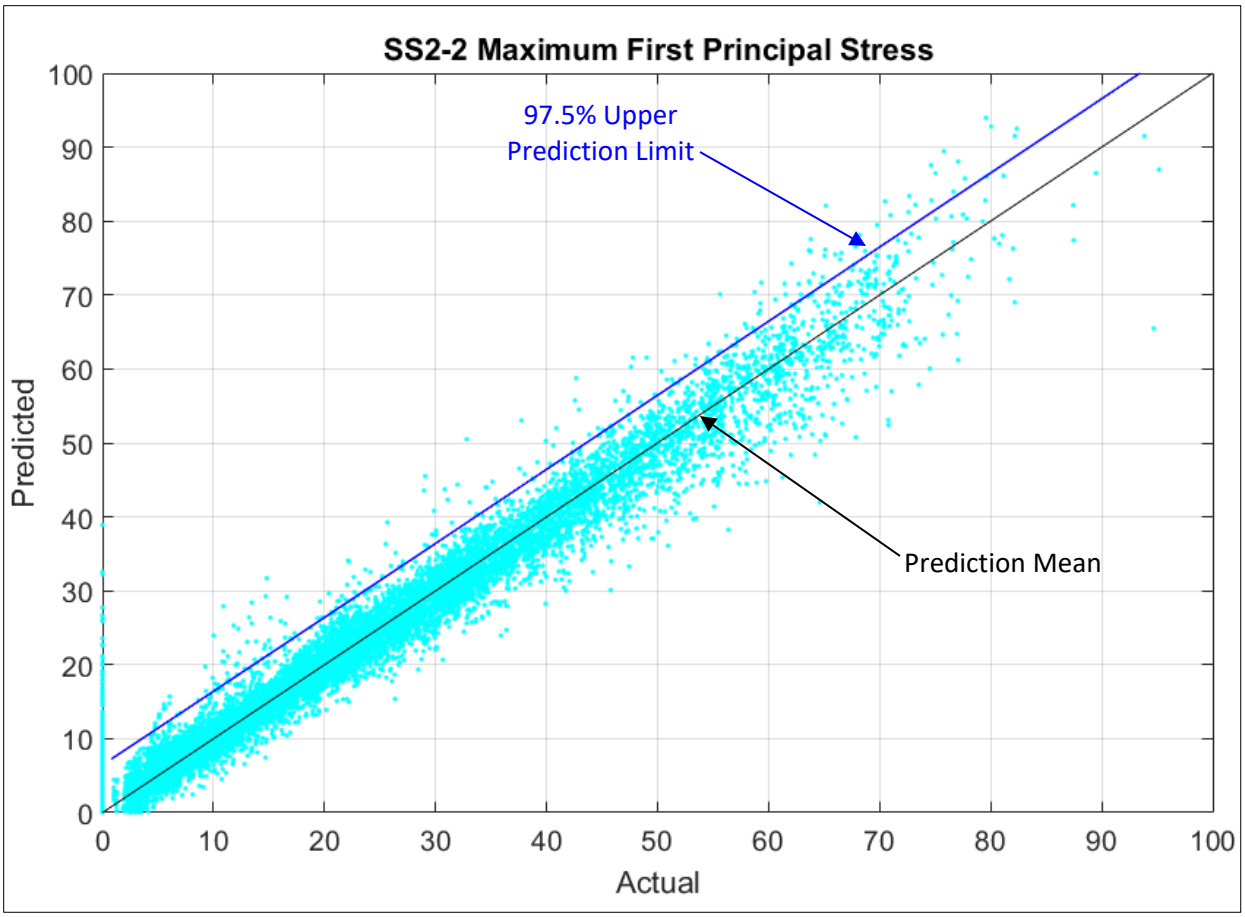

Figure 13. SS2-2 Maximum First Principal Stress, Predicted versus Actual, adjusted R^2=0.9641, with 97.5% upper prediction limit

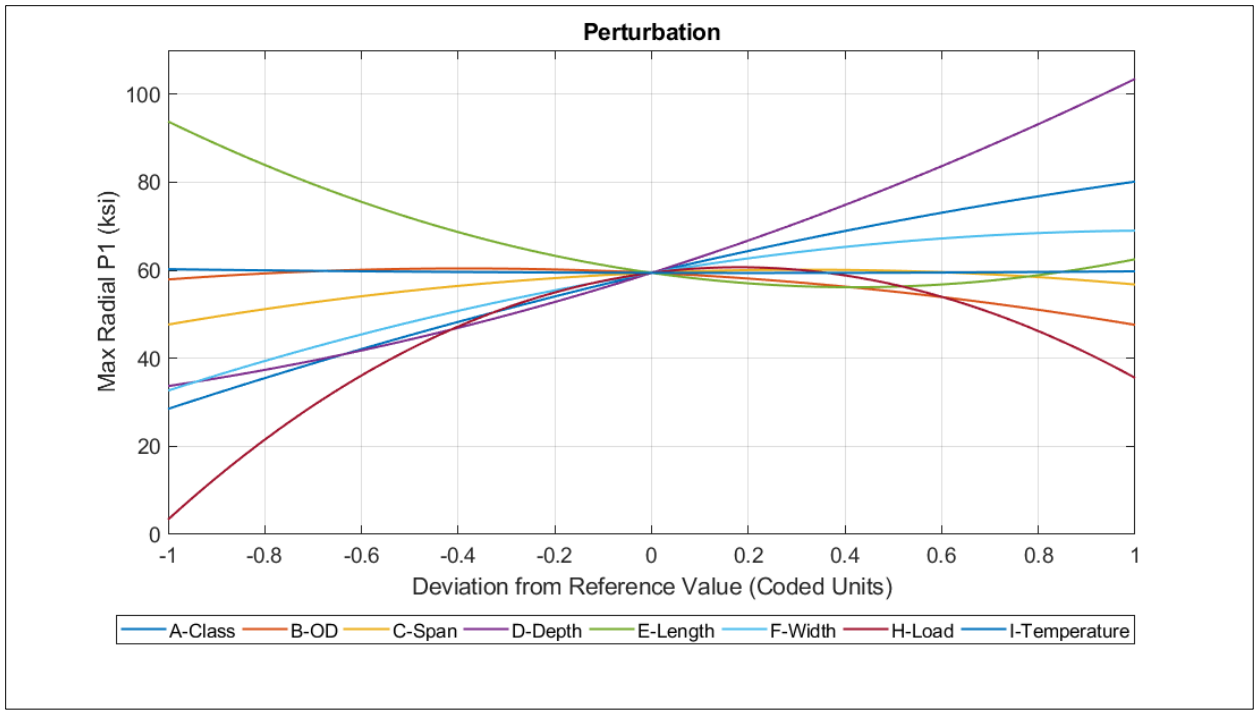

Figure 14. SS2-2 Maximum First Principal Stress, perturbation graph

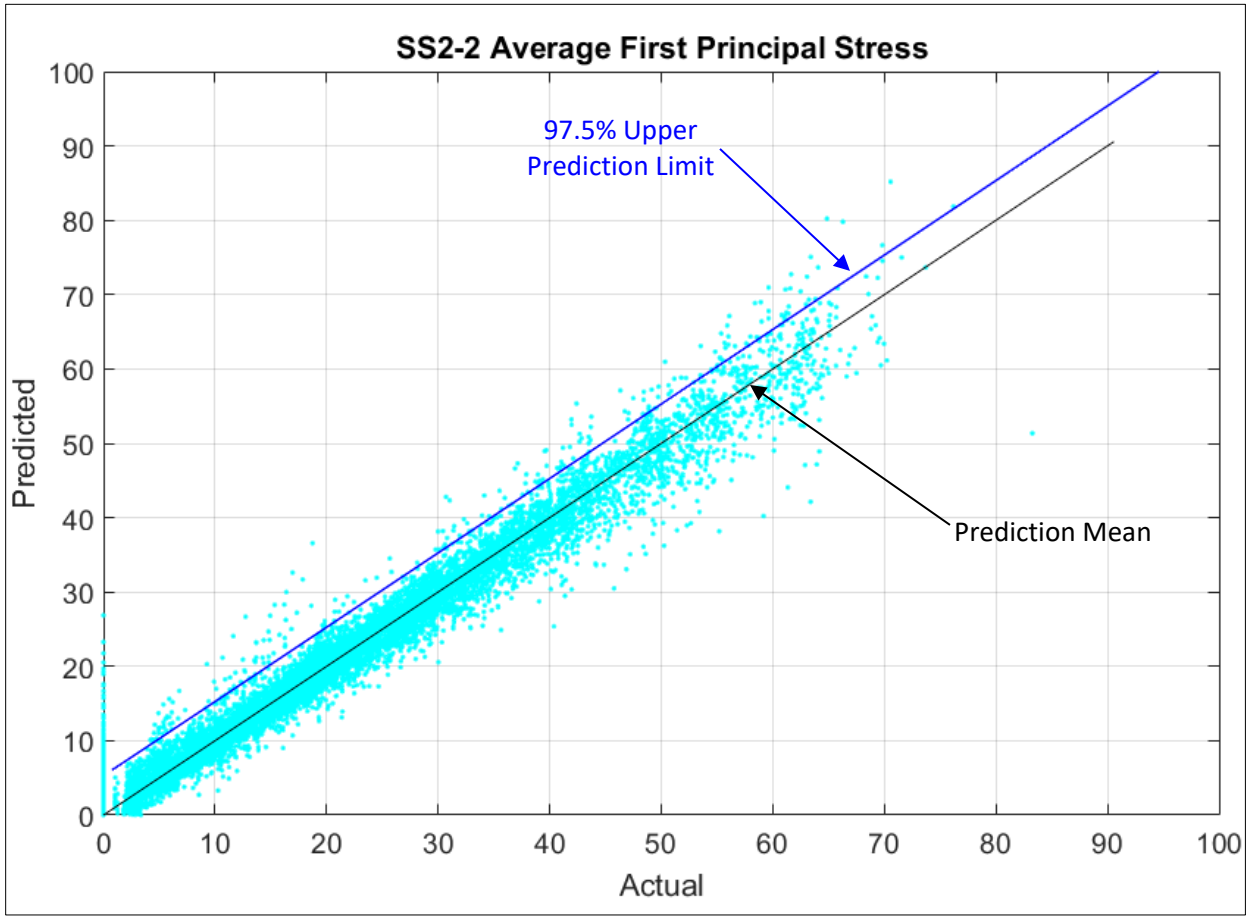

Figure 15. SS2-2 Average Radial First Principal Stress, Predicted versus Actual, adjusted R^2=0.9693, with 97.5% upper confidence bound

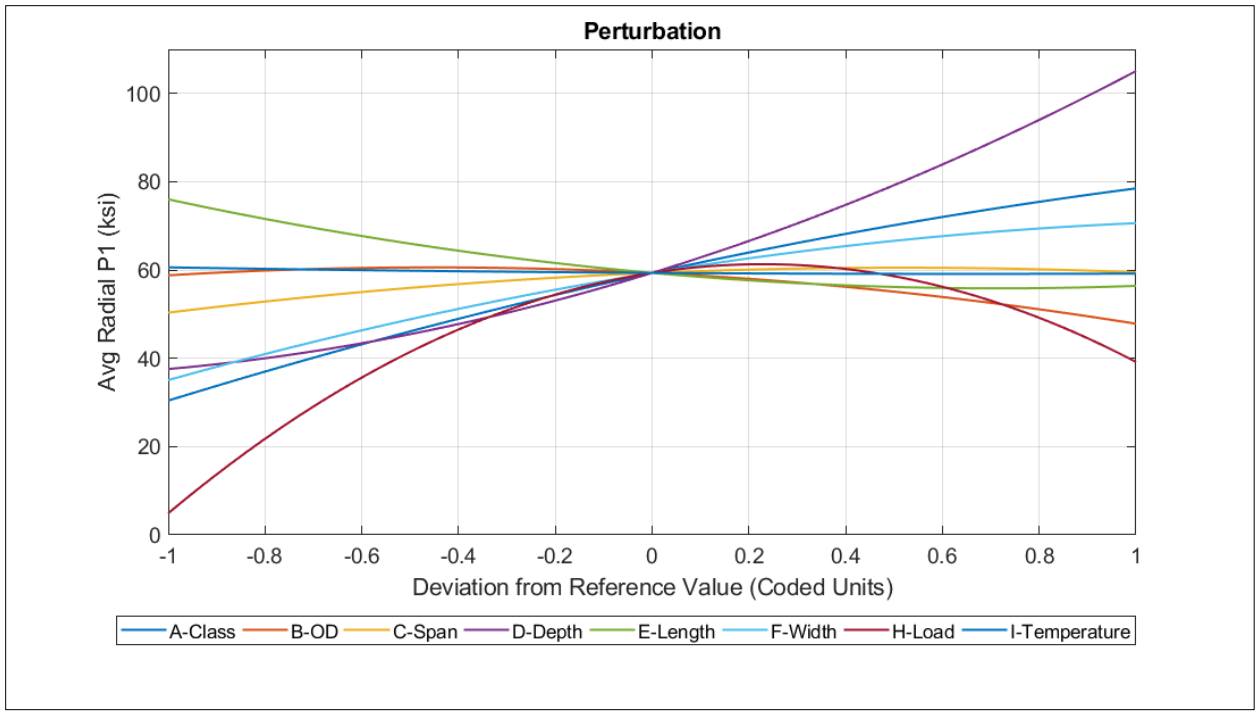

Figure 16. SS2-2 Average Radial First Principal Stress, perturbation graph

Response Surface SS3-1 – Large diameter pipe without flaw, axially free end

Response surface SS3-1 applies to a non-axially restrained, large-diameter pipe segment without wall loss.

The response surfaces for the maximum and average first principal stresses are based on 1496 data points and have the input variables given in Table 1:

Table 5. Design Variables for SS3-1

	Units	Lower Value	Upper Value
Class	-	10	60
Outer Diameter	in	15.3	50.5
Pipe Span	ft	12	18
Vertical Load Pressure	psi	0	80

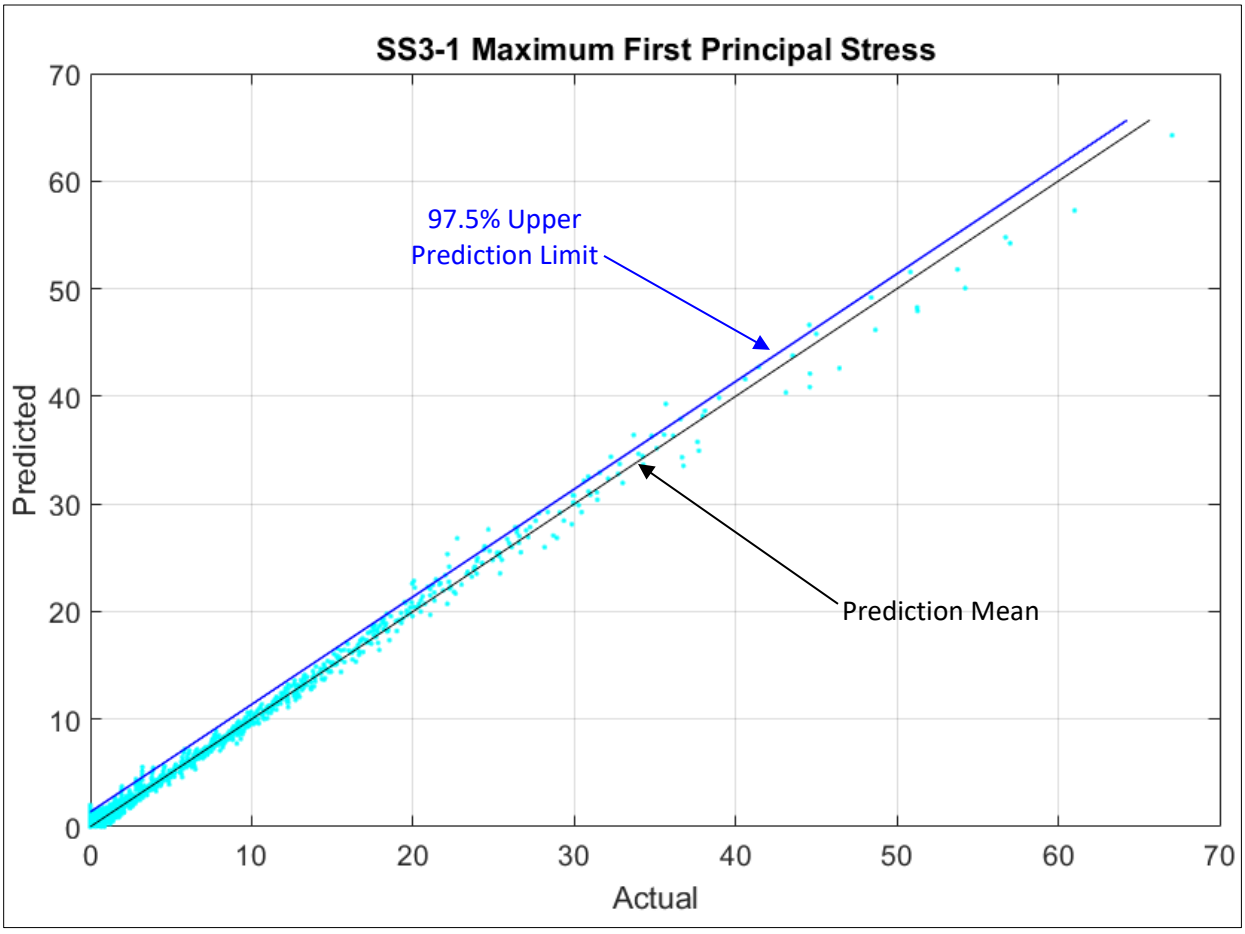

Figure 17. SS3-1 Maximum First Principal Stress, Predicted versus Actual, adjusted R^2=0.9948, with 97.5% upper confidence bound

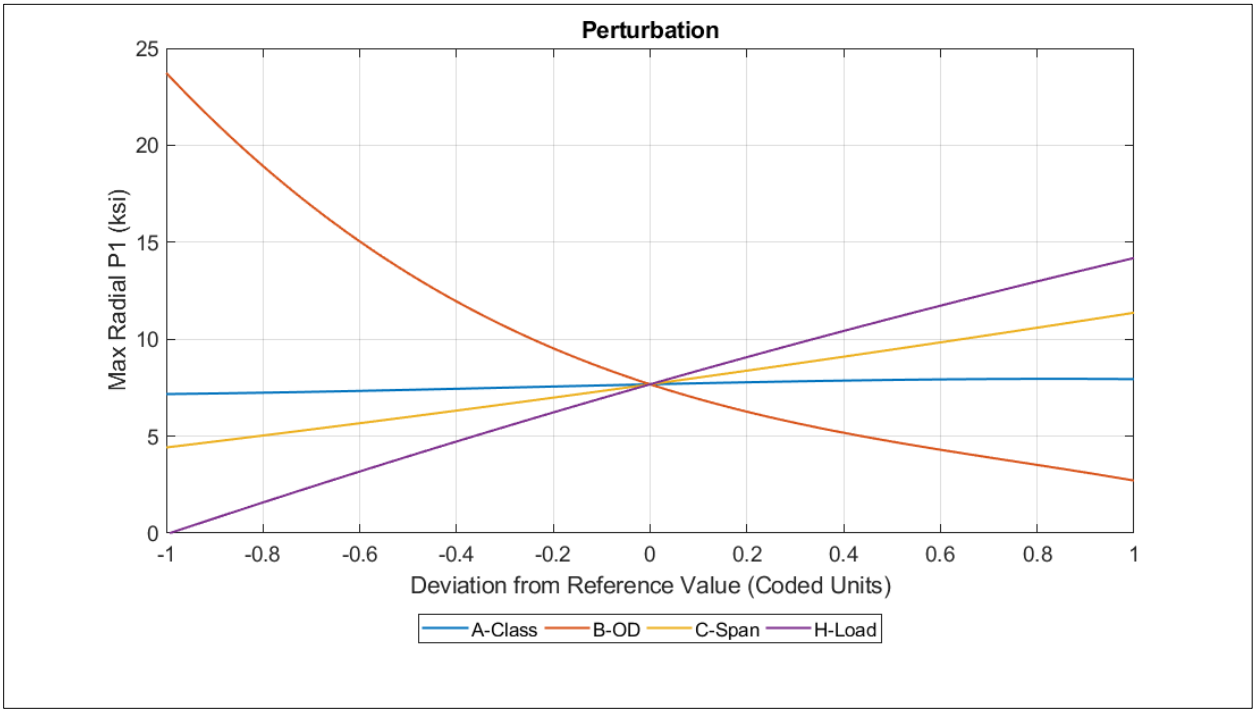

Figure 18. SS3-1 Maximum First Principal Stress, perturbation graph

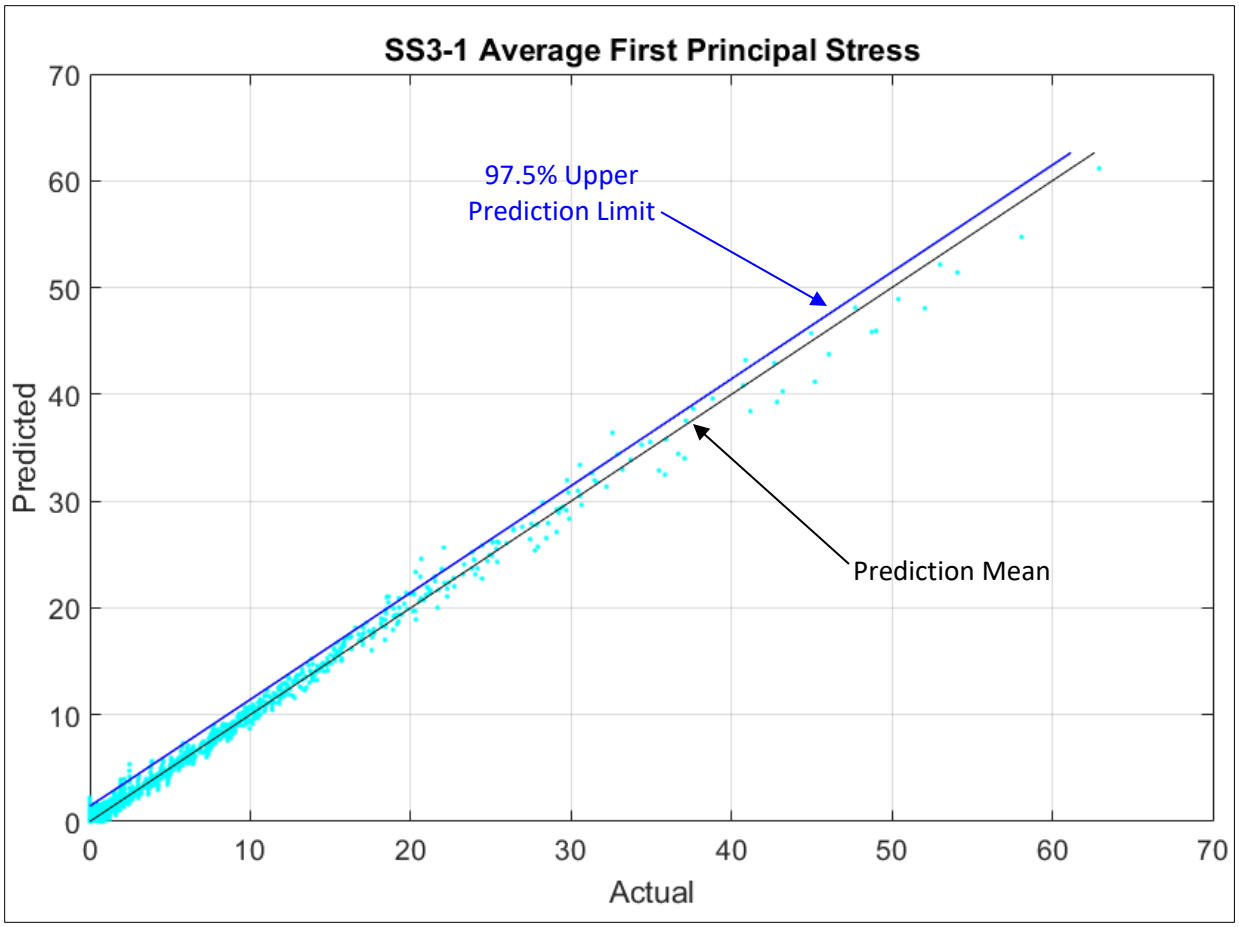

Figure 19. SS3-1 Average Radial First Principal Stress, Predicted versus Actual, adjusted R^2=0.9934, with 97.5% upper confidence bound

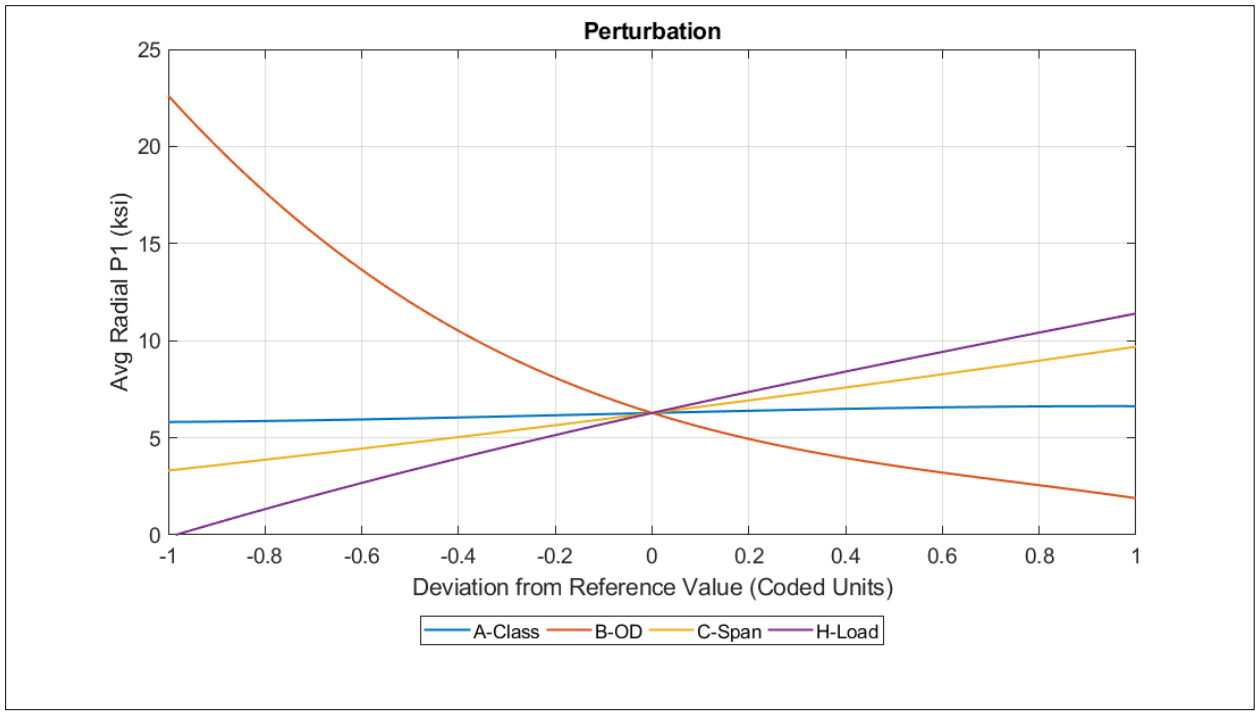

Figure 20. SS3-1 Average Radial First Principal Stress, perturbation graph

Response Surface SS3-2 – Large diameter pipe without flaw axially restrained ends

Response surface SS3-2 applies to an axially restrained, large-diameter pipe segment without wall loss.

The response surfaces for the maximum and average first principal stresses are based on 4395 data points and have the input variables given in Table 2:

Table 6. Design Variables for SS3-2

	Units	Lower Value	Upper Value
Class	-	10	60
Outer Diameter	in	15.3	50.5
Pipe Span	ft	12	18
Temperature Change	degC	-20	0
Vertical Load Pressure	psi	0	80

Figure 21. SS3-2 Maximum First Principal Stress, Predicted versus Actual, adjusted R^2=0.9931, with 97.5% upper confidence bound

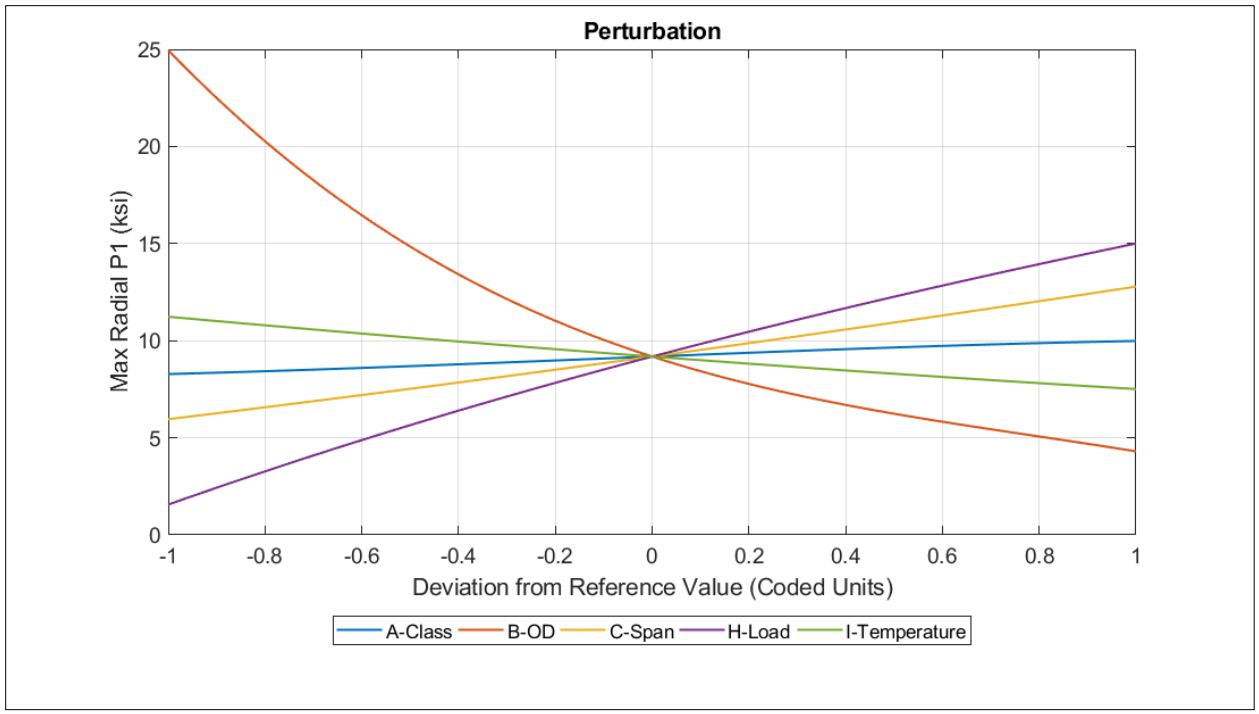

Figure 22. SS3-2 Maximum First Principal Stress, perturbation graph

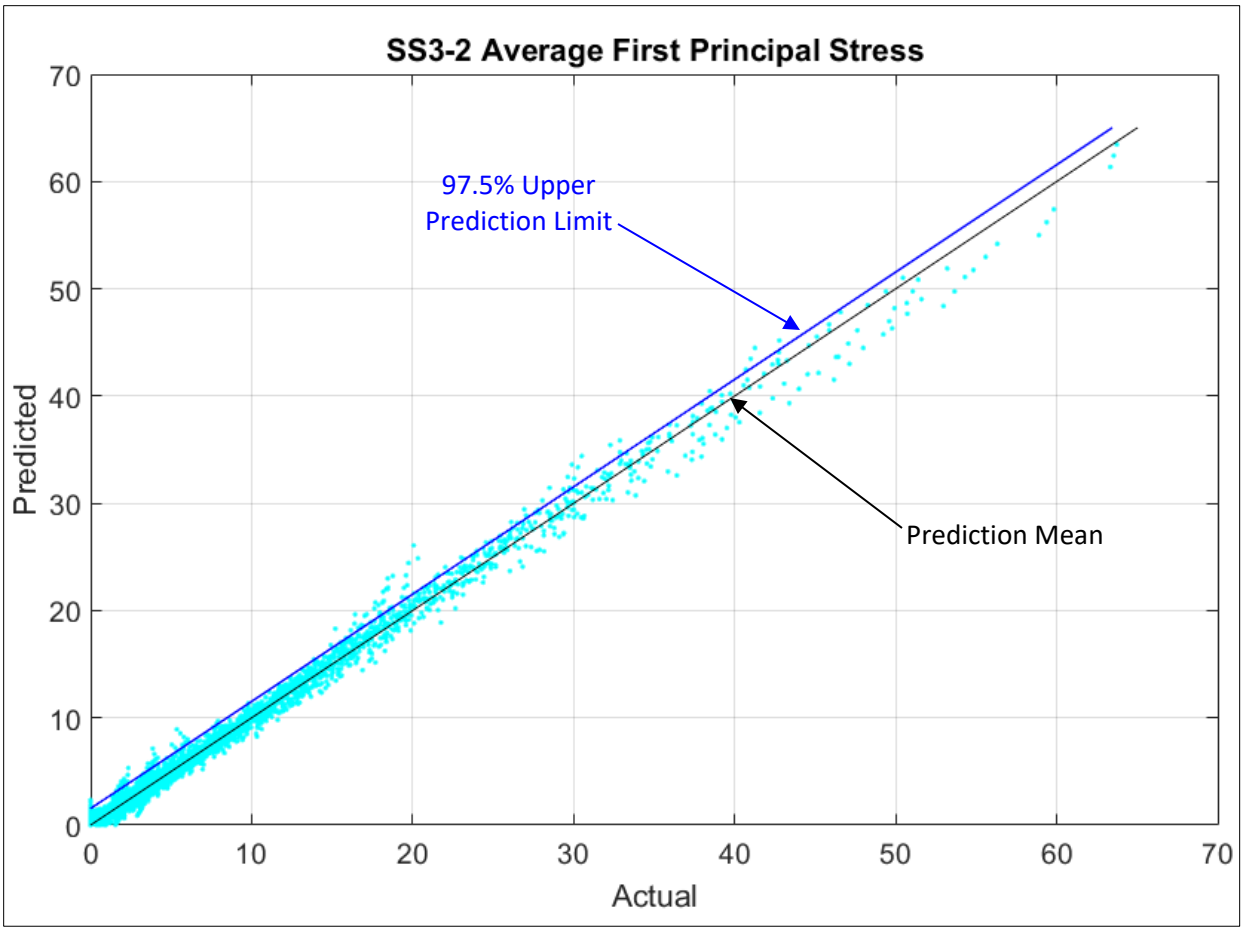

Figure 23. SS3-2 Average First Principal Stress, Predicted versus Actual, adjusted R^2=0.9923, with 97.5% upper confidence bound

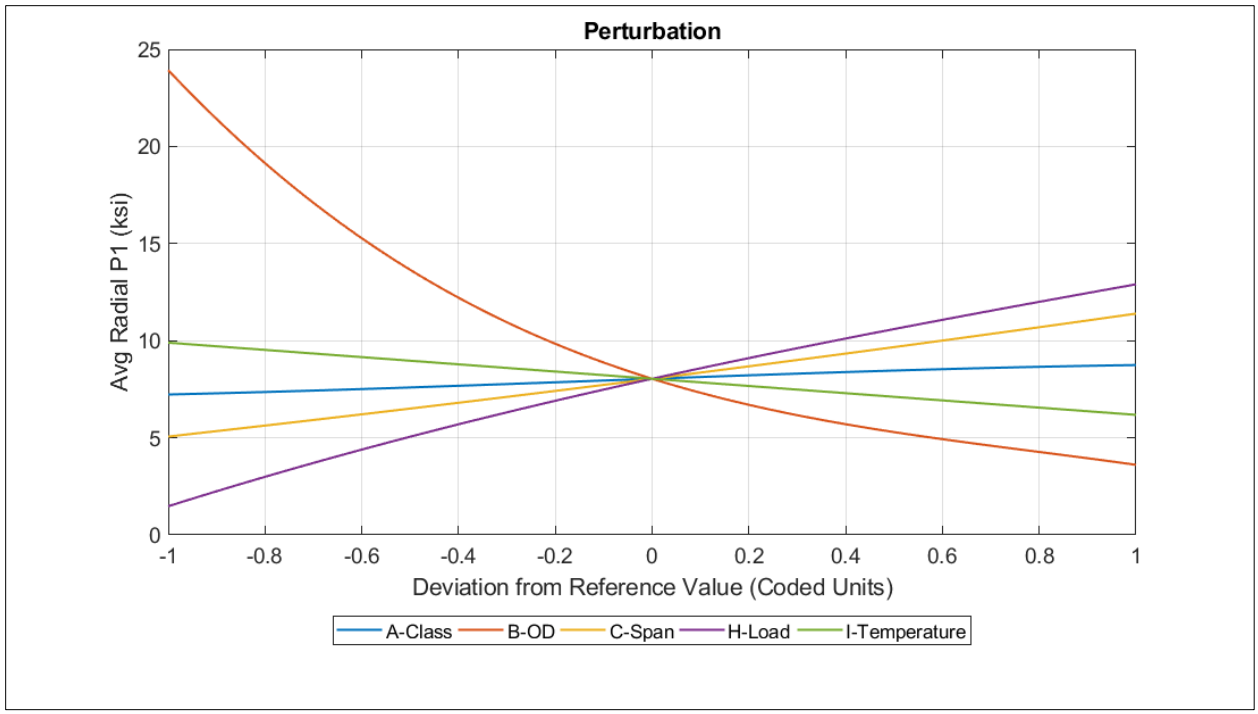

Figure 24. SS3-2 Average Radial First Principal Stress, perturbation graph

Response Surface SS4-1 – Large diameter pipe with flaw, axially free end

Response surface SS4-1 applies to a non-axially restrained, large-diameter pipe segment with wall loss.

The response surfaces for the maximum and average first principal stresses are based on 11376 data points and have the input variables given in Table 3:

Table 7. Design Variables for SS4-1

	Units	Lower Value	Upper Value
Class	-	10	60
Outer Diameter	in	15.3	50.5
Span	ft	12	18
Flaw Depth	% of WT	5	80
Flaw Length	C	0.1	3
Flaw Width	% of Pipe Circumference	5	49
Vertical Load Pressure	psi	0	80

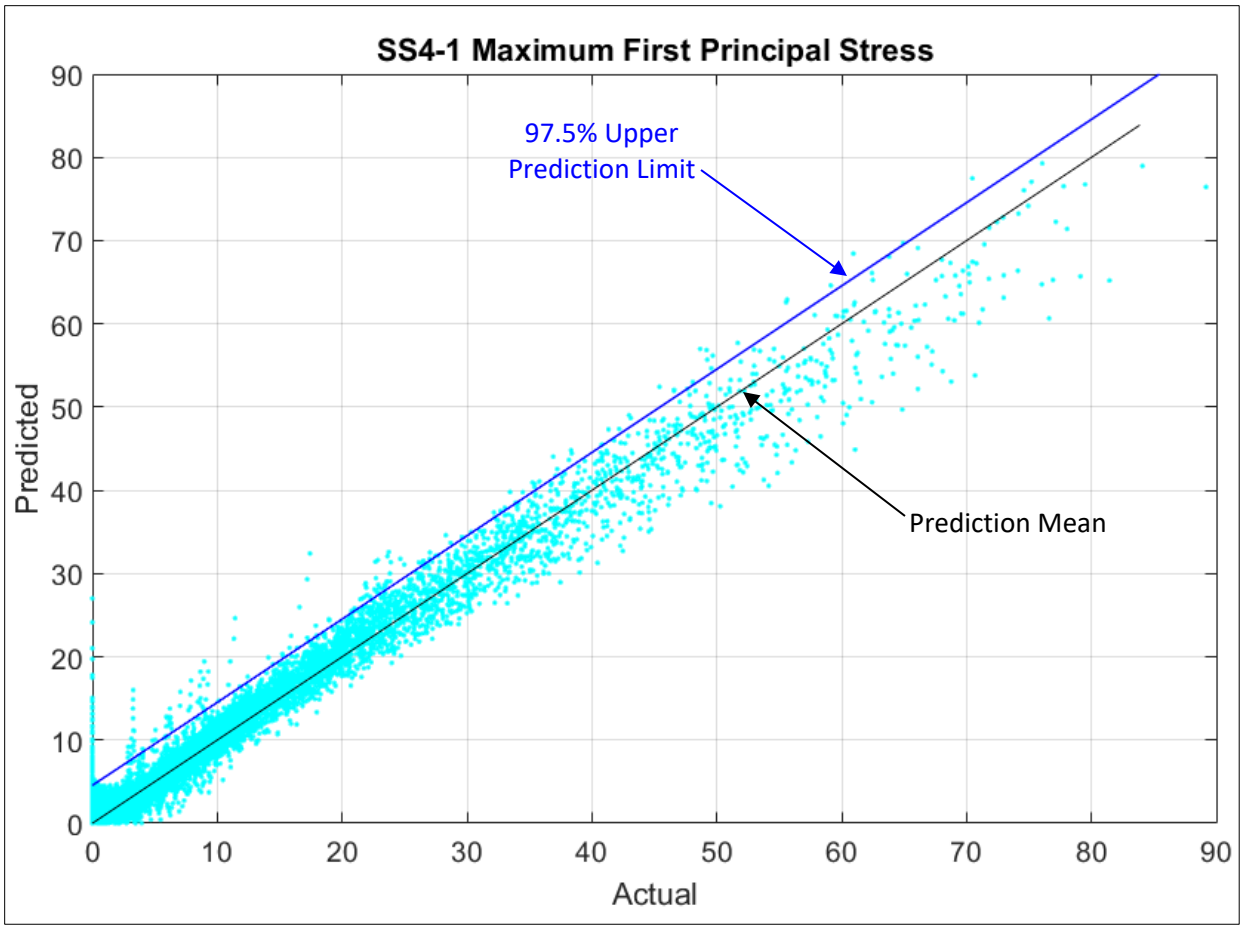

Figure 25. SS4-1 Maximum First Principal Stress, Predicted versus Actual, adjusted R^2=0.9696, with 97.5% upper confidence bound

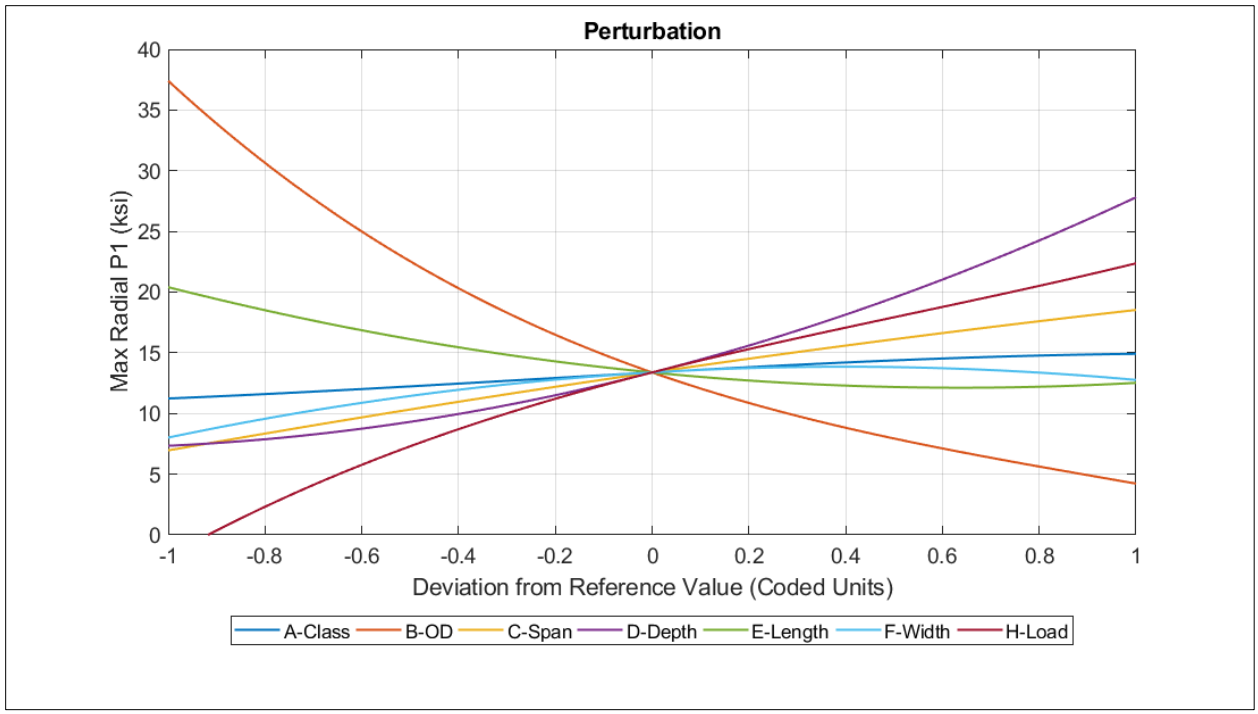

Figure 26. SS4-1 Maximum First Principal Stress, perturbation graph

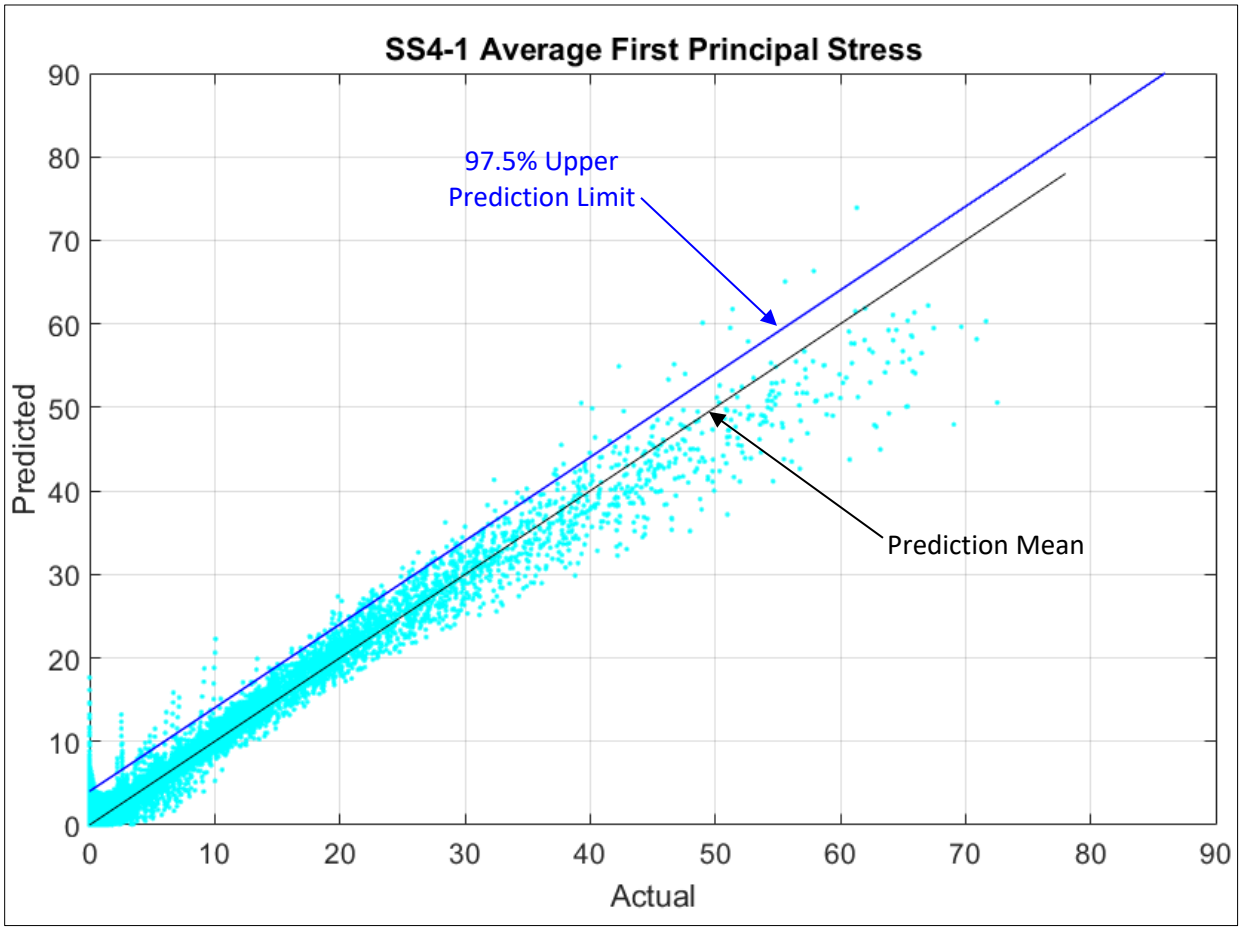

Figure 27. SS4-1 Average Radial First Principal Stress, Predicted versus Actual, adjusted R^2=0.9682, with 97.5% upper confidence bound

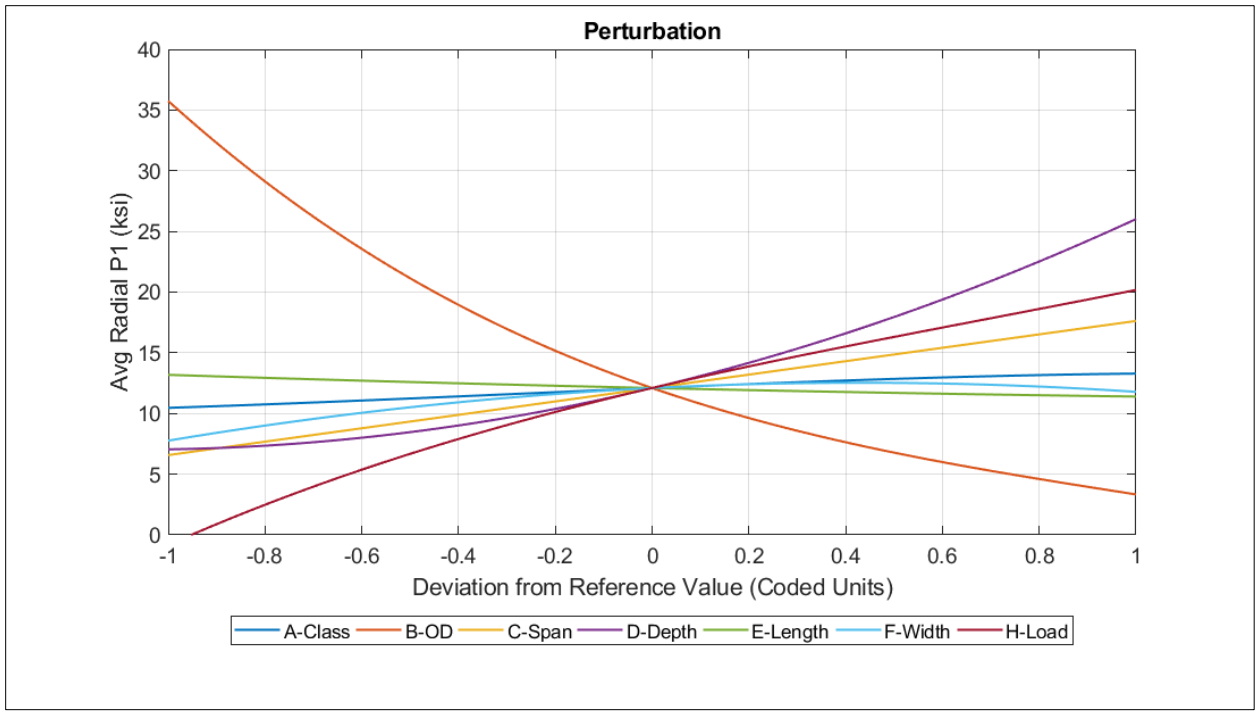

Figure 28. SS4-1 Average Radial First Principal Stress, perturbation graph

Response Surface SS4-2 – Large diameter pipe with flaw, axially restrained ends

Response surface SS4-2 applies to an axially restrained, large-diameter pipe segment with wall loss.

The response surfaces for the maximum and average first principal stresses are based on 29513 data points and have the input variables given in Table 4:

Table 8. Design Variables for SS4-2

	Units	Lower Value	Upper Value
Class	-	10	60
Outer Diameter	in	15.3	50.5
Span	ft	12	18
Flaw Depth	% of WT	5	80
Flaw Length	C	0.1	3
Flaw Width	% of Pipe Circumference	5	49
Vertical Load Pressure	psi	0	80
Temperature Change	degC	-30	0

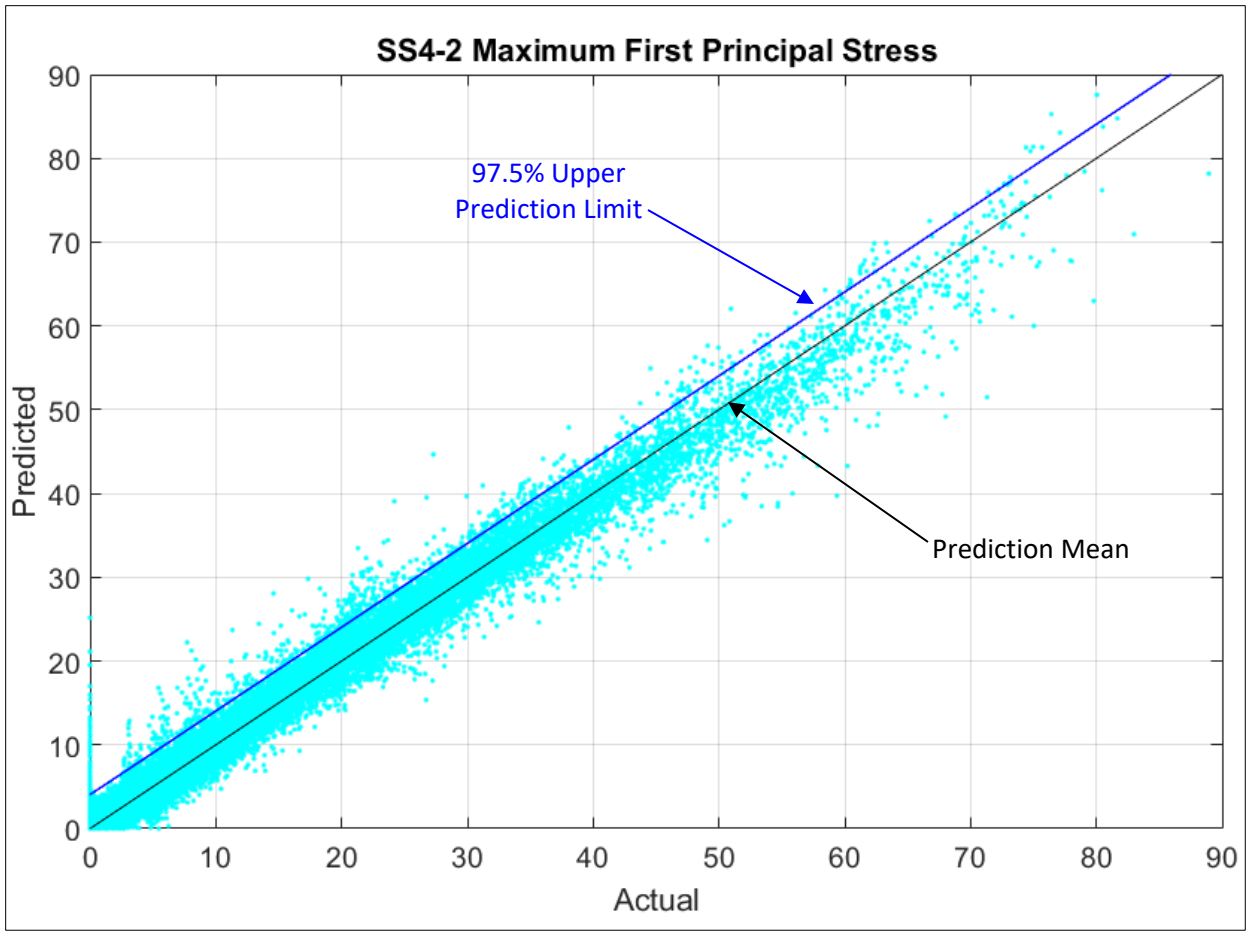

Figure 29. SS4-2 Maximum First Principal Stress, Predicted versus Actual, adjusted R^2=0.9770, with 97.5% upper prediction limit

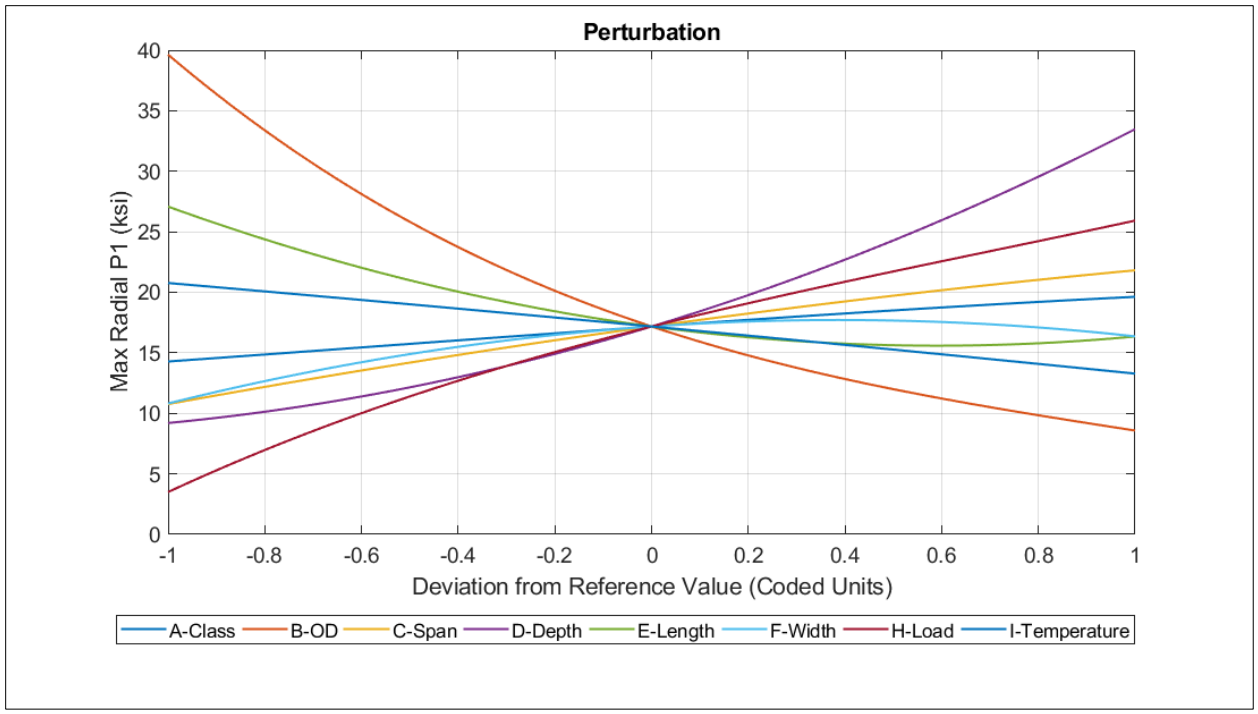

Figure 30. SS4-2 Maximum First Principal Stress, perturbation graph

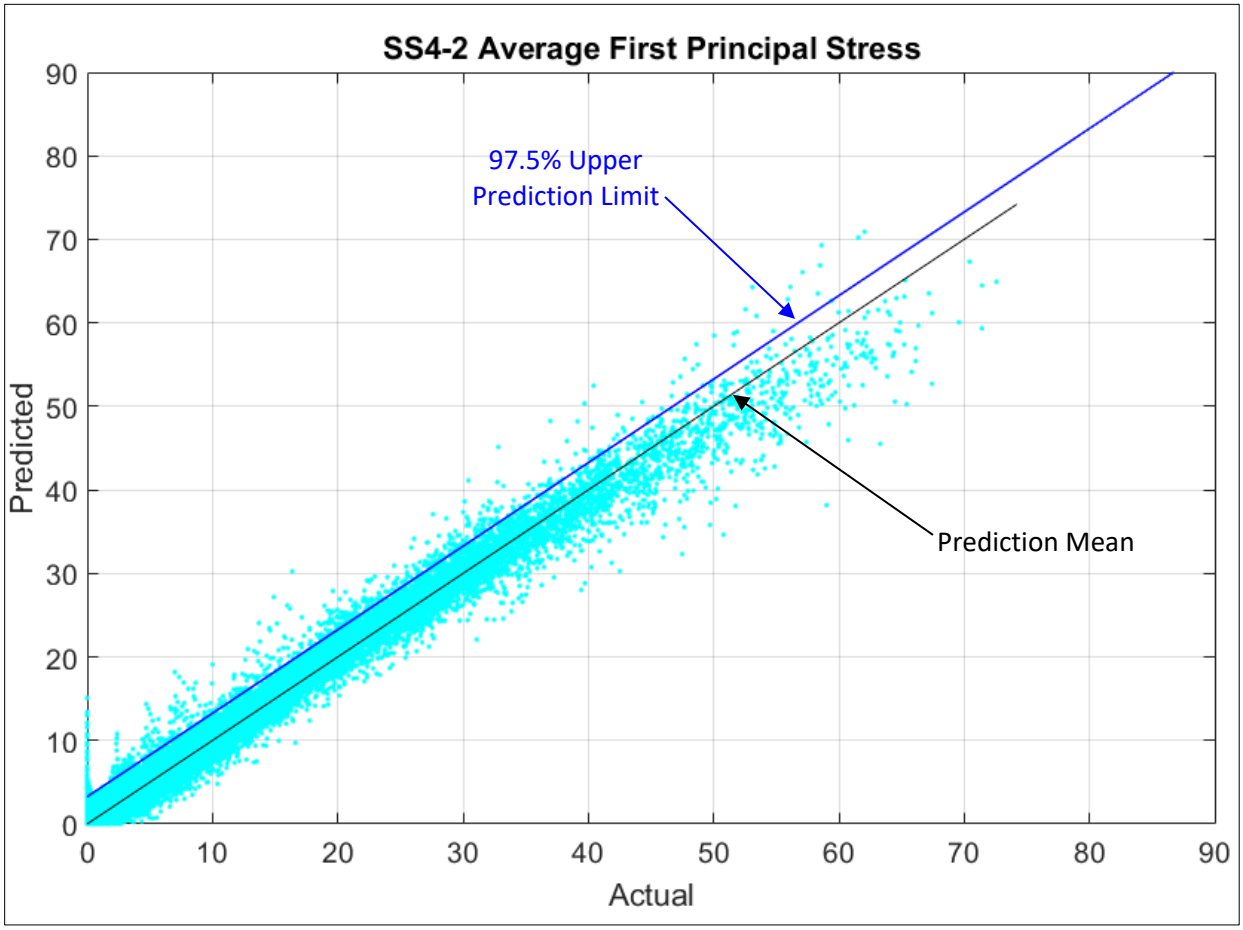

Figure 31. SS4-2 Average Radial First Principal Stress, Predicted versus Actual, adjusted R^2=0.9790, with 97.5% upper confidence bound

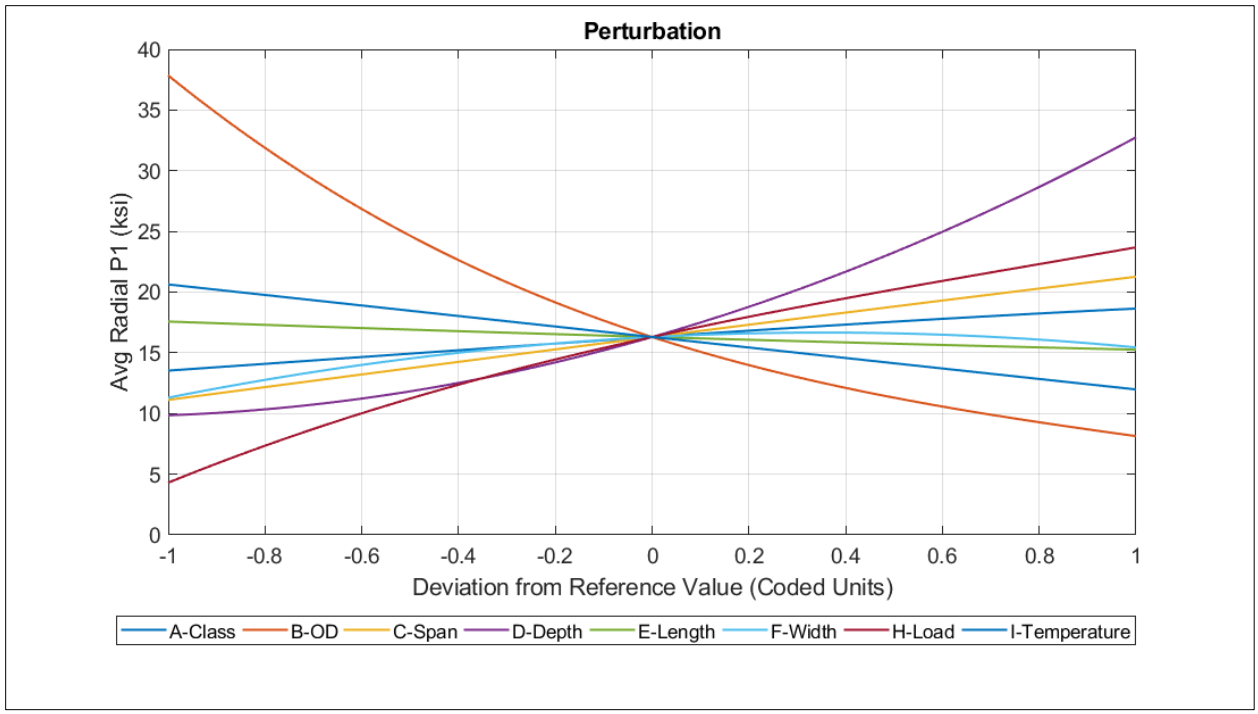

Figure 32. SS4-2 Average Radial First Principal Stress, perturbation graph

References

1. Seica, M.V., Jeffrey, A.P., “Finite Element Evaluation of the Remaining Mechanical Strength of Deteriorated Cast Iron Pipes”, Journal of Engineering Materials and Technology, January 2004.
2. Seica, M.V., Jeffrey, A.P., “Simplified Numerical Method to Evaluate the Mechanical Strength of Cast Iron Water Pipes”, Journal of Infrastructure Systems, March 2006.

End of Addendum Report

the Energy to Lead

gti

ADDENDUM REPORT NUMBER 2
GTI PROJECT NUMBER 21874
Contract Number: DTPH56-15-T-00006

Characterization and Fitness for Service of Corroded Cast Iron Pipe

Addendum Report #2 – Geospatial Example

Report Issued
December 31, 2018

Prepared For
U.S. Department of Transportation
Pipeline and Hazardous Materials Safety Administration
Office of Pipeline Safety
Chris McLaren
chris.mclaren@dot.gov

Technical Team
Daniel Ersoy
Ernest Lever
Oren Lever
Khalid Farrag
Brian Miller

Project Manager
Kristine Wiley
R&D Director, GTI
kristine.wiley@gastechnology.org

Technical Contact
Daniel Ersoy
R&D Executive Director, GTI
daniel.ersoy@gastechnology.org

Gas Technology Institute
1700 S. Mount Prospect Rd.
Des Plaines, Illinois 60018

SIGNATURE PAGE

			Date
CO-AUTHOR			
Daniel A. Ersoy		Daniel Ersoy//S//	12/31/2018
	Title:	R&D Exec. Dir. and PI	
CO-AUTHOR			
Ernest Lever		Ernest Lever//S//	12/31/2018
	Title:	R&D Dir.	
REVIEWED BY			
Kristine Wiley		Kristine Wiley//S//	12/31/2018
	Title:	R&D Dir. and PM	

LEGAL NOTICE

This information was prepared by Gas Technology Institute ("GTI") for U.S. DOT/PHMSA under agreement DTPH56-15-T-00006.

Neither GTI, the members of GTI, the Sponsor(s), nor any person acting on behalf of any of them:

Makes any warranty or representation, express or implied with respect to the accuracy, completeness, or usefulness of the information contained in this report, or that the use of any information, apparatus, method, or process disclosed in this report may not infringe privately-owned rights. Inasmuch as this project is experimental in nature, the technical information, results, or conclusions cannot be predicted. Conclusions and analysis of results by GTI represent GTI's opinion based on inferences from measurements and empirical relationships, which inferences and assumptions are not infallible, and with respect to which competent specialists may differ.

Assumes any liability with respect to the use of, or for any and all damages resulting from the use of, any information, apparatus, method, or process disclosed in this report; any other use of, or reliance on, this report by any third party is at the third party's sole risk.

The results within this report relate only to the items reviewed.

TABLE OF CONTENTS

LIST OF FIGURES

LIST OF TABLES

Page

EXECUTIVE SUMMARY

The project final report, “Characterization and Fitness for Service of Corroded Cast Iron Pipe” dated February 15, 2018 provided a Cast Iron (CI) Fitness-For-Service (FFS) model, calculator, and method for operators to characterize and grade graphitic corrosion defects on cast iron natural gas pipe. The project deliverables will help make monitoring, repair, and replacement decisions, as well as prioritize their replacement program decisions leading to improved safety and supply stability.

The Technical Advisory Panel (TAP) suggested that the project expand the applicability of the calculator solution to include larger diameter pipe, 20-inch and larger, which several of them are currently using. Another suggestion was to provide a full geo-spatial implementation example showing the solution applied to a cast iron network with rankings for an accelerated mains replacement program.

These revised and new project deliverables are provided in four additional files in addition to the previously distributed project Final Report:

1. DTPH56-15-T-00006_**FinalReport**_2018-02-15, original final report.
2. DTPH56-15-T-00006_**Addendum-01**_2018-12-31, which describes the expanded (larger diameter pipe inclusion) model development.
3. **[THIS REPORT]** DTPH56-15-T-00006_**Addendum-02**_2018-12-31, which uses the model solution and applies it to a geo-spatial scenario for accelerated mains replacement.
4. DTPH56-15-T-00006_**Model_Calculator_v0.3**_2018-12-31, which includes the expanded model use case range for larger diameters. The v0.3 is the first version released under the project.
5. DTPH56-15-T-00006_**Calculator_Training_Manual_v0.3**_2018-12-31, which explains how to use the calculator.

Simulation of a Cast Iron Gas Distribution Network

The Cast Iron Fitness-For-Service model described in the main body of this report forms an ideal basis for a simulation tool that can display aggregate system performance in a geospatial database. This simulation tool can provide the operator risk-informed geospatial input into their mitigation programs. The tool can also be extended to temporal consideration of future repair/replace programs.

Geospatial Database

Staten Island was chosen as a conveniently sized and well contained geographic region to build the synthetic database. The coastline of Staten Island was extracted from the Global Self-consistent, Hierarchical, High-resolution Shoreline (GSSHS) database compiled by Wessel et. al. [1]. The coastline is shown in Figure 1.

Figure 1. Coastline extracted from GSSHS

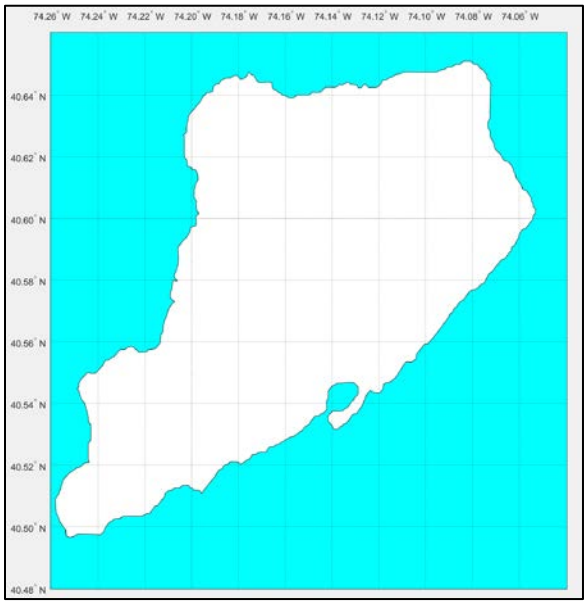

Several buffer-zones were generated internal to the shoreline prior to laying a synthetic gas distribution pipeline system:

1. A coastal buffer approximately 1000 feet from the shoreline
2. A sand zone,
3. A loam zone,
4. A clay zone, and
5. A rock zone.

These zones are used to determine the soil density for the soil=loading calculations and to ensure that pipelines do not extend into the sea. The zones are shown in Figure 2.

Figure 2. Concentric coastal buffer zones: Coastal buffer, Sand, Loam, Clay, Rock

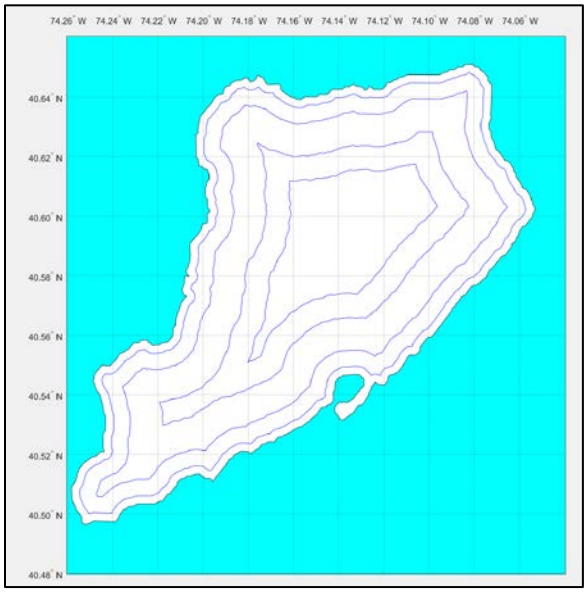

The entire island internal to the coastal buffer was divided into a rectangular grid utilizing the dimensions of a standard Manhattan city block, 264' x 900'. The resultant grid is shown in Figure 3.

Figure 3. Rectangular pipeline grid

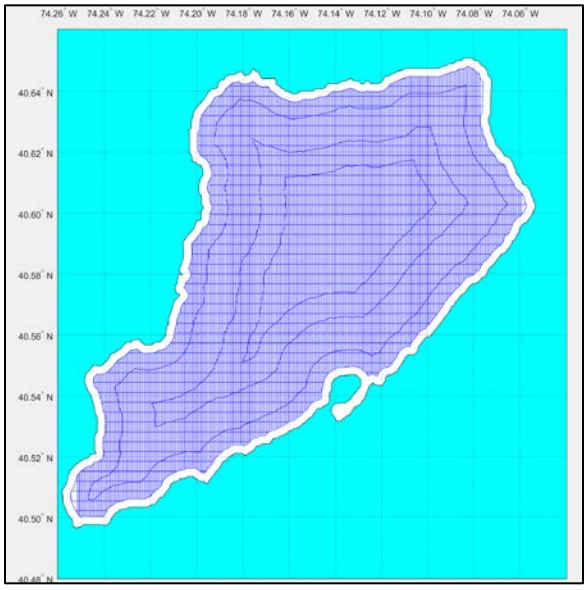

The rough allocation of pipe sizes is shown in Figure 4. A large north-south main line shown as 32” in the figure was upsized to 36” in the final allocation. Smaller mains of 12” were allocated in the north-south direction with 6” for the remaining north-south lines. A 24” east-west main was allocated with the remaining lines a mixture of 8” and 4” sizes.

Table 1 summarizes the number of lines, segments and length per pipe size as well as the totals for each metric.

Figure 4. Allocation of pipe sizes

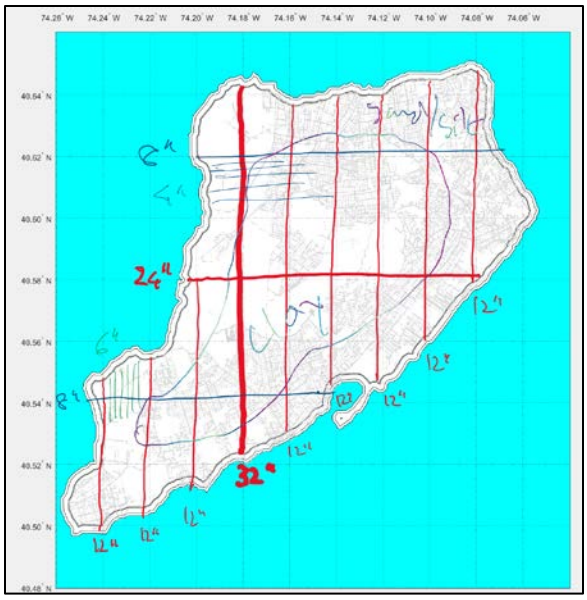

Table 1. Allocation of Pipe Sizes: Counts per size and Totals

	4 inch	6 inch	8 inch	12 inch	24 inch	36 inch	Totals
Lines	39	277	9	13	1	1	340
Segments	41,330	288,188	8,302	9,460	1,065	1,355	349,700
Length [ft]	495,960	3,458,256	99,624	113,520	17,040	21,680	4,206,080

Each segment was generated independently with the orientation in x- horizontal axis, y-depth axis varying randomly within specified tolerances. The nominal depth of cover was set to 4.5 feet with a tolerance of ± 1.5 foot.

Each pipe segment thus has a unique average depth of cover. The density of the soil cover was set in accordance with the calculator values for sand, clay and gravel in accordance with the soil

type regions described above. Traffic loading was applied in accordance with the calculator values for rail, highway and none.

Probability distribution for the proportion of pipe with defects and the width, length and depth of the defects were generated and are shown in Figure 5. The defect size bounds correspond to the ranges for the calculator.

The pipes were grouped into 20 coarse geographic regions. The regions were assigned vintages in the range 1911 – 1960 with each region spanning 2 ½ years of vintage range. Tensile strength distributions were generated that accurately match the distributions covered in the main body of the report.

Values for each parameter were randomly drawn from the appropriate probability distribution on a segment by segment basis. Variability was introduced for specific lines in specific geographic regions. Corrosion rate was adjusted in a subset of 200 sub-regions. The geographic regions and sub-regions are shown in Figure 6 and Figure 7.

Figure 5. Distribution for input parameters

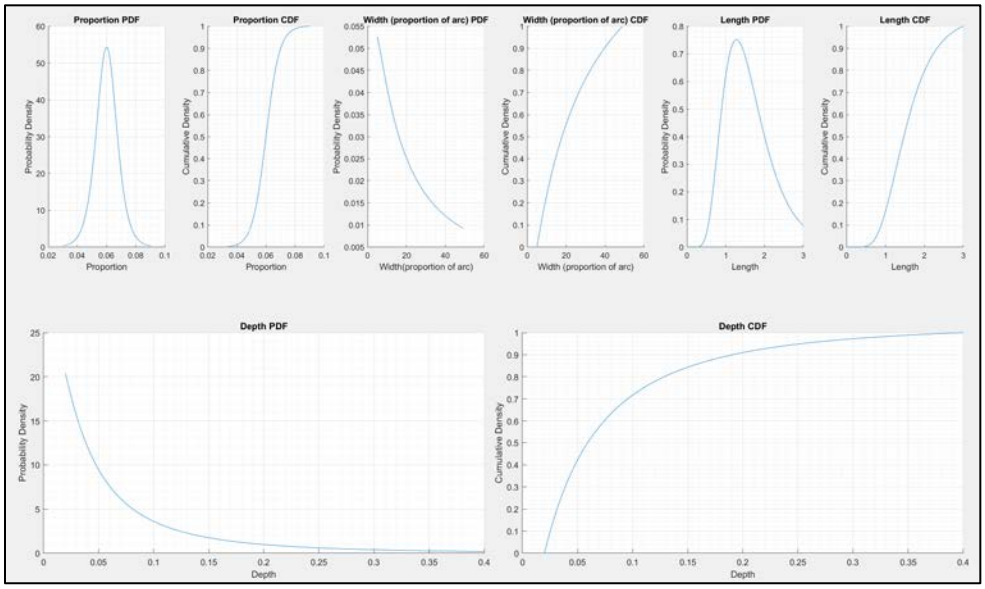

Figure 6. Coarse geographic regions

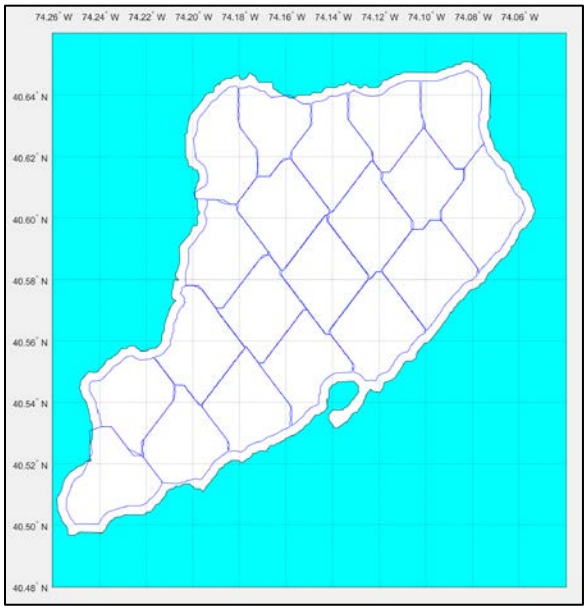

Figure 7. Geographic sub-regions

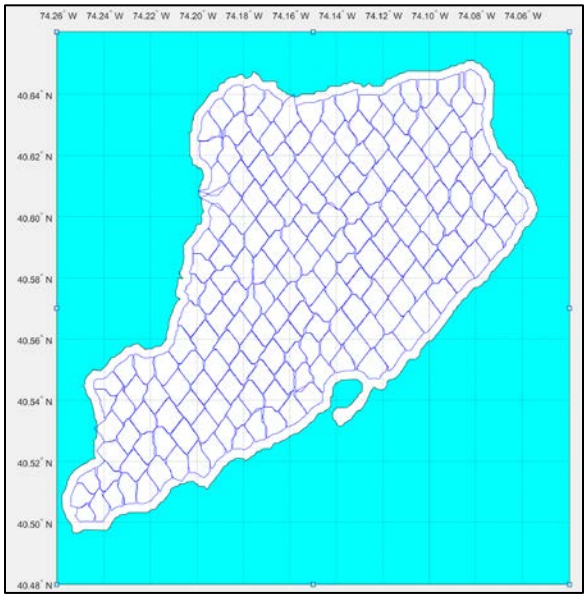

Figure 11 shows the results of a full simulation run. The plots show a 1% sampling of the 349,700 segments next to a 2% sampling of the same results. The results of separate samplings at each of the two sampling rates are shown overlaid on the soil type regions, geographic regions and geographic sub regions.

The result shown is the factor of safety relative to the average flaw stress as defined in the main report Figure 98, Figure 8.

Figure 8. Average Stress Probe

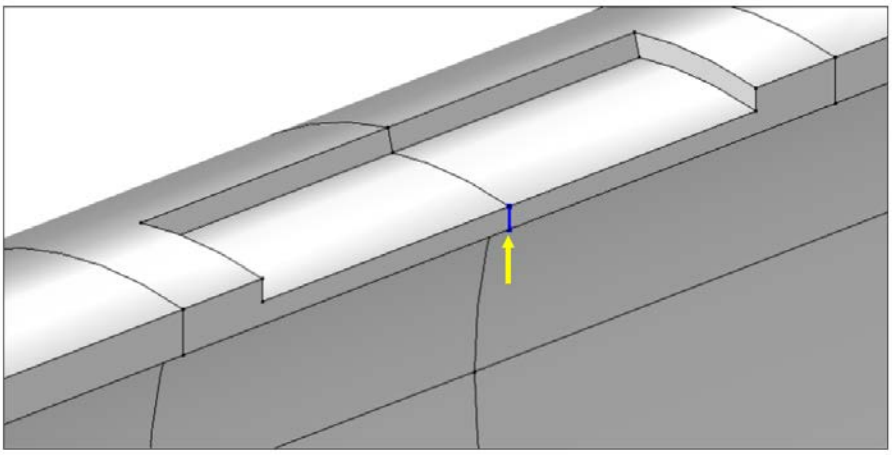

(Figure 98 in main report) - Radial line (highlighted in blue) at center of flaw for average stress probe (model cross-section shown for illustration)

The factor of safety is the average stress from the calculator model for free pipe ends divided by the segment tensile strength. The plots in Figure 9 show a large filled red circle for all segments with a factor of safety less than or equal to 1.4. Smaller orange filled circles depict a factor of safety in the range $1.4 < FS \leq 1.6$ and the smallest green filled circles depict a factor of safety in the range $1.6 < FS \leq 2.0$.

Figure 9 is a plot of the entire system calculated safety factors. Figure 10 and Figure 11show the results from random samplings of the region using 1% and 2% sampling rates. It can clearly be seen in the plots that the sampling picks up the pre-1920 pit cast pipe, lines with reduced corrosion resistance due to morphology and sub-regions with corrosive environments due to local soil conditions.

The three factor of safety ranges can be used to prioritize mitigation programs. They also reflect the temporal aspect of corrosion: Red -current problem segments, Orange can be expected to be problematic in the short term, Green can be expected to be problematic in the medium term.

Figure 12 shows the histogram of the average flaw stress across all segments. It is clearly a complex distribution of stresses indicating that multiple factors are interacting to produce the

result. Figure 13 shows the distribution of safety factors due to these stresses. The safety factors reflect the tensile strength of the individual segments. The distribution is highly skewed.

Figure 14 through Figure 19 show histogram plots of the likelihood of safety factor ≤ 1.4 conditioned on: line number, strength class, vintage, sub-region, region and diameter.

It is immediately apparent that strength class of 10 ksi, which is highly correlated with pre=1920 pit cast pipe, is the dominant risk factor. Four-inch diameter is pipe most likely to have a low safety factor. The regions that had pipe installed pre-1920 are obviously the riskiest regions. There are several sub-regions that can be identified as having more corrosive environments, and there is a well-defined set of lines that are high risk.

The breakdown remains essentially unchanged for 1.4 < safety factor ≤ 1.6. The first noticeable difference can be seen in the range 1.6 < safety factor ≤ 2.0, where the histogram for likelihood by diameter is distinctly different as shown Figure 20. In this safety factor range 6” pipe has the greatest probability of being present.

The analyses presented here are a small sub-set of the possible analyses that can be conducted on database generated by the simulation. It is clear that the results match actual system behavior quite well and that combining this simulation approach with historical leak and repair histories will provide a powerful tool for forensically understanding past events and improving the predictive capabilities of the analysis for future system states.

Figure 9. Full system - calculated safety factors

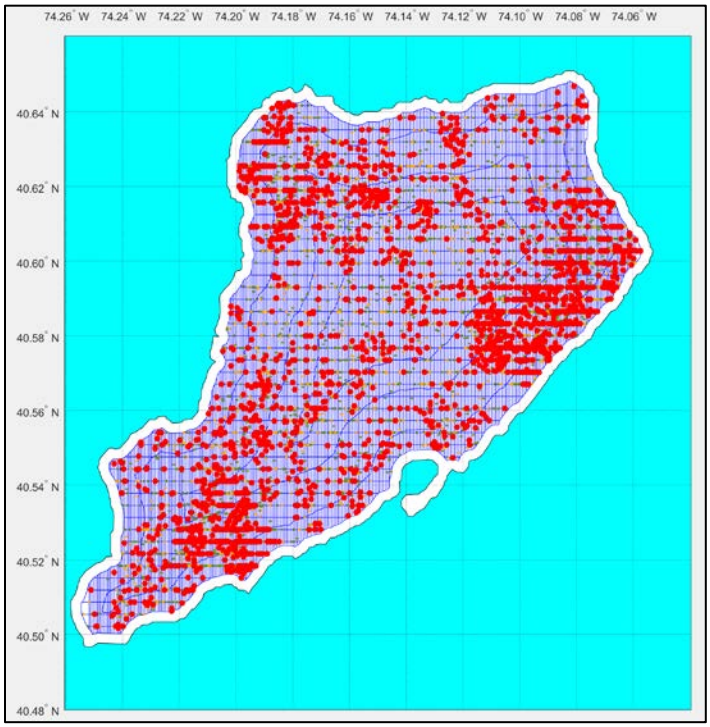

Figure 10. 1% sampling of region – calculated safety factors

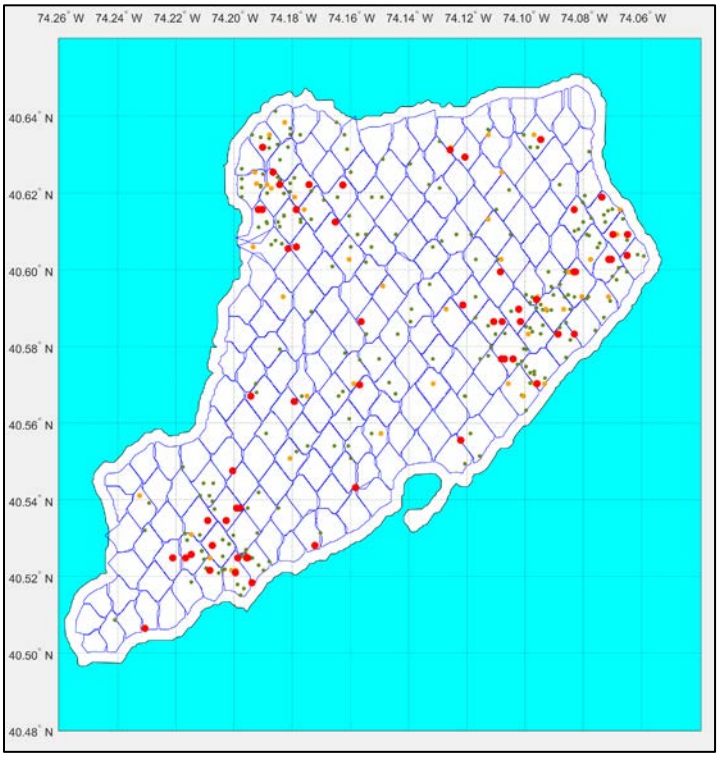

Figure 11. Simulation results 1% sampling left, 2% sampling right

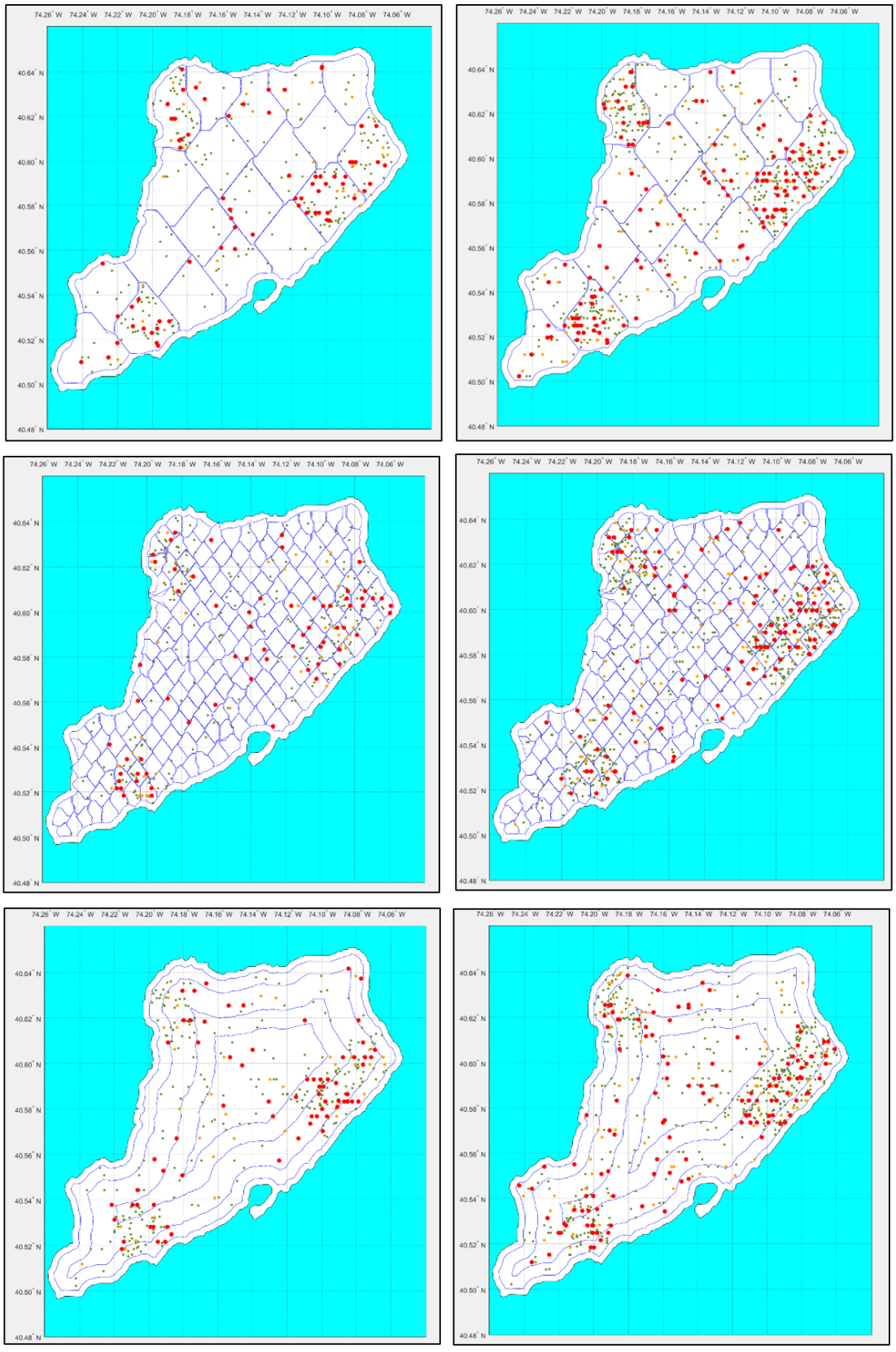

Figure 12. Histogram of ave. flaw stress in [ksi] per segment (all segments)

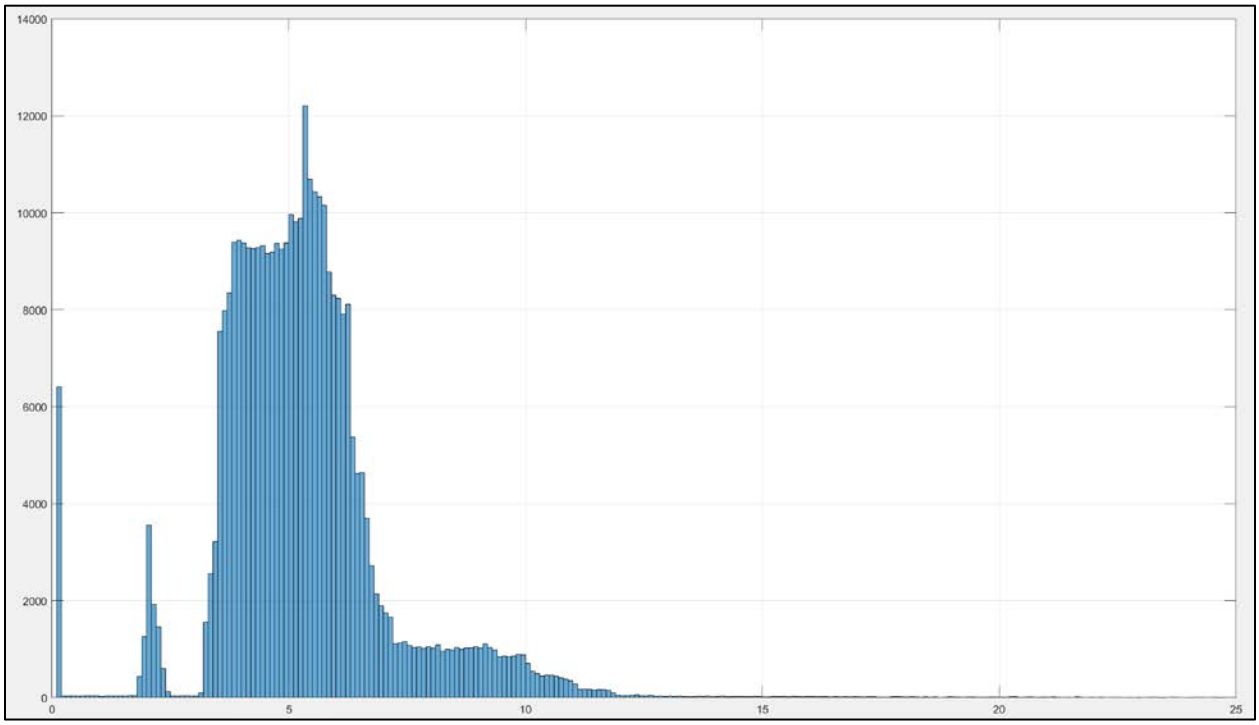

X-axis flaw stress in ksi; y axis segment count

Figure 13. Histogram of safety factor for ave. flaw stress.

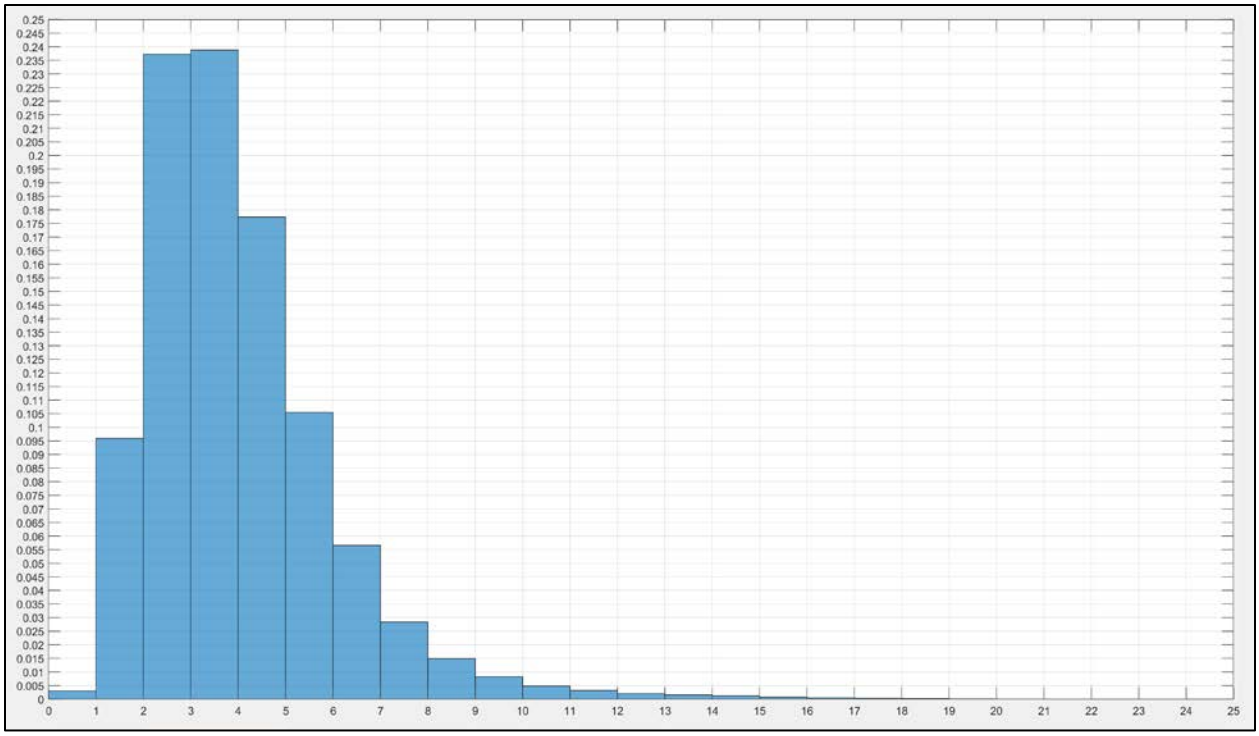

X- axis SF; Y - axis probability density

Figure 14. Histogram of lines with safety factor < 1.4

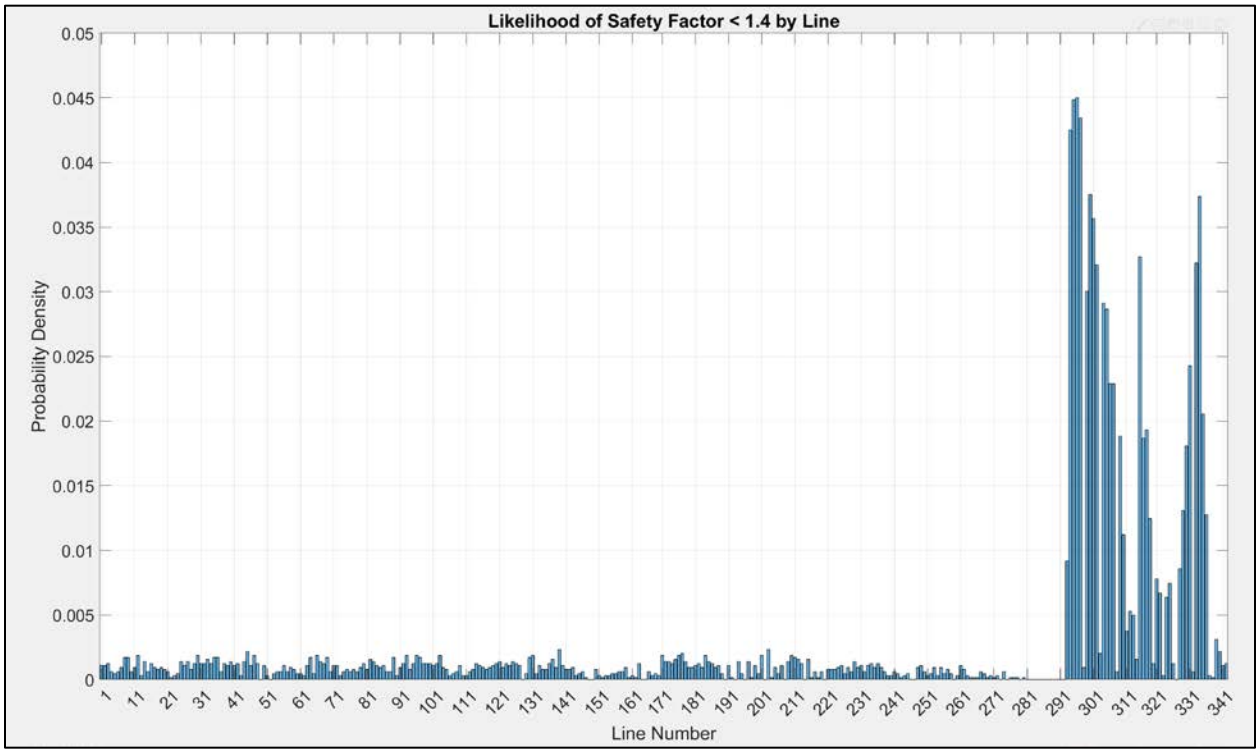

Figure 15. Histogram of strength class with safety factor < 1.4

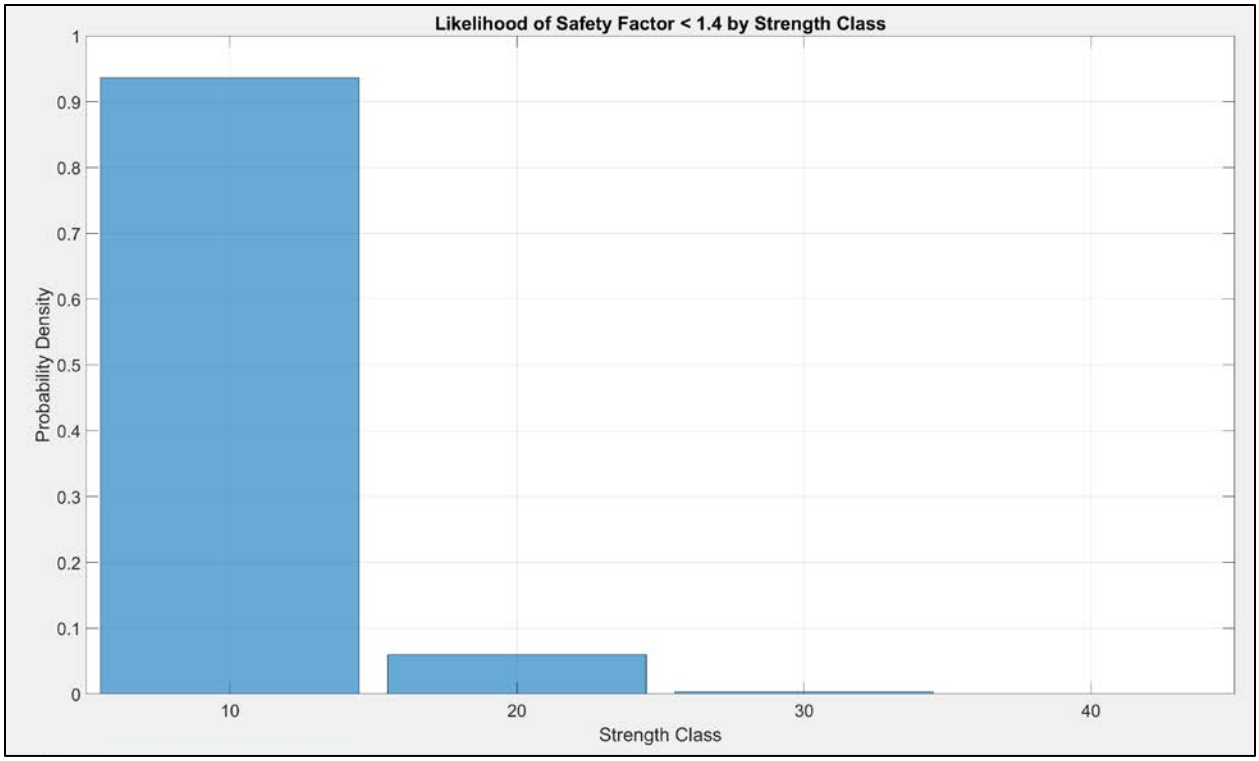

Figure 16. Histogram of vintage with safety factor < 1.4

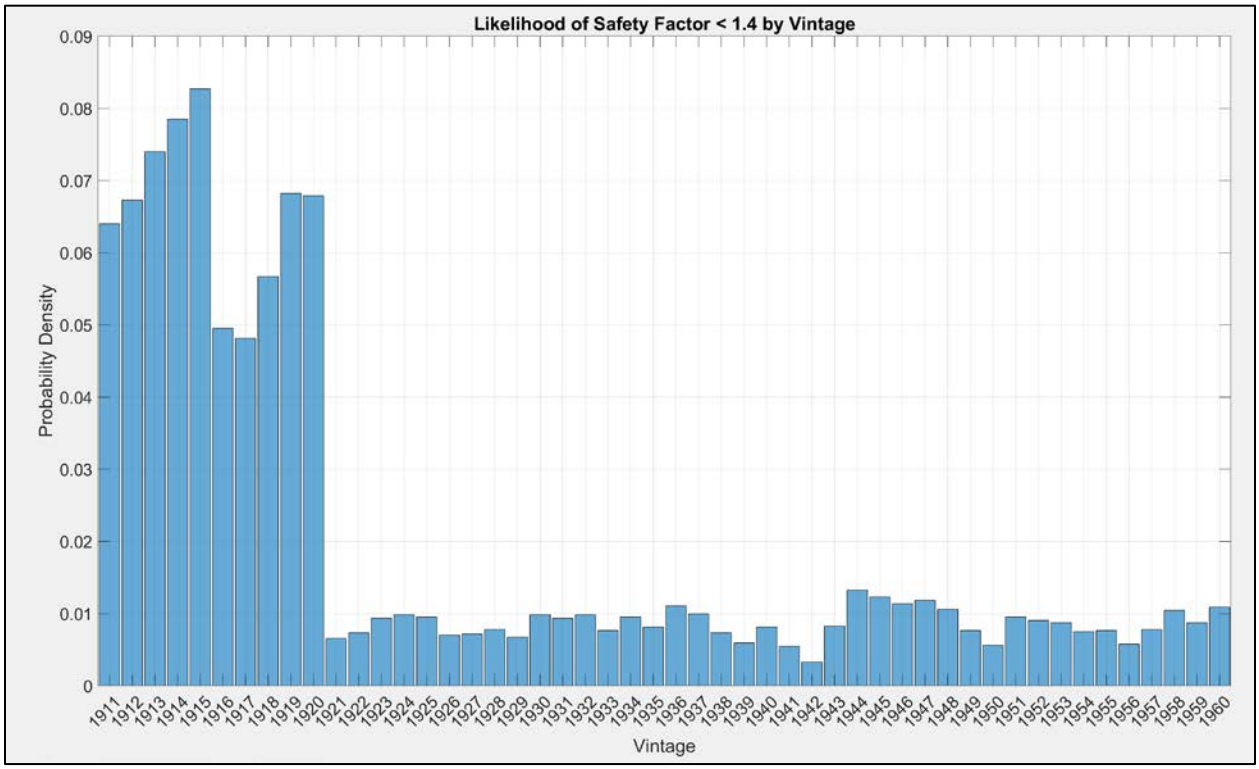

Figure 17. Histogram of sub-region with safety factor < 1.4

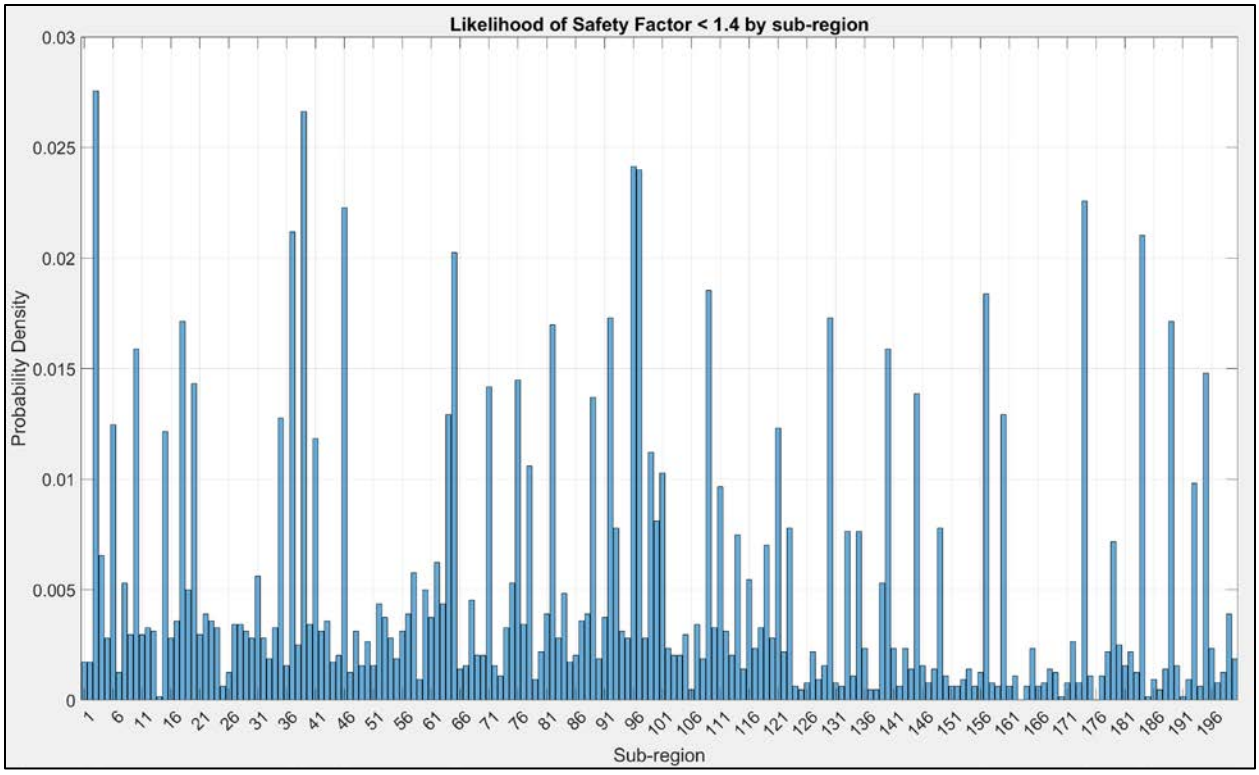

Figure 18. Histogram of region with safety factor < 1.4

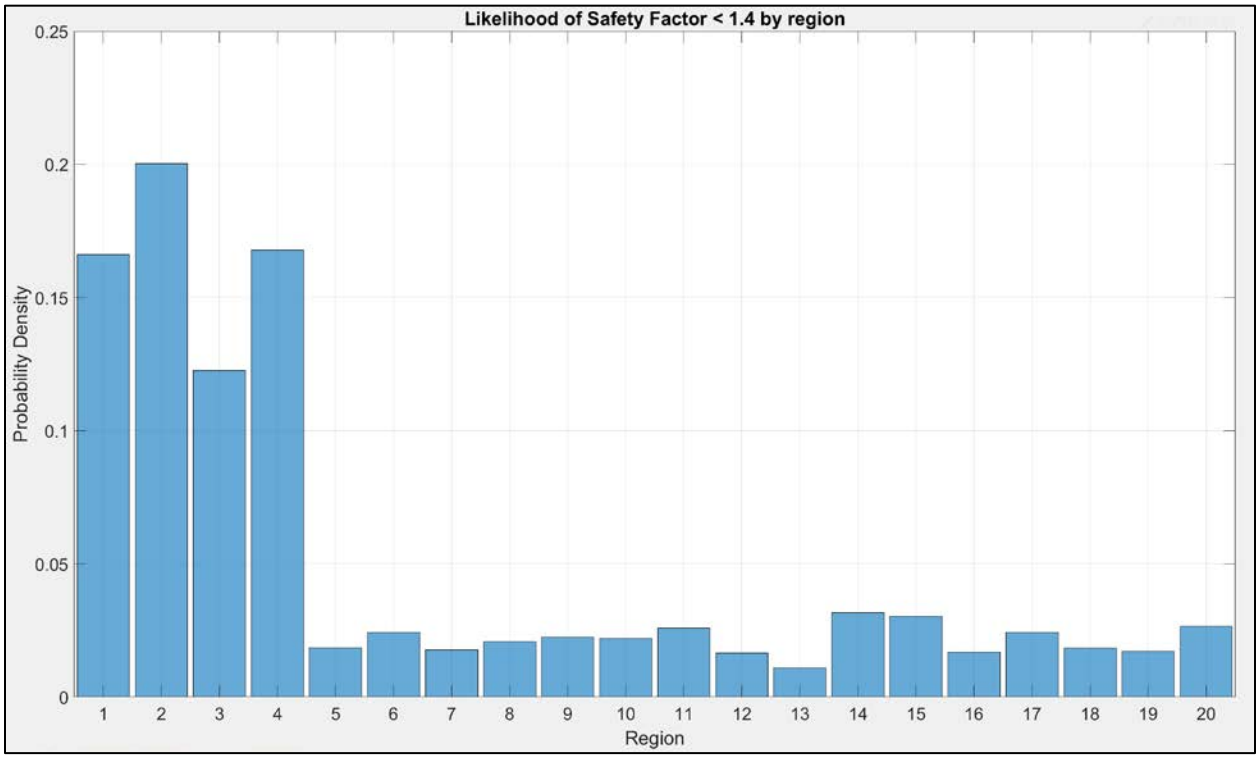

Figure 19. Histogram of diameter with safety factor < 1.4

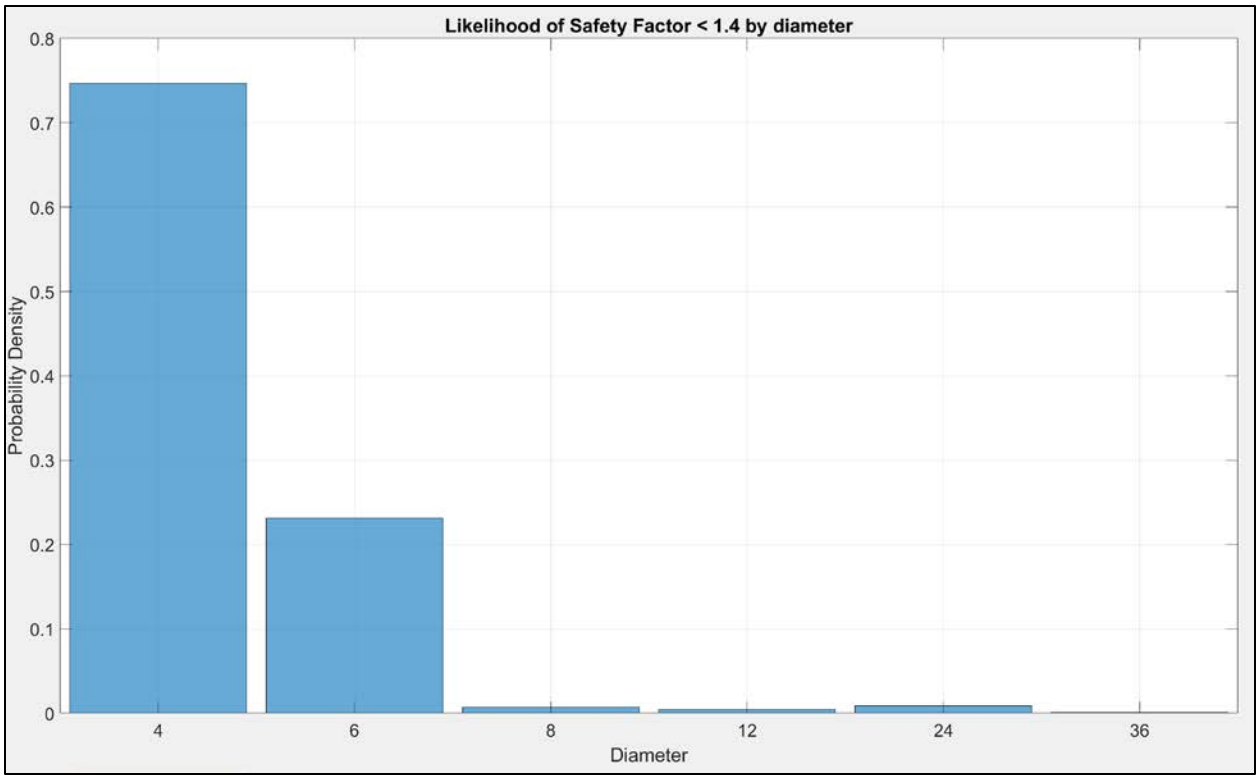

Figure 20. Histogram of diameter with 1.6 < safety factor ≤ 2.0

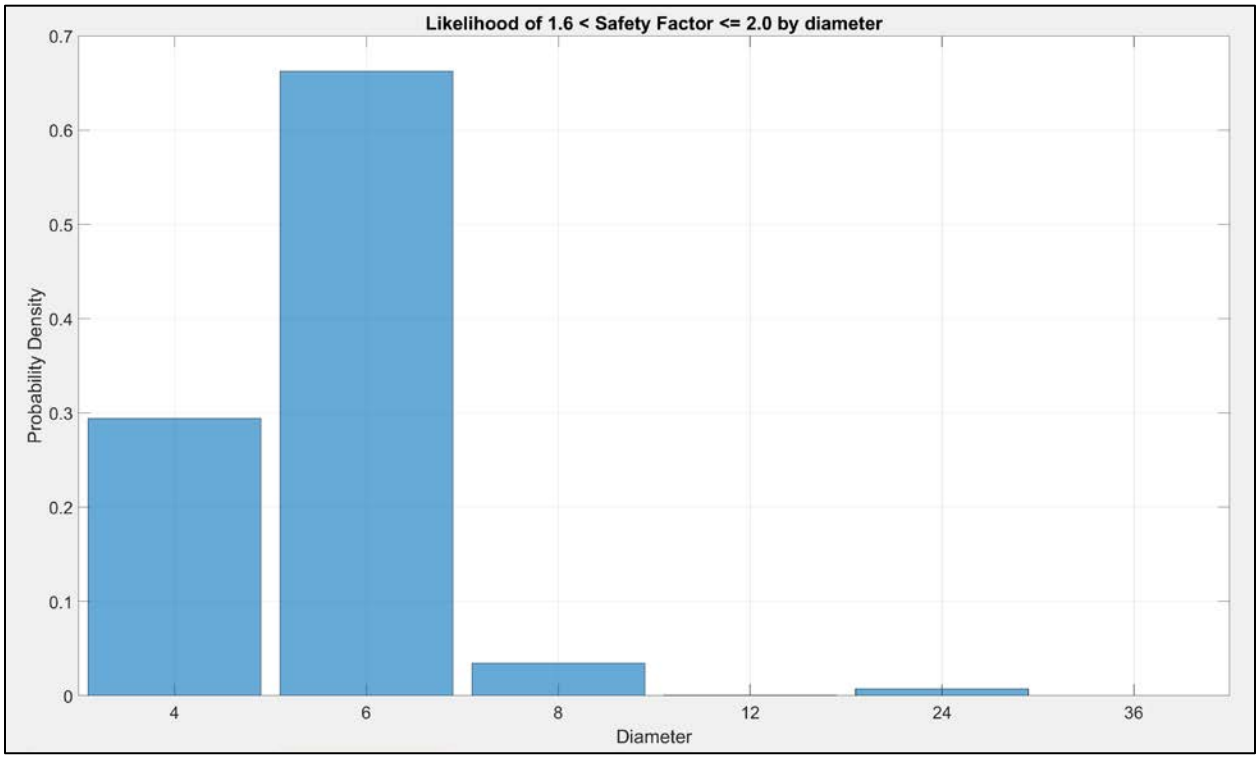

References

1. Wessel, P. and W.H.J.J.o.G.R.S.E. Smith, *A global, self-consistent, hierarchical, high-resolution shoreline database.* 1996. **101**(B4): p. 8741-8743.

End of Addendum Report

TRAINING MANUAL FOR CALCULATOR V0.3
GTI PROJECT NUMBER 21874
Contract Number: DTPH56-15-T-00006

Characterization and Fitness for Service of Corroded Cast Iron Pipe
Calculator Training Manual v0.3

Report Issued
December 31, 2018

Prepared For
U.S. Department of Transportation
Pipeline and Hazardous Materials Safety Administration
Office of Pipeline Safety
Chris McLaren
chris.mclaren@dot.gov

Technical Team
Daniel Ersoy
Oren Lever
Khalid Farrag
Brian Miller

Project Manager
Kristine Wiley
R&D Director, GTI
kristine.wiley@gastechnology.org

Technical Contact
Daniel Ersoy
R&D Executive Director, GTI
daniel.ersoy@gastechnology.org

Gas Technology Institute
1700 S. Mount Prospect Rd.
Des Plaines, Illinois 60018

Signature Page

			Date
Principal Investigator			
Daniel A. Ersoy		Daniel Ersoy//S//	12/31/2018
	Title:	R&D Exec. Dir. and PI	
Author			
Oren Lever		Oren Lever//S//	12/31/2018
	Title:	Principal Engineer	
Reviewed by			
Kristine Wiley		Kristine Wiley//S//	12/31/2018
	Title:	R&D Director and PM	

Legal Notice

This training manual and the associated calculator software applications were developed by the Gas Technology Institute (GTI) for U.S. DOT/PHMSA under agreement DTPH56-15-T-00006.

The information provided in this manual and the associated software are offered in good faith and believed to be accurate at the time of its preparation. Neither GTI, the projects funding agencies, nor any person acting on behalf of any of them:

a. Makes any warranty or representation, express or implied with respect to the accuracy, completeness, or usefulness of the information contained in this software and manual, or that their use may not infringe privately-owned rights. Inasmuch as these programs are experimental in nature, the technical information, results, or conclusions cannot be predicted. The results represent GTI's opinion based on inferences from the empirical relationships.

b. Assumes any liability with respect to the use of these programs by any third party, which use is at the third party's sole responsibility.

c. Assumes any responsibility for regulatory compliance. Third party users must assess and satisfy their compliance with any related standards and regulations when using this information.

By using this manual and/or the associated software, the user acknowledges reading the above disclaimer and accepts their use in accordance with these terms.

Table of Contents

Page

Table of Figures

1. Background

This is the training manual for the Excel-based cast-iron FFS calculator developed under DOT PHMSA project DTPH56-15-T-00006 *Characterization and Fitness for Service of Corroded Cast Iron Pipe*. For more detailed information see this project's final report.

End of Section 1

2. Navigating the Calculator

The calculator contains the following sheets:

- Calculator – used to calculate the maximum stress and safety factor given the user's inputs.
- Corrosion Measurement Guideline – Contains the *Graphitic Corrosion Field Measurement Guideline* that is provided in this manual in Section 4.

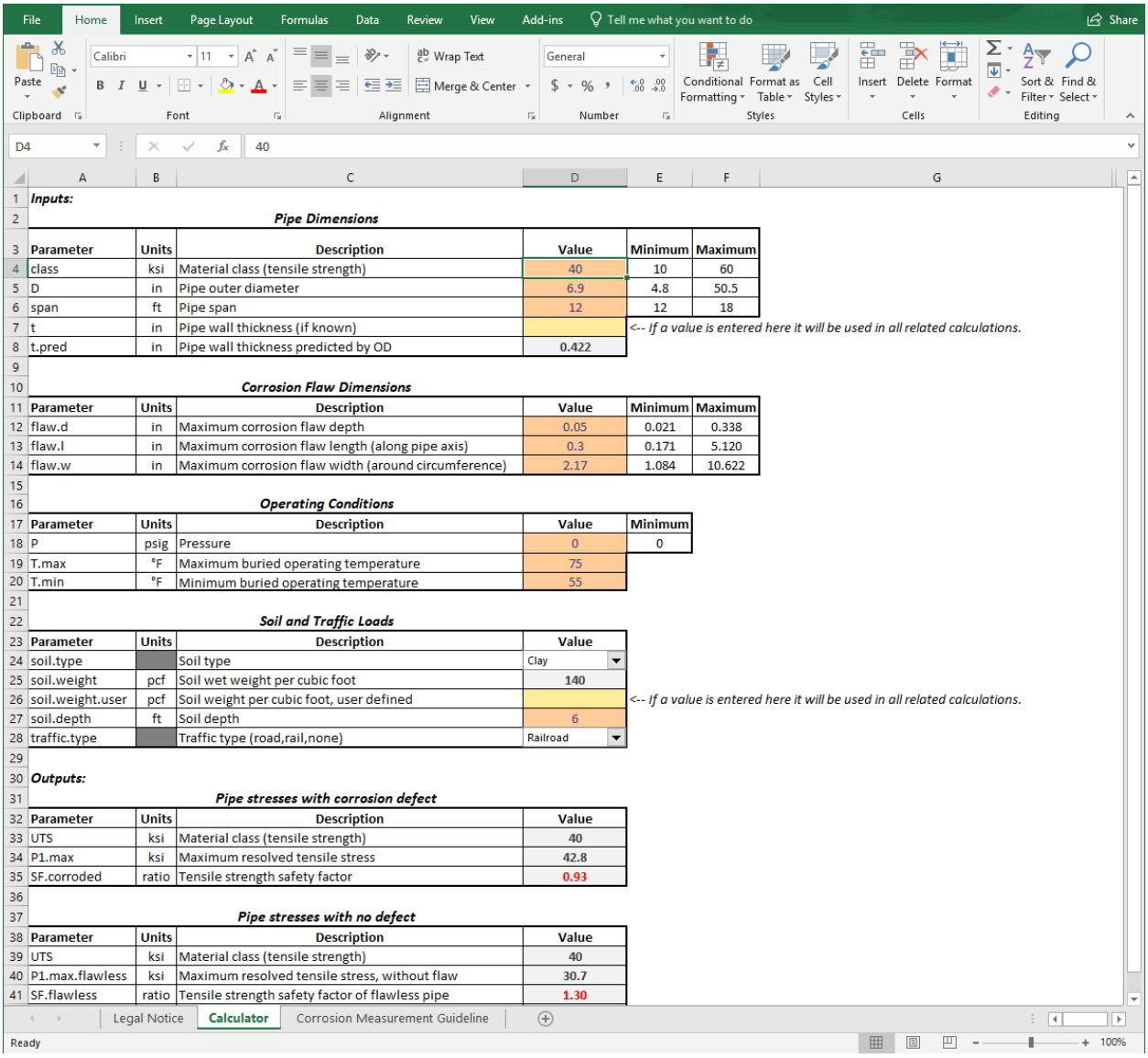

Inputs:

Pipe Dimensions

Parameter	Units	Description	Value	Minimum	Maximum	
class	ksi	Material class (tensile strength)	40	10	60	
D	in	Pipe outer diameter	6.9	4.8	50.5	
span	ft	Pipe span	12	12	18	
t	in	Pipe wall thickness (if known)				*<-- If a value is entered here it will be used in all related calculations.*
t.pred	in	Pipe wall thickness predicted by OD	0.422			

Corrosion Flaw Dimensions

Parameter	Units	Description	Value	Minimum	Maximum
flaw.d	in	Maximum corrosion flaw depth	0.05	0.021	0.338
flaw.l	in	Maximum corrosion flaw length (along pipe axis)	0.3	0.171	5.120
flaw.w	in	Maximum corrosion flaw width (around circumference)	2.17	1.084	10.622

Operating Conditions

Parameter	Units	Description	Value	Minimum
P	psig	Pressure	0	0
T.max	°F	Maximum buried operating temperature	75	
T.min	°F	Minimum buried operating temperature	55	

Soil and Traffic Loads

Parameter	Units	Description	Value	
soil.type		Soil type	Clay	
soil.weight	pcf	Soil wet weight per cubic foot	140	
soil.weight.user	pcf	Soil weight per cubic foot, user defined		*<-- If a value is entered here it will be used in all related calculations.*
soil.depth	ft	Soil depth	6	
traffic.type		Traffic type (road,rail,none)	Railroad	

Outputs:

Pipe stresses with corrosion defect

Parameter	Units	Description	Value
UTS	ksi	Material class (tensile strength)	40
P1.max	ksi	Maximum resolved tensile stress	42.8
SF.corroded	ratio	Tensile strength safety factor	0.93

Pipe stresses with no defect

Parameter	Units	Description	Value
UTS	ksi	Material class (tensile strength)	40
P1.max.flawless	ksi	Maximum resolved tensile stress, without flaw	30.7
SF.flawless	ratio	Tensile strength safety factor of flawless pipe	1.30

Figure 1. Calculator sheet with input and output fields

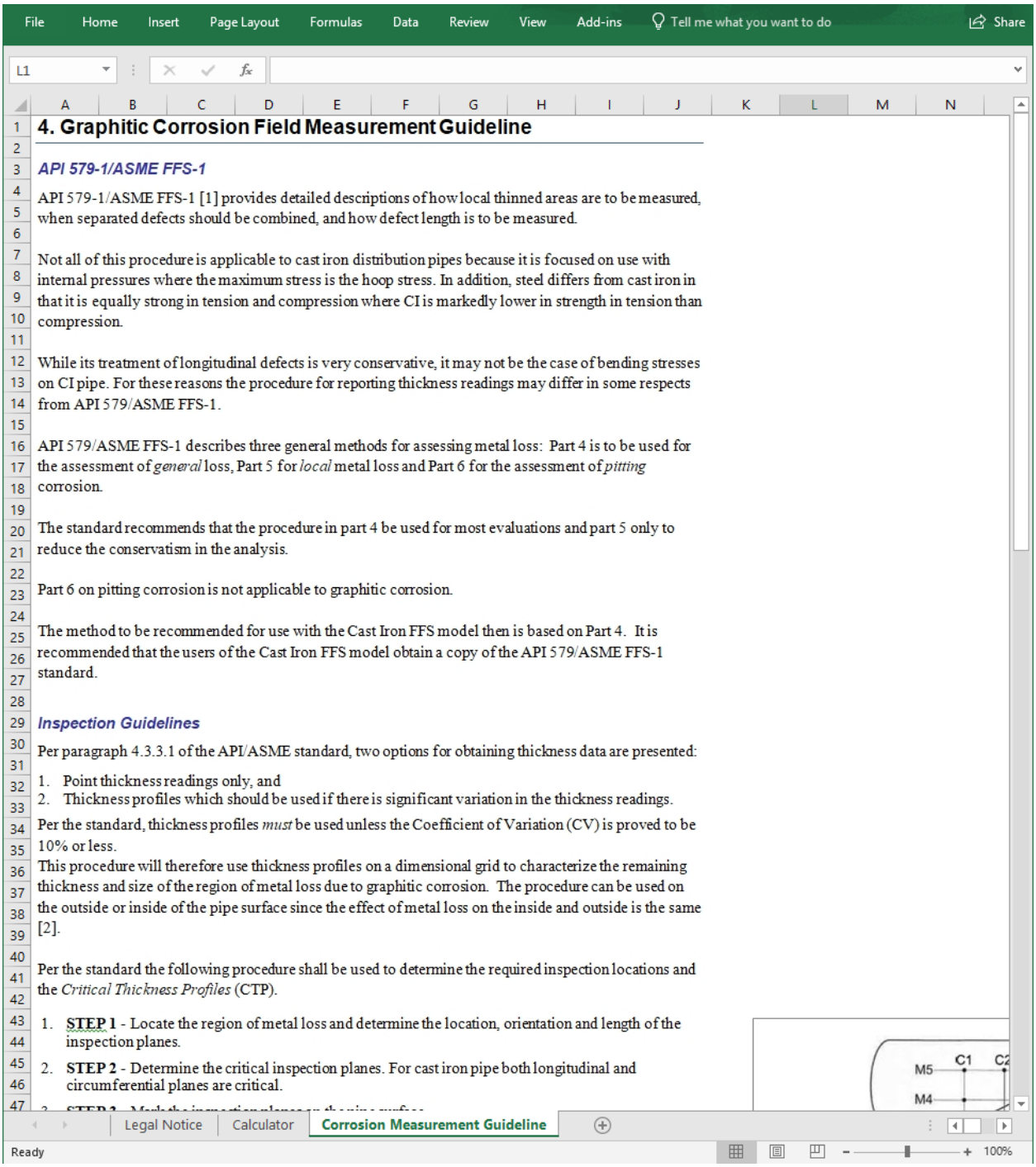

Figure 2. Corrosion Measurement Guideline

End of Section 2

3. Using the Calculator

Pipe Dimensions Inputs

There are three required inputs that define the pipe in the calculator:

1. **Material class** (ksi) - range: 10 to 60 ksi
2. **Pipe diameter** (inches) - range: 4.8 to 50.5 inches
3. **Pipe span (feet)** - range: 12 to 18 ft

The calculator user enters these three data inputs into their respective cells. The three cells are circled in red in Figure 3. The respective ranges are shown on the right of the input cells.

An optional input for defining the pipe geometry is pipe wall thickness, which is used for calculating the percent of wall thickness depth of a flaw. If a wall thickness is not entered, the calculator will use a predicted wall thickness based on the outer diameter of the pipe. This wall thickness input cell is shown in Figure 3, highlighted in yellow, and the predicted wall thickness is highlighted in gray.

Inputs:

Pipe Dimensions

Parameter	Units	Description	Value	Minimum	Maximum
class	ksi	Material class (tensile strength)	40	10	60
D	in	Pipe outer diameter	6.9	4.8	50.5
span	ft	Pipe span	12	12	18
t	in	Pipe wall thickness (if known)		*<-- If a value is entered h*	
t.pred	in	Pipe wall thickness predicted by OD	0.422		

Figure 3. Pipe dimensions input cells (circled in red).

Corrosion Flaw Dimensions Inputs

There are three inputs that define the corrosion flaw size:

1. **Flaw depth** (inches) - range: depends on wall thickness
2. **Flaw length** (inches) - range: depends on wall thickness and outer diameter
3. **Flaw width** (inches) - range: depends on outer diameter

The flaw dimensions are entered in the cells highlighted in red in Figure 4. The minimum and maximum values that can be input are shown to the right of the input cells.

Corrosion Flaw Dimensions					
Parameter	Units	Description	Value	Minimum	Maximum
flaw.d	in	Maximum corrosion flaw depth	0.05	0.021	0.338
flaw.l	in	Maximum corrosion flaw length (along pipe axis)	0.3	0.171	5.120
flaw.w	in	Maximum corrosion flaw width (around circumference)	2.17	1.084	10.622

Figure 4. Corrosion flaw dimensions input cells (circled in red).

Operating Conditions Inputs

There are three inputs that define the operating conditions:

1. **Pressure** (psig) - range: 0 to unlimited
2. **Maximum operating temperature** (°F) - range: unlimited
3. **Minimum operating temperature** (°F) - range: unlimited

The pressure input does not affect the response surface based stress calculation, but is provided for a complimentary hoop stress calculation that uses Barlow's equation. The absolute values of the minimum and maximum operating temperature inputs do not matter, as the calculator only uses the difference between these inputs. Should the difference between these temperatures exceed the calculator's input range, a warning will appear and the calculator will use the maximum temperature difference it can.

Operating Conditions				
Parameter	Units	Description	Value	Minimum
P	psig	Pressure	0	0
T.max	°F	Maximum buried operating temperature	75	
T.min	°F	Minimum buried operating temperature	55	

Figure 5. Operating conditions input cells (circled in red).

Soil and Traffic Loads Inputs

Three inputs define the vertical loading on the pipe:

1. **Soil type** - selection from list
2. **Soil depth (ft)** - range: 0 to unlimited
3. **Traffic type** - selection from list

These inputs are circled in red in Figure 6.
Soil types are given in a drop-down list, each defined with a specific wet weight per cubic foot. The soil loading is calculated from the soil weight density and soil depth input. The user may also enter a custom value for soil weight, which will automatically override the selection from the drop-down list. The custom value input cell is highlighted in yellow, as shown in Figure 6.

Traffic types are given in a drop-down list. This list contains industry standard traffic loads and uses the soil depth input to calculate the applied traffic load on the pipe.

Soil and Traffic Loads			
Parameter	**Units**	**Description**	**Value**
soil.type		Soil type	Clay
soil.weight	pcf	Soil wet weight per cubic foot	140
soil.weight.user	pcf	Soil weight per cubic foot, user defined	
soil.depth	ft	Soil depth	6
traffic.type		Traffic type (road,rail,none)	None

Figure 6. Soil and traffic loads input cells (circled in red).

Calculator Outputs

The calculator sheet displays the results from the FFS model calculations in a tabulated format. The outputs are described in the sheet (see Figure 7).

Outputs:

Pipe stresses with corrosion defect

Parameter	**Units**	**Description**	**Value**
UTS	ksi	Material class (tensile strength)	40
P1.max	ksi	Maximum resolved tensile stress	42.8
SF.corroded	ratio	Tensile strength safety factor	0.93

Pipe stresses with no defect

Parameter	**Units**	**Description**	**Value**
UTS	ksi	Material class (tensile strength)	40
P1.max.flawless	ksi	Maximum resolved tensile stress, without flaw	30.7
SF.flawless	ratio	Tensile strength safety factor of flawless pipe	1.30
P.hoop	ksi	Hoop stress due to internal pressure (Barlow's Formula)	0.00

Figure 7. Tabulated calculator outputs.

The maximum resolved tensile stress is the maximum stress calculated by the applicable response surfaces (pipe with corrosion defect, pipe with no defect).
The tensile strength safety factor results are based on the maximum resolved tensile strength and material class. If a safety factor is less than 1.5, it will display in red.
The hoop stress of a pipe with no defect is provided for reference and is calculated according to Barlow's equation.

End of Section 3

4. Graphitic Corrosion Field Measurement Guideline

API 579-1/ASME FFS-1

API 579-1/ASME FFS-1 [1] provides detailed descriptions of how local thinned areas are to be measured, when separated defects should be combined, and how defect length is to be measured.

Not all of this procedure is applicable to cast iron distribution pipes because it is focused on use with internal pressures where the maximum stress is the hoop stress. In addition, steel differs from cast iron in that it is equally strong in tension and compression where CI is markedly lower in strength in tension than compression.

While its treatment of longitudinal defects is very conservative, it may not be the case of bending stresses on CI pipe. For these reasons the procedure for reporting thickness readings may differ in some respects from API 579/ASME FFS-1.

API 579/ASME FFS-1 describes three general methods for assessing metal loss: Part 4 is to be used for the assessment of *general* loss, Part 5 for *local* metal loss and Part 6 for the assessment of *pitting* corrosion.

The standard recommends that the procedure in part 4 be used for most evaluations and part 5 only to reduce the conservatism in the analysis.

Part 6 on pitting corrosion is not applicable to graphitic corrosion.

The method to be recommended for use with the Cast Iron FFS model then is based on Part 4. It is recommended that the users of the Cast Iron FFS model obtain a copy of the API 579/ASME FFS-1 standard.

Inspection Guidelines

Per paragraph 4.3.3.1 of the API/ASME standard, two options for obtaining thickness data are presented:

1. Point thickness readings only, and
2. Thickness profiles which should be used if there is significant variation in the thickness readings.

Per the standard, thickness profiles *must* be used unless the Coefficient of Variation (CV) is proved to be 10% or less.

This procedure will therefore use thickness profiles on a dimensional grid to characterize the remaining thickness and size of the region of metal loss due to graphitic corrosion. The procedure can be used on the outside or inside of the pipe surface since the effect of metal loss on the inside and outside is the same [2].

Per the standard the following procedure shall be used to determine the required inspection locations and the *Critical Thickness Profiles* (CTP).

1. **STEP 1** - Locate the region of metal loss and determine the location, orientation and length of the inspection planes.
2. **STEP 2** - Determine the critical inspection planes. For cast iron pipe both longitudinal and circumferential planes are critical.
3. **STEP 3** - Mark the inspection planes on the pipe surface.
4. **STEP 4** - Determine the uniform thickness away from the local metal loss t_{rd}.
5. **STEP 5** - Measure and record thickness readings along each inspection plane and determine the minimum measured wall thickness t_{mm} , see Figure 8 (figure 4.6a from API 579-1/ASME FFS-1).
    a. The spacing distance for thickness readings (the grid) should allow for an accurate characterization of the thickness profile.
    b. A guideline is that the spacing should be done in a manner that the path of minimum measured thickness (t_{mm}) can be determined in both the longitudinal and circumferential directions (explained in STEP 6 below).
6. **STEP 6** - Determine the Critical Thickness Profile (**CTP**) in the longitudinal and circumferential directions.
    a. The CTP in each direction is determined by projecting the minimum remaining thickness for each position along all parallel inspection planes onto a common plane as shown in Figure 9 (figure 4.6a from API 579-1/ASME FFS-1) and Figure 10 (figure 4.6c from API 579-1/ASME FFS-1). These also show the corroded wall thickness, t_c.
    b. One can see in these two figures that there are two planes of minimum thickness, one for the circumferential (dotted line C) and one for the longitudinal (solid line M) direction.
    c. The length of the profile is established by determining the end point locations where the remaining wall thickness is greater than the uniform thickness away from local metal loss, t_{rd}, in both the longitudinal and circumferential directions. Note, t_{rd}, can be less than the nominal, t_{nom}, (non-corroded) wall thickness away from the local areas of metal loss. This is a determination that must be made in the field with careful measurements made in and around areas of metal loss.

d. If there are multiple flaws in close proximity to one another, then the size of the flaw to be used in the assessment is established considering the effects of neighboring flaws using the *intersecting box methodology* shown in Figure 11 (figure 4.7 in API 579-1/ASME FFS-1).

e. The final CTP can be established as shown in Figure 12 (figure 4.8 in API 579-1/FFS-1).

f. The thickness profile for both the longitudinal and circumferential planes should be evaluated in this manner.

7. **Step 7** – The operator will also record the measurements in a way to determine the axial direction of the pipe relative to the measurements.

   a. This can be a simple annotation on the drawing of the pipe's center line as shown in Figure 8.

   b. This information will be needed to determine the angle of the overall wall loss measurement relative to the pipe's axial direction, in degrees.

The above process will provide the graphitic corrosion defect (wall loss): length, depth, and width of the wall loss. These measurements are inputs to the CI FFS model calculator.

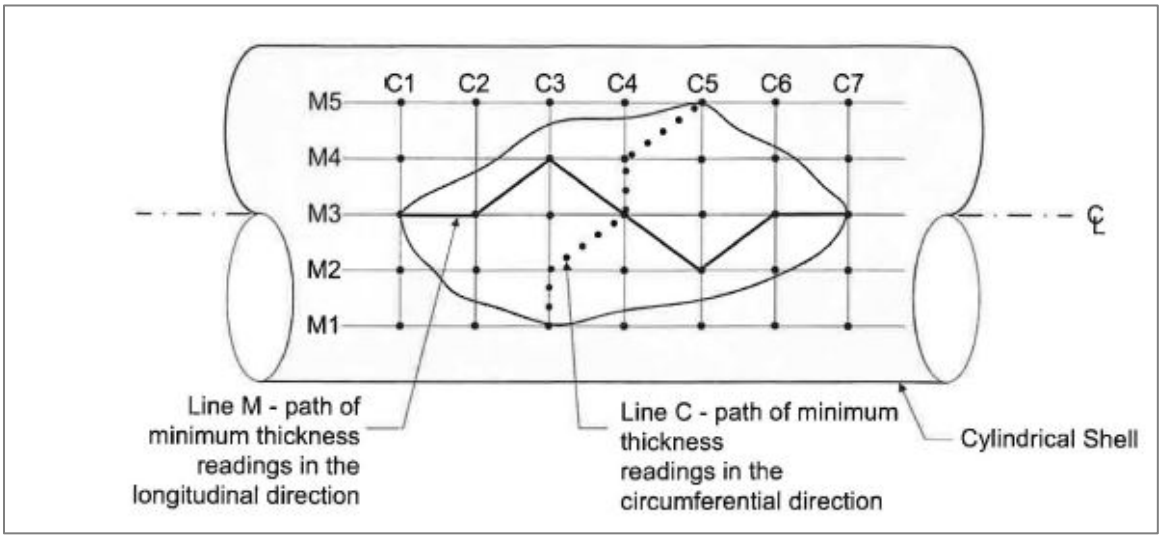

Figure 8. Inspection planes per API 579-1/FFS-1 fig 4.6a and the critical thickness profiles

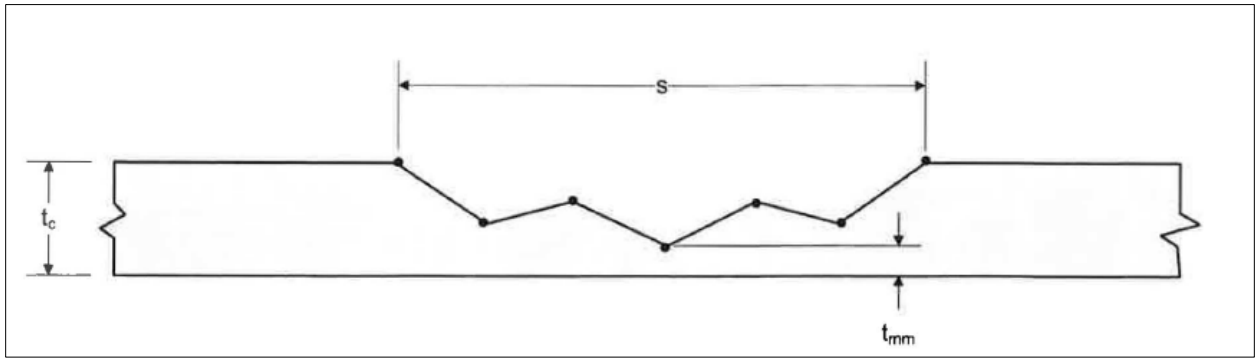

Figure 9. Critical Thickness Profile (CTP) – Longitudinal Plane (Projection of Line M) API 579-1/FFS-1 fig 4.6b

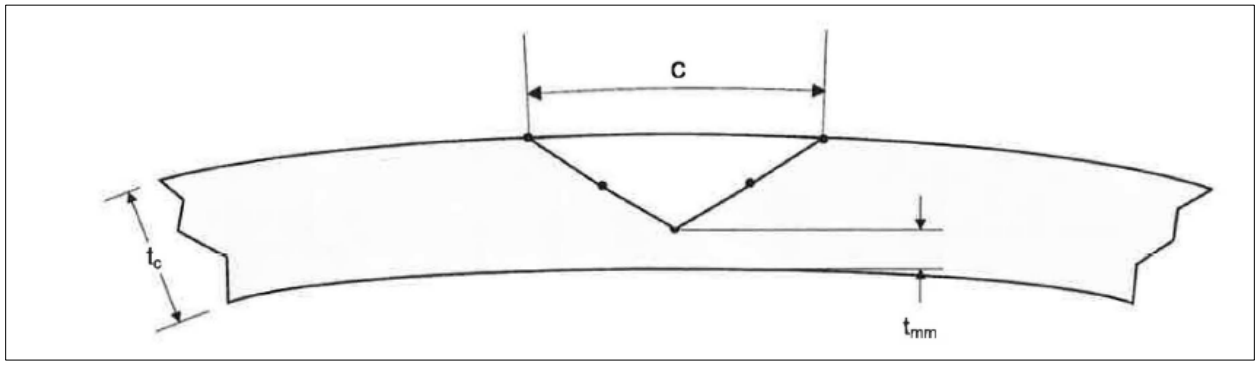

Figure 10. Critical Thickness Profile (CTP) – Circumferential Plane (Projection of Line C) API 579-1/FFS-1 fig 4.6c

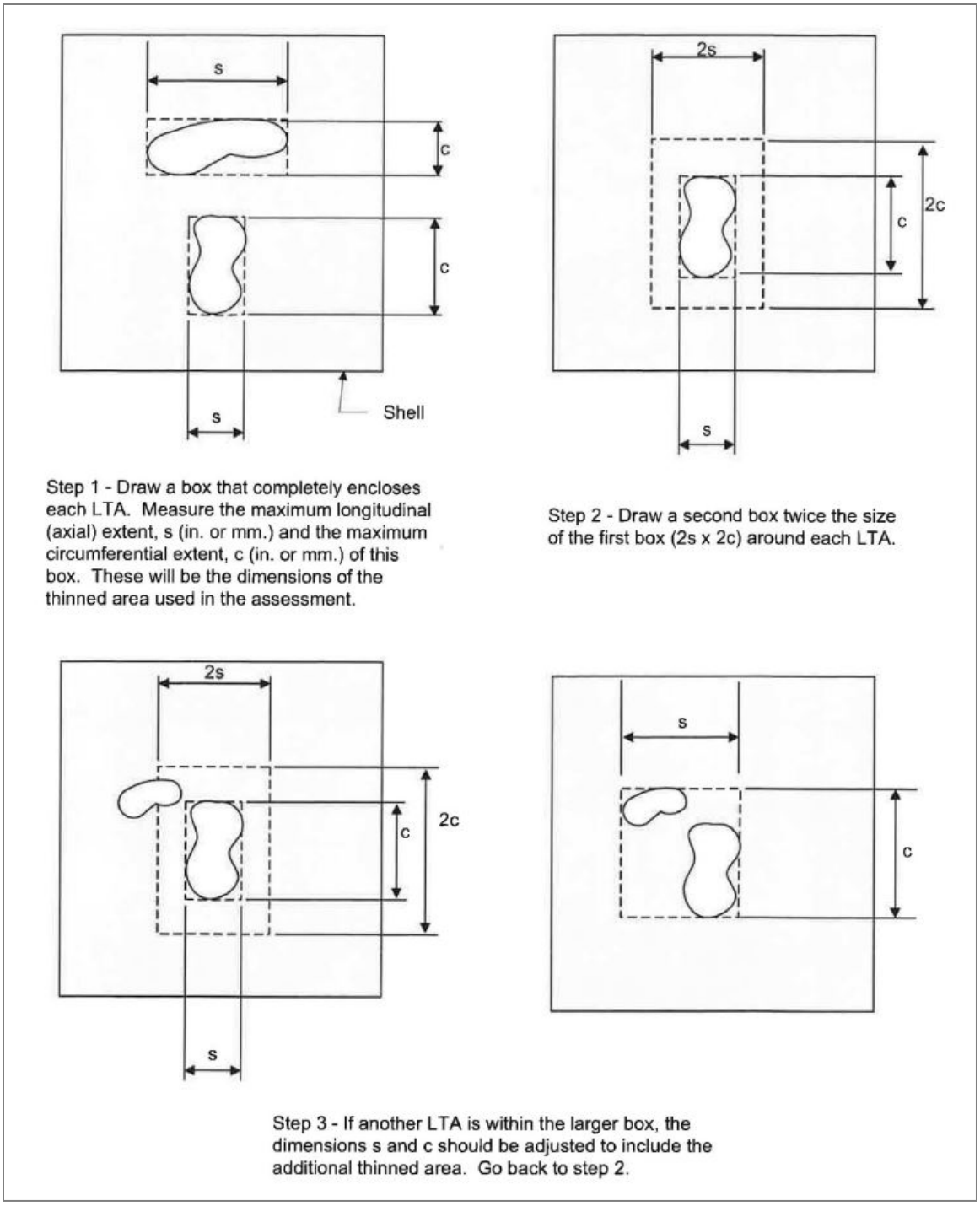

Figure 11. Combining and resizing flaws per API 579-1/ASME FFS-1 fig 4.7

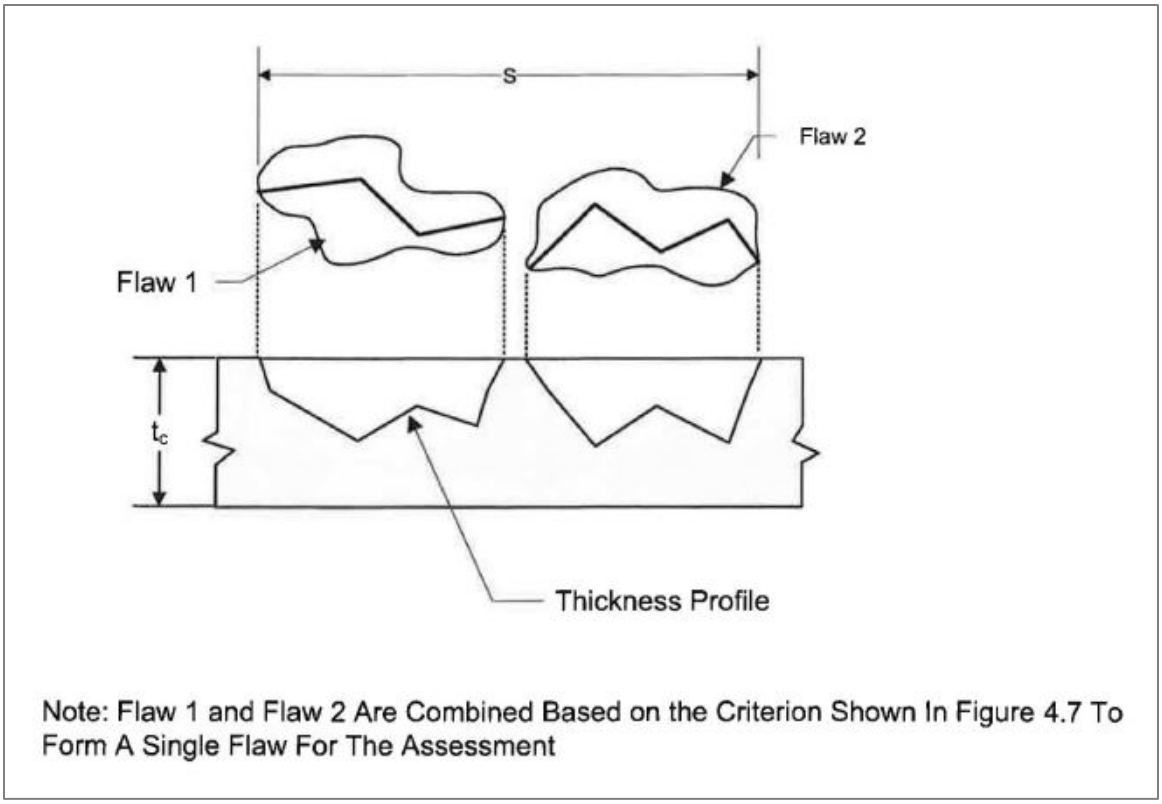

Figure 12. Sizing of a network of flaws from API 579-1/ASME FFS-1 fig 4.8

End of Section 4

5. References

1. API 579-1/ASME FFS-1 Fitness for Service, The American Society of Mechanical Engineers and the American Petroleum Institute, 2nd Edition, June 5, 2007, Washington D.C.
2. Escoe, K. A., Piping and Pipeline Assessment Guide, Elsevier Publishing, New York, 2006.

End of Training Manual